THE UNIVERSITY OF HULL

Elemental Speciation and Miniaturised Sample Introduction Studies for Inductively Coupled Plasma Mass Spectrometry

being a Thesis submitted for the Degree of

Doctor of Philosophy

in the University of Hull

by

Gareth F. Pearson M.Chem. MRSC

July 2007

Summary of Thesis submitted for Ph.D. degree

by Gareth F. Pearson M.Chem. MRSC

on

Novel Sample Introduction for Inductively Coupled Plasma Mass Spectrometry

This thesis describes two approaches towards the development of rapid speciation analysis employing ICPMS detection.

Firstly rapid separation of arsenic species is described by HPLC – ICPMS using a commercial monolithic silica column (Chromolith™). Arsenic species were separated within 3 minutes, greatly reducing the time required for analysis with conventional columns. The separation was achieved by ion-pair liquid chromatography using 2.5 mM tetrabutylammonium bromide as the ion-pair reagent. Good detection limits, accuracy and precision were achieved with the optimised method. The technique was applied to speciation analysis of urine and food samples in an ingestion experiment carried out in collaboration with De Montfort University to investigate the effect of rice consumption on arsenic exposure in humans. For the first time this study reveals that ingestion of American long grain rice significantly increases the excretion of dimethylarsinate (DMA) in human urine. This is consistent with a recent study which reported that DMA was the predominant arsenic species in rice from the USA, which also contained the highest mean arsenic level compared to rice grown in Europe, Bangladesh and India.

Secondly a novel sample introduction system specifically designed for interfacing microfluidic devices with ICPMS is presented. The development and optimisation of this highly efficient interface is described. This system uses an extremely low flow micro-cross-flow nebuliser sited directly at the liquid exit of the microchip. An evaporation chamber has been incorporated into the interface in order to prevent the losses associated with spray chambers, allowing the entire sample aerosol to enter the plasma. The optimised system demonstrated good sensitivity and stability. Sample recondensation was never observed in the evaporation chamber at liquid flow rates < 20 μl min^{-1}. Hydrodynamic sample injection was performed *via* a manual switching valve allowing sample volumes of > 40 nanolitres to be analysed. The advantages and potential applications, in particular for microchip electrophoresis to conduct elemental speciation, are discussed.

Acknowledgements

Firstly I would like to thank Professor Gillian Greenway my research supervisor. I am indebted to Gillian for the opportunity to carry out this research, her expert guidance and support throughout. I am also grateful to my collaborators Dr. Parvez Haris and Prof. Henryk Matusiewicz for the opportunities they provided me.

Bob Knight has become a good friend throughout this work and has always been there for me to share the successes and frustrations. I have learnt a lot from Bob and am very thankful to him for welcoming me into his lab, his good humour and constant encouragement.

I am grateful to Nigel Parkin, Mike Dunn and Mike Bailey, from the engineering and glass blowing workshops, who have provided the skills to transform even my most abstract ideas into reality.

I thank my friends within the analytical chemistry research group (and beyond) at the University of Hull. They have provided me with their assistance and entertainment throughout including countless scientific discussions (often in the bar).

Without the constant support and encouragement of my parents I could have never achieved half of what I have to date. They have provided for me in every way and made it possible for me to get where I am today. I cannot ever thank them enough.

Finally I would like to acknowledge PTFE tape, epoxy resin, Torr Seal® and Blu Tack™. Without these none of the chip work would have ever been successful.

Abstract

The work presented in this thesis describes the development of sample introduction for inductively coupled plasma mass spectrometry (ICPMS). The ultimate aim is to develop methods for conducting rapid speciation analysis. This is approached in two ways; firstly using liquid chromatography (LC) employing a column with a monolithic silica stationary phase, and secondly by the development of a highly efficient sample introduction system designed for interfacing an electrophoresis microfluidic chip with ICPMS.

Chapter 1 gives a comprehensive introduction to the project. The background and fundamentals of ICPMS are presented, with particular attention drawn to the sample introduction systems used. A brief history of elemental speciation analysis is discussed along with elements that have found particular interest. Arsenic speciation analysis is considered in detail since it was a focus of the work presented on LC – ICPMS. Separation schemes used in conjunction with ICPMS for speciation are then reviewed, including the principles and application of chromatographic and electrophoretic techniques.

Chapter 2 details the instrumentation and standard operating procedures used throughout this work. Operating parameters for each instrument are given along with details of calibration, optimisation and maintenance. The use of reagents, gases and certified reference materials are also described in this section. Common procedures for

trace elemental analysis, including liquid handling and equipment cleaning are considered.

Chapter 3 describes the rapid separation of arsenic species by application of a commercial monolithic silica column (Chromolith™). The optimisation of the chromatographic conditions suitable for use with this column and ICPMS detection is described. Separation is achieved by ion-pair chromatography using a mobile phase consisting of 2.5 mM tetrabutylammonium bromide, 10 mM phosphate buffer (pH 5.6) and 1.0 % ($^{v}/_{v}$) methanol. The analysis time required for separation with conventional columns is greatly reduced with the separation being completed within 3 minutes. This affords a dramatic reduction in detector idle time and an increase in sample throughput. Detection limits of 0.107, 0.084, 0.120, 0.121 and 0.101 μg As L^{-1} for As(III), arsenobetaine (AsB), dimethylarsinate (DMA), monomethylarsonate (MMA) and As(V), respectively have been achieved. The precision of the method, based upon analysis of 15 μg As L^{-1}, is better than 5.9 % for all species. The technique is applied to the speciation analysis of urine and food samples in an ingestion experiment carried out in collaboration with De Montfort University to investigate the effect of rice consumption on arsenic exposure in humans. For the first time this study reveals that ingestion of American long grain rice, widely consumed in the UK and purchased from a local supermarket, significantly increases the excretion of DMA in human urine. This is consistent with a recent study which reported that DMA was the predominant arsenic species in rice from the USA, which also happened to contain the highest mean arsenic level in the grain compared to rice grown throughout Europe, Bangladesh and India.

Chapter 4 introduces the development of a sample introduction system specifically designed for interfacing laboratory on a chip devices with ICPMS. Low flow sample introduction is discussed in which it is possible to allow the entire sample aerosol to enter the plasma. The design and optimisation of an evaporation chamber is presented in order to prevent the losses associated with traditional spray chambers. A low flow micro-concentric nebuliser (MicroMist) is used to generate the sample aerosol. No sample recondensation is ever observed in the evaporation chamber at flow rates up to 20 μl min^{-1}. A comparison with a commercial low volume cyclonic spray chamber (Cinnabar) is performed. The optimised evaporation chamber results in a 400 % increase in signal intensity and instrumental detection limits are improved by an average 34 %.

Chapter 5 describes the development of a nebuliser designed specifically for use with microfluidic devices and its incorporation into a sample introduction system for ICPMS. This system uses an extremely low flow micro-cross-flow nebuliser (MCFN) sited directly at the liquid exit of the chip. The evaporation chamber described in Chapter 4 has been incorporated into this highly efficient microchip interface. The optimised system has been shown to achieve a sensitivity of 13 500 cps for 10 μg L^{-1} indium at an extremely low flow rate of 5 μl min^{-1}. The stability of the sample introduction over 10 min is 2.6 % RSD (n = 453) and sample volumes of > 40 nl can be analysed. The advantages and potential applications, in particular for elemental speciation, are discussed. The system is then applied to sample introduction for microchip electrophoresis.

Chapter 6 reviews the use of hydrodynamic sample injection for microfluidic devices. The performance of a manual switching valve is evaluated, achieving a reproducibility of 5.10 % RSD (n = 6). Suggestions for improvement of the sample injection specifically for small ionic species are discussed. The use of microvalves formed in *situ* within the microchip channels is investigated. Photo-polymerisation with a UV laser source is performed to produce rigid (highly cross-linked), non-stick (highly fluorinated) monoliths which do not adhere to the glass channel walls. Incorporation of these microvalves into a microchip in order to create a discrete sample loop is discussed.

Chapter 7 summaries the general conclusions of the work presented and gives suggestions for future work.

Table of Contents

1 Introduction

The aim of this work was to investigate methods to achieve rapid speciation using detection by inductively coupled plasma mass spectrometry (ICPMS). This ultimate aim was approached in two ways.

Firstly by the application of a new commercial monolithic silica stationary phase material to ion-pair liquid chromatography. This system was evaluated for the rapid separation of arsenic species. An ingestion study was performed in collaboration with De Montfort University to elucidate the effect of American long-grain rice consumption on arsenic exposure in humans.

The second approach was the instrumental development of a novel highly efficient sample introduction system for interfacing microfluidic chips with ICPMS. Lab on a chip devices had previously been used to conduct electrophoretic separations and successfully interfaced to ICPMS using commercial low flow sample introduction systems. The objective was to overcome specific problems experienced with the use of commercial sample introduction. This was achieved by designing a microfluidic chip assembly incorporating a micro cross-flow nebuliser and integrated evaporation chamber.

The scope of this introduction is to introduce the historical background and development of the research areas, techniques and applications associated with the work presented.

1.1 Inductively Coupled Plasma Mass Spectrometry

Plasma spectroscopy was originally developed based upon work by Gray in the 1970's.[1-3] Gray utilised an atmospheric pressure plasma source (the capillary arc plasma) for the direct ionisation of nebulised liquid samples, which could then be detected by quadrupole mass spectrometry (MS). Simple spectra were achieved with a low background signal and high sensitivity. Prior to this gaseous samples were easily analysed by MS, but aqueous solutions could only be indirectly analysed by evaporation to dryness and then analysing the solid residues.[1] The plasma source was soon changed to an inductively coupled plasma (ICP) to obtain higher temperatures for ionisation and the first publication of an ICPMS system was presented in 1980.[4]

The interface of the ICP source to the quadrupole MS described in this original paper remains the same up to the present day. Two water cooled metal cones link the high temperature (6000K), atmospheric pressure argon ICP and room temperature, low pressure quadrupole mass analyser (10^{-5} Torr). These are electrically grounded to reduce the potential between the plasma and the interface, hence preventing potential electrical discharge. Douglas and French presented an alternative method of electrical grounding. Radiofrequency (RF) voltage was applied to either end of a coil, which was earthed in the centre; hence resulting in a plasma potential of almost zero so there is no potential between the interface and plasma.[5] This plasma spectrometer interface is shown schematically in Figure 1.1 and described further regarding ion transport later.

Only four years after the pioneering work of Gray and Houk *et al.*[4] the first commercial ICPMS instruments became available. SCIEX (Canada and US) adopted the work of Douglas and French, while the VG Elemental (UK) system was based upon

Gray and Houk's work. Since then the technique has continued to mature rapidly and has had a massive impact on atomic spectrometry.

There are a number of different types of mass analysers that can be used with ICPMS. Quadrupole (Q –) ICPMS is the most widely used, offering good sensitivity, robustness, reliable software and has a large market. High resolution (HR –), double focussing (DF –) and sector field (SF –) ICPMS can all achieve lower detection limits (*cf.* Q – ICPMS) and adjustable improvement in resolution helping to minimise polyatomic interferences; however this all comes at greater expenditure. Time of flight (TOF –) ICPMS has poorer detection limits (*cf.* Q – and DF – ICPMS) but higher scan speeds which makes it particularly suited to isotope ratio measurements or for detection of rapid analyte signals (e.g. originating from CE or laser ablation). Additionally collision or reaction cells are becoming increasingly popular as a method for avoiding polyatomic interferences, discussed further in Section 1.1.4. Current quadrupole ICPMS instruments available on the market include:

- PerkinElmer SCIEX Elan range (PerkinElmer LAS Ltd., Beaconsfield, UK), featuring dynamic reaction cell (DRC) and axial field technology (AFT)

- Agilent Technologies 7500 series (Agilent Technologies Ltd., Cheshire, UK), featuring octapole reaction system (ORS)

- Varian 820 (Varian Ltd., Oxford, UK), featuring collision reaction interface (CRI)

- Thermo X Series (Thermo Fisher Scientific, Cheshire, UK), featuring collision cell technology (CCT)

- GV Instruments Platform XS (GV Instruments, Manchester, UK), featuring HEX™ collision cell (GV established in 2003 from VG Elemental, which became Fisons, Micromass and Waters)

1.1.1 Principles of ICPMS

There are several excellent texts written by experts in the field of ICPMS which describe the technique in detail,[6-8] however it is important to explain the basic principles. A schematic of a modern quadrupole ICPMS instrument is shown in Figure 1.1. The ICP is formed within a quartz torch consisting of three concentric tubes. The central tube, termed the injector, contains the sample aerosol in a flow of argon nebuliser gas flow, typically at 0.5 – 1.5 L min^{-1}. The intermediate and outer tubes carry the argon plasma gas (typically 15 L min^{-1}) and auxiliary gas (typically 1.2 L min^{-1}). These sustain and shape the plasma, and cool the torch to prevent it from melting. The torch is encircled by a copper induction or load coil. This coil is cooled by water and is connected to a radiofrequency (RF) generator giving typical output powers of 1 to 2 kW. The oscillating RF current produces a magnetic field in the coil which induces a current in the argon gas flow. The plasma is formed when the argon gas is seeded with energetic electrons, typically produced by a spark from a high voltage Tesla discharge. Electrons continuously collide with argon atoms, transferring energy, causing further ionisation. A stable, self-sustained plasma is maintained as long as sufficient RF power is supplied.

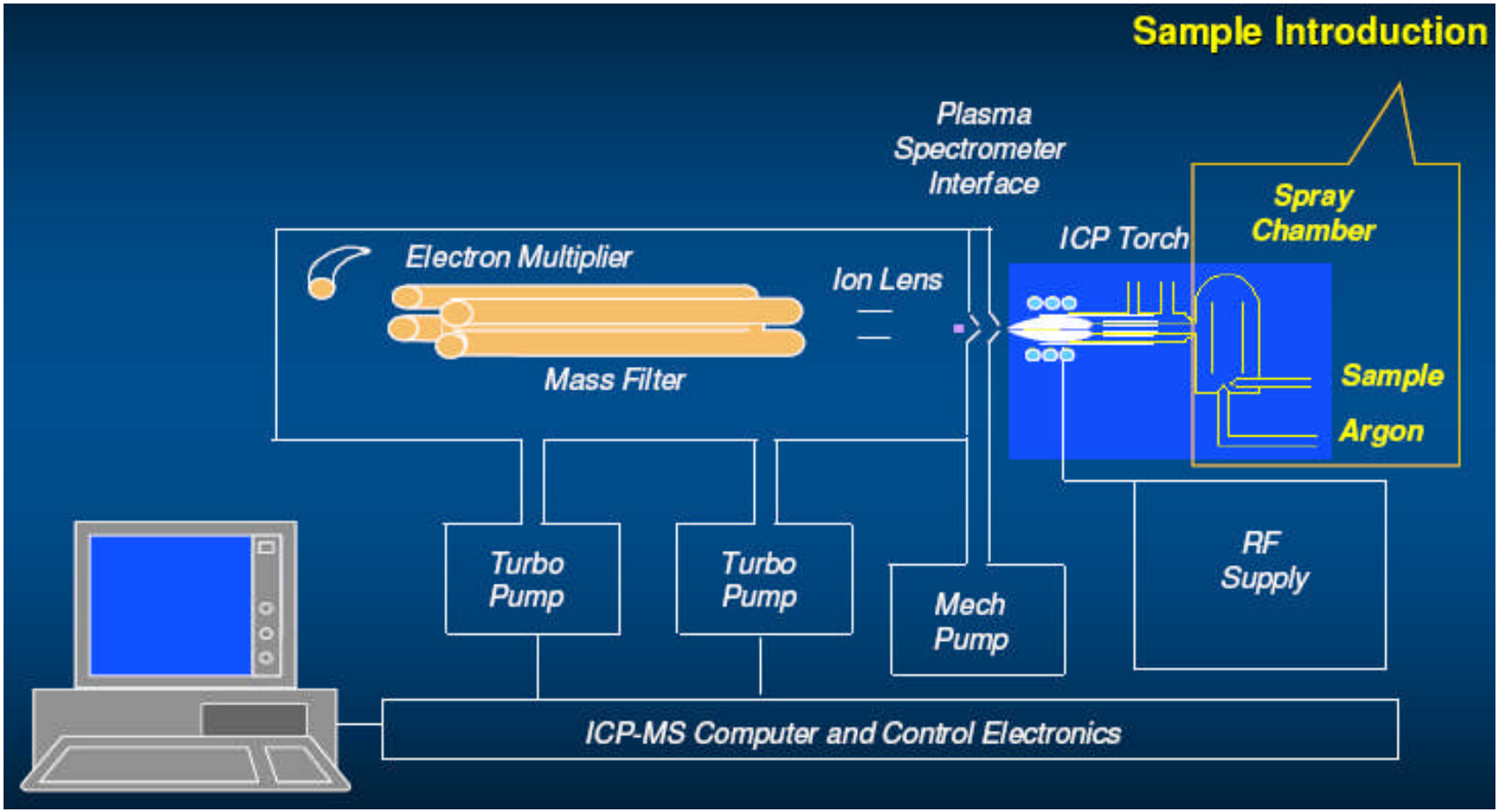

Figure 1.1 Schematic of the components of a quadrupole ICPMS instrument (ICPMS and DRC training course, PerkinElmer LAS, Seer Green, UK. 11-15 July 2005).

In an ICP the largest current flow occurs on the outside of the plasma giving it an annular configuration providing efficient sample introduction *via* the channel created through the centre of the plasma. The collisions release an enormous amount of energy creating plasma gas temperatures of up to 8 000 K (5 – 7 000 K in the central channel) and electron temperatures of up to 10 000 K. This combined with high electron number density (1 – 3 x10^{15} cm^{-3}) and relatively long residence time of sample in the plasma (2 – 3 ms) results in efficient vaporisation – atomisation – ionisation of the sample.

1.1.1.1 Ion source

The argon plasma is an intense source of inert ions in which the bulk plasma consists of > 99.9 % argon. The atmospheric pressure plasma is not in chemical or physical equilibrium, and is best thought of as a dynamic reactor. The plasma is considered to be in local thermal equilibrium (LTE) in order to evaluate the partitioning which occurs between particle states within the plasma; however in reality it may not be fully in LTE.[6] The degree of ionisation of an element can be calculated by considering the equilibrium between an atom (M), ion (M^+) and electron (*e*):

$$M \Leftrightarrow M^+ + e \qquad \textbf{Equation 1.1}$$

The equilibrium constant for this equilibrium being:

$$K = \frac{[M^+][e]}{[M]} \qquad \textbf{Equation 1.2}$$

Within an ICP thermal ionisation predominates. Considering a singly charged ion for a system in LTE the degree of ionisation can be estimated from the Saha equation:

$$\frac{[M^+]}{[M]} = \frac{1}{n_e}\left(\frac{2\pi m_e kT_e}{h^2}\right)^{3/2}\frac{Q^+}{Q^0}\exp\left(-\frac{IP}{kT_{ion}}\right) \qquad \textbf{Equation 1.3}$$

Where n_e is the electron number density in the plasma (typically 1 x10^{15} cm^{-3} Ar ICP), m_e the mass of the electron (9.11 x10^{-31} kg), k is Boltzmann's constant (1.38 x10^{-23} J K^{-1}), h is Planck's constant (6.63 x10^{-34} J s), T_e the free electron temperature (typically 7500 K Ar ICP), Q^+ the electronic partition function of the ion, Q^0 the electronic partition function of the atom, IP the ionisation potential of the element, and T_{ion} the ionisation temperature (typically 7500 K Ar ICP).[6] According to the Saha equation the degree of ionisation is a function of the ionisation energy of the elements in the plasma. Generally ionisation energies below 9 eV result in very good sensitivity, up to 11 eV is acceptable, above 11 eV the degree of ionisation becomes low and over 13 eV atoms are not ionised sufficiently in the plasma. The majority of the elements in the periodic table have first ionisation energies below 10 eV, with significantly higher second ionisation energies. Therefore the majority of elements are > 90 % ionised and singly charged positive ions predominate. There is however a small molecular and doubly charged ion population which can present isobaric interferences in quadrupole MS. Doubly charged ions originate from elements with relatively low second ionisation potentials. Prime examples are barium (10.004 eV), cerium (10.851 eV), calcium (11.871 eV) and strontium (11.03 eV). The most significant molecular ions generated in an ICP are the oxides of atomic ions; however argides, nitrides and chlorides are also often present.

1.1.1.2 Ion transport

Following ionisation the analyte ions must be transported from atmospheric pressure plasma region at 6000 K to the low vacuum (10^{-5} Torr) mass analyser region at room temperature. Ions must be transported from the plasma into the mass spectrometer in a representative and reproducible manner. The interface must also be able to handle the high temperature generated by the ICP. This is achieved by a two stage, differentially pumped extraction procedure: firstly using a sampler cone to extract ions into an 1 – 3 Torr vacuum region, and secondly using a skimmer cone to extract ions into a high vacuum region (see Figure 1.1). The sampler cone directly faces the plasma and hence is water cooled to efficiently dissipate the heat generated from the plasma. This cone is generally made of nickel and has a 1 mm diameter orifice through which the plasma and analyte ions are sampled. Behind this cone is a mechanically pumped intermediate pressure region. The sampled plasma jet forms a shock wave structure, rapidly expanding and cooling. The skimmer cone samples the analyte ions within the freely expanding region, termed the zone of silence, which is surrounded by two shock waves called the barrel shock and the Mach disc. The shock waves are caused by collision of the supersonic jet with the surrounding background gas. The position of the skimmer cone precedes the Mach disc and is essential to achieve representative sampling whilst avoiding ion losses due to collisions and scattering. Only the central part of the jet is sampled through the 0.7 mm diameter skimmer cone orifice, representing approximately 1 % of the ion beam. Ions passing through skimmer cone undergo supersonic expansion in a further reduced pressure region, controlled by the first turbo-pump. The ions are refocused by an electrostatic ion lens system before entering the quadrupole. A potential is applied to the ion lens(es) in order to permit the transmission of only ions, discarding neutral atoms, electrons and photons.

1.1.1.3 Quadrupole mass spectrometer

The ion beam enters the analyser region which is held at approximately 10^{-6} to 10^{-7} bar by a second turbo-pump. The role of a mass filter is to be capable of separating ions with different mass to charge ratios. The analytical parameters of a mass filter are: resolution, abundance sensitivity and stability. The quadrupole consists of four perfectly cylindrical rods mounted in a circle, shown in Figure 1.2. AC (RF frequency 2.5 MHz) and DC potentials are applied to each pair of opposing rods creating an oscillating hyperbolic field in the central channel formed by the rods. The RF and DC potentials are selected so that only ions with a specific mass to charge ($^{m}/_{z}$) ratio have a stable trajectory and can pass through the path of the rods to the detector.

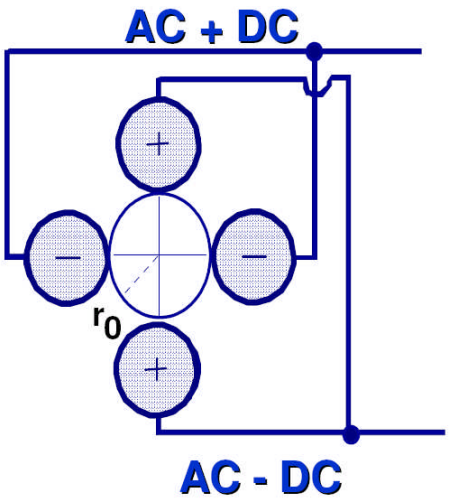

Figure 1.2 Schematic of quadrupole rods in mass filter (ICPMS and DRC training course, PerkinElmer LAS, Seer Green, UK. 11-15 July 2005).

The Mathieu equation is used in order to select the appropriate AC and DC voltages in order to transmit ions with the desired mass to charge ratio and reject all others:

$$a_n = 2n(n-1)\frac{eU}{m\omega^2 r_0^2}$$
$$q_n = n(n-1)\frac{eV}{m\omega^2 r_0^2}$$

Equation 1.4

Where *n* is the number of rods (i.e. 4), *e* is the charge on the ion, *m* is the mass of the ion, ω is the frequency, r_0 is the inner radius of the quadrupole (Figure 1.2) and U and V are the DC and AC rod offsets respectively. The Mathieu equation shows the relationship in Equation 1.5.

$$a \propto \frac{U}{m}$$
$$q \propto \frac{V}{m}$$

Equation 1.5

The *q* value is selected in order to reject lighter masses and the *a* value to reject heavier masses. The quadrupole is usually operated within the stability region where: $0 < q < 0.908$; $0 < a < 0.24$ (usually illustrated in a stability diagram).[9] A mass calibration is performed to select the working line of the quadrupole across the mass range.

Resolution is expressed in terms of the signal from two adjacent peaks. If the mean mass of the peaks is m, and the separation is δm, the resolving power (R) is given by Equation 1.6.

$$R = \frac{m}{\delta m}$$

Equation 1.6

In quadrupole ICPMS resolution is typically defined as the peak width at 10 % of the peak height. The quadrupole mass filter is generally operated at nominal unit mass resolution (1 amu), capable of resolving 0.6 – 0.8 amu peak widths. This is appropriate for atomic spectra but does provide one the major limitations of quadrupole ICPMS.

Abundance sensitivity is the measure of signal due to analyte at one amu higher and one amu lower than analyte. This defines the ability of a quadrupole to determine an ultra-trace analyte concentration next to a major matrix ion mass. Typical values are 10^6 at (amu -1) and 10^7 at (amu +1).

The role of the detector is to count the number of ions leaving the mass filter. The most commonly used detector is the electron multiplier, which can be operated in both pulse counting and analogue modes. Figure 1.3 shows a schematic of a discrete dynode electron multiplier. A large negative potential is applied to the entrance of the electron multiplier (typically –2.5 kV) and the collector end has a positive potential (+1.2 kV). Ions are attracted to the surface, coated with a lead oxide semi conducting material, and upon striking it initiate the release of a cascade of secondary electrons. These electrons continue to strike the successive dynodes as they travel down the tube resulting in a large gain of between 10^7 to 10^8 (*cf.* the original collision), which generates a large electron pulse. The rate at which pulses emerge from the detector corresponds to the rate of ions striking the surface coating. This is related to the number of ions present, hence the concentration of analyte in the sample. The signal generated is therefore presented as the number of counts per second (cps). Pulse counting mode is the most sensitive, but saturation of the detector occurs at high analyte concentrations at which point the detector cannot respond quickly enough to count individual pulses (counting rate above 2 x10^6 cps). In this case analogue mode can be utilised which

monitors the constant signal half way down the detector, resulting in a lower gain of 10^3 – 10^4. In practise both modes are operated simultaneously and if the signal is too high upon reaching an electronic gate following the analogue output the gate is closed and the pulse signal is not measured in order to protect the detector. This technology gives rise the large linear dynamic range of ICPMS, up to 8 orders of magnitude. In order to achieve this linear range a cross-calibration must be performed using any elements which are to be measured in both pulse and analogue modes, generally between 1 x10^5 and 2 x10^6 cps.

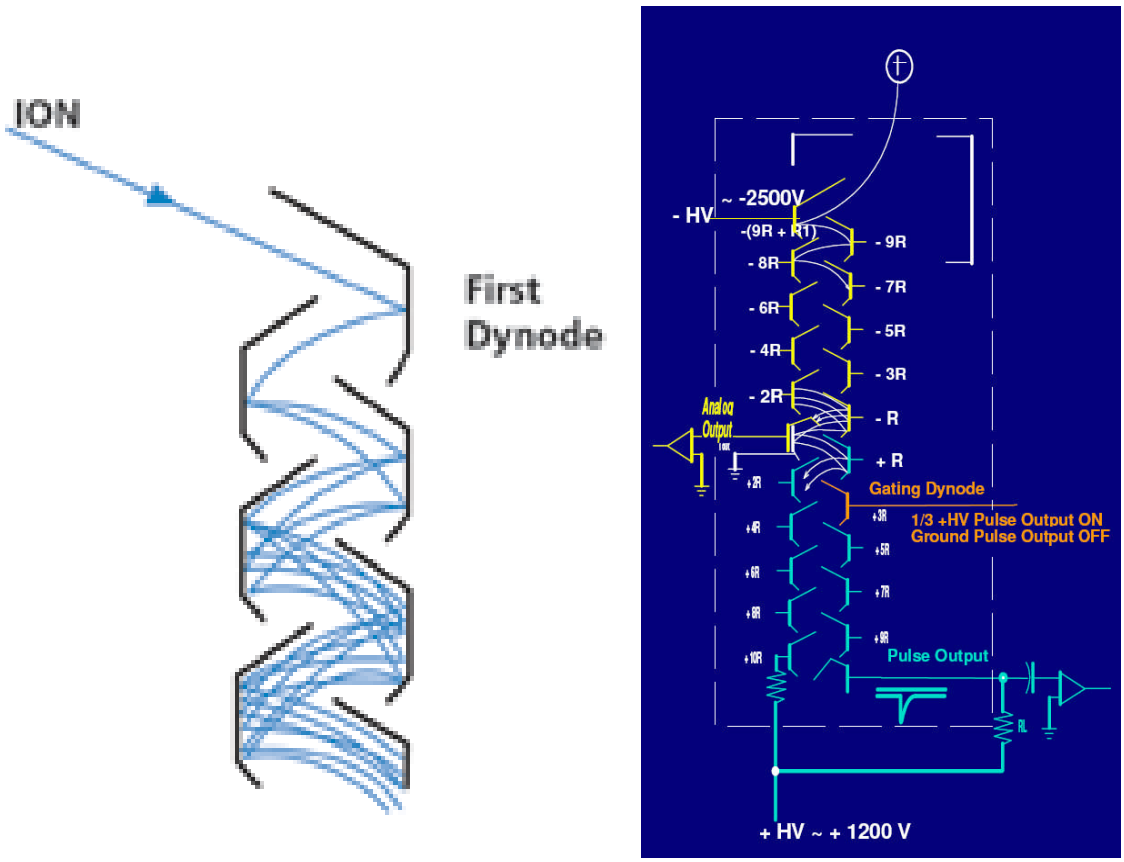

Figure 1.3 Schematic of electron multiplier operation[10] and the ICPMS discrete dynode detector featuring simultaneous pulse and analogue modes *via* gating dynode (ICPMS and DRC training course, PerkinElmer LAS, Seer Green, UK. 11-15 July 2005).

1.1.2 Sample Introduction

The most common form of sample introduction for ICPMS is liquid. Liquid phase samples provide excellent measurement accuracy and precision, owing to the ease of sample handling, preparation, dilution and calibration. The typical sample introduction system for ICPMS consists of a peristaltic pump, nebuliser, spray chamber and plasma torch with injector. The peristaltic pump pumps the liquid sample to the nebuliser in a constant and reproducible manner, allowing controllable flow rates with minimal pulsation. This compensates for differences in viscosities between samples, standards and blanks.

1.1.2.1 Nebulisation

The function of a nebuliser is to reproducibly form a smooth nebular or aerosol, i.e. transform a stream of liquid into a cloud of droplets. A size distribution of droplets are produced, in which the smaller the droplet size the higher proportion of the sample can be introduced to the plasma. The typical desired droplet size is less than 2 μm, any droplets in excess of 10 μm are considered too large, and are removed to waste in the spray chamber. It is desirable for the nebuliser to have good tolerance to high dissolved solids (particulates) and chemically corrosive materials (e.g. strong acids) both present from the sample digestion / preparation processes. It should also be robust and offer suitable uptake rates for the application and introduction into the ICP.

There are many types of nebuliser, each with distinct advantages / disadvantages which make them suited to certain applications. Pneumatic (PN) and ultrasonic nebulisers (USN) are the most common types and are based upon well established

technology. PN were developed based upon early work by Gouy in 1879 and USN were first reported later by Wood and Loomis in 1927.[6]

1.1.2.1.1 Pneumatic Nebulisers

Aerosol transport efficiency is defined as the percentage of the mass of nebulised solution that actually reaches the plasma.[6] The analyte transport efficiency is generally more important, representing the percentage of analyte actually detected. Pneumatic nebulisers (PN) have a typical efficiency of 1 – 3 %; i.e. the majority of sample is pumped to waste, as they produce an aerosol distribution. Approximately 90 % of droplets are too large and do not reach the plasma, instead they are removed to waste *via* a spray chamber. The basic components of a PN are a nozzle which accelerates the propellant gas and a means of introducing the liquid into the flowing gas stream. Figure 1.4 illustrates the three basic types of PN are most commonly used in analytical spectrometry: the glass concentric (a.k.a. Meinhard), cross-flow and Babington or V-groove (De Galan and Ebdon).

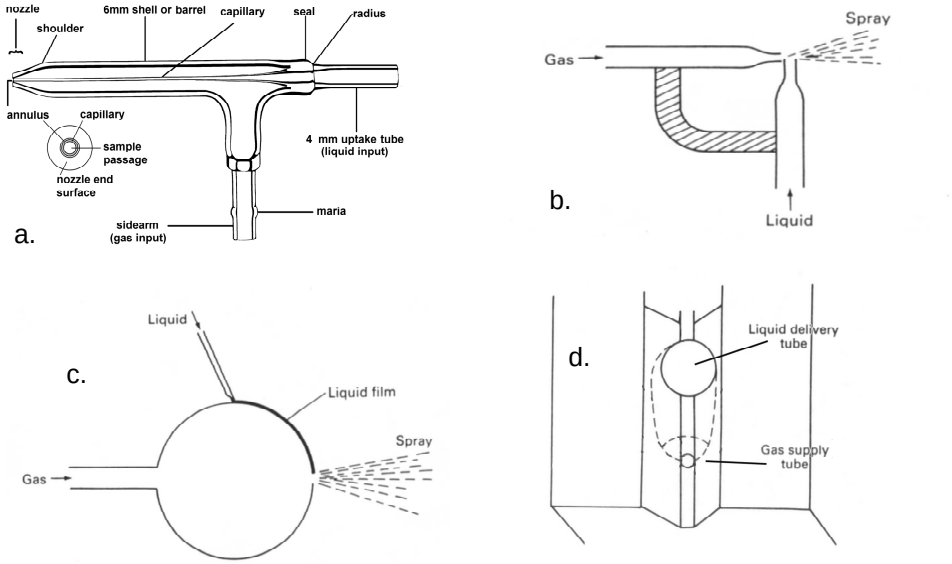

Figure 1.4 Schematic of conventional nebuliser designs used for sample introduction into ICP. a. Glass concentric, b. Cross flow, c. Babington, d. V-groove.[11, 12]

The **glass concentric** PN (Figure 1.4 a) is currently the most widely used, often being the standard arrangement for typical ICPMS analysis. It consists of an outer glass tube through which a nebuliser gas (routinely Argon) flows at high velocity (500 to 1500 ml min^{-1}). The sample solution flows parallel to this inside the inner capillary. As the nebuliser gas passes across the end of the inner capillary it produces a reduction in pressure by the *Venturi* effect, which results in the uptake of liquid sample. Upon reaching the end of the inner tube the liquid is nebulised by the flowing Argon gas. Advantages of glass concentric nebulisers which have made them so popular include; low background with higher signal intensity. No essential requirement for a pump to introduce sample (natural uptake), hence eliminating any pump background noise. The placement of the sample intake capillary inside the nebuliser gas tube reduces the liquid dead volume, consequently increasing the sample throughput and reducing associated memory effects. They do however have some disadvantages which make them unsuitable for some applications. They can easily become blocked, especially if solutions consist of high dissolved solid content or suspensions. Solutions in excess 0.25 % solids (particularly samples containing NaOH or HF) should not be nebulised in this way. However they can be unblocked relatively easily (by immersion in an ultrasonic bath, inserting a thin piece of wire through the nozzle, soaking in strong acid to dissolve the obstruction, or back-flushing nebuliser with a stream of liquid), but this can still cause instrument shutdown which can be very inconvenient during analysis. Also if the nebuliser's natural liquid uptake is being employed there is no control over flow rate between samples with different viscosities. Being made of glass they are not HF resistant, and are relatively expensive to replace if damaged. A common type are the Meinhard® nebulisers (J E Meinhard Associates, Inc., Santa Ana, CA, USA), which are supplied in several configurations, to offer a range of operating characteristics and

nozzle types. If the inner capillary tip is recessed from the end of the tube (~0.5mm) it creates an increase in the pressure differential, and therefore natural uptake rates can be elevated by 1.5 to 2 times. The nebuliser consistency is affected by the aspiration rate, nozzle type and nebuliser pressure. Higher pressure and lower flow rates produce a greater percentage of smaller droplets, i.e. increased sensitivity as more sample reaches the plasma, but give more inconsistency in the nebulisation, i.e. increased % RSD. Micro-concentric nebulisers (MCN) have been developed for the analysis of low sample volumes, using low liquid flow rates. As implied by their name these have reduced critical dimensions. Areas in which MCN have found application are discussed further in Section 4.1.1.

Cross-flow PN (Figure 1.4 b) use a sample capillary set perpendicular to the nebuliser gas tube. As in the concentric nebuliser a reduction in pressure at the tip is produced, providing a mechanism for sample uptake. The shape and position of the two capillary tips relative to each other critically affects the performance of the nebuliser. The cross-flow is a good all purpose PN which is inexpensive and can be made from a variety of chemically resistant materials. It generally suffers less from clogging and finds wide application for solutions with high solid content, or salt containing solutions. **V-groove** PN (Figure 1.4 d) are considered to be a type of cross-flow nebuliser, as they are a modification on the general design. The sample flows through an orifice, down a smooth V-groove with another small orifice through which the argon flows. The nebular is formed as the argon flow shears the liquid layer. The V-groove design prevents the clogging at the nebuliser tip caused by solutions containing salts and suspended solids, even allowing slurries to be successfully nebulised.

Parallel path PN (Figure 1.5) works on the basic principal that a body of liquid will produce a fine mist with a gas stream, if the two are in close proximity to each other. Critical alignment of the gas stream and the liquid is not required. Gas streams in capillaries have a pressure driven flow profile creating velocity gradients across the diameter of the capillary. The gas velocity is zero at the sides of the capillary and twice the average velocity in the centre. Ideally the sample solution should meet the nebuliser gas flow in the centre, at the point where the gas is travelling at the highest velocity. Since energy is related to the square of the velocity, an increase in gas velocity creates a large increase in energy transfer from the gas to the liquid, consequentially shattering the liquid into much smaller droplets.

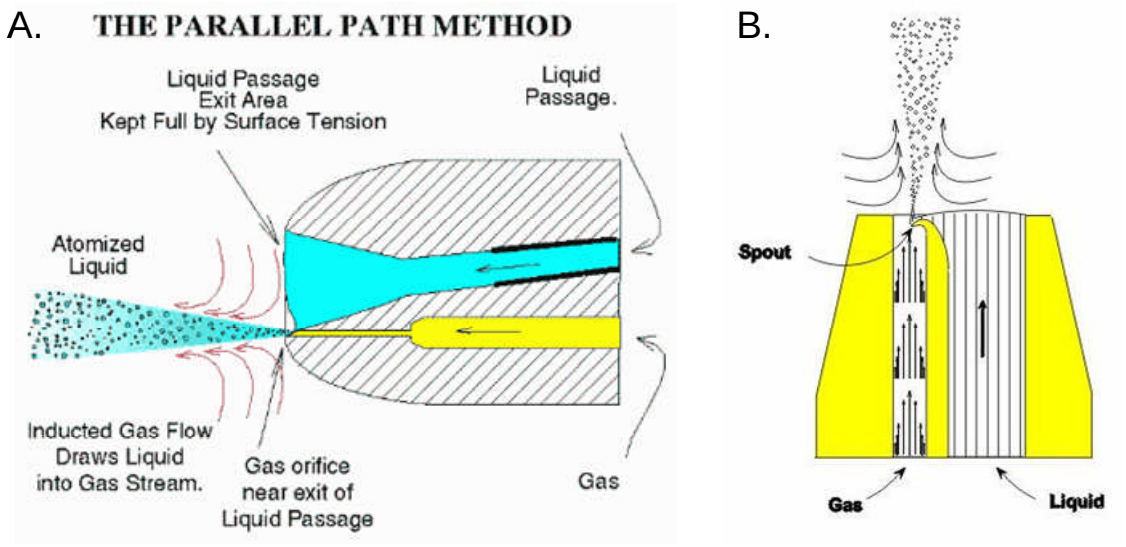

Figure 1.5 Schematic of Burgener parallel path nebulisers. A. Parallel path PN, B. Enhanced parallel path PN.[13]

The enhanced parallel path PN (Figure 1.5 B.) enables the liquid to enter the centre of the gas stream.[13] The design uses an intricate spout created at the end of the liquid orifice, which directs the liquid towards the centre of the gas stream. The spout reduces the surface tension of the liquid, in much the same way as a teapot spout works.[14] This

design can significantly improve sample throughput to the torch and enable much lower flow rates. Additionally the gas orifice is larger compared to concentric nebulisers; hence there is less chance of the nebuliser tip becoming blocked by salt formation, as usually such salts are blown away.[14] A parallel path nebuliser has been specifically designed for use with CE (Mira Mist CE, Burgener Research International, Maidenhead, UK) and has recently been evaluated for speciation coupled with a cyclonic spray chamber.[15] It proved successful at separating a mixture of four cobalamin species standards.

The mechanisms by which PN operate are complex and out of the scope of this introduction. Literature is available on the topic, including an extensive review focussed specifically on the three most common types (concentric, cross-flow and V-groove) of PN.[11]

1.1.2.1.2 Ultrasonic Nebulisers

Ultrasonic nebulisers (USN) were first developed in the 1920s and have two main advantages. They are able to provide improved LOD compared with PN, typically by an order of magnitude. This is because USN have a typical efficiency of 35 % as use of an ultrasonic transducer produces a higher proportion of smaller droplets. Secondly they have relative freedom from clogging, as the nebular is not formed through a small-bore capillary, but as a thin film of solution. The sample solution is pumped to the surface of a piezoelectric transducer, which has an operating frequency of 200 kHz to 10 MHz. The resulting longitudinal ultrasonic waves propagate perpendicular to the surface of the crystal towards the liquid – air interface. When the wave amplitude becomes sufficiently large disruption of the film of sample solution occurs, creating a pressure that shatters the film into a nebular of extremely fine droplets. The droplets are

transported to the plasma by a flow of Argon gas, the efficiency of the droplet formation is independent of the Argon gas flow rate; so lower flow rates can be employed. This is useful for hard to ionise elements, since their residence time in the plasma is increased.

The use of low flow rates and improved efficiency increases solvent loading to the plasma, which can cool or even extinguish the plasma. For this reason most USN are generally used in conjunction with a desolvation unit. This consists of a heated tube (typically 150 ^{o}C) to evaporate the droplets and a condenser (cooled to ~ 0 ^{o}C) that removes the resulting water vapour. The dried aerosol particles are then transported to the plasma. Even higher analyte transport efficiency can be achieved by reducing the solution flow rate to a few μl. With micro-flow USN solution uptake rates of 5 to 20 μl min^{-1} transport efficiency close to 100 % can be achieved.[16]

Disadvantages associated with USN include: the high purchase cost (several thousand pounds), the requirement of a separate RF generator, poorer precision (typically 2 – 3 % RSD, *cf.* 1 % RSD for PN), severe memory effects requiring long washout times 60 – 90 seconds, *cf.* 30 seconds for PN (as an increased amount of matrix constituents are transmitted to the plasma a long with an increased amount of analyte), and enhanced responses due to interfering species (for the same reason).

1.1.2.2 Spray Chamber

The spray chamber is required to remove large droplets and turbulence created by nebulisation of the liquid sample into a primary aerosol. Only droplets below approximately 8 – 10 μm in diameter can be efficiently volatilised in an ICP, with typical RF power used in order to maintain the plasma between 0.8 and 2.0 kW.[6] The sample has a residence time in the plasma in the order of ms, in which time it can only

absorb a little of this power. A pneumatic nebuliser (PN) commonly generates droplets in excess of 30 μm. Several processes occur within the spray chamber to convert the primary aerosol generated by the PN into a finer, more stable tertiary aerosol. A thorough review of spray chambers for ICP spectrometry, discussing the functions, mechanisms of operation and design considerations has been presented by Sharp.[17] All of these processes are not completely known but include; evaporation, coagulation, gravitational forces, decay of turbulence and inertial losses. The effect is to remove, or to reduce the size of the larger droplets and dampen turbulence within these chambers in order to satisfy plasma requirements.

Spray chambers are typically made from glass, but plastic alternatives are available. Glass presents the problem of the surface being attacked by certain corrosive reagents, e.g. HF, and the absorption of some trace analytes, which can lead to significant memory effects.[8] Ryton or PTFE chambers are less surface active, so fewer analytes absorb onto the surface.

The analysis time is dictated by the spray chamber wash-out, or fall time, which is defined as the time taken to reduce the steady-state signal to 1 % of its initial value.[17] Recently spray chambers have been designed with a small internal volume in order to reduce this time. Other variables that affect this time interval are the element being nebulised and the gas velocity. Wash-out times are generally minutes rather than seconds in conventional spray chambers, however this can be reduced to around 20 seconds if the chamber is flushed with a high volume of gas between runs.

Spray chambers are often cooled to 2 – 4 ^{o}C throughout analysis, in order to ensure a small, constant amount of solvent enters the plasma. This improves the stability of the plasma and maximises the signal intensity. In the case of organic

solvents, it is important to use a cooled spray chamber and this can be cooled further. Aqueous solvents should not be cooled below 0 ^{o}C as this can cause the solution to freeze within the spray chamber, which could damage it and create blockages for subsequent samples. This cooling is usually achieved by circulating a cool liquid around an outer jacket on the spray chamber.

The most common design is the Scott double-pass spray chamber, shown in Figure 1.6 a.[18] It is a barrel-shaped spray chamber that removes the larger droplets by deposition on the inner walls, or by gravity. An inner concentric tube reduces aerosol density changes, which cause random fluctuations in signal intensity. Minor changes in pressure can greatly affect the plasma and inefficient draining can cause severe noise spikes in the spectra. For this reason chambers should be designed so liquid drains away smoothly (e.g. through capillaries or sand beds, etc) and liquid build up in the chamber is avoided. The chamber has a number of 'dead volume' areas that introduce memory effects. In an attempt to reduce memory effects within the spray chamber a single-pass design can be used, which has fewer dead volume areas, or by using a reduced volume spray chamber. However these designs are not as efficient at filtering the droplet size and dampening noise.

Other popular designs include spray chambers employing an impact bead in order to further break down the nebular and the cyclone spray chamber (Figure 1.6 b.). Cyclonic spray chambers are essentially wall impact devices in which the aerosol enters through a tangential inlet and spirals downwards within the chamber. When the aerosol reaches the bottom of the chamber a tighter, concentric spiral is produced as it ascends up the chamber and finally the small droplets exit *via* an outlet tube at the top. Centrifugal force acts upon the larger droplets, which impact with the chamber wall,

recondense and are removed by the drain. A re-circulatory flow can entrain the nebuliser jet and particles into the exit flow.[19] However it has been noted that entrainment of the particles by the re-circulatory flow can lead to increased response times and particle losses. Cyclonic chambers can achieve significantly higher transport efficiency compared to other designs, however this is at the expense of allowing the passage of larger droplets.[17]

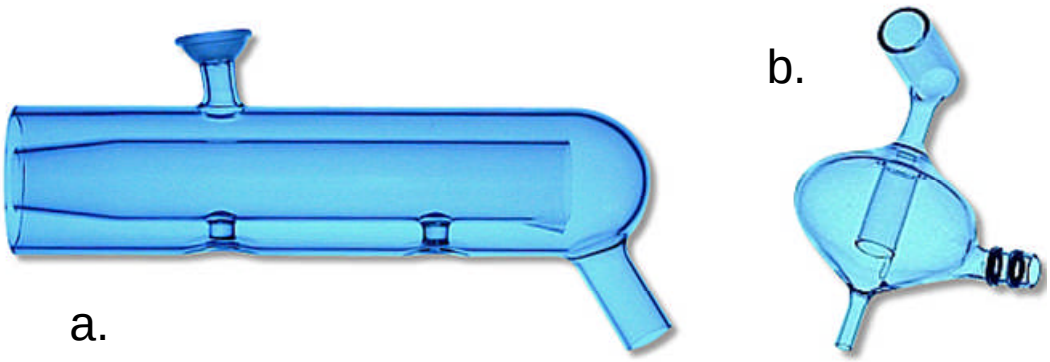

Figure 1.6 Images of a. Scott double pass and b. cyclonic spray chamber.[20]

1.1.2.3 Direct sample introduction

Although the most common method of liquid sample introduction for ICPMS is *via* nebulisation (pneumatic or ultrasonic) used in conjunction with spray chambers or desolvation units several direct sample introduction systems have been investigated. Particularly successful schemes have included electrothermal vaporisation (ETV), thermospray and hydride generation (HG) as methods to convert the liquid sample into a gaseous state ideal for introduction into the plasma. ETV has the advantages of permitting introduction of any sample type into the plasma, achieving high transport efficiencies (< 80 %) and removal of matrix interferences (*via* solvent drying and pyrolysis).[21] Often poor reproducibility is obtained however (> 10 % RSD) and memory effects can be a significant problem.[22] Thermospray nebulisation involves the

electrical heating of the solvent through a narrow-bore stainless steel tube (100 – 150 μm)[8], with pressure produced by the liquid pump producing a mixed aerosol – vapour phase.[17, 23] Thermospray is often applied to LC – MS and lends itself towards LC – ICPMS. HG is the production of volatile hydride species of the analyte with chemical pre-treatment; generally achieved using sodium borohydride [$NaBH_4$]. The application is limited since only certain elements are capable of forming gaseous hydrides at room temperatures (As, Sn, Pb, Sb, Bi, Ge, Se and Te). However 100 % transport efficiency of the gaseous hydride can be achieved and matrix interferences reduced.[22]

Direct injection nebulisers (DIN) and direct injection high efficiency nebulisers (DIHEN) have been developed and applied to the analysis of small sample volumes.[21] As implied by their name they produce an aerosol that is not first passed though a spray chamber, but directly into the plasma. The DIN suffered from being extremely fragile, expensive and complex to use.[24] The high efficiency nebuliser (HEN), introduced in 1992, is a modification on the glass concentric nebuliser (Meinhard®), which is significantly longer in length with reduced critical dimensions.[12] The DIHEN is effectively a hybrid of the DIN and HEN. In comparison to the HEN the DIHEN is longer, to facilitate fitting directly into the torch, and has slightly larger critical dimensions. The typical operating conditions for the DIHEN are a high as possible RF power (e.g. 1500 W) with low as possible nebuliser gas flow (e.g. 0.1 – 0.3 L min^{-1} argon) and μl min^{-1} delivery rate of sample. The liquid flow rate must be low to avoid overloading the plasma as the transport efficiency to the plasma is close to 100 %. Consequently sensitivity and LOD can be significantly improved in comparison with a concentric nebuliser and spray chamber. However both DIN and DIHEN have associated problems due to the analytical behaviour being strongly related to the primary aerosol produced and a high solvent loading on the plasma (the plasma has a

tolerance to solvent of approximately 20 – 40 mg min^{-1}). Droplets larger than 10 – 20 mm in diameter can often be introduced into the plasma.[21] This results in increased signal noise and degraded plasma excitation conditions. Matrix effects are still present, from both organic and inorganic species, which are likely to be due to the deterioration of the plasma conditions. Additionally the tip can be easily blocked due to the longer narrow sample capillary or melted due to operating conditions.[21] A large bore (LB) – DIHEN has been developed to overcome these drawbacks of the DIHEN and permit the analysis of high salt and slurries. However coarser aerosols are generated resulting in poorer sensitivity and precison for the LB-DIHEN.[24]

1.1.3 Limitations of ICPMS

Despite the numerous advantages of ICPMS which has revolutionised trace elemental analysis and speciation it does suffer from some particular limitations. One of the main problems with quadrupole MS detectors is the presence of interferences based upon isobaric overlap. An obvious example is for Ca which is 96.9 % abundant at ^{40}Ca and hence cannot be determined by quadrupole ICPMS since the argon plasma gas produces a much greater signal due to ^{40}Ar (99.6 %). Often this problem can be overcome by careful selection of alternative isotopes that do not suffer from interference; however this is usually at a compromise to sensitivity due to lower % abundance. This problem is compounded further by the presence of polyatomic interfering ions generated in the plasma; for example ^{56}Fe with $^{40}Ar^{16}O$ or ^{75}As with $^{40}Ar^{35}Cl$ (which is a particular problem since As is monoisotropic). These interferences are generally well known and can be overcome by use of correction equations within the instruments software. High resolution ICPMS instruments are capable of eliminating isobaric interferences due to their much greater resolving power. However these instruments are much more

expensive and generally find specific application rather than widespread use. Modern quadrupole ICPMS instruments now often use a collision or reaction cell in order to remove interfering species prior to reaching the quadrupole mass filter. This technique is discussed in more detail later (Section 1.1.4).

Limitations with sample introduction into the ICPMS include the low tolerance to total dissolved solids (TDS). It is customary to limit the TDS below 2000 μg ml^{-1} (practically < 0.5 – 0.1 % $^{w}/_{v}$) in order to prevent blocking of the sampler cone, torch injector and concentric nebulisers.[7] Obviously this restricts the sensitivity of analysis for sample matrices with a high TDS content as they must be diluted. Introduction of organic solvents also causes problems in ICPMS since carbon (IE 11.26 eV) is not fully ionised in the plasma and forms an increased number of carbon containing molecular species. This results in deposits onto the torch and sampler cone. These problems can be reduced by using a water cooled spray chamber, higher RF power and the addition of oxygen gas into the plasma (typically 1 – 3 %) in order to oxidise the C to CO_2 and prevent its deposition.[6, 7]

The use of ICPMS as a detector for speciation analysis is desirable for the ability to provide the low LOD required. ICPMS cannot directly provide any speciation information, apart from isotopic information, owing to the destructive nature of the plasma. Traditional users of ICPMS often consider its use as a detector for lengthy chromatography to be a waste of the instruments capability, especially if only one element is being monitored. Therefore it is desirable to reduce separation times and increase the number of different element species that can be interrogated in a single sample analysis.

1.1.4 Collision / reaction cell technology

The reduction of spectral interferences in ICPMS is achieved by taking advantage of differences existing between analyte and interfering ions. Gas phase ion-molecule chemistry generated in the ICP can be used in order to shift the interferent or analyte ions into another part of the mass spectrum. This approach has the advantage of being employed with conventional sample introduction, using normal analytical ICP conditions with no additional sample pre-treatment required.[25] It is achieved by a collision or reaction cell located between the ion optics and the mass analyser quadrupole in the ICPMS. The first commercial collision cell ICPMS was introduced in 1987.

There are three key considerations in the use of a collision / reaction cell.[25] Firstly identifying a suitable reaction gas, specific interference problems can be addressed using tailored methods, utilising different reaction gases selected on a per element basis. If methods have not previously been published for the analyte / interferent of interest, kinetic rate information, or thermodynamic data can be used to predict an appropriate reaction gas.[26]

Secondly the elevation of the chemical background must be considered; as rather than removing interfering ions a collision / reaction cell converts them into other (hopefully non-interfering) ions. Ideally these product ions will be ejected from the quadrupole, owing to their small mass to charge ratio outside of stability region, and are therefore not detected (for example H_2 gives the product ion H_3^+). If this is not the case the product ions will continue to react further and to follow sequential reaction pathways. This process is favoured by the high reaction efficiency of the cell. High reaction efficiency is favourable when applied to the removal of Ar^+ signal by up to 9

orders of magnitude; however any contamination present, e.g. water vapour, can react with most elemental and molecular argide ions and may create new interferences of similar magnitude. Additionally ArH^+, H_3O^+ and H_3^+ are efficient proton donors and can increase spectral background by several orders of magnitude across the entire mass range *via* proton transfer reactions with hydrocarbons.

Thirdly the properties of the cell as an ion-molecule reactor must be considered. It is desirable for the cell to be in thermally controlled to promote useful ion-molecule reactions, so it operates close to thermal equilibrium conditions. Chemical resolution is achieved by the reaction of an interfering species with a reaction gas within the cell to form a product which does not interfere in the analyte $^m/_z$ region. The instrument used in this study uses dynamic bandpass tuning (DBT) to remove interfering species by setting a high and low $^m/_z$ limit by means of a quadrupole situated inside the reaction cell cavity.[9] These limits change according to the analyte $^m/_z$ range of the detector, hence are dynamic. Interferents are removed by the removal of reactive species that produce the interfering species. For example Cl^- ions can be removed which prevents the ArCl interferent from being formed.

Despite the complex chemistry involved within collision / reaction cells they can be used with relative ease. Argide interferences on K^+, Ca^+ and Fe^+ can be efficiently removed allowing detection below ng L^{-1} concentrations.[27] Extensive applications of collision / reaction cells can be found in the literature. They have been particularly applied for analytes contained within complex sample matrices, for example biological fluids[28-34] and foodstuffs[35, 36] and for selenium speciation.[37-42] Some of the most common interferences and their removal using the Elan DRC are presented in Table 1.1.

Table 1.1 Most common interferences in ICPMS and their removal by Elan DRC

Analyte	Isotope	Relative abundance / %	Interference	Reaction gas	Notes
Mg	24	78.990	C_2	NH_3	
Al	27	100.000	CN, CNH	NH_3	only NH_3 reacts with CN
K	39	93.258	ArH	NH_3	
Ca	40	96.941	ArH	NH_3	
V	51	99.750	ClO	NH_3	H_2 / CH_4 does not remove ClO
Cr	52	83.789	ArC	NH_3, H_2, CH_4	
Cr	53	9.501	ArC, ClO	NH_3	H_2 / CH_4 does not remove ClO
Fe	54	5.800	ArN	NH_3, H_2, CH_4	
Mn	55	100.000	ArNH	NH_3, H_2, CH_4	
Fe	56	91.720	ArO	NH_3, H_2, CH_4	
In	58	68.077	ArO	NH_3, H_2, CH_4	
Co	59	100.000	ArOH	NH_3, H_2, CH_4	
In	60	26.223	ArO	NH_3, H_2, CH_4	CaO lowest with CH_4
Cu	63	69.170	ArNa	NH_3, H_2, CH_4	
As	75	100.000	ArCl	H_2, CH_4	$^{75}As^{16}O$ with 0.3ml/min O_2
Se	78	23.780	ArAr	NH_3, H_2, CH_4	
Se	80	49.610	ArAr	NH_3, H_2, CH_4	NH_3 removes Br^+

1.2 Elemental Speciation

Interest in trace elements, i.e. those elements present in samples with such low concentration that they can only just be detected, dates back to the beginning of the 20th century. For the next 60 years total element concentration was used to determine the effect of these trace elements and research was focussed upon developing more sensitive detection methods. Aquatic geochemists first made the distinction between 'dissolved metal' and 'particulate metal' fractions in waterways at the beginning of the 1950's. A simple filtering membrane was used to discriminate between the two phases and electrochemistry was used to distinguish between free and complexed metal species in water samples.[43] In the early 1960's concern was first raised regarding the chemical form of trace elements, prompting a need for the development of analytical schemes for speciation. The first instrumental coupling was presented by Kolb *et al.* in the mid-1960's.[44] A gas chromatograph (GC) flame atomic absorption spectrometry (FAAS) system was used in the determination of alkyllead compounds in gasoline. The first global speciation approach was published by Florence in the 1980's, in which different metal fractions in water were discriminated by preconcentration followed by electrochemical detection or by AAS.[45] Rapid development in speciation analysis has been brought about over the past 25 years by the acceptance that the chemical, biological and toxicological properties of an element are highly dependant on the form in which the element occurs within a sample. Subsequently research on trace element analysis has become more focussed on trace element species to the present day.[46] Publications in the field of speciation increased dramatically midway through the 1990's and have continued to increase at a steady rate since; as demonstrated in Figure 1.7. The number of publications is now approaching 2000 per year, which illustrates

the interest in the area and the wide application of speciation analysis made possible by instrumental advances.

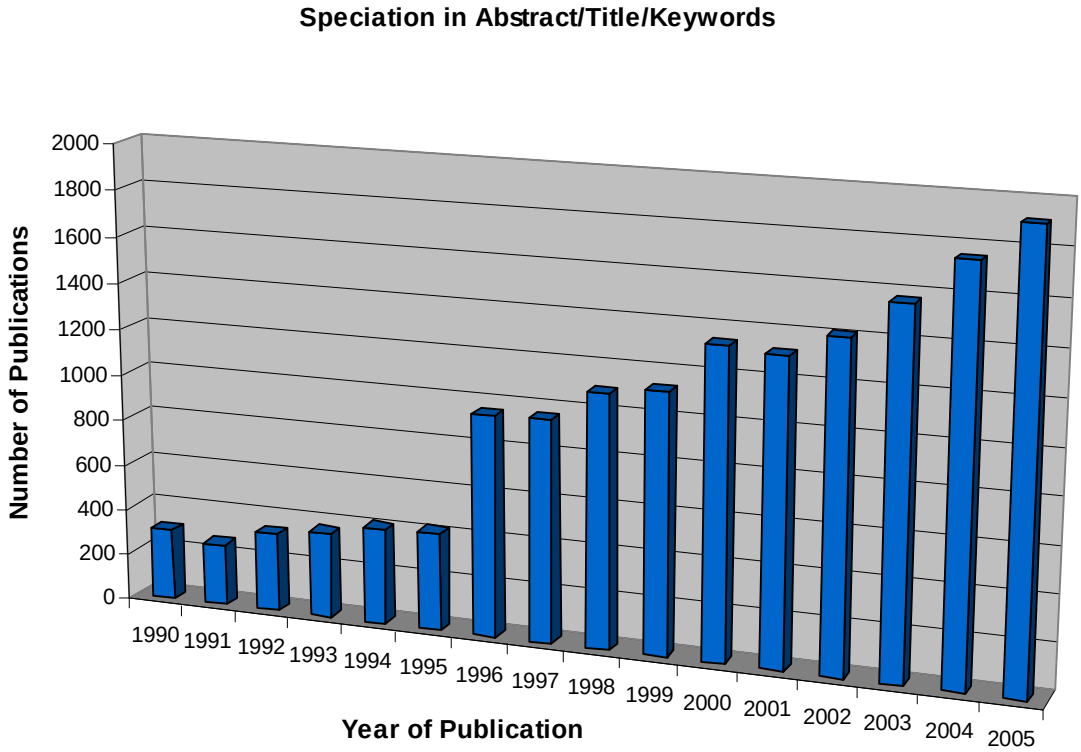

Figure 1.7 Number of publications with SPECIATION appearing in the abstract, title or keywords. Sourced from the Scopus electronic database covering physical, life, health and social sciences.[47]

The use of the term speciation in analytical chemistry has been derived from its use in biological science. In order to clearly define the meaning of speciation analysis, chemical species and speciation the IUPAC definitions for analytical chemistry are followed.

> i. *Chemical species*. Chemical elements: specific form of an element defined as to isotopic composition, electronic or oxidation state, and/or complex or molecular structure
>
> ii. *Speciation analysis*. Analytical chemistry: analytical activities of identifying and/or measuring the quantities of one or more individual chemical species in a sample
>
> iii. *Speciation of an element; speciation*. Distribution of an element amongst defined chemical species in a system
>
> (IUPAC Recommendations 2000)[48]

Where speciation is not possible, another term is defined:

> iv. *Fractionation.* Process of classification of an analyte or a group of analytes from a certain sample according to physical (e.g., size, solubility) or chemical (e.g., bonding, reactivity) properties.
>
> (IUPAC Recommendations 2000)[48]

Fractionation is often employed since the sum of the chemical species detected rarely equals the total concentration of an element in a sample matrix. This is due to the chemical species not being stable enough to remain unchanged by the analytical procedure or the number of different species present being too great to allow full identification.

The development of speciation has been reliant upon advances in analytical instrumentation. There has been continued development towards lowering detection

limits in optical and mass spectroscopy which has allowed the progression from quantification of total element concentration to speciation. Background levels of species in biological systems were previously below the achievable limit of detection (LOD) and therefore the effect of elemental species could not be studied. There is still a requirement for achieving lower LOD in order to evaluate the effect of low background level of elemental species.[46]

There is a wealth of literature available on the speciation and fractionation of elements. This should always be the first starting point in the development of any speciation analysis. Conducting speciation analysis requires a good knowledge of the sample, analyte and analytical techniques / instrumentation. On development of a speciation strategy the several important factors must be considered. These include what species / form(s) of sample are present and in what sample matrix, ensuring the natural composition and distribution of species in the original sample is preserved, the selectivity and LOD of quantisation required and how to calibrate for the species (especially since many are not available as commercial compounds). Speciation procedures can be classified into three experimental categories, based upon the physical, chemical and biochemical properties of the analyte species; see Table 1.2.

Table 1.2 Principal classification of Speciation Processes[49]

Methods based upon Physical properties
adsorption phenomena; centrifugation; some chromatographic techniques (e.g. size exclusion chromatography); cold trapping; dialysis; distillation; element-specific detection; filtration
Methods based upon Chemical properties
some chromatographic techniques; complexation; derivatisation; element-specific detection; extraction; ion-exchange processes; redox reactions
Methods based upon Biochemical properties
enzymatic reactions; immunoassay

Any strategy usually requires two complementary techniques; firstly to isolate and / or separate the various species / forms of analyte and secondly to detect and quantify the analyte following separation. Separation requires sufficiently high specificity to adequately separate all types of component present, often involving discrimination between chemically very similar species. For this reason modern chromatographic or electrophoretic methods have generally been utilised. Detection methods require sufficiently high sensitivity to reliably provide accurate and precise quantification, usually requiring specialist detection techniques since concentration of trace element analytes are frequently below the LOD for common detectors used with separation systems. For these reasons the coupling of chromatographic separation and atomic

spectrometric detection has found wide application in the field of speciation analysis based upon the resulting systems ability to fulfil the requirements outlined above.[50-53] An ideal speciation system should be simple, robust, low cost and portable to allow rapid results to be obtained in the field. Additionally the system should present minimal perturbation on the sample so that reliable results representing the original speciation of an element can be achieved. Currently speciation analysis is not routine. Development of routine speciation analysis will require the automation of systems, employing computer control, and an increase in analysis speed in order to increase sample throughput and make it financially viable. Speciation analysis can be time consuming owing to the related sample pre-treatment and separation processes. Ideally sample pre-treatment should be minimised and if possible eliminated, however this is not always possible particularly when analysing solid samples. Attention should be focussed upon reducing the time taken by the separation method used in speciation analysis, which is typically in excess of 10 minutes. This is achievable for the majority of systems using recent advances in the instrumentation / techniques. The need for routine speciation analysis can be expected to increase due to regulatory requirements. This includes enforcement of new legislation regarding acceptable levels of element species (for example in the environment and workplace) with the aim of limiting exposure to living systems. Current legislation defines limits of total element concentration; however this is rapidly becoming outdated. Increased knowledge of the effect of different species on toxicity and bioavailability necessitate legislation to be updated to govern limits of elemental species. This will drive future development in speciation analysis.

1.2.1 Elements of particular interest

Knowledge of elemental speciation is relevant to scientists from a range of disciplines; these include chemists, biologists, geologists, physicists and specialists in nutrition and medicine.[54] Biological science is interested in studying the transport, metabolism and conversion within living systems. The aim of this is to understand an elements toxicity or essential requirement to the system. Geologists have a great interest in speciation since trace element species contained in sediments and geological features can provide a wealth of information on land use, biogeochemical cycles and the transport and storage of elements.[55-57]

Elements that have provoked extensive interest in the field of elemental speciation generally have been found to be highly damaging to living systems. Often exposure to these elements results from their industrial use leading to increased levels present in the environment. Chromium has two main oxidation states; Cr(III) and Cr(VI) and is greatly used in industry. The two oxidation states result in significantly different in biological and toxicological nature of chromium. Cr(III) (determined as the Cr-EDTA complex) is considered relatively non-toxic and essential in the human diet, while Cr(VI) (occurring in 2 forms chromate [CrO_4^{2-}] and dichromate [$Cr_2O_7^{2-}$], both eluted at same time in HPLC) is highly toxic to humans. Recent interest has involved the speciation of Cr oxidation state within different biological systems to gain an understanding of the transport, localisation and absorption of the metal species, in order to assess the resulting health hazards.[58] Mercury is sourced from contaminated mining and industrial environments (in particular mercury and gold mines, and coal fired power stations). It is present in flue gases, river sediments and aquatic food chains. Alkyl-Hg species are the most highly toxic. Speciation is required to ascertain its transport and

bioavailability.[59-61] Lead speciation is often necessary due to the high toxicity of organolead compounds. Combustion of leaded petrol is tightly controlled now, but historically presented the most common source of organolead environmental pollution. Although sources and hazards to human health have been well investigated, less is known about the effect of lead on wildlife. Recent research has involved the effect of old leaded paint on the surrounding environment.[62] Platinum has become present in elevated concentrations in the urban environment since the introduction of the catalytic converter in motor vehicles. Hence concern over the potential environmental and health effects has arisen.[63, 64]

Generally speaking inorganic forms of an element are more toxic than organic forms; for instance arsenic is extremely toxic in its inorganic forms while it is relatively innocuous as arsenobetaine (form commonly found in seafood). However examples of the reverse can be found; for example organo-tin compounds, such as the antifouling agent tributyltin, are generally more toxic than inorganic tin species.[54]

The main routes of exposure to elements are *via* ingestion, inhalation or absorption. This can affect humans directly or via introduction of the elemental species into the food chain. Speciation is conducted in order to investigate the route of exposure and bioavailability. Another source of exposure to elemental species is *via* drugs and medication. Speciation is required during drug development in order to ensure the elemental form presented to the patient is bioavailable, monitor the metabolism / species conversion within the body and evaluate the mechanism by which the drug acts. A good example of this is platinum, which is used in drugs used for chemotherapy, e.g. cis-platin. Non-metallic elements (S, P, Br, Cl) are also of interest

in drug development (e.g. P in phosphorylation of drugs).

Some elements essential to biological systems can exhibit toxicity when present in excess. Selenium is both essential, used in the body's antioxidant defence system, immune system and thyroid gland,[65] and toxic dependant on concentration and species present. It also has proven to have cancer chemo-preventative properties, shown for breast, colon, lung and prostate cancers.[65] Accurate and precise determination of selenium concentration / speciation is important since there is a narrow range between beneficial and toxic levels.[54, 65, 66] A useful review on the speciation analysis of selenium using hyphenated analytical techniques has been presented by Uden.[66] There is concern regarding falling selenium levels in the UK, originating from a low selenium concentration in soil through many parts of Europe, resulting in low levels in foods.[46] Selenium has been permitted and investigated as a food additive / supplement. It is crucial that supplements provide selenium in a bioavailabile form, organic selenium sources are claimed to be the most valuable.[67] Despite the common lack of selenium, toxic levels can be found in the locality of various industrial processes. Selenium contamination can result from numerous sources including; the production of glass, pigments, inks and lubricants, and the combustion of fossil fuels.[68] It is one of the most volatile elements present in flue gas from coal power stations.[60] Manganese displays unique toxicological behaviour[69] having a very low toxicity except in humans, where in chronic overdose 'manganism' can result (causing similar symptoms to Parkinson's disease).[46] Mn compounds are neurotoxic substances that target the central nervous system,[70] however the exact mechanism of manganese's toxicity and how the brain handles Mn is not fully understood.[71-73] Nevertheless it is an essential element in the human diet, activating many enzymes used in metabolic processes[74] and termed the 'cell

protector' as it intervenes in antioxidant activity, and Mn deficiency can lead to dysfunction of the central nervous system.[75] Exposure to Mn is usually *via* inhalation,[72] as it is one of the most frequently used metals in industry[69] being a hardening agent in the steel industry,[76, 77] principle component of dry cell batteries and used in the production of Mn alloys. Manganese is difficult to measure in clinical samples as there are many potential sources of contamination.[70] A comprehensive review of recent developments in manganese speciation has been presented by the author.[78]

Discussion of the speciation for every element that has found interest in speciation analysis is beyond the scope of this thesis. Numerous speciation reviews can be found,[43, 50, 52, 53, 79-85] along with an increasing amount of texts giving an overview of many of the elements.[46, 54, 86, 87] There is a wide variety of literature available specific to the study of single elements with almost 2000 speciation papers currently being published annually.[47] The speciation of arsenic in particular has been a focus of this research, therefore it is introduced in greater detail.

1.2.1.1 Arsenic

For some time there has been a global concern about arsenic contamination to groundwater supplies. Arsenic is commonly found throughout the earth's surface, being the 20th most abundant element in the earth's crust, 14th in seawater and 12th in the human body.[88] Natural release of arsenic is most commonly caused by volcanic activity and erosion processes in soils.[89] These processes give rise to natural contamination of groundwater by arsenic. Forty million people in the West Bengal and Bangladesh regions alone are thought to be at risk from arsenic-contaminated water supplies from arsenic released from rocks into underground water supplies.[90] Inorganic arsenic is

found in groundwater generally in the form of arsenate [As(V)] and / or arsenite [As(III)]. Acute exposure to arsenic leads to death, typically within 30 minutes. Symptoms of chronic arsenic exposure include skin thickening, lesions, skin cancers, diabetes, and nervous system damage.[90] Additionally arsenic has a wide range of industrial (glass and semiconductor), agricultural (pesticides / herbicides and food additives) and military (as chemical warfare agents) uses and therefore presents the requirement for tight controls.[91]

In 1993, the World Health Organization (WHO) set 10 μg L^{-1} (ppb) as the recommended limit for arsenic in drinking water. The 15 nation European Union adopted 10 ppb as a mandatory standard for arsenic in drinking water in 1998. Legislation from the US Environmental Protection Agency has recently enforced the reduction in maximum permissible arsenic levels in drinking water to 10 ppb total arsenic concentration, from 50 ppb, to protect consumers served by public water systems from the effects of long-term, chronic exposure to arsenic.[92] Water systems were ordered to comply by 23rd January 2006, providing additional protection to an estimated 13 million Americans. This legislation has raised concerns about the agricultural use of arsenic containing bio-solids (e.g. poultry litter) in the US as it provides a significant source of groundwater contamination.[93] Poultry litter contains arsenic species originating from organo-As(V) compounds (e.g. roxarsone) which are added to poultry feed for coccidiosis control, as a growth promoter and egg production stimulant.

Despite this legislation total arsenic concentration alone has long been realised insufficient for addressing clinical and environmental considerations. The toxicity and bioavailability of arsenic is highly dependant on the chemical species present. The

most toxic species are inorganic arsenic (e.g. arsenite and arsenate), whereas in comparison organic species have much lower toxicity (e.g. arsenobetaine, which is considered innocuous). Speciation studies of arsenic are important to evaluate resulting physiological and toxicological effects from its various chemical forms. These studies help to provide more information about the environmental impact and health risks associated with exposure and extensive research has been published on arsenic speciation along with numerous reviews.[94-100]

In addition to exposure *via* drinking water another significant source of arsenic to humans is through food. Products consumed from the marine environment contain the highest arsenic concentrations, and many different arsenic species have been detected, however only about half of the arsenic compounds detected in marine animals have yet to be identified.[84] In the marine environment the total arsenic concentration in animals and plants typically ranges between 0.5 and 50 mg kg^{-1}. Plant food sources have much lower concentrations, below 0.2 mg kg^{-1}, except for rice (at approximately 0.2 mg kg^{-1}) and some types of mushroom which can have several mg kg^{-1}.[46] Arsenic intake from food is highly dependant on the amount of seafood in the diet. In order to evaluate the toxicology of arsenic intake speciation information is essential.[46] Generally knowledge regarding the arsenic species present in the majority of food is still quite limited.[94]

Use of the arsenic containing poultry feed additives, discussed previously, has also raised concern about associated increase in arsenic concentration in chicken meat for human consumption. This has prompted a study by the Institute for Agriculture and Trade Policy, Minnesota, who found widespread elevated levels of arsenic in chicken.[101] A recent publication highlighted that USA long grain rice, widely consumed in the UK

and other parts of the world, showed the highest mean arsenic level in the grain compared to rice from Europe, Bangladesh and India.[102] In a more recent study it was reported that rice contained the highest level of arsenic compared to other common food items (bread, milk, pork meat, chicken meat, cabbage and potatoes) collected from a study area in Slovakia.[103]

The primary pathway for removal of arsenic from the human body is *via* urinary excretion. Arsenic speciation in urine can be considered as a biomarker for arsenic exposure since arsenic levels in urine have a relatively short half life; and hence represent recent exposure. After ingestion inorganic arsenic species are methylated within the human body to produce monomethylarsonate (MMA) and dimethylarsinate (DMA). This process has generally been considered to be a detoxification process. Recently however trivalent methylated arsenic metabolites have been reported to be more toxic than inorganic arsenic species.[94] However, discussion regarding the validity of these species existence has arisen owing to the storage and analytical methods used to identify them.[95] Inorganic arsenic and its metabolites are excreted by humans in urine with the following percentages: 10 – 15 % inorganic As, 10 – 15 % monomethylated species and 60 – 80 % dimethylated species.[104, 105] Recently dietary selenium has been shown to assist the excretion of toxic inorganic arsenic species and help to prevent effects of arsenic poisoning. Urinary arsenic excretion significantly increases with a related increase in selenium intake.[106] It was also noted that the percentage DMA increased while the percentage inorganic arsenic decreased.[107] Additionally a link has been proposed between arsenic and manganese concentration and neuropsychological function. In a recent study in Bangladesh; exposure to Mn from drinking water has been associated with neurotoxic effects in children.[108] High As

and Mn concentrations in combination resulted in significantly lower scores on an IQ test and tests of verbal learning and memory.[109] The effects of exposure to chemical mixtures are not widely known. Further research is required on the effect of exposure to combinations of toxic element species in order to assess any contributory effects.

1.2.2 Separation Systems for Elemental Speciation

The aim of analytical separation systems is to achieve the greatest possible resolution and selectivity for components from a complex sample in order to obtain quantitative and / or qualitative information in an accessible and appropriate manner.[66]

The most common chromatographic separation schemes investigated for elemental speciation analysis are gas chromatography (GC) and liquid chromatography (LC), usually high performance liquid chromatography (HPLC). GC has been the most frequently used separation technique in the past.[53] However it is the most labour intensive technique owing to the extremely small sample volumes injected onto a GC column. To achieve required sensitivity preconcentration factors of > 1000 are typically necessary and additionally ionic species must be derivatised. LC has proved to be the most popular separation technique and can be applied to a wide variety of sample types / matrices. LC, mainly HPLC, has two major advantages over GC; being no requirement for derivatisation and the ability to detect inorganic and essentially all organometallic species.[53] Both HPLC and GC are easily interfaced with a variety of detectors, particularly with ICPMS which is highly desirable for speciation.

Capillary electrophoresis (CE) has been applied to speciation analysis to a lesser degree than chromatography,[81, 83, 110-112] but offers some specific advantages. The principal advantage of electrophoretic separations over chromatographic methods is less

severe disruption to the natural distribution of elemental species. This is due to the separation mechanism, based upon the mobility of analytes in an applied electric field rather than upon partitioning between a stationery and mobile phase, which prevents perturbation on species equilibria.[113] However this is not always true; distribution can be greatly disturbed if complexing agents or pH conditions required for separation affect the sample. Additional advantages include low sample volume requirement, high efficiency separation (high plate number), ability to separate positive, neutral and negative species in a single run, and short run times.[81]

The reason behind CE not being used to the same extent as chromatography in speciation is difficulties with interfacing CE to suitable detectors. While interfacing HPLC to ICPMS is routine, interfacing CE-ICPMS is more challenging and commercial interfaces have only recently become available (CEI-100, Cetac Technologies, Omaha, Nebraska, USA, developed in 1999).[114] However, while LC remains by far the most commonly used separation method; the application of CE has now overtaken that of GC which is reflected in a growing number of bioanalytical applications.[115] CE–ICPMS interface schemes are discussed in further detail later (Section 1.4.5).

A concern when using chromatographic or electrophoretic separation in speciation analysis is the requirement that the species of interest needs to be stable over the separation timescale and not be present in equilibrium. If species equilibrium exists within the sample during the separation the species will rapidly interconvert, possibly resulting in a group of unresolved bands.[79] With care this can be avoided in many sample situations so chromatographic and electrophoretic separation is extremely useful for speciation analysis.

Chemical and / or physical pre-treatment can be used in place of or to compliment chromatographic or electrophoretic separation. Precipitation, volatilisation, extractability and further chemical reactions can all occur as a result of chemical pre-treatment. If the chemical pre-treatment is species-selective it can be considered a snapshot of the species information so subsequent detection is unambiguous. The advantages of this procedure are chemical selectivity, high sensitivity, low cost, flexibility and ease of automation (by flow-injection). However it generally requires a difficult chemical treatment for each species of interest so can be extremely time-consuming; therefore best suited to specific applications and single elements.[79] GC, LC and CE are all often used with some form of analyte preconcentration process.

1.2.3 Detection Systems for Elemental Speciation

Speciation analysis inherently involves very low level trace analysis, typically in the ng L^{-1} (solutions) or ng g^{-1} (solids) range.[53] The concentration of individual species is inevitably lower, often a great deal lower, than the total concentration of an element in a given sample. For this reason the LOD of common commercial detectors, particularly those used with separation systems, is rarely sufficient. Commercial CE and chromatographic instruments most commonly employ UV detectors. UV detectors give LOD in the concentration range between 0.1 and 100 mg L^{-1}; hence this is usually not sufficient in real samples without the requirement of high preconcentration factors. This presents a higher risk of errors and frequently involves more manual work and time per sample. Additionally most metal ions, metallic or metalloid species do not absorb in the ultraviolet region. To overcome this problem pre- or on-column derivatisation can be employed to produce a chromophore, which does absorb in the UV region. Indirect UV detection can also be used in which a highly absorbing species is

added to sample and the decay in absorbance is measured. The decay is assumed to be due to elution of a non-absorbing species, i.e. the analyte. It is clear that the use of common detectors induces the requirement for sample pre-treatment which must be carried out with extreme care and provides a frequent source of errors in speciation analysis. Even minor changes in the sample conditions and / or environment can significantly influence the species distribution.[53]

Other more sensitive and selective detectors, such as electrochemical and fluorescence detectors or ion selective electrodes, can give lower LOD but often suffer from problems with interferences.[83] They are also not rugged enough and their sensitivity changes over time. Therefore they are rarely used in speciation analysis.[81]

Elemental mass spectrometry has revolutionised elemental speciation in the last decade.[116] The ideal atomic spectrometer is capable of decomposing a sample into its constituent atoms allowing these to then be probed by atomic emission, fluorescence, absorption, or mass spectrometry.[79] The ability of atomic spectrometers to isolate atoms results in simple, readily acquired spectra, high sensitivity, broad dynamic range, the ability to perform mass balance and only exhibit moderate levels of spectral and matrix interferences. Obviously atomisation of a sample destroys any speciation information; therefore coupling with an auxiliary instrument (e.g. chromatography) and / or chemical / physical pre-treatment is required to obtain speciation information prior to detection.

Atomic absorption spectrometry (AAS), atomic emission spectrometry (AES) and atomic fluorescence spectrometry (AFS) have been applied to speciation analysis, and continue to be. However; AAS and AES often suffer from a lack of sensitivity,

requiring a sample preconcentration step, and AFS has only limited applicability.[116] Typically speciation analysis using these detectors requires further investigation, often with more sensitive detection, to confirm results / findings. In the past few years GC-AAS has been used for studying butyl- and phenyltin species[117] and LC-AAS has been applied to As and Se speciation with limited success.[118] LC-AES has been used for Al, As, Se and U speciation. GC-AFS has almost exclusively found application to mercury speciation, usually in fish products or seafood, while LC-AFS has been used to determine As,[119] Hg, Se, Sb and Te species.[118]

Inductively coupled plasma mass spectrometry (ICPMS) has proved a highly versatile detector and is ideally suited to elemental speciation on account of its ability to provide high efficiency atomisation and ion formation (ICP) with specific and sensitive multielement detection (atomic MS). The detector response is directly related to the number of analyte atoms present in the plasma, i.e. analyte concentration within the sample. Plasma spectrometry is widely used in analytical laboratories owing to its high sensitivity (LOD ng L^{-1} or less, allowing ultra-trace detection) and precision (0.5 - 5.0 %) with a wide linear dynamic range (up to 5 - 6 orders of magnitude, permitting detection of major constituents and trace components in one sample dilution). ICPMS detection limits are often 3 orders of magnitude lower than those for ICPAES, primarily as there is no source of continuous background. ICPMS also permits the observation of individual isotopes, which permits the use of isotope-dilution techniques for internal standardisation and to monitor species transformations. A potential disadvantage is the plasma instability and build up of carbon (resulting from the use of organic solvents for separations) or salt (from buffers) residue on the sampling cone.[6, 23, 84, 120] A key advantage of ICPMS for speciation analysis results from the detector response not being

significantly influenced by the molecular occurrence of the analyte, hence producing a species independent response. Therefore stable elemental species can be used for quantification purposes and applied to a range of different species for that element. This is excellent for the analysis of unstable or unknown elemental species and for those with no pure standard available.[116] Despite ICPMS traditionally being used for the detection of metals and metalloids it has recently found application in the analysis of non-metals such as organophosphorous (pesticides in river water,[121] chemical warfare agents[122]), sulphur (selenotrisulfides / Se and S oxides by LC–DRC–ICPMS[37]), bromate (drinking water,[123, 124]) and iodine (seawater[125, 126], seaweed[127]). Reasonable LOD can be achieved generally using reaction / collision cells or high-resolution instruments.

As stated previously hybrid / coupled systems using either a chromatographic or electrophoretic separation technique with atomic mass spectrometric detection are frequently applied in speciation analysis. This is reflected in the number of publications using chromatography or electrophoresis and ICP for speciation; presented in Figure 1.8. Chromatographic separation has found the widest application, representing approximately 10 % of all papers published in speciation annually. Electrophoresis accounts for approximately 2 % of speciation publications. Both separation systems follow a similar trend to each other and the total number of speciation papers (shown in Figure 1.7) increasing in number annually.[47]

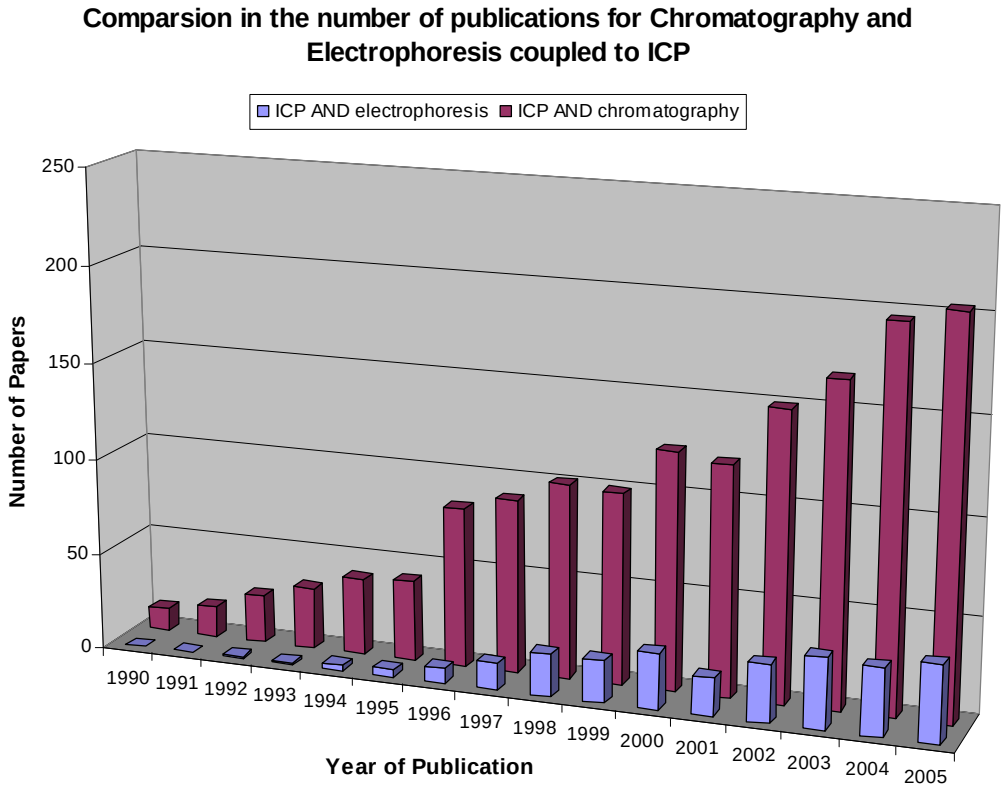

Figure 1.8 Number of publications with (*chromatography* OR *electrophoresis*) AND *inductively coupled plasma* appearing in the abstract, title or keywords. Sourced from the electronic database of Scopus covering physical, life, health and social sciences.[47]

Welz predicted in 1998 that HPLC–ICPMS would gain further importance in speciation analysis since it was undoubtedly the most powerful system available at the time.[53] This prediction has come to fruition with HPLC–ICPMS becoming an almost routinely applied speciation system. However; HPLC–ICPMS is the most expensive system for speciation analysis both in terms of purchase price and running cost.[53] There is therefore an incentive for reducing the cost of analysis. This can be achieved by investigating lower cost, but highly sensitive, detection methods or increasing the speed

of analysis, to increase sample throughput and hence reduce the cost per sample.

An excellent review focussed on detectors used in elemental speciation was presented by Feldmann in 2005.[116] The application of molecular MS and dual detection system was also discussed which are out of the scope of this thesis.

1.3 Liquid Chromatography

Liquid chromatography (LC) was introduced by Tswett in 1906, in which a glass column (inner diameter of between 1 and 5 cm and a length of 50 to 500 cm) was used with 150 to 200 μm particle packing in order to achieve practicable flow rates up to 1ml min^{-1}. It was quickly realised that to achieve improved separation power the particle size of the stationary phase packing material had to be reduced. However this created high backpressures which could not be overcome using original LC equipment. Practical HPLC was realised in the 1960's, with particle diameters between 3–10 μm. Since the conception the technique has been developed and applied extensively and is a fundamental tool in analytical chemistry.[128]

1.3.1 Chromatographic theory

Several characteristics of a chromatogram are assessed for the use of HPLC method development. Resolution (R_s) is used to evaluate the quality of the separation achieved. Two bands that overlap badly are poorly resolved and have a low R_s value.[129]

$$R_s = \frac{2(t_2 - t_1)}{W_1 + W_2} \qquad \textbf{Equation 1.7}$$

Where t_1 and t_2 are the retention times of the first and second adjacent bands and W_1 and W_2 are their respective band widths. Resolution is equal to the distance between peak centres divided by the average bandwidth. An increase in resolution is achieved either by the two bands moving further apart or a decrease in bandwidth. Alternatively using the bandwidth at half the peak height ($W_{0.5}$) can give more reliable results since it is not affected by poor peak shape, tailing effects and band overlap.[129]

$$R_s = \frac{1.18(t_2 - t_1)}{W_{0.5,1} + W_{0.5,2}} \qquad \textbf{Equation 1.8}$$

Equations 1.7 and 1.8 may not be reliable for poorly resolved bands, generally when R_s is less than 1. For accurate quantitative HPLC baseline resolution of all bands is desirable to allow an accurate baseline to be drawn. This is used for integration of the peak area and measurement of peak height which is related to component concentration. Baseline resolution corresponds to $R_s > 1.5$ for bands of a similar size, while $R_s \geq 2.0$ is desirable to allow for bands dissimilar in size and normal deterioration of HPLC methods through continued use.

Resolution can also be expressed in terms of three parameters (α, N, k), which permit systematic variation of the experimental conditions to give desired R_s (Equation 1.9). This is particularly useful in HPLC method development since it classifies experimental variables into three categories, namely selectivity (α), column efficiency (in terms of plate count, N) and retention (k). While it is convenient to regard these variables as independent this is only partially true, especially regarding k and α.

$$R_s = \frac{(\alpha - 1)}{4} N^{1/2} k'(1 + k) \qquad \textbf{Equation 1.9}$$

Where k is the average retention factor of the two bands (a.k.a. capacity factor, k'), N is the column plate number and α is the separation factor. $\alpha = k_2 / k_1$, where k_1 and k_2 are the values of k for adjacent bands 1 and 2. The retention factor is given by Equation 1.10.[129]

$$k = \frac{t_R - t_0}{t_0} \qquad \textbf{Equation 1.10}$$

Where t_R is the band retention time and t_0 is the column dead time. t_0 is related to the column dead volume (V_m) and mobile phase flow rate (F); as described in Equation 1.11.[129]

$$t_0 = \frac{V_m}{F} \qquad \textbf{Equation 1.11}$$

V_m (ml) can be estimated from the column length, L, (cm) and internal diameter, d_c, (cm) using:

$$V_m \approx 0.5 L d_c^2 \qquad \textbf{Equation 1.12}$$

For the most typical HPLC column size of 4.6 mm i.d. this equation can be simplified further:

$$V_m \approx 0.1 L \qquad \textbf{Equation 1.13}$$

However these estimations can lead to errors of 10 – 20 % in t_0, but this is acceptable for the purpose of method development. Ideally k should be between 0.5 and 20, in order to avoid problems with resolution of compounds from any unretained compounds eluted at t_0 and to prevent excessive band broadening and long run times for strongly

retained compounds.

Experimentally the resolution is generally improved by increasing the retention time (i.e. *k*) and significantly increased by greater selectivity (α) which moves the two bands further apart. Increasing column efficiency (*N*) causes the bands to become narrower and hence better resolved. *k* and α are determined by the composition of the mobile and stationary phase, while *N* is dependant on the column conditions (length, particle size) and flow rate. Therefore *k* and α are more easily adjusted to achieve a good separation, and only if this fails *N* is increased. The temperature of the column can be used in order to improve the separation efficiency. Raising the temperature reduces the viscosity of the mobile phase allowing greater flow rates. Hydrogen bonding effects in water are reduced, making it less polar, which can be used to improve retention or eliminate the requirement for a binary solvent gradient system. Improvement in *N* comes at the expense of longer run times, since the column length must be increased or mobile phase flow rate reduced. Classical theory presents discrete partition steps on a column at which equilibration of the analyte takes place between the mobile and stationary phase. As the compound moves down the column it moves from one equilibrated stage to another. These steps are called theoretical plates (*N*) and result from the height equivalent to the theoretical plate (or plate height, *H*) and the column length (L).[128]

$$N = \frac{L}{H} \qquad \textbf{Equation 1.14}$$

In practice the column plate number is determined directly from the chromatogram using the relationship defined by Equation 1.15.[129]

$$N = 16\left(\frac{t_R}{W}\right)^2 \qquad \textbf{Equation 1.15}$$

However as mentioned previously $W_{0.5}$ is usually more reliable than W so Equation 1.16 is more practicable.

$$N = 5.54\left(\frac{t_R}{W_{0.5}}\right)^2 \qquad \textbf{Equation 1.16}$$

Several models have been suggested in order to mathematically approximate the plate height of which the van Deemter equation (1.17) is widely used.[128]

$$H = A + \frac{B}{u} + Cu \qquad \textbf{Equation 1.17}$$

In which the plate height is dependant on the linear flow rate in the mobile phase (*u*, in cm s^{-1}). Constant A is the Eddy diffusion, B the longitudinal diffusion and C the mass transfer between mobile and stationary phase. There exists an optimum flow rate at which *H* is a minimum and *N* is a maximum. From these theoretical considerations low *H* minimum values are achievable with small stationary phase particle sizes, which are homogenous and tightly packed, small column diameters and large diffusion coefficients in the stationary phase, small in the mobile phase.[128] Generally flow rates are operated at higher than this optimum since they allow shorter run times with sufficient resolution.[129]

While resolution, run time and column pressure are generally of prime concern in the variation of column conditions and *N*; in trace analysis minimising bandwidth (maximising *N*) is important to obtain maximum sensitivity of the method.

1.3.2 Types of LC for speciation analysis

It has previously been discussed that LC, in particular HPLC, is the most common form of separation system applied to speciation analysis,[53] this is particularly true if detection by atomic spectrometry is employed. A typical HPLC system comprises of solvent reservoir(s), pump unit (introducing minimum dead volume and pulsation, and capable of achieving pressures up to 15 MPa), sample injector (typically a 6-way valve with 5 to 500 μl sample loop), (pre- / guard column), separation column and detector (UV being the most common, but numerous types available dependant on application). The main separation mechanisms utilised in HPLC include: partitioning (normal and reversed phase), ion exchange (anionic and cationic) and size exclusion (based upon the molecular sieve effect). The most popular form of HPLC remains reversed phase (RP), in which the column consists of a non-polar stationary phase. A polar mobile phase is pumped over the stationary phase and a small sample volume injected into this eluent flow. Components in the sample are separated based upon partitioning between the non-polar stationary phase and polar mobile phase. The analytes polarity governs the retention time in which it is eluted from the column. The separating power of RP-HPLC can be improved or tailored for specific applications in several ways. If isocratic elution, using a fixed mobile phase composition, is not sufficient gradient elution can be employed. Additionally the elution strength of the MP can be modified by variation of the pH or addition of an ion-pair reagent (IPR). Gradient elution is not recommended when using ICPMS detection, since it involves increasing the solvent load on the plasma. Aqueous rather than organic MP compositions are much more desirable for introduction into an ICPMS.

The most common stationary phase materials for RP-HPLC are silica bonded C_{18} (*n*-octadecyl) followed by C_8 (*n*-octyl) consisting of 3 – 5 μm packed silica particles. Problems which remain with the use of such stationary phases are high backpressures, which limit flow rates, and a limited number of theoretical plates (i.e. column efficiency); both of which limit the speed of separation. This becomes a major issue when using ICPMS detection, owing to the high running cost, and application of the system to routine analysis of large sample numbers.

1.3.3 Monolithic Columns for Rapid Separations

The development of porous monolithic stationary phase media is considered to be the most significant advance in stationary phase design for liquid chromatography since the development of the technique.[130] Monolithic silica stationary phases have a bimodal structure consisting of a macroporous and mesoporous structure; as shown in Figure 1.9.[131]

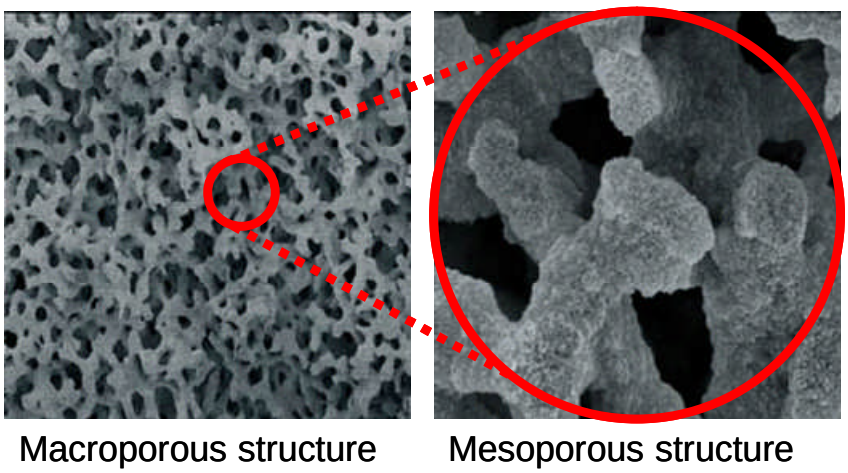

Figure 1.9 Bimodal structure of monolithic silica stationary phase[132]

These monolithic stationary phases are made *via* a sol-gel method used to form bimodal highly porous monolithic silica rods. The macroporous structure consists of relatively large holes (2 μm diameter) forming a dense network of through-pores or transport channels (with pore volume 1 ml g^{-1}). These allow rapid liquid flow without inducing a high backpressure (as observed in traditional packed columns); hence separation times can be dramatically reduced. The mesoporous structure forms the fine porous structure of column (with 13 nm diameter pores), which create a very high surface area for adsorption of the analyte (surface area 300 m^2 g^{-1}); therefore resulting in a high separation efficiency.[132] Recent investigation into use of monolithic stationary phases for the separation of ions has resulted in new possibilities of low- and medium-pressure chromatography and ultra-fast separations.[130] Results have shown that short monolithic columns can exhibit similar or superior peak efficiencies to traditional sized packed columns. This demonstrates the potential of this stationary phase material for increasing separation speed for speciation analysis, which is extremely desirable when using ICPMS detection. Previous applications have been focussed upon separation of large organic and bio-molecules, particularly with MS detection,[130, 133] while there are limited examples of the separation of small inorganic and transition metal ions.[134-139]

1.3.4 Reversed-phase ion-pair chromatography

The main advantage of ion pair chromatography (IPC) over ion exchange is the high degree of flexibility in adjustment of the chromatographic conditions in order to tailor them to a specific separation.[140] The stationary phase consists of a neutral, porous, low polarity, high specific surface area, chemically bonded silica phase. The selectivity of the column is determined solely by the mobile phase. An ion pair reagent (IPR) is added to the eluent (water / aqueous buffer solution) and is chosen according

to the chemical nature of the analytes. IPC is particularly suited to separate surface-active anions / cations and transition metal complexes. The dominating separation mechanism is adsorption; however the retention mechanism is not fully understood.[129] Two hypotheses have been presented and it is likely that both occur to some extent. The first proposed mechanism is that the analyte ions form neutral pairs with the ion-pair reagent in the aqueous mobile phase, and are then retained at the non-polar stationary phase. The second proposal is the ion-exchange model in which the IPR first adsorbs at the stationary phase surface giving it ion-exchange characteristics, and then separation of the analyte ions is possible.

Chromatographic separation of cations is achievable using long-chain alkanesulphonic acids or mineral acids as an ion-pair reagent. Anion separations are generally performed using quaternary ammonium salts. The choice of lipophilic ion depends entirely on the degree of hydrophobicity of the analyte ion. A hydrophobic reagent is selected for the separation of surface inactive ions and the separation of ions with long alkyl chains requires a strongly hydrophilic reagent. The hydrophobicity of an IPR is determined primarily by the length of its alkyl groups, and more generally by its number of carbon atoms. The sodium salts of alkanesulphonic acids or quaternary ammonium salts are used as IPR's. Retention increases with increasing chain length, due to increasing hydrophobicity which results in a stronger interaction with the stationary phase and reduced solubility in the mobile phase. Adjusting the chain length therefore allows very efficient adjustment of selectivity of chromatography. Commonly used IPR are presented in Table 1.3 in order of increasing hydrophobicity.

Table 1.3 Commonly used ion pair reagents used in reverse phase ion pair LC.

Cation separation	**Anion separation**
hydrochloric acid or perchloric acid *(least hydrophobic)*	ammonium hydroxide *(least hydrophobic)*
hexanesulphonic acid	tetramethylammonium hydroxide
heptanesulphonic acid	tetrapropylammonium hydroxide
octanesulphonic acid *(most hydrophobic)*	tetrabutylammonium hydroxide; *(most hydrophobic)*

1.4 Electrophoresis

Electrophoresis is defined as:

> the movement of electrically charged particles or molecules in a conductive liquid medium, usually aqueous, under the influence of an electric field.
>
> (D. R. Baker, Capillary Electrophoresis)[141]

A schematic of a typical experimental setup and electrophoretic separation is described in Figure 1.10. Electrophoresis is a relatively new technique for the separation and analysis of chemical compounds and compliments chromatographic techniques.[141]

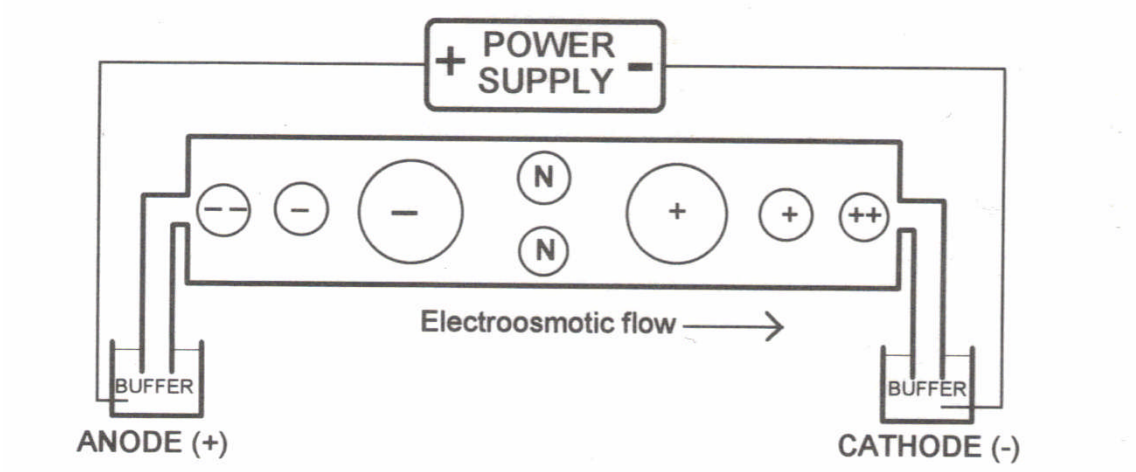

Figure 1.10 Schematic representation of electrophoresis system. Sample mixture introduced at anode. N; neutral species, +; cationic species, –; anionic species.[141]

1.4.1 Electrophoretic theory

Assuming a sample contains a mixture of neutral and electrically charged molecules (ions) the rate and direction of migration depends upon the size of the ions and the magnitude and sign of their charge. Positively charged cations will migrate towards the negatively charged cathode while negatively charged anions will migrate towards the positively charged anode. The rate of this migration is governed by the ions electrophoretic mobility (μ_{EP}) which is relative to its charge – to – size (i.e. radius, assuming spherical ion) ratio (q/r) and also associated with the buffer viscosity (η) as described in Equation 1.18.[141]

$$\mu_{EP} = \frac{q}{6\pi\eta r} \qquad \textbf{Equation 1.18}$$

A smaller molecule will travel faster in comparison to a larger molecule with the same charge. The electrophoretic velocity (υ_{EP}) can be calculated from the electrophoretic mobility and the magnitude of the applied electric field (E):

$$\upsilon_{EP} = \mu_{EP} E \qquad \textbf{Equation 1.19}$$

Where the magnitude of the applied electric field is given by the applied voltage (V) and the length of the capillary (L):

$$E = \frac{V}{L} \qquad \textbf{Equation 1.20}$$

Neutral molecules (i.e. q = 0) have zero electrophoretic mobility and hence will not be influenced by the electric field and migrate at the same rate as the run buffer.

The buffer moves through the capillary by electroosmotic flow (EOF), which conventionally flows towards the negatively charged cathode. The EOF of the buffer is usually greater than the electrophoretic mobilities of negatively charged solutes; therefore allowing separation and detection of both negative and positive ions and neutral species in a single run. EOF originates from the inner surface of the capillary becoming charged when filled with a buffer. This can be a result of ionisation of the capillary surface or adsorption of ions from the buffer onto the capillary. In silica capillaries the surface silanol groups (Si–OH) are ionised to silanoate groups ($Si–O^-$) when the pH is above 3. This ionisation can be enhanced by flushing the surface with a basic solution (e.g. KOH or NaOH) prior to the run buffer. This charged surface then attracts a layer of cations at the capillary wall, however this is not sufficient to neutralise the charge. Therefore a second outer layer of cations forms creating a diffuse double layer of cations. On application of an electric field the more mobile outer layer of

cations are attracted towards the negatively charged cathode. These solvated ions drag the bulk solution along with them as they travel towards the cathode. The electroosmotic mobility of a buffer (μ_{EOF}) is given by Equation 1.21[141]

$$\mu_{EOF} = \frac{\varepsilon\zeta}{4\pi\eta} \qquad \textbf{Equation 1.21}$$

Where ε is the dielectric constant of the buffer, ζ is the zeta potential and η is the viscosity of the buffer. The zeta potential is the result of an electrical imbalance created at the plane between the diffuse double layer of cations. The zeta potential is proportional to the thickness of this double layer (δ) and is given by Equation 1.22.

$$\zeta = \frac{4\pi\delta e}{\varepsilon} \qquad \textbf{Equation 1.22}$$

Where *e* is the charge per unit surface area.

EOF has a relatively flat flow profile in comparison to pumped flow which produces a parabolic flow profile. This has the advantage of all analyte ions being subjected to the same velocity profile regardless of their cross-sectional position in the capillary. This means they elute as very narrow bands producing narrow peaks and high separation efficiency. The velocity of the EOF (υ_{EOF}) is calculated from the electroosmotic mobility and the applied electric field (E):

$$\upsilon_{EOF} = \mu_{EOF} E \qquad \textbf{Equation 1.23}$$

The observed velocity of an ion (υ_{OBS}) is the combination of both the electrophoretic mobility of the ion and the EOF of the buffer.

$$\upsilon_{OBS} = \upsilon_{EP} + \upsilon_{EOF} \qquad \textbf{Equation 1.24}$$

This relationship demonstrates how cations will have a $\upsilon_{OBS} > \upsilon_{EOF}$ while anions will oppose the EOF resulting in $\upsilon_{OBS} < \upsilon_{EOF}$. Neutral molecules will have $\upsilon_{OBS} = \upsilon_{EOF}$.

1.4.2 Modes of Electrophoresis

There are several different types of electrophoresis that can be employed to suit the desired application. For speciation analysis the coupling of capillary electrophoresis (CE) with atomic spectrometric detection is highly desirable. The most common modes of CE are capillary zone electrophoresis (CZE), micellar electrokinetic capillary chromatography (MEKC), capillary gel electrophoresis (CGE) and capillary isotachophoresis (CITP).[141] CZE is performed in capillaries containing a buffer (and modifier) and separates anionic and cationic species based on their size – to – charge ratio. It cannot separate different neutral species from each other; this can be achieved with MEKC. MEKC uses a detergent added to the buffer and separation is achieved based upon partitioning of the species between the hydrophobic environment of the micelle and the hydrophilic environment of the buffer. CGE uses the molecular sieve mechanism to separate molecules with a different size but similar size to charge ratios (e.g. DNA fragments).

CITP is a moving boundary technique in which the sample is effectively sandwiched between two buffers. A steady state is reached in which all ions migrate at the same velocity in distinct zones, each containing just one ion. The length of each zone indicates the concentration of the species within the sample, and is determined by the concentration of the leading buffer rather than potential applied. This has found use as a sample preconcentration step,[142] as a separation technique,[143] and for the speciation

of iodine.[125] It has also been incorporated into miniaturised microchip based devices[144] and applied to inorganic arsenic speciation.[145]

1.4.3 Advantages for speciation

The major advantage of electrophoresis as a separation technique for elemental speciation is that the natural distribution of elemental species is less severely disturbed compared with chromatography. This originates from the separation being based solely upon the mobility of analytes in an applied electric field, while chromatography relies on partitioning between a stationery and mobile phase. Partitioning alters any species equilibrium present in the sample causing conversion of species to re-establish equilibrium. However electrophoresis can cause disruption to the original species distribution if complexing agents or pH conditions required for separation effect the sample. Additional advantages are the simplicity and low cost of the procedure, low sample size requirement, high number of theoretical plates (i.e. high efficiency), short run times (possible to conduct on-line analysis), potential to be easily automated, ability to separate positive, negative and neutral species in a single run.

Limiting factors in the use of electrophoresis result from the effect of sample composition, e.g. conductivity, and the detection limits required. Historically electrophoresis could only achieve detection limits in the low mg L^{-1} range using common detectors, which limits its application to speciation analysis. The analyte concentration can be increased by pre-separation clean up (i.e. preconcentration), electrokinetic sample introduction, electrostacking, or isotachophoresis. This introduces an additional step to the analysis, which is highly undesirable in speciation analysis, and can present a significant source of errors. The development of a CE interface for

ICPMS can provide access to the LOD required for speciation analysis without sample preconcentration. An extensive review on the use of capillary electrophoresis for speciation has been presented by Dabek-Zlotorzynska *et al.*.[83]

1.4.4 Microchip Electrophoresis

Microfluidic devices are well suited to rapid on chip pre-treatment of samples, electrophoretic separation for speciation studies and the analysis of very small sample volumes. Microfabricated electrophoretic analytical systems can drastically reduce the separation time and allow a simplified instrumental design. Reducing both the capillary diameter and length also reduces the separation time considerably. The application of pre-etched channel networks removes the requirement of tubing connectors and hence minimises any associated dead volumes. High-speed separations have been achieved in the order of < 10 seconds.[146, 147] Another possible way of reducing the separation time is to apply a higher separation voltage; however maximum voltages possible from the power supply and consequential heating effects produced impose limits. A low-voltage microchip electrophoresis system has been designed to overcome these limitations, which involves use of a moving electrical field.[148] The general principle is that the potential is only applied to a small portion of the channel in which the sample plug is travelling through; this is sequentially moved along the channel as the sample moves. Due to this reduced length over which the voltage is applied identical electric field strengths can be created using one-fifth of the potential.

Glass chips inherently have an EOF active surface; however it is possible to modify the surface of the channel within the chip (e.g. surface charge, stability to pH) in order to control EOF through the channel.[149] Chips can be constructed from numerous

materials including; polydimethylsiloxane (PDMS), glass, calcium fluoride (desirable for use with optical detection)[150] and plastics.[151] Similarly chips can be fabricated in a number of different ways; of which lithography, wet and dry chemical etching, direct laser machining, embossing and moulding are the most common. Developments in fabrication using polymers make it possible to rapidly construct readily reproducible, inexpensive chips.[152] This presents the potential for tailoring the chip to each analyte species and sample matrix, and can even facilitate the use of disposable chips.

The benefits of microchip electrophoresis make it ideal for use with ICPMS detection. The reduction in separation time is highly desired since it reduces the time the ICPMS is idle. Since conventional CE systems take several minutes or even longer to separate the analyte species the sample throughput is reduced and running cost per analysis is increased. There have been few attempts in combining the advantages of chip technology with the sensitivity of ICPMS.

1.4.4.1 Sample Injection

Precise control of fluids is a key advantage of microfluidic devices. Accurate and precise sample introduction is crucial in quantitative electrophoretic analysis to obtain good quality data. Small known sample volumes, typically 50 nl, must be reproducibly injected into the separation capillary as a well-defined discrete sample plug. The majority of capillary and microchip electrophoresis systems use electrokinetic sample injection. This is due to the majority of separations conducted with these devices are upon large biomolecules (DNA fragments, proteins, peptides, etc). These molecules have relatively low charge to size ratios, however in inorganic elemental analysis when the analyte species consist of low molecular mass highly charged ions the electrokinetic

method is not always suitable. Since these molecules have relatively high electrophoretic mobilities electrokinetic injection would lead to severe sample bias. For example a positive injection potential would cause a bias in favour of anions, over cations and neutral species.[153] For this reason in elemental speciation a hydrodynamic injection technique is more appropriate.[154-156]

1.4.5 Interfacing capillary and microchip electrophoresis to ICPMS

The design of a suitable interface between CE and ICPMS is not trivial and presents a number of requirements. Effective electrical contact must be maintained at the CE outlet. Laminar flow in the capillary should be countered / minimised by offsetting the suction created by pneumatic nebulisation. Band broadening must be minimised and high transport efficiency obtained. Olesik *et al.*, first reported a CE-ICP-MS system for rapid elemental speciation in 1995.[157] The system comprised of a conventional concentric nebuliser and conical spray chamber. The CE outlet end was coated with 4 – 5 cm of silver paint, and directly inserted into the nebuliser so that the front end of the capillary was recessed 0.5 mm from the tip of the nebuliser. This gave a dead volume close to zero and provided electrical connection between the solution and ground for the CE system (ground contact between silvered end and nebuliser shell). It was found an applied voltage of 10 kV was sufficient for the separation of inorganic ions and the RSD for repeat injections was below 3 %. However, LOD were 6 to 200 times greater *cf.* continuous flow of 1 ml min^{-1} and the resolution was degraded as the solution flow rate through the capillary was approximately 40 times greater than EOF (0.05 μl min^{-1}). This is due to the suction produced by the 1 ml min^{-1} nebuliser flow and resulted in broader, parabolic peaks that in normal circumstances are very sharp.

The main problem associated with the interface is that the flow rate of sample in CE is typically less than 1 μl min^{-1}, containing only nanolitres of sample, which is too low for traditional ICPMS nebuliser uptake flow rate. A negative pressure at the end of the capillary is produced by the *Venturi* effect caused by high nebuliser gas flow passing over the outlet of the capillary. This induces suction throughout the capillary length, creating laminar flow throughout the capillary. Laminar flow impairs the separation profile of analyte, providing a significant source of band broadening, hence degrading the resolution. This is due to the loss of EOF control in the capillary, causing dispersal of separated analyte bands. Dispersion due to laminar flow depends strongly upon capillary diameter and analyte diffusion coefficient.[158] Laminar flow (F_L) in the capillary can be calculated using Equation 1.25.[113]

$$F_L = \frac{\left(\pi d_i^2 L\right)}{4t_m} \qquad \textbf{Equation 1.25}$$

Where L is the length, d_i the internal diameter of the capillary and t_m the migration time of a compound through the capillary with no electric field applied. Hence a make up buffer, previously termed sheath flow, is introduced to increase the flow rate after CE separation, prior to nebulisation. It is possible to tune the sheath flow so that laminar flow in the capillary is eliminated. However this presents another problem as it introduces a dead volume to the detector, which results in additional peak broadening / tailing and reduction in analyte concentration in the sample (i.e. decrease in sensitivity). Sheath flow can be provided by self-aspiration or peristaltic pump. In self-aspiration the uptake is automatic and variation in flow rate is due to sample viscosity. Use of a peristaltic pump offers control over the sheath flow rate and therefore requires optimisation (too low a flow rate will not provide adequate compensation for the suction

effect, too high a flow rate will create a backpressure to the CE capillary). Ideally the sheath flow rate should be minimal in order to minimise the dead volume introduced to the detector, which in turn minimises band broadening and any loss in sensitivity.

Lu *et al.*, reported use of this sheath flow interface later in 1995.[159] As in Olesik's design a conventional concentric nebuliser was used with a 35ml spray chamber. Various interface designs based on different commercial nebulisers have investigated and compared including glass concentric,[160, 161] glass frit,[162] HEN,[160] DIN,[163] USN,[164, 165] MCN,[114, 166] and cross-flow nebuliser.[167] In 1998 Mei *et al.* developed an interface design independent of the nebuliser so that any nebuliser could be used.[168] The general findings have shown that cross-flow nebulisers give better performance over glass concentric, however the best hyphenation has been shown by MCN, particularly the MicroMist (Glass Expansion, Australia).[113, 158, 169, 170] A particularly successful interface was developed by Schaumlöffel and Prange in 1999.[114] This was based upon a MCN with very low flow rate of 6 μl and small single pass spray chamber. This design has been commercialised as the CEI-100 (Cetac Technologies, Omaha, Nebraska, USA). This interface is now finding increasing application.[33, 171] Another interesting interface was presented in 2001 by Li *et al.* using a high-efficiency cross-flow micronebuliser.[172, 173] This is a robust design, free from glass and permitting easy replacement of all capillaries as required. Liquid flow rates down to 5 μl min^{-1} with transport efficiencies up to 95 % were achieved.

Interfacing of microchip electrophoresis to ICPMS has been presented by Song *et al.* in 2003.[174, 175] The microchip electrophoresis system was designed to be interfaced to the ICPMS using commercial sample introduction, consisting of a MicroMist MCN with miniature cyclonic spray chamber (Cinnabar, Glass Expansion, Australia). A

short length of encapsulated capillary was inserted into the exit of the microchip allowing connection with the MCN. The electrophoretic separation was conducted using an 8 cm separation channel with flow rate of 0.585 μl min^{-1}. The nebuliser was allowed to freely aspirate a make up buffer to avoid laminar flow resulting in a flow rate of 42.5 μl min^{-1}. Rapid speciation was demonstrated with the system for Cr (30 seconds), Cu (30 seconds) and As (2 minutes). Problems however remained due to the transfer capillary between the chip and the nebuliser and the design of the spray chamber resulting in low transport efficiency and creating band broadening. A nebuliser designed specifically for a chip based system has been presented by Hui *et al.* in 2006.[176] A PDMS electrophoresis chip was interfaced directly with ICPAES using a cross-flow nebuliser arrangement with stainless steel tip at the end of the separation channel. This was coupled to a vertical single pass spray chamber. A make up buffer was used at 3.5 μl min^{-1} to facilitate the nebulisation of the 0.4 μl min^{-1} electrophoretic flow and transport efficiencies of 10 % were achieved.

1.5 Conclusions

Speciation analysis is essential for the assessment of an element's mobility, toxicity and bioavailability. It has now become widely accepted throughout the scientific community that total elemental concentration is not sufficient for this assessment. Recent instrumental developments have instigated a massive growth in speciation analysis owing to improved capability. There is a wealth of techniques and applications reported in the literature covering a wide range of elements. In order to facilitate routine speciation analysis and enforcement of species specific legislation development must be focussed towards increasing the speed of analysis, sample throughput and

reducing the cost. The main obstacles in achieving this are the requirement of extremely low detection limits and highly specific discrimination between analyte species. While ICPMS has high associated running costs it is often the detector of choice for speciation analysis owing to its simultaneous multielement capability and superior limits of detection. Therefore the reduction of detector idle time and sample throughput is of utmost importance.

1.6 References

1 A.L. Gray, *Proc. Soc. Analyt. Chem.*, 1974, **11**, 182.

2 A.L. Gray, *Anal. Chem.*, 1975, **47**, 600.

3 A.L. Gray, *Analyst*, 1975, **100**, 289.

4 R.S. Houk, V.A. Fassel, G.D. Flesch, H.J. Svec, A.L. Gray and C.E. Taylor, *Anal. Chem.*, 1980, **52**, 2283.

5 D.J. Douglas and J.B. French, *Spectrochim. Acta, Part B*, 1986, **41**, 197.

6 A. Montaser, *Inductively Coupled Plasma Mass Spectrometry*, Wiley-VCH, 1998.

7 K.E. Jarvis, A.L. Gray and R.S. Houk, *Handbook of Inductively Coupled Plasma Mass Spectrometry*, Blackie, Glasgow, 1992.

8 S.J. Hill, *Inductively Coupled Plasma Spectrometry and its Applications*, Sheffield Academic Press, Sheffield, 1999.

9 S.D. Tanner and V.I. Baranov, *J. Am. Soc. Mass. Spectrom.*, 1999, **10**, 1083.

10 *http://www.etpsci.com/images/etp/elec_mult_work_fig_3.gif* (accessed 01/07/2007)

11 B.L. Sharp, *J. Anal. At. Spectrom.*, 1988, **3**, 613.

12 J.E. Meinhard, *http://www.meinhard.com/pages/nebulizers.html* (accessed 25/05/2004)

13 J. Burgener, *http://www.burgenerresearch.com* (accessed 10/12/2003)

14 J. Burgener, *New Developments in Burgener Nebulisers*, New Directions in ICP Mass Spectrometry at University of Sheffield, 05/11/2003

15 E.G. Yanes and N.J. Miller-Ihli, *Spectrochim. Acta, Part B*, 2004, **59**, 883.

16 M.A. Tarr, G. Zhu and R.F. Browner, *Anal. Chem.*, 1993, **65**, 1689.

17 B.L. Sharp, *J. Anal. At. Spectrom.*, 1988, **3**, 939.

18 R.H. Scott, V.A. Fassel, R.N. Kniseley and D.E. Nixon, *Anal. Chem.*, 1974, **46**, 75.

19 G. Schaldach, H. Berndt and B.L. Sharp, *J. Anal. At. Spectrom.*, 2003, **18**, 742.

20 *http://www.geicp.com* (accessed 10/06/2005)

21 J.L. Todoli and J.-M. Mermet, *Trends Anal. Chem.*, 2005, **24**, 107.

22 L.K. Olson, N.P. Vela and J.A. Caruso, *Spectrochim. Acta, Part B*, 1995, **50**, 355.

23 J. Mora, S. Maestre, V. Hernandis and J.L. Todoli, *Trends Anal. Chem.*, 2003, **22**, 123.

24 J.L. Todoli and J.-M. Mermet, *Spectrochim. Acta, Part B*, 2006, **61**, 239.

25 V.I. Baranov and S.D. Tanner, *J. Anal. At. Spectrom.*, 1999, **14**, 1133.

26 J.W. Olesik and D.R. Jones, *J. Anal. At. Spectrom.*, 2006, **21**, 141.

27 S.D. Tanner, V.I. Baranov and U. Vollhopf, *J. Anal. At. Spectrom.*, 2000, **15**, 1261.

28 C.C. Chery, K. De Cremer, R. Cornelis, F. Vanhaecke and L. Moens, *J. Anal. At. Spectrom.*, 2003, **18**, 1113.

29 S.D. D'Ilio, N. Violante, M. Di Gregorio, O. Senofonte and F. Petrucci, *Anal. Chim. Acta*, 2006, **579**, 202.

30 L.A. Simpson, R. Hearn, S. Merson and T. Catterick, *Talanta*, 2005, **65**, 900.

31 D.E. Nixon, K.R. Neubauer, S.J. Eckdahl, J.A. Butz and M.F. Burritt, *Spectrochim. Acta, Part B*, 2004, **59**, 1377.

32 C.-F. Yeh, S.-J. Jiang and T.-S. Hsi, *Anal. Chim. Acta*, 2004, **502**, 57.

33 M. Montes-Bayon, D. Profrock, A. Sanz-Medel and A. Prange, *J. Chromatogr. A*, 2006, **1114**, 138.

34 S.J. Christopher, R.D. Day, C.E. Bryan and G.C. Turk, *J. Anal. At. Spectrom.*, 2005, **20**, 1035.

35 K.-L. Chen and S.-J. Jiang, *Anal. Chim. Acta*, 2002, **470**, 223.

36 V. Dufailly, L. Noel and T. Guerin, *Anal. Chim. Acta*, 2006, **565**, 214.

37 S. Sturup, L. Bendahl and B. Gammelgaard, *J. Anal. At. Spectrom.*, 2006, **21**, 201.

38 P. Giusti, D. Schaumloffel, H. Preud'homme, J. Szpunar and R. Lobinski, *J. Anal. At. Spectrom.*, 2006, **21**, 26.

39 D. Layton-Matthews, M.I. Leybourne, J.M. Peter and S.D. Scott, *J. Anal. At. Spectrom.*, 2006, **21**, 41.

40 S. Mounicou, M. Shah, J. Meija, J.A. Caruso, A.P. Vonderheide and J. Shann, *J. Anal. At. Spectrom.*, 2006, **21**, 404.

41 B. Gammelgaard, L. Bendahl, N.W. Jacobsen and S. Sturup, *J. Anal. At. Spectrom.*, 2005, **20**, 889.

42 D. Wallschlager and J. London, *J. Anal. At. Spectrom.*, 2004, **19**, 1119.

43 O.F.X. Donard and J.A. Caruso, *Spectrochim. Acta, Part B*, 1998, **53**, 157.

44 B. Kolb, G. Kemmer, F.H. Schelser and E. Wideking, *Fresenius J. Anal. Chem.*, 1966, **221**, 166.

45 T.M. Florence, *Trends Anal. Chem.*, 1983, **2**, 162.

46 R. Cornelis, J.A. Caruso, H.M. Crews and K. Heumann, *Handbook of Elemental Speciation - Techniques and Methodology*, John Wiley & Sons Ltd., Chichester, 2003.

47 *http://www.scopus.com/scopus/home.url* (accessed 28/11/2006)

48 D.M. Templeton, F. Ariese, R. Cornelis, L.-G. Danielsson, H. Muntau, H.P. Van Leeuwen and R. Lobinski, *Pure Appl. Chem.*, 2000, **72**, 1453.

49 S. Caroli, *Element Speciation in Bioinorganic Chemistry*, Wiley-Interscience, New York, 1996, p. 3.

50 W. Lund, *Fresenius J. Anal. Chem.*, 1990, **337**, 557.

51 J.L. Gomez-Ariza, T. Garcia-Barrera, F. Lorenzo, V. Bernal, M.J. Villegas and V. Oliveira, *Anal. Chim. Acta*, 2004, **524**, 15.

52 Y.K. Chau, *Analyst*, 1992, **117**, 571.

53 B. Welz, *Spectrochim. Acta, Part B*, 1998, **53**, 169.

54 A.M. Ure and C.M. Davidson, *Chemical Speciation in the Environment*, Blackie Academic & Professional, Glasgow, 1995.

55 P. Masque, J.K. Cochran, D. Hebbeln, D.J. Hirschberg, D. Dethleff and A. Winkler, *Environ. Sci. Technol.*, 2003, **37**, 4848.

56 S. Knusel, D.E. Piguet, M. Schwikowski and H.W. Gaggeler, *Environ. Sci. Technol.*, 2003, **37**, 2267.

57 M. Pitz, J. Cyrys, E. Karg, A. Wiedensohler, H.-E. Wichmann and J. Heinrich, *Environ. Sci. Technol.*, 2003, **37**, 4336.

58 J.A. Howe, R.H. Loeppert, V.J. Derose, D.B. Hunter and P.M. Bertsch, *Environ. Sci. Technol.*, 2003, **37**, 4091.

59 C.S. Kim, N.S. Bloom, J.J. Rytuba and J. Brown, G.E., *Environ. Sci. Technol.*, 2003, **37**, 5102.

60 J.R. Otero-Rey, J.M. Lopez-Vilarino, J. Moreda-Pineiro, E. Alonso-Rodriguez, S. Muniategui-Lorenzo, P. Lopez-Mahia and D. Prada-Rodriguez, *Environ. Sci. Technol.*, 2003, **37**, 5262.

61 K.A. Warner, E.E. Roden and J.-C. Bonzongo, *Environmental Science and Technology*, 2003, **37**, 2159.

62 M.E. Finkelstein, R.H. Gwiazda and D.R. Smith, *Environ. Sci. Technol.*, 2003, **37**, 3256.

63 S. Rauch and H.F. Hemond, *Environ. Sci. Technol.*, 2003, **37**, 3283.

64 S. Rauch, H.F. Hemond and B. Peucker-Ehrenbrink, *Environ. Sci. Technol.*, 2004, **38**, 396.

65 S.S. Kannamkumarath, K. Wrobel and R.G. Wuilloud, *Talanta*, 2005, **66**, 153.

66 P.C. Uden, *Anal. Bioanal. Chem.*, 2002, **373**, 422.

67 Y. Ogra, K. Ishiwata and K.T. Suzuki, *Anal. Chim. Acta*, 2005, **554**, 123.

68 D.B. Vickerman, J.T. Trumble, G.N. George, I.J. Pickering and H. Nichol, *Environ. Sci. Technol.*, 2004, **38**, 3581.

69 G.B. Gerber, A. Leonard and P. Hantson, *Crit. Rev. Oncol. Hematol.*, 2002, **42**, 25.

70 R. Cornelis, *Handbook of Elemental Speciation - techniques and methodology*, John Wiley & Sons Ltd., Chichester, 2003, p. 37.

71 J.S. Crossgrove, D.D. Allen, B.L. Bukaveckas, S.S. Rhineheimer and R.A. Yokel, *NeuroToxicology*, 2003, **24**, 3.

72 H. Roels, G. Meiers, M. Delos, I. Ortega, R. Lauwerys, J.P. Buchet and D. Lison, *Arch. Toxicol.*, 1997, **71**, 223.

73 M. Aschner, *NeuroToxicology*, 2002, **23**, 123.

74 B. Michalke, *J. Chromatogr. A*, 2004, **1050**, 69.

75 J.S. Crossgrove and R.A. Yokel, *NeuroToxicology*, 2004, **25**, 451.

76 D.G. Ellingsen, S. Hetland and Y. Thomassen, *J. Environ. Monit.*, 2003, **5**, 84.

77 K.C. Teo and J. Chen, *Analyst*, 2001, **126**, 534.

78 G.F. Pearson and G.M. Greenway, *Trends Anal. Chem.*, 2005, **9**, 803.

79 G.M. Hieftje, *Spectrochim. Acta, Part B*, 1998, **53**, 165.

80 K. Sutton, R.M.C. Sutton and J.A. Caruso, *J. Chromatogr. A*, 1997, **789**, 85.

81 S.S. Kannamkumarath, K. Wrobel, K. Wrobel, C. B'Hymer and J.A. Caruso, *J. Chromatogr. A*, 2002, **975**, 245.

82 T.M. Florence, *Analyst*, 1986, **111**, 489.

83 E. Dabek-Zlotorzynska, E. P.C. Lai and A. R. Timerbaev, *Anal. Chim. Acta*, 1998, **359**, 1.

84 A.L. Rosen and G.M. Hieftje, *Spectrochim. Acta, Part B*, 2004, **59**, 135.

85 F.C. Adams, *J. Anal. At. Spectrom.*, 2004, **19**, 1090.

86 S. Caroli, *Element Speciation in Bioinorganic Chemistry*, Wiley-Interscience, New York, 1996.

87 E. Merian, *Metals and Their Compounds in the Environment:occurrence, analysis, and biological relevance*, VCH, Weinheim, 1991.

88 B.K. Mendal and K.T. Suzuki, *Talanta*, 2002, **58**, 201.

89 A. Huerga, I. Lavilla and C. Bendicho, *Anal. Chim. Acta*, 2005, **534**, 121.

90 *http://news.bbc.co.uk/1/health/medical_notes/459078.stm* (accessed 05/06/2006)

91 M. Leermakers, W. Baeyens, M. De Gieter, B. Smedts, C. Meert, H.C. De Bisschop, R. Morabito and P. Quevauviller, *TrAC - Trends in Analytical Chemistry*, 2006, **25**, 1.

92 http://www.epa.gov/safewater/arsenic/index.html (accessed 08/07/2006)

93 Y. Arai, A. Lanzirotti, S. Sutton, J.A. Davis and D.L. Sparks, *Environ. Sci. Technol.*, 2003, **37**, 4083.

94 Z. Gong, X. Lu, M. Ma, C. Watt and X.C. Le, *Talanta*, 2002, **58**, 77.

95 K.A. Francesconi and D. Kuehnelt, *Analyst*, 2004, **129**, 373.

96 M. Burguera and J.L. Burguera, *Talanta*, 1997, **44**, 1581.

97 D. Chakraborti, M.M. Rahman, K. Paul, U.K. Chowdhury, M.K. Sengupta, D. Lodh, C.R. Chanda, K.C. Saha and S.C. Mukherjee, *Talanta*, 2002, **58**, 3.

98 D.G. Kinniburgh and W. Kosmus, *Talanta*, 2002, **58**, 165.

99 W.R. Cullen and K.J. Reimer, *Chem. Rev.*, 1989, **89**, 713.

100 B.K. Mandal and K.T. Suzuki, *Talanta*, 2002, **58**, 201.

101 D. Wallinga, *Playing Chicken. Avoiding arsenic in your meat.*, Institute for Agriculture and Trade Policy, Minneapolis, 2006.

102 P.N. Williams, A.H. Price, A. Raab, S.A. Hossain, J. Feldmann and A.A. Meharg, *Environ. Sci. Technol.*, 2005, **39**, 5531.

103 A.-L. Lindberg, W. Goessler, E. Gurzau, K. Koppova, P. Rudnai, R. Kumar, T. Fletcher, G. Leonardi, K. Slotova, E. Gheorghiu and M. Vahter, *J. Environ. Monit.*, 2006, **8**, 203.

104 C. Hopenhayn-Rich, M.L. Biggs, A.H. Smith, D.A. Kalman and L.E. Moore, *Environ. Health Perspect.*, 1996, **104**, 620.

105 Y. Hsueh, H. Chiou, Y. Huang, W. W., C. Huang, M. Yang, M. Lue, G. Chert and C. Chen, *Cancer Epidemiol Biomarkers Prev.*, 1997, **6**, 589.

106 Y.-M. Hsueh, Y.-F. Ko, Y.-K. Huang, H.-W. Chen, H.-Y. Chiou, Y.-L. Huang, M.-H. Yang and C.-J. Chen, *Tox. Lett.*, 2003, **137**, 49.

107 W.J. Christian, C. Hopenhayn, J.A. Centeno and T. Todorov, *Environ. Res.*, 2006, **100**, 115.

108 G.A. Wasserman, X. Liu, F. Parvez, H. Ahsan, D. Levy, P. Factor-Litvak, J. Kline, A. van Geen, V. Slavkovich, N.J. Lolacono, Z. Cheng, Y. Zheng and J.H. Graziano, *Environ. Health Perspect.*, 2006, **114**, 124.

109 R.O. Wright, C. Amarasiriwardena, A.D. Woolf, R. Jim and D.C. Bellinger, *NeuroToxicology*, 2006, **27**, 210.

110 M.V. Holderbeke, Y. Zhao, F. Vanhaecke, L. Moens, R. Dams and P. Sandra, *J. Anal. At. Spectrom.*, 1999, **14**, 229.

111 G. Forte, M. D'Amato and S. Caroli, *Microchem. J.*, 2005, **79**, 15.

112 S. Pozdniakova and A. Padarauskas, *Analyst*, 1998, **123**, 1497.

113 C. Casiot, O.F.X. Donard and M. Potin-Gautier, *Spectrochim. Acta, Part B*, 2002, **57**, 173.

114 D. Schaumloffel and A. Prange, *Fresenius J. Anal. Chem.*, 1999, **364**, 452.

115 J.R. Bacon, K.L. Linge, R.R. Parrish and L.V. Vaeck, *J. Anal. At. Spectrom.*, 2006, **21**, 785.

116 J. Feldmann, *Trends Anal. Chem.*, 2005, **24**, 228.

117 D.N. Van, B. Radziuk and W. Frech, *J. Anal. At. Spectrom.*, 2006, **21**, 708.

118 E.H. Evans, J.A. Day, C. Palmer, W.J. Price, C.M.M. Smith and J.F. Tyson, *J. Anal. At. Spectrom.*, 2006, **21**, 592.

119 C.-G. Yuan, G.-b. Jiang and B. He, *J. Anal. At. Spectrom.*, 2005, **20**, 103.

120 J.W. Olesik, *Anal. Chem.*, 1991, **63**, 12A

121 N. Fidalgo-Used, M. Montes-Bayon, E. Blanco-Gonzalez and A. Sanz-Medel, *J. Anal. At. Spectrom.*, 2005, **20**, 876.

122 D.D. Richardson, B.B.M. Sadi and J.A. Caruso, *J. Anal. At. Spectrom.*, 2006, **21**, 396.

123 K.C. Thompson, J.L. Guinament, V. Ingrand, A.R. Elwater, C.W. M^{c}Leod, F. Schmitz, G. De Swaef and P. Quevauviller, *J. Environ. Monit.*, 2000, **2**, 416.

124 J. Diemer and K.G. Heumann, *Fresenius J. Anal. Chem.*, 1997, **357**, 74.

125 Z. Huang, K. Ito, A.R. Timerbaev and T. Hirokawa, *Anal. Bioanal. Chem.*, 2004, **378**, 1836.

126 Z. Huang, K. Ito and T. Hirokawa, *J. Chromatogr. A*, 2004, **1055**, 229.

127 M. Shah, R.G. Wuilloud, S.S. Kannamkumarath and J.A. Caruso, *J. Anal. At. Spectrom.*, 2005, **20**, 176.

128 R. Kellner, J.-M. Mermet, M. Otto and H.M. Widmer, *Analytical Chemistry*, Wiley-VCH, Weinheim, 1998.

129 L.R. Snyder, J.J. Kirkland and J.L. Glajch, *Practical HPLC Method Development*, Wiley-Interscience, New York, 1997.

130 B. Paull and P.N. Nesterenko, *Trends Anal. Chem.*, 2005, **24**, 295.

131 N. Tanaka, H. Kobayashi, N. Ishizuka, H. Minakuchi, K. Nakanishi, K. Hosoya and T. Ikegami, *J. Chromatogr. A*, 2002, **965**, 35.

132 *http://chrombook.merck.de/chrombook/index.jsp?alias=1A1A4A1&j=1* (accessed 08/12/2006)

133 T. Ikegami and N. Tanaka, *Current Opinion Chem. Bio.*, 2004, **8**, 527.

134 E. Sugrue, P.N. Nesterenko and B. Paull, *Anal. Chim. Acta*, 2005, **553**, 27.

135 E. Sugrue, P.N. Nesterenko and B. Paull, *J. Chromatogr. A*, 2005, **1075**, 167.

136 Q. Xu, M. Mori, K. Tanaka, M. Ikedo and W. Hu, *J. Chromatogr. A*, 2004, **1026**, 191.

137 E. Sugrue, P.N. Nesterenko and B. Paull, *Analyst*, 2003, **128**, 417.

138 P. Hatsis and C.A. Lucy, *Analyst*, 2002, **127**, 451.

139 J. Scancar and R. Milacic, *Analyst*, 2002, **127**, 629.

140 J. Weiss, *Ion Chromatography*, VCH, Weinheim, 1995.

141 D.R. Baker, *Capillary Electrophoresis*, Wiley-Interscience, New York, 1995.

142 J. Lichtenberg, N.F. de Rooij and E. Verpoorte, *Talanta*, 2002, **56**, 233.

143 J.E. Prest and P.R. Fielden, *Anal. Commun.*, 1999, **36**, 333.

144 J.E. Prest, S.J. Baldock, P.R. Fielden and B.J. Treves Brown, *Analyst*, 2001, **126**, 433.

145 J.E. Prest, S.J. Baldock, P.R. Fielden, N.J. Goddard and B.J. Treves Brown, *J. Chromatogr. A*, 2003, **990**, 325.

146 J. Wang, M.P. Chatrathi, B. Tian and R. Polsky, *Anal. Chem.*, 2000, **72**, 2514

147 R. Wilke and S. Buttgenbach, *Biosens. Bioelectron.*, 2003, **19**, 149.

148 Y.-C. Lin, *Sens. Actuators, B*, 2001, **80**, 33.

149 Y. Liu, J.C. Fanguy, J.M. Bledsoe and C.S. Henry, *Anal. Chem.*, 2000, **72**, 5939.

150 T. Pan, R.T. Kelly, M.C. Asplund and A.T. Woolley, *J. Chromatogr. A*, 2004, **1027**, 231.

151 T. M^{c}Creedy, *Anal. Chim. Acta*, 2001, **427**, 39.

152 B. Graβ, G. Weber, A. Neyer, M. Schilling and R. Hergenroder, *Spectrochim. Acta, Part B*, 2002, **57**, 1575.

153 S.C. Jacobson, R. Hergenroder, L.B. Koutny, R.J. Warmack and J.M. Ramsey, *Anal. Chem.*, 1994, **66**, 1107.

154 C.-C. Lin, C.-C. Chen, C.-E. Lin and S.-H. Chen, *J. Chromatogr. A*, 2004, **1051**, 69.

155 S. Buttgenbach and R. Wilke, *Anal. Bioanal. Chem.*, 2005, **383**, 733.

156 U. Backofen, F.-M. Matysik and C.E. Lunte, *Anal. Chem.*, 2002, **74**, 4054.

157 J.W. Olesik, J.A. Kinzer and S.V. Olesik, *Anal. Chem.*, 1995, **67**, 1.

158 J.E. Sonke, D.J. Furbish and V.J.M. Salters, *J. Chromatogr. A*, 2003, **1015**, 205.

159 Q. Lu, S.M. Bird and R.M. Barnes, *Anal. Chem.*, 1995, **67**, 2949.

160 J.A. Kinzer, J.W. Olesik and S.V. Olesik, *Anal. Chem.*, 1996, **68**, 3250.

161 B. Michalke and P. Schramel, *Fresenius J. Anal. Chem.*, 1997, **357**, 594.

162 M.J. Tomlinson, L. Lin and J.A. Caruso, *Analyst*, 1995, **120**, 583.

163 Y. Liu, V. Lopez-Avila, J.J. Zhu, D.R. Wiederin and W.F. Beckert, *Anal. Chem.*, 1995, **67**, 2020.

164 Q. Lu and R.M. Barnes, *Microchem. J.*, 1996, **54**, 129.

165 P.W. Kirlew, M.T.M. Castillano and J.A. Caruso, *Spectrochim. Acta, Part B*, 1998, **53**, 221.

166 K.A. Taylor, B.L. Sharp, D.J. Lewis and H.M. Crews, *J. Anal. At. Spectrom.*, 1998, **13**, 1095.

167 V. Majidi and N.J. Miller-Ihli, *Analyst*, 1998, **123**, 803.

168 E. Mei, H. Ichihashi, W. Gu and S. Yamasaki, *Anal. Chem.*, 1997, **69**, 2187.

169 E.G. Yanes and N.J. Miller-Ihli, *Spectrochim. Acta, Part B*, 2003, **58**, 949.

170 J. Chamoun and A. Hagege, *J. Anal. At. Spectrom.*, 2005, **20**, 1030.

171 T.-h. Lee and S.-J. Jiang, *J. Anal. At. Spectrom.*, 2005, **20**, 1270.

172 J. Li, T. Umemura, T. Odake and K. Tsunoda, *Anal. Chem.*, 2001, **73**, 5992.

173 J. Li, T. Umemura, T. Odake and K. Tsunoda, *Anal. Chem.*, 2001, **73**, 1416.

174 Q.J. Song, G.M. Greenway and T. McCreedy, *J. Anal. At. Spectrom.*, 2003, **18**, 1.

175 Q.J. Song, G.M. Greenway and T. McCreedy, *J. Anal. At. Spectrom.*, 2004, **19**, 883.

176 A.Y.N. Hui, G. Wang, B. Lin and W.-T. Chan, *J. Anal. At. Spectrom.*, 2006, **21**, 134.

2 Experimental

This chapter describes the fundamental instrumentation, reagents and procedures used throughout the work presented in this thesis. Specific details for the individual studies are presented within the relevant chapter for ease of reference.

2.1 Instrumentation

2.1.1 ICPMS instrumentation

Two ICPMS instruments were used for this work since the original instrument was replaced with a new instrument approximately half way through the study. The original PlasmaQuad II+ instrument was removed in October 2004, with installation of the new instrument being completed in April 2005. A training course for the new Elan DRC II ICPMS was provided in July 2005 (PerkinElmer LAS, Beaconsfield, UK).

2.1.1.1 PlasmaQuad II+

The first part of the work was conducted with a PlasmaQuad II+ (VG Elemental, Winsford, Cheshire, UK) operated using PlasmaLab software (Thermo Elemental, Winsford, Cheshire, UK). The instrument was allowed to warm up for a minimum of 30 minutes and optimised prior to use. Optimisation was based upon the maximum sensitivity for indium ($^{m}/_{z}$ 115). A 10 μg L^{-1} tune solution was aspirated comprising of Be, Co, In, Ce and U in 2 % nitric acid (described later in reagents). The stability of the instrument was evaluated based upon a real-time display showing the % RSD (n = 5) of the measured intensity (cps). The torch position was adjusted in the X, Y and Z planes

using micrometers. The extraction lens was then tuned followed by the collector lens, lenses 1, 2, 3 and 4 and finally the pole bias. The argon nebuliser gas flow was optimised and was highly dependant on the sample introduction system (type of nebuliser and spray chamber). The standard sample introduction for the PlasmaQuad II+ used throughout this work comprised of a low flow glass concentric nebuliser (MicroMist, Glass Expansion, Australia) with a miniature jacketed (water cooled at 4^{o}C) cyclonic spray chamber (Cinnabar, Glass Expansion, Australia). This arrangement was selected in order to provide high transport efficiency with low liquid flow rates. This was well suited to the development of interfacing a microfluidic chip to ICPMS. The standard operating conditions of the PlasmaQuad II+ are in Table 2.1; any variation to these conditions is described in the relevant Section.

Table 2.1 Standard operating conditions for the PlasmaQuad II+ ICPMS

RF Forward power / W	1350
Reflected power / W	0
Auxiliary gas flow rate / L min^{-1}	1.0
Coolant gas flow rate / L min^{-1}	11
Nebuliser gas flow rate / L min^{-1}	0.88
Data acquisition mode	Peak jumping
Points per peak	3
Dwell time per amu / ms	10.24
Detector mode	Pulse counting

2.1.1.2 Elan DRC II

The majority of the work was conducted upon the newly installed Elan DRC II ICPMS (PerkinElmer SCIEX, Ontario, Canada). The instrument was allowed to warm up for a minimum of 30 minutes and optimised prior to use. A tune solution containing 1 μg L^{-1} of Mg, Ce, In, U and 10 μg L^{-1} of Ba in 2 % HNO_3 was aspirated for instrument optimisation and performance checks. Firstly the torch position was adjusted in the X and Y planes in order to give the greatest sensitivity based upon 1 μg L^{-1} Mg, In and U. The nebuliser gas was optimised *via* the instrument software to give below 3 % oxide formation (based upon CeO / Ce ratio). The Elan series of ICPMS instruments have an Autolens system, as well as the static lens option, comprising of a single ion lens. The Autolens adjusts the lens voltage for the optimum transmission for each mass into the mass spectrometer, replacing a compromise condition. In combination with the single ion lens a grounded shadow stop is employed to assist in only allowing ions to enter the quadrupole. The Autolens voltage was optimised based upon a linear calibration across the mass range weighted towards the low mass end (using 1 μg L^{-1} Be, Co and In). The standard operating conditions for the Elan DRC II are shown in Table 2.2. The standard sample introduction system used with the Elan DRC II comprised of a glass concentric nebuliser and cyclonic spray chamber (PerkinElmer SCIEX, Ontario, Canada). Mass calibration (Elan Tuning) was performed to give a resolution of 0.7 amu and dual detector cross calibration (pulse to analogue conversion) was performed for a suite of elements across the entire mass range. The detector dead time was optimised to give the greatest cross calibration coefficient at 35 ns.

Table 2.2 Standard operating conditions for the Elan DRC II ICPMS

RF Forward power / W	1100
Auxiliary gas flow rate / L min^{-1}	1.2
Plasma (previously coolant) gas flow rate / L min^{-1}	15
Nebuliser gas flow rate / L min^{-1}	0.88
Sweeps per reading	25
Readings per replicate	1
Replicates	3
Dwell time per amu / ms	50
Data acquisition mode	Peak hopping
Autolens	On
Detector mode	Dual

The instrument performance was monitored daily based upon the sensitivity across the mass range (cps measured for 1 μg L^{-1} Mg, In, U), stability (% RSD) of 5 replicate readings, oxide formation (based on CeO / Ce ratio), doubly charged ion formation (based upon Ba^{2+} / Ba^{+}) and background signal (cps measured at 8.5 and 220 amu). Specifications were checked against the instrument manufacturer's guidelines, given in Table 2.3, and the performance of the instrument at the time of installation. If the instrument fell out of these specifications optimisation was performed and if poor performance was still obtained more thorough optimisation, cleaning and maintenance were undertaken in order to correct the problem.

Table 2.3 Elan DRC II instrument performance specifications for daily check

Sensitivity / cps ppb^{-1}	Mg	> 6000
	In	> 30 000
	U	> 20 000
Background / cps	8.5 amu	< 2
	220 amu	< 2
Doubly charged ratio / %	Ba^{2+} / Ba^{+}	< 3
Oxide ratio / %	CeO / Ce	< 3

The instrument was equipped with a dynamic reaction cell (DRC), which in standard mode was vented. This provides chemical resolution by the introduction of a reactive gas into the cell placed in the ion path prior to the quadrupole mass filter (described in Section 1.1.4). The cell was conditioned prior to use by flowing 0.6 ml min^{-1} reaction gas through the cell for a minimum of 2 hours. When the DRC was used the nebuliser gas was optimised since this is often marginally higher than in standard mode (i.e. with cell vented). Ammonia was the only reaction gas available throughout this work and was used to remove the $^{40}Ar^{12}C$, $^{40}Ar^{15}NH$ and $^{40}Ar^{40}Ar$ interferences on ^{52}Cr, ^{55}Mn and ^{80}Se respectively. This was achieved predominantly by charge transfer to remove $^{40}Ar^{+}$ as shown in Equation 2.1.

$$^{40}Ar^{+} + NH_3 \rightarrow NH_3^{+} + Ar$$
$$k = 1.60x10^{-9}\,cm^{-3}molecule^{-1}s^{-1} \qquad \textbf{Equation 2.1}$$
$$\Delta H_r = -5.6eV$$

The ammonia gas flow rate was optimised based upon the background equivalent correction (BEC) for matrix matched blank and 1000 ng L^{-1} analyte in the matrix. typically at 0.5 ml min^{-1}. The instrument detection limit (DL) was calculated using Equation 2.2.

$$DL(ppt) = \frac{3SD_{(Blank)} x Concentration_{(S\tan dard)}}{I_{(S\tan dard)} - I_{(Blank)}} \qquad \textbf{Equation 2.2}$$

Where $SD_{(Blank)}$ is the standard deviation of the blank (matrix) and I is the intensity (cps). An example of the results achieved for manganese in a 2 % HNO_3 matrix was the reduction in the detection limits from 5.7 ng L^{-1} Mn in standard mode to 2.9 ng L^{-1} Mn with 0.35 ml min^{-1}.

The DRC also utilises dynamic bandpass tuning (DBT) by means of a second quadrupole within the cell prior to the detector quadrupole. The RPq value upon this quadrupole can be set in order to prevent constituents of byproducts / interferents passing through the cell. The RPa defines the high $^{m}/_{z}$ bandpass limit and is therefore often not used. However it can be beneficial in reducing sensitivity for example elements in analogue mode can be suppressed to pulse mode.

2.1.1.3 Temperature regulators

A Neslab mini-chiller (Life Sciences International Ltd., Basingstoke, UK) was used to control the temperature of the jacketed cyclonic spray chamber when used with the PlasmaQuad II+ ICPMS. A 10 % ($^{v}/_{v}$) solution of ethylene glycol in UHQ water was circulated to maintain the temperature at 4^{o}C.

A refrigerating / heating circulating bath (Model 9106, PolyScience, Illinois, USA) was used with the Elan DRC II ICPMS. This was filled with a 30 % ($^{v}/_{v}$) solution of ethylene glycol in UHQ water in order to maintain the same 4 ^{o}C temperature of the jacket spray chamber. An air cooled recirculator (Model 3370, PolyScience, Illinois, USA) was used to cool the Elan DRC II interface region. This was filled with coolant solution (PerkinElmer SCIEX, Ontario, Canada), mainly comprising of deionised water and an algaecide.

2.1.1.4 Autosampler

A Cetac ASX-510 AutoSampler (Cetac Technologies, Omaha, Nebraska, USA) was used for the batch analysis of samples. This has the capacity for 10 x 50 ml sample vials (generally for blanks and standards) and 240 x 10 ml sample vials within 4 x 60 vial removable racks. It also has an integrated peristaltic pump supplying a wash position, which is ordinarily used with 2 % ($^{v}/_{v}$) nitric acid. This was controlled by the Elan instrument control software.

2.1.2 Liquid pumps

2.1.2.1 Peristaltic pumps

Liquid sample introduction for ICPMS was supplied by peristaltic pumps. The PlasmaQuad II+ used an independent MiniPuls3 (Gilson Inc., Middleton, USA) pump, while the Elan DRC II had an integrated pump unit. Both comprised of stainless steel rollers and were fitted with Tygon pump tubing (Elkay Laboratory Products Ltd., Basingstoke, UK). The desired liquid flow rate was achieved by selection of pump tubing with an appropriate internal diameter and by setting the pump speed. Pump

speed (rev min^{-1}) was controlled either on the pump unit (Gilson) or *via* the instrument software (Elan).

2.1.2.2 Syringe pumps

When very low liquid flow rates were required, particularly for the microfluidic chips, solutions were delivered using Baby Bee™ syringe pumps (Bioanalytical Systems Ltd., Kenilworth, UK). Equipped with a Worker Bee™ controller these were capable of delivering 0.1 – 100 μl min^{-1} when used with a 1 ml syringe. Clean, single use syringes were used with the pumps in order to prevent any contamination of the solutions.

2.1.3 Chromatographic instrumentation

2.1.3.1 HPLC pump

A Speck Analytical HPLC pump model SA103 (Speck & Burke Analytical, Alva, UK) was used to deliver the mobile phase for liquid chromatography. This was capable of providing a flow rate of 0.01 to 10.00 ml (0.01 ml increments) at pressures up to 6000 p.s.i. using a low pulsation reciprocating single piston pump.

2.1.3.2 Sample injection

Sample injection was performed using a 6-way injection valve (Rheodyne, Cotati, USA) equipped with a 20 μl sample loop.

2.1.3.3 Monolithic silica HPLC column

The chromatographic column used throughout all speciation analysis was a Chromolith™ performance RP-18e (Merck KGaA, Darmstadt, Germany). The column

dimensions were 100 mm (L) x 4.6 mm (i.d.). The stationary phase material was monolithic high purity silica. The structure of the column consists of 2 μm macropores and 13 nm mesopores with a pore volume of 1 ml g^{-1} and total porosity of >80 %. This provides a surface area of 300 m^2 g^{-1}. The significance of this stationary phase is described in more detail in Section 1.3.3 and Chapter 3. The column was conditioned by flushing for 5 minutes at 3 ml min^{-1} with 100 % acetonitrile (HPLC grade, Fisher Scientific Ltd., Loughborough, UK), 5 minutes at 3 ml min^{-1} with UHQ water and finally the mobile phase until a stable baseline was achieved. As the ICPMS was being used as the detector this process was completed with the column disconnected from the instrument, only being connected after 10 minutes conditioning with the appropriate mobile phase. A 25cm length of PEEK tubing (250μm i.d.; 1/16" o.d.) was used to connect the chromatographic column to the nebuliser. The column was operated at room temperature throughout the work and the pH was limited to between 2.0 to 7.5 to avoid any damage to the silica stationary phase.

2.1.4 Balances

The electronic balance used for all weighing of samples and reagents was a Precisa 205A SCS (Precisa Balances Ltd., Milton Keynes, UK), which was accurate to 0.0001g and was cleaned and calibrated regularly.

2.1.5 Liquid handling

All liquids were transferred using a range of Sealpette® pipettes (Jencons Scientific Ltd., Leighton Buzzard, UK). Both variable (5 – 50 μl, 50 – 200 μl, 200 – 1000 μl and 1 – 5 ml) and fixed volume pipettes (100 and 1000 μl) were employed in the preparation

of samples and standard solutions. Clean single use pipette tips were used once only to avoid contamination of solutions. All pipettes were dismantled, cleaned and calibrated regularly and were checked prior to use by weighing the amount of water expelled from the tip.

Volumetric flasks used for the preparation of standard solutions were Volac grade A (Poulten & Graf Ltd., Barking, UK). Once prepared all sample and standard solutions were stored and used from disposable sample tubes. Clean 15 and 50 ml screw top tubes (SARSTEDT Ltd., Leicester, UK) were used once only and were a suitable size for the ICPMS autosampler racks.

2.2 Reagents

All solutions were prepared using Analytical Grade reagents and ultra high quality (UHQ) water de-ionised to a resistivity of 18 mΩ cm^{-1} (ELGA LabWater, High Wycombe, UK). Nitric acid 69 %; super purity acid™, (Romil Ltd., Cambridge, UK) was used throughout.

2.2.1 Standards

All calibration standards and spike solutions were prepared from 1000 mg L^{-1} single element reference solutions. Generally PrimAg® – xtra certified reference material (Romil Ltd., Cambridge, UK) stock solutions were used. These were diluted using pipettes and volumetric flasks as required. Any deviation from these will be included in the relevant chapter, particularly for the source of certified speciation standards and matrix matched certified reference materials (CRM's).

2.2.1.1 Standards for conducting ICPMS optimisation and performance

The PlasmaQuad II+ was optimised and checked using a 10 μg L^{-1} tune solution comprising of Be, Co, In, Ce and U. This was prepared by dilution from the respective 1000 mg L^{-1} single element reference solutions in 2 % nitric acid.

The Elan DRC II daily performance, nebuliser gas flow optimisation and X-Y torch positioning was performed using a tune solution comprising of 1 μg L^{-1} Mg, Ce, In and U with 10 μg L^{-1} Ba. Optimisation of the autolens voltage was conducted using 1 μg L^{-1} Be, Co and In solution. These solutions were prepared by dilution from the respective 1000 mg L^{-1} single element reference solutions in 2 % nitric acid. Upon installation of the instrument a number of certified PerkinElmer Pure atomic spectroscopy standards were supplied. These included:

- Elan 6100DRC setup/stab./mass cal. solution; consisting of 1 μg L^{-1} Mg, Al, Cr, Mn, Cu, Rh, Cd, In, Ce, Pb, Th and 10 μg L^{-1} Ba in 0.5 % nitric acid.

- Elan 6100DRC sensitivity detection limit solution; consisting of 1 μg L^{-1} Be, Co, In, U, Mg, Rh, Pb, Na, Fe, Ca, K, Ba and Ce in 0.5 % nitric acid.

- Elan 6100 detection limit solution; consisting of 10 μg L^{-1} Be, Co, In and U in 2 % nitric acid.

These certified multielement solutions were used to check the accuracy of the laboratory prepared tune and autolens solutions and confirm the instrument performance.

2.2.2 Gases

The ICPMS instruments were supplied with argon gas from a 200 L dewar (Statebourne Cryogenics, Washington, UK) filled with pure liquid argon 99.999% (BOC Gases Cryospeed, Rotherham, UK).

Ammonia was used as a reaction gas within the Elan DRC II reaction cell. Anhydrous ammonia >99.99999% (Praxair, Optogas Ltd., Wirral, UK) was supplied from a cylinder (Engineering and Welding Ltd., Hull, UK) contained within a stainless steel cupboard with fume extraction.

2.3 Procedures

2.3.1 Washing/cleaning glassware

All glassware was washed following a strict procedure to avoid contamination and elevated blank levels in trace analysis. The following protocol was followed;

1. Soak in 2% Lipsol® (Bibby Sterilin Ltd., Stone, UK) solution in UHQ water for 24 hours
2. Rinse in UHQ water minimum of five times
3. Soak in 5% nitric acid for a further 24 hours
4. Rinse in UHQ water minimum of five times
5. Store filled with 2% nitric acid to avoid any exposure to air

2.3.2 Elan DRC II maintenance

Periodical cleaning of sampler and skimmer cones, the ion lens and shadow stop, the torch and injector and changing of the pump oil was undertaken as described by the instrument manufacturer. A decrease in sensitivity was an indicator of dirty cones and / or injector. An increase in the lens voltage was indicative of a dirty ion lens. Other parameters were routinely optimised approximately every month, or upon significant change to the sample introduction system. These included RF power, detector (pulse and analogue stage voltage) and dual detector calibration. These were all done according to the manufacturers guidelines *via* the instruments software. Specific optimisation of significance to the work presented will be discussed in the relevant chapter.

2.4 Conclusion

In order to achieve reliable results in ultra–trace elemental analysis it is vital to work with high quality assurance. Contamination and the introduction of an elevated background signal must be avoided in order to achieve the best analytical results. This is the basis of the procedures described within this chapter. The instrumentation must regularly be carefully maintained and optimised. All gases and reagents used should be of high purity. The glassware and liquid handling equipment is used exclusively used for trace analysis, and the washing / cleaning and storage procedures are strictly adhered to.

3 Rapid Speciation Analysis using a Monolithic Silica Column for HPLC – ICPMS

3.1 Introduction

As discussed in the introduction (Section 1.3.2), reverse phase (RP) high performance liquid chromatography (HPLC) with a packed silica column is the most commonly applied separation technique for speciation analysis.[1] The stationary phase material typically consists of packed *n*-octadecyl (C_{18}) or *n*-octyl (C_8) bonded silica particles 3 – 5 μm in diameter. This type of liquid chromatography (LC) is routinely coupled with ICPMS detection in order to achieve the limits of detection (LOD) required by elemental speciation analysis. Limitations with this type of stationary phase material include the generation of high backpressures and limited column efficiency (i.e. number of theoretical plates). This restricts the flow rates achievable through the column and the speed of separation. The speed of separation is a major issue when using ICPMS detection since the detector is idle during the separation. High running costs associated with the ICPMS dictate a high analysis cost for samples requiring lengthy separation prior to detection. Therefore the major drive of this work is to reduce the separation time associated with trace element speciation by HPLC.

As stated in Section 1.3.3; the development of monolithic silica stationary phases for reversed phase LC has been considered as the most significant advance in stationary phase design since its conception.[2] A monolithic silica stationary phase enables much greater liquid flow rates to be achieved without the introduction of

excessive backpressure (macroporous through-pores) and has an increased surface area (fine mesoporous structure) *cf.* traditional packed silica columns. These factors combined allow much faster separations to be realised as discussed in the introduction (Section 1.3.3). This is the basis for the use of such a LC column for reducing the separation time while conducting trace elemental speciation by HPLC-ICPMS.

The selected analyte for the development of rapid trace element speciation is arsenic. The requirement for arsenic speciation is extensive and has been discussed in detail in Section 1.2.1.1. Inorganic arsenic is a group A human carcinogen.[3] Recently it has been reported that rice contains higher levels of arsenic compared to other common food types (bread, milk, pork meat, chicken meat, cabbage and potatoes)[4] and presents the primary source of dietary arsenic exposure in a non-seafood diet (typically containing higher levels of inorganic arsenic than seafood).[5] The specific interest for this work has arisen from the recent findings highlighting American long grain rice having the highest mean arsenic level in comparison to rice originating from Europe, Bangladesh and India.[6] Consequently a large scale market basket survey of the arsenic content of rice grown in the United States has been conducted by Meharg *et al.*[7] 134 supermarket rice samples from the main rice producing regions of the US, south central states (Arkansas, Louisiana, Mississippi, Texas and Missouri) and California, were analysed. The mean arsenic concentration was 0.27 μg As g^{-1} from the south central states and 0.16 μg As g^{-1} from California with 0.66 μg As g^{-1} found in rice from the Louisiana mills. A significant contribution to the high arsenic concentrations stems from rice being grown in old cotton fields previously treated with arsenic pesticides,[6] along with geological sources. Rice is widely consumed throughout the world and American long grain rice is one of the most common types consumed. Therefore this

could present a significant source of arsenic exposure *via* the human diet. The U.S. national standard of daily inorganic arsenic intake is 10 μg. The U.S. daily per capita rice consumption in 2003 was 25 g dry weight. Coupled with the average daily drinking water intake of 1 L exposure standards could easily be breached by the average American. Certain population groups known to have a high rice intake in their diet (Hispanics, Asians, sufferers of Celiac disease and infants) are at significant risk from high dietary arsenic exposure.[7]

HPLC is the most commonly applied separation technique for arsenic speciation[8] and has been considered as state-of-the-art.[9] Using ICPMS detection imposes restrictions upon the conditions that can be used in LC. The most obvious of these is the introduction of organic solvents into the plasma. Despite the numerous advantages of ICPMS for speciation analysis, including high specificity and sensitivity, it cannot be considered the ideal detector for routine speciation analysis owing to its high running costs.[9] The most common HPLC separation mechanisms applied to arsenic speciation are ion exchange and ion-pairing. Both cation and anion exchange chromatography have been used for arsenic speciation analysis. Anion exchange is the most commonly applied approach for separation of inorganic arsenic (As(III), As(V)), monomethylarsonate (MMA) and dimethylarsinate (DMA) with a polymeric anion-exchange column (Hamilton PRP X-100) being the most frequently used.[10-16] This column has been shown to be stable over a wide pH range and to give good separations taking approximately 15 – 20 minutes per sample. While being a tried and trusted separation method this leaves the detector idle for a significant amount of time. The applicability for routine arsenic speciation, involving large numbers of samples, is hence limited owing to the analysis cost and time.

Reversed phase ion-pair chromatography (IPC) is well suited to ICPMS detection since the mobile phase consists of water or aqueous buffer into which an ion-pair reagent (IPR) is added. This eluent composition can be carefully selected to be suitable for direct introduction into the ICP *via* standard sample introduction systems. The principle advantage of IPC over ion exchange is the high degree of flexibility in adjustment of the chromatographic conditions in order to tailor them to a specific separation / analyte. IPC and IPR's have been discussed in Section 1.3.4. IPC has been developed for arsenic speciation and there have been many different mobile phase compositions and IPR's suggested in the literature. Some particularly interesting and more recent schemes are presented in Table 3.1.

Table 3.1 Previously reported mobile phase compositions for ion-pair chromatographic separation of arsenic species[17]

Refs.	Mobile phase	Flow rate	Inj. vol.
K. Sathrugnan and S. Hirata, *Talanta*, 2004, **64**, 237	5 mM butanesulfonic acid (BSA) 2 mM malonic acid 0.3 mM hexanesulfonic acid (HSA) 0.5% methanol	1 mL min^{-1}	25 µL
X. C. Le and M. J. Ma, *J. Chromatogr., A*, 1997, **764**, 55	10 mM hexanesulfonate 1 mM tetraethylammonium hydroxide 0.5% methanol	0.8 mL min^{-1}	20 µL
S. Wangkarn and S. A. Pergantis, *J. Anal. At. Spectrom.*, 2000, **15**, 627	5 mM tetrabutylammonium hydroxide Malonic acid (adj. to pH 6.2)	0.7 mL min^{-1}	1 µL
H. Ding, J. Wang, J. G. Dorsey and J. A. Caruso, *J. Chromatogr., A*, 1995, **694**, 425	0.05 M cetyltrimethylammonium bromide (CTAB) 10% propanol 0.02 M borate buffer	1 mL min^{-1}	100 µL
R. Chen, B. W. Smith, J. D. Winefordner, M. S. Tu, G. Kertulis and L. Q. Ma, *Anal. Chim. Acta*, 2004, **504**, 199	10 mM cetyltrimethylammonium bromide (CTAB) 20 mM ammonium phosphate buffer (pH 6) 2% methanol		20 µL
K. Ackley, C. B'Hymer, K. Sutton and J. A. Caruso, *J. Anal. At. Spectrom.*, 1999, **14**, 845	25 mM citric acid 10 mM 1-pentanesulfonic acid sodium salt	0.15 mL min^{-1}	20 µL
A. Huerga, I. Lavilla and C. Bendicho, *Anal. Chim. Acta*, 2005, **534**, 121	7 mM tetrabutyl ammonium bromide 0.5 mM potassium phosphate buffer (pH 5.75) 5% methanol	1.2 mL min^{-1}	100 µL

Both anion-pairing and cation-pairing techniques have been developed for the separation of arsenic species. Tetrabutylammonium salts are generally the most successful IPR's for separation of inorganic arsenic, MMA and DMA, giving a consistent elution order of As(III), DMA, MMA, As(V).[8] The optimal pH for the separation has been found to be between pH values of 5.0 and 7.0. However separation of As(III) and arsenobetaine (AsB) is not achieved as they are unretained under these conditions. As(III), pK_a 9.2, and AsB, which is a zwitterion, are both neutral species in this pH range. Rapid speciation was achieved by Wangkarn *et al.*[9] utilising narrow-bore (2.1 mm i.d.) ion-pairing HPLC–ICPMS. Six species were separated within 3 minutes, however the LOD achieved were relatively high (mean 0.7 μg As L^{-1}, max. 1.3 μg As L^{-1}).[9] This could limit the application of the method to biological samples since they often require dilution to reduce the total dissolved solid content prior to ICPMS analysis. Cationic arsenic species have been separated using long-chain alkanesulphonic acids IPR's (butane-, pentane-, hexane- sulphonic acid as described in Table 3.1).

3.1.1 Aim

The aims of this work were to firstly investigate the use of a commercial monolithic silica stationary phase column (Chromolith™) for the rapid separation of arsenic species. Namely the two most common forms of inorganic arsenic; arsenate (As(V)) and arsenite (As(III)), and three organic arsenic species; arsenobetaine (AsB, most commonly found in marine environment), monomethylarsonate (MMA) and dimethylinate (DMA). The intention was to reduce separation times in order to reduce ICPMS detector idle time, increase sample throughput and therefore decrease the cost of analysis per sample.

The aim was then to demonstrate the applicability of this novel rapid and highly sensitive method for arsenic speciation to a dietary study. As high levels of arsenic have recently been reported in rice;[4, 6] a study designed by E. Brima and Dr. P. Haris (De Montfort University, Leicester) was conducted to identify arsenic species excreted in urine after ingestion of rice.

3.2 Experimental

3.2.1 Instrumentation

The Elan DRCII ICPMS was used for all analyses with a glass concentric nebuliser and cyclonic spray chamber for sample introduction. The instrument performance was monitored daily as described in the Experimental (Section 2.1.1.2). The operating conditions for ICPMS both for total element concentration and HPLC-ICPMS are shown in Table 3.2.

The Cetac ASX-510 AutoSampler was used for batch analysis of filtered and diluted urine samples. The chromatographic instrumentation (pump, injector and column) was as described in Section 2.1.3.

Table 3.2 Operating conditions for Elan DRC II ICPMS and ion-pair HPLC

ICPMS	**Total**	**Speciation**
RF forward power / W	1100	1100
Plasma gas flow rate / (L/min)	15	15
Nebuliser gas flow rate / (L/min)	0.88	0.88
Dwell time per AMU / ms	50	500
Sweeps per reading	25	1
Readings per replicate	1	160
Replicates	3	1
Time per sample / s	103	240
HPLC		
C18 reversed phase column	Chromolith™ RP-18e 100 x 4.6mm i.d.	
Mobile phase	2.5mM tetrabutylammonium bromide (TBAB) 10mM phosphate buffer (pH 5.6) 1% (v/v) methanol	
Flow rate	1.0ml/min	
Injection volume	20μl	

3.2.2 Reagents

Arsenic standards were prepared from their appropriate 1000 mg L^{-1} As stock solutions as follows: As(V) in 2 % NaOH and As(III) in 2 % HCl (1000 ± 3 mg L^{-1}, CPI International, Amsterdam), Dimethylarsinic acid [DMA; $(CH_3)_2AsOOH$] (Sigma-Aldrich, Germany), Monomethylarsonic acid [MMA; $CH_3AsO(OH)_2$] (Greyhound, Dorset, England), and Arsenobetaine [AsB; $(CH_3)_3AsCH_2COO^-$] (Fluka, Fisher Scientific UK Ltd., Loughborough, UK). All stock solutions were prepared in deionized water and stored in the fridge at 4 ^oC. Fresh diluted solutions were prepared daily for analysis.

Ion-pair reagents investigated were tetrabutylammonium bromide [TBAB], sodium 1-hexanesulfonate monohydrate [HSA], 1-butanesulfonic acid sodium salt [BSA] and 1-octanesulfonic acid sodium salt [OSA] (Sigma-Aldrich, Germany).

Buffer solutions were prepared daily from analytical grade reagents as described in "Practical HPLC Method Development", Appendix IV.[18] Phosphate buffer components were sodium dihydrogen *ortho*-phosphate [$NaH_2PO_4.2H_2O$] and *ortho*-phosphoric acid (Fisher Scientific Ltd., Loughborough, UK), and disodium hydrogen *ortho*-phosphate [Na_2HPO_4] (BDH, Poole, UK). Citrate buffers were prepared from citric acid (BDH Chemicals Ltd., Poole, UK) and sodium citrate (Fisher Scientific Ltd., Loughborough, UK). Acetate buffers were prepared using glacial acetic acid (Fisher Scientific Ltd., Loughborough, UK) and sodium acetate (Avocado Research Chemicals Ltd., Heysham, UK).

HPLC grade methanol (Fisher Scientific Ltd., Loughborough, UK) was added by % ($^{v}/_{v}$) as an organic modifier.

3.2.3 Procedures

3.2.3.1 Samples

All urine samples were filtered prior to analysis through a 0.45 μm mixed cellulose ester filter unit (Millex HA, MF-Millipore, Cork, Ireland) which was fitted to a 5 ml disposable syringe (Discardit II, B-D, Fraga, Spain). 1 ml of each sample was diluted with 4 ml of 2 % (0.3 M) nitric acid in order to reduce the amount of total dissolved solids, which could cause the glass concentric nebuliser to become blocked.

3.2.3.2 Collection and treatment of urine samples

Urine sample collection and storage were carried out as generally reported in the literature.[19, 20] Creatinine adjustment is routinely used to reduce some factors that are not related to As exposure, such as urine concentration and urine volume.[21] Creatinine

was analysed photometrically by using a Metra Creatinine Assay Kit (Quidel Corporation, USA). The actual concentration of arsenic in all urine samples were expressed as As µg/g creatinine.

3.2.3.3 Extraction of food samples for speciation analysis

The food samples were extracted, as described by Rmalli,[22] using 50 % methanol: 50 % water. Microwave digestion (Microdigest A301, Prolabo, Fontenay-sous-Bois, France) was performed at 25 % power (200 W) for 10 minutes. The resulting solution was centrifuged at 3000 rpm for 15 minutes in a Chilspin centrifuge (MSE Ltd., London, UK), then the methanol was evaporated using a rotary evaporator (Rotavapor® R-114, Buchi Ltd., Oldham, UK). The final extract was made up to 10 ml in a volumetric flask with UHQ water.

3.2.3.4 Digestion of food samples for total element analysis

The digestion procedure as previously described was followed.[23] Digestion was performed using 5 ml concentrated HNO_3 (69 %) for 20 min and 2 ml 30 % H_2O_2 for 10 min. Both steps involved the application of microwave digestion (Microdigest A301, Prolabo, Fontenay-sous-Bois, France) at 25 % power (200 W). The digests were made up to 10 ml in a volumetric flask with UHQ water. This method was validated for food analysis by the analysis of certified reference material (IMEP®-20, Institute for Reference Materials and Measurements, Belgium) tuna fish (4.93 ± 0.21 mg As kg^{-1}); in which 4.65 ± 0.02 mg As kg^{-1} was found. There was no available rice certified reference material at the time of the work.

3.2.3.5 Chromatography

The chromatographic column used was a Chromolith™ Performance RP-18e (100 x 4.6 mm i.d.) with monolithic silica stationary phase material (Merck KGaA, Darmstadt, Germany). The optimised ion pair separation was performed using a mobile phase consisting of 2.5 mM tetrabutylammonium bromide (TBAB), 10mM phosphate buffer (pH 5.6) and 1.0 % ($^{v}/_{v}$) methanol. The mobile phase flow rate used throughout was 1.0 ml min^{-1} generating a backpressure of approximately 1000 psi. The mobile phase eluent was prepared freshly prior to analysis. Constituents were added to UHQ water and made up to either 500 or 1000 ml (or 50 ml during optimisation and method development) volume in a volumetric flask. This was then sonicated for 30 minutes, before being transferred to a polyethylene bottle. The prepared mobile phase was degassed, by further sonication, and filtered through a 0.45 μm filter immediately prior to use. The column was conditioned with acetonitrile (100 %) followed by UHQ water (100 %) and connected to the ICPMS nebuliser *via* PEEK capillary, whose dimensions were minimised to limit any peak broadening (250 μm i.d.; 25 cm in length). Finally the mobile phase was flushed for approximately 30 minutes (at the same time as the instrument was allowed to warm up). Any minor changes to mobile phase composition during optimisation were made allowing 10 minutes for the column and system to be flushed with the new composition prior to injection of the next sample or standard.

3.2.3.6 Chromatographic data processing

The chromatographic data was processed using a Turbochrom Workstation and Chromlink™ for the Elan ICPMS (PerkinElmer LAS Ltd., Beaconsfield, UK). Chromlink™ was used to export the data files generated by the ICPMS control software

into Turbochrom. Within Turbochrom the peaks were integrated automatically and were reviewed and reprocessed manually as required.

3.2.3.7 Online internal standard addition

Selection of an appropriate internal standard is crucial to ensure reliable standardisation of results. An internal standard corrects for minor differences in sample introduction between samples, standards and blanks resulting from differences in viscosity. The internal standard should have an $^{m}/_{z}$ close to that of the analyte masses it is associated with and it should not be interfered by any of the constituents in the sample matrix. Initially ^{71}Ga was investigated since it fits well with ^{75}As and ^{82}Se and has no obvious interference; however the ^{71}Ga response decreased significantly between running a standard and sample (60 – 65 000 cps for standard *cf.* 50 – 55 000 cps for sample). This led to high recoveries (115 – 120 %) due to the internal standard correction being excessive. ^{115}In also gave inaccurate results and for this reason monoisotopic ^{89}Y was finally selected as the internal standard as it gave good recoveries, and a stable intensity throughout (RSD 5.71 %; n = 100). 10 μg L^{-1} yttrium was added to all blanks, standards and samples as an internal standard to correct for the variation due to non-matrix matched calibration standards and minor variation in sample introduction.

To simplify sample preparation the internal standard was introduced on-line. Sample and internal standard were pumped to the nebuliser and the streams were combined before reaching it using a 3-way cap ‘T’-shaped connector with PTFE cones (Omnifit, Cambridge, UK). This resulted in the sample effectively being diluted with an equivalent volume of internal standard solution. Since all solutions are diluted

identically, the dilution factor did not need to be taken into account for quantification; however it should be considered if sensitivity becomes an issue. The stability of this arrangement was assessed by analysis of a 10 μg Y L^{-1} solution over approximately 10 minutes. The relative standard deviation of the cps for 100 replicates was 1.30 %, proving the addition was consistent and good mixing has been achieved within the connector. This arrangement was used for all total arsenic analyses.

3.2.3.8 Removal of chloride interference

Matrices with high chloride concentrations can cause interference on the arsenic signal. This originates from the formation of $^{40}Ar^{35}Cl$ within the plasma, which has the same mass – to – charge ratio as monoisotropic ^{75}As and is unresolved by the quadrupole mass filter. Since urine contains a significant amount of salts a correction for this interference was applied. A dynamic correction equation was applied to the method in order to monitor the ArCl signal, and remove this from the total signal at $^{m}/_{z}$ 75 to leave just the signal due to arsenic. This was achieved by monitoring $^{40}Ar^{37}Cl$ at $^{m}/_{z}$ 77 and relating this to the proportion present at $^{m}/_{z}$ 75 by the known relative abundance of the natural isotopes of ^{37}Cl (24.23 %) and ^{35}Cl (75.77 %). There is however selenium present in the samples as well and this adds to the signal at $^{m}/_{z}$ 77 at which selenium is 7.63 % abundant. Therefore an additional correction to remove this signal was applied by monitoring ^{82}Se. The resulting dynamic correction equation for removal of the chloride interference on the arsenic signal is shown in Equation 3.1.

$$^{75}As = -3.1288191 \times (^{77}Se - 0.8739977 \times ^{82}Se) \qquad \textbf{Equation 3.1}$$

The effectiveness of the correction equation applied to ^{75}As was evaluated by the analysis of standards containing a high chloride concentration, comparable to the

concentration found in urine. In the preparation of artificial urine 122 mM Cl was added from NaCl, to give a comparable matrix to real urine samples.[24] A calibration was obtained for arsenic over the range 1 – 20 μg L^{-1}. Then a blank and 5 standards, each containing 1 – 20 μg As L^{-1} with 85.4 μg Cl L^{-1} in 0.45 M nitric acid, were analysed for ^{75}As. The results were processed both with and without the correction equation applied and are shown in Table 3.3.

Table 3.3 Total arsenic concentration determined in high chloride matrix (85.4 μg Cl L^{-1}, 0.45 M nitric acid). Results processed both with and without dynamic correction equation applied (Equation 3.1).

Expected conc. / μg As L^{-1}	Meas Conc / μg As L^{-1}	Std Dev n = 3	%RSD n = 3	Recovery / %	Error / μg As L^{-1}	Error / %
Dynamic correction equation applied						
2.0	**2.15**	0.13	6.04	107.5	0.2	**7.5**
0.0	**0.04**	0.12	283.56		0.0	
20.0	**23.13**	0.32	1.38	115.7	3.1	**15.7**
1.0	**1.16**	0.05	4.45	115.5	0.2	**15.5**
5.0	**5.74**	0.12	2.01	114.8	0.7	**14.8**
10.0	**11.47**	0.09	0.80	114.7	1.5	**14.7**
Dynamic correction equation not applied						
2.0	**3.63**	0.06	1.68	181.3	1.6	**81.3**
0.0	**1.40**	0.05	3.87		1.4	
20.0	**24.81**	0.23	0.93	124.1	4.8	**24.1**
1.0	**2.54**	0.03	1.04	254.3	1.5	**154.3**
5.0	**7.22**	0.08	1.10	144.4	2.2	**44.4**
10.0	**12.95**	0.02	0.13	129.5	3.0	**29.5**

The error in the expected arsenic concentration for the uncorrected results ranged from 24.1 – 154.3 %, while the corrected results gave an error of 7.5 – 15.7 %. This proved the effectiveness of the equation to significantly reduce the interference in a high chloride matrix (85.4 μg Cl L^{-1}). Therefore it was applied throughout the analysis of all urine samples.

3.3 Results and discussion

3.3.1 Optimisation of Ion Pair Chromatographic Conditions

The mechanism by which IPC separation is achieved is presented in Section 1.3.4. Separation is affected by the following parameters: the type of lipophilic counter ion (i.e. IPR) in the mobile phase, the concentration of the IPR in the mobile phase, the type and concentration of organic modifier in the mobile phase, the type and concentration of inorganic additives, and the mobile phase pH.

3.3.1.1 Selection of Ion Pair Reagent

The properties of some ion pair reagents are discussed in Section 1.3.4 and presented in Table 1.3. There have been many different mobile phase compositions and ion-pair reagents suggested in the literature for the separation of arsenic species (various significant schemes are presented in Table 3.1). These methods can be separated into cation separation, using sodium salts of alkanesulphonic acids as IPR's, and the more commonly applied anion separation, using quaternary ammonium salts. Additionally both IPR types can be used simultaneously as in the scheme presented by Le and Ma.[25] It was decided to investigate both cationic and anionic separation schemes for arsenic speciation since both have been proven successful in the literature. The two schemes would be compared in order to evaluate the most suitable method for a column with monolithic silica stationary phase.

Firstly cationic separation was investigated using a scheme adapted from that presented by Sathrugnan *et al.*.[26] Despite the arsenic species being anionic good separation was achieved for As(III) and As(V), alongside selenium species, in water

samples. The mobile phase comprised of 5.0 mM butanesulphonic acid (BSA), 2.0 mM malonic acid, 0.3 mM hexanesulphonic acid (HSA) and 0.5 % methanol at pH 2.5. Initially this was prepared without adjusting the pH, which was 3.1. A sample containing 100 μg As L^{-1} of both As(III) and As(V) was prepared in both UHQ water and the mobile phase. No separation of the two species was achieved and they were poorly retained on the column, retention time 1.62 min and 1.54 min respectively. An increase in retention can be achieved by increasing the IPR concentration (limited by saturation of stationary phase typically at 10 mM), increasing the hydrophobicity of the IPR by use of longer chain alkanesulphonic acids (BSA < HSA < OSA) or lowering pH since the degree of dissociation of multivalent ions increases. Therefore hexanesulphonic acid (HSA) and octanesulphonic acid (OSA) were both investigated as IPR's at 5.0 mM upon the same samples. These failed however to increase the retention and separation of the two species sufficiently.

Secondly an anion separation scheme was investigated, based upon that presented by Huerga *et al*.[27] The IPR was tetrabutylammonium bromide (TBAB) and the mobile phase was prepared with 7.0 mM TBAB, 1.0 mM phosphate buffer and 1.0 % methanol. The pH was adjusted prior to addition of the organic modifier (which can cause inaccuracies in the pH measurement) to 6.0 using 0.1 M NaOH / 0.1 M malonic acid as suggested by Wangkarn *et al*.[9] A sample containing 5 arsenic species (As(III), As(V), AsB, MMA and DMA) at 100 μg As L^{-1} in UHQ was injected. Three peaks were baseline resolved with retention times of 1.42, 2.25 and 5.48 min. Therefore optimisation of the IPC conditions was continued with TBAB.

3.3.1.2 Concentration of Ion Pair Reagent

Increasing the concentration of the selected IPR increases the retention of analytes up to a maximum achievable limit. The limiting factor that governs the maximum retention that can be achieved with an IPR is the saturation of the stationary phase with IPR at which point the resulting excess of Na^+ drives the equilibrium back causing a decrease in retention, as demonstrated for cationic IPR's in Equation 3.2.

$$CH_3(CH_2)_n - SO_3 - Na^+ + X^+ \leftrightarrow C_6 - SO_3 - X^+ + Na^+ \qquad \textbf{Equation 3.2}$$

Generally the concentration range of IPR in the mobile phase is 0.5 – 10.0 mM; typically 2.0 mM is a suitable concentration. The retention factor (*k*) is used as a measure of retention; given by Equation 3.3.

$$k = \frac{t_R - t_0}{t_0} \qquad \textbf{Equation 3.3}$$

Where t_R is the retention time of the species and t_0 is the column dead time given by:

$$t_0 = \frac{V_m}{F} \qquad \textbf{Equation 3.4}$$

Where F is the flow rate (1 ml min^{-1}) and V_m is the column dead volume given by:

$$V_m \approx 0.5Ld_c^2 \qquad \textbf{Equation 3.5}$$

Where L is the column length (10.0 cm) and d_c is the column internal diameter (0.46 cm), Equation 3.5 provides a column dead volume of 1.06 ml, which results in a column dead time of 1.06 min at 1.0 ml min^{-1} from Equation 3.4. Hence;

$$k = \frac{t_R - 1.058}{1.058} \qquad \textbf{Equation 3.6}$$

Optimisation was performed for cation separation with BSA concentration covering the range of 0.0 to 10.0 mM. 10 mM sodium phosphate buffer was prepared at pH 2.6, to which 0.5 % methanol and BSA was added. The sample contained 100 μg As L^{-1} of both As(III) and As(V) in 0.5 % methanol. Figure 3.1 suggests that 5.0 mM gives the greatest retention as suggested by Sathrugnan *et al.*;[26] however the change in retention is minimal and not sufficient to achieve separation of As(III) and As(V). Ideally *k* should be between a minimum of 0.5 and maximum of 20. At 5.0 mM it was 0.49, which is too low resulting in the species being eluted close to the column void volume. Therefore 5.0 mM BSA was adopted and the HSA concentration was optimised in the same way. For this the mobile phase consisted of 5.0 mM BSA, 2.0 mM malonic acid and 0.5 % methanol and the HSA concentration was varied from 0 to 10 mM, however this did not achieve separation of the two species or significantly increase retention. For this reason cation separation was not investigated any further.

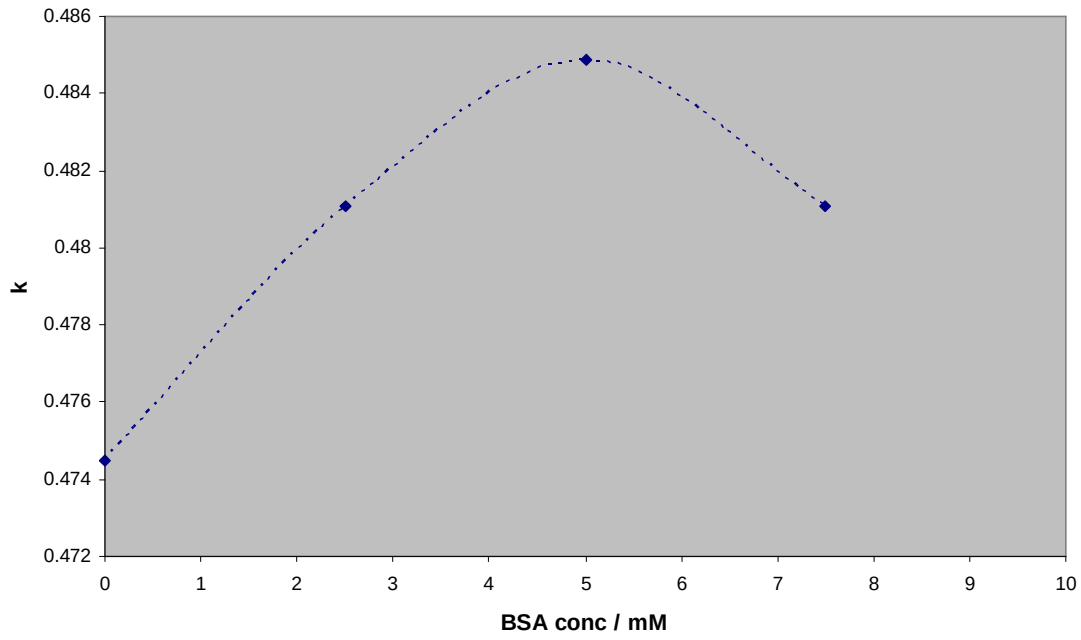

Figure 3.1 Effect of butanesulphonic acid (BSA) concentration in the mobile phase on the retention of 100 μg As L^{-1} As(III) / As(V)

Subsequently anion separation was investigated, which had shown greater potential initially. Separation of a mixed arsenic standard solution consisting of As(III), As(V), MMA, DMA and AsB at 50 μg As L^{-1} in UHQ water was carried out using TBAB as the IPR. TBAB concentration was optimised from 0.0 to 15.0 mM within an aqueous mobile phase consisting of 1.0 % methanol at pH 6.0. The analysis time was initially set at 10 minutes (defined by 400 replicate readings); however all species were eluted within 5 minutes. The resulting effect on the retention factor of the five arsenic species is presented in Figure 3.2.

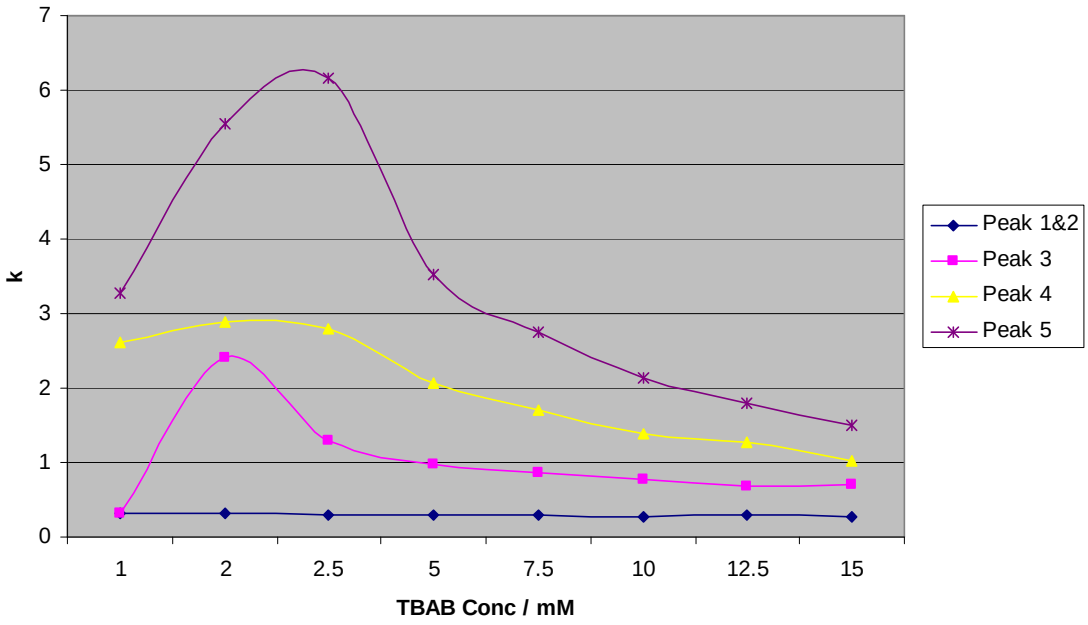

Figure 3.2 Optimisation of tetrabutylammonium bromide (TBAB) concentration within the mobile phase in order to achieve the greatest retention of the arsenic species investigated.

Figure 3.2 shows that the retention increased with increasing concentration, as expected, and that the optimal was reached at 2.0 – 2.5 mM TBAB for all arsenic species. As the stationary phase becomes saturated with IPR, the associated loss of retention is seen and therefore an optimal concentration of 2.5 mM TBAB was selected based upon these results and used in all subsequent mobile phase compositions. The chromatograms presented in Figure 3.3 show the separation achieved.

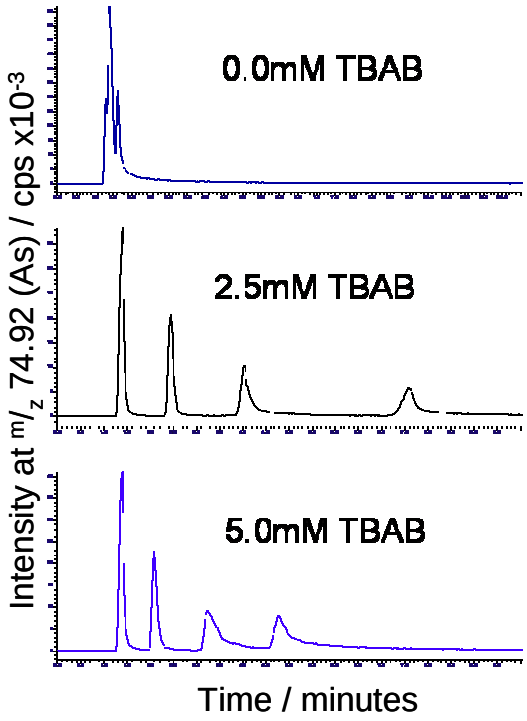

Figure 3.3 Effect of increasing TBAB concentration within the mobile phase on the separation of five arsenic species.

3.3.1.3 Mobile phase pH and buffer selection

Generally for the separation of multivalent ions it is necessary to alter the pH of the mobile phase with an appropriate acid or base. Retention increases with the degree of dissociation of the multivalent ion, which can be controlled by pH. In this work malonic acid was used to lower the pH and sodium hydroxide was used to raise pH. These were not found to increase any background signal or interfere with the speciation of the arsenic analytes.

To obtain the optimal pH for the separation of the five arsenic species (50 μg As L^{-1} mixed standard) the pH of a mobile phase containing 2.5 mM TBAB in UHQ water

was varied between 2.0 and 7.5. Extreme values outside of this range were avoided to prevent degradation of the monolithic stationary phase. The optimal pH was found to be between pH 5.0 and 6.0. Several buffer systems were then investigated to find a suitable scheme for effectively controlling the pH.[18] The buffer systems evaluated were citrate (pH 5.0 – 6.6), acetate (pH 4.6 – 5.6) and phosphate (pH 5.6 – 6.6), prepared from both sodium and potassium salts. The use of citrate buffer is desirable since it has a wide working pH range, however it does have the potential for degrading stainless steel components in the HPLC system. For this application, citrate buffers were found to severely degrade the separation of the arsenic species over all the pH values investigated. The highest pH possible for acetate buffer (pH 5.6) gave the best results, however the separation obtained was worse than that seen without the presence of buffer in the mobile phase. Phosphate buffer was found to be the most suitable for the separation of the five arsenic species and a pH value of 5.6 sodium phosphate buffer was found to give the best peak resolution as shown in Figure 3.4. From comparison of Figures 3.3 and 3.4 it can be seen that the phosphate buffer reduces the broadening of peaks 4 and 5.

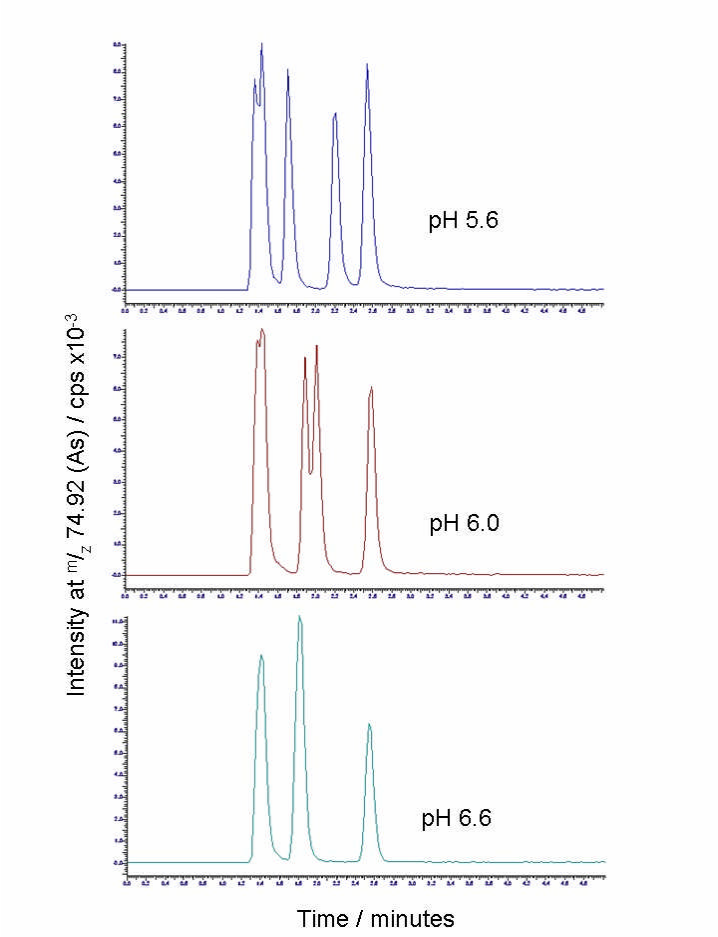

Figure 3.4 Effect of the sodium phosphate buffer pH upon the separation of the five arsenic species

The concentration of phosphate buffer in the mobile phase was also investigated. It is important to use the lowest possible concentration possible while still effectively controlling the pH, so as not to cause any increase in background signal by contamination of the column or detector. A concentration of 10 – 50 mM is usually adequate; relying on the assumption that the volume of injected sample is small and / or the sample is not buffered at very different pH to the mobile phase.[18] The lowest concentration found to give reproducible results was 10.0 mM.

As a result 10.0 mM sodium phosphate buffer was used to control the mobile phase pH at 5.6 in order to achieve arsenic speciation. This was prepared from 94.8 ml

L^{-1} of 0.1 M sodium dihydrogen orthophosphate [$NaH_2PO_4.2H_2O$] and 5.2 ml L^{-1} 0.1 M disodium hydrogen orthophosphate [Na_2HPO_4].

3.3.1.4 Signal enhancement via methanol addition to mobile phase

Organic solvents can be added to the mobile phase to reduce tailing of peaks. Their addition decreases the retention time because they adsorb onto the stationary phase in competition with IPR. This effect is much greater for acetonitrile compared to methanol, since methanol can form hydrogen bonds (hence has potential for greater interaction with the mobile phase).

It is important to note that when using ICPMS as a detector the concentration of organic modifier in the mobile phase must be limited to avoid the build up of carbon on the sample and skimmer cones. The addition of methanol in the mobile phase does however enhance the signal intensity for both arsenic and selenium by a chemical ionisation process. Methanol in the mobile phase introduces carbon containing polyatomic ions into the plasma which lead to an increased population of C^+, ionisation energy (IE) 11.26 eV, and polyatomics. The ionisation of analytes is promoted by electron transfer to carbon atoms with higher IE; therefore an increase in ionisation is possible for elements not completely ionised in the plasma, but with ionisation energy below that of carbon, i.e. 9 – 11 eV. Arsenic (IE 9.82 eV) is only 52 % ionised with standard ICP conditions and selenium (IE 9.75 eV) is just 33 % ionised. 3.0 % ($^v/_v$) methanol has previously been reported as an optimum for this enhancement effect.[28]

To evaluate the addition of methanol to the selected mobile phase composition 0 – 5 % ($^v/_v$) methanol was added to the mobile phase. The optimal mobile phase composition found from method development previously described was used

comprising of 2.5 mM TBAB in 10 mM phosphate buffer at pH 5.6. The separation of the five arsenic species (50 μg As L^{-1}) was conducted in triplicate. Figure 3.5 shows the relationship between peak area and methanol concentration. This shows that the maximum signal enhancement was achieved upon addition of 1.0 % ($^{v}/_{v}$) methanol to the mobile phase, despite the previously quoted 3.0 % optimal.[28] The enhancement achieved was reproducible with an average increase in signal intensity of 94 % for all arsenic species.

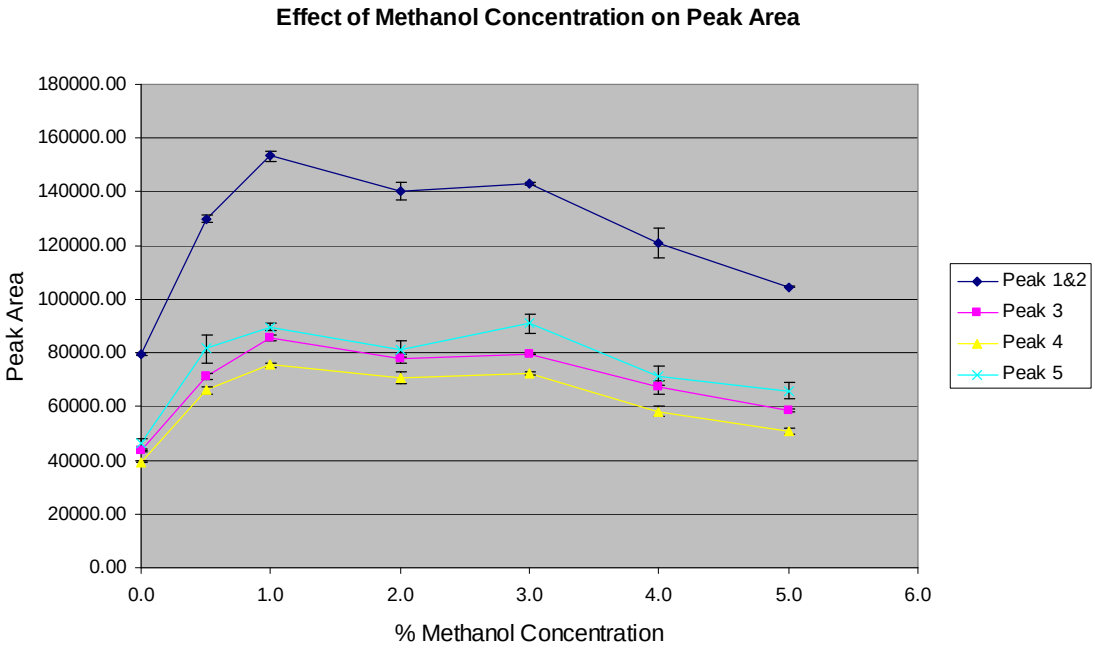

Figure 3.5 Optimisation of sensitivity enhancement produced by addition of methanol to mobile phase

The chromatograms presented in Figure 3.6 also show how the retention of the arsenic species is reduced as the methanol concentration is increased leading to a loss of resolution as the methanol concentration increases from 0.0 % and 5.0 %. It can be seen that using a methanol concentration of 1.0 % ($^{v}/_{v}$) gives the signal enhancement sought after (*cf.* 0.0 % methanol chromatogram) whilst maintaining the resolution of the

species, which is lost at higher methanol concentrations (*cf.* 5.0 % methanol chromatogram).

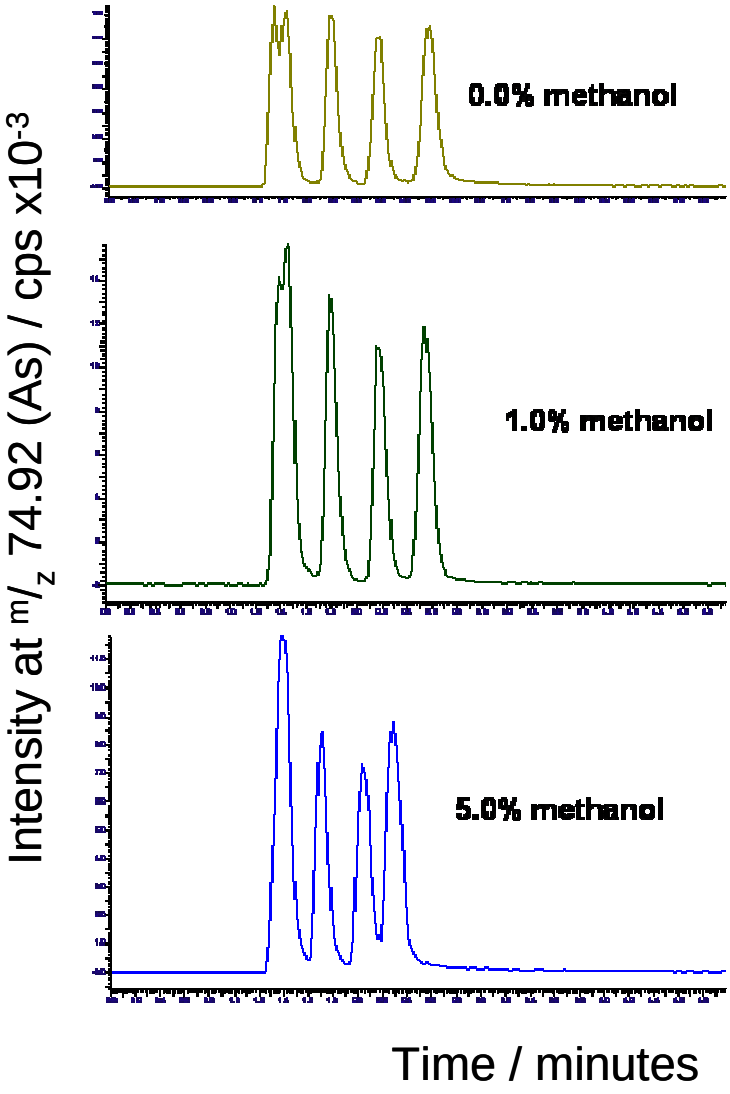

Figure 3.6 Chromatograms produced from optimisation of methanol addition to mobile phase demonstrating enhancement in sensitivity (cps) and separation resolution.

It is important to note that when using organic components in the mobile phase pH measurement is unreliable due to drift of the pH meter.[18] Therefore in the preparation of the mobile phase the pH was measured and adjusted prior to the addition of methanol.

3.3.1.5 Optimised ion-pair chromatographic separation of arsenic species

The final composition of the mobile phase used for arsenic speciation was 2.5 mM TBAB ion-pair reagent with 10.0 mM sodium phosphate buffer at pH 5.6 and 1.0 % ($^{v}/_{v}$) methanol. The optimised separation of the arsenic species is shown in Figure 3.7. Peak identification was achieved by spiking a mixed standard with 100 μg L^{-1} of each individual arsenic species in turn. The order elucidated is in agreement with that consistently described in the literature using various reversed phase columns.[8] It is shown that baseline resolution is achieved for DMA, MMA and As(V). As(III) is unretained under these chromatographic conditions. At the optimal pH for the separation As(III) is a neutral species (pK_a = 9.2) and hence eluted in the void volume.[8] Partial retention for AsB has been achieved, however under these conditions it is not fully resolved from unretained compounds. This was expected with an anionic IPR separation scheme since AsB is zwitterionic and therefore not sufficiently retained under anionic-pairing chromatographic conditions. In order to fully separate As(III) and AsB using anionic-paring LC the pH of the mobile phase should be raised above 9.0, requiring a resin-based column (e.g. Hamilton PRP1), to afford retention of As(III).[29] Quantisation of As(III) and AsB would ideally require a complementary separation scheme. Since this method was to be applied to arsenic speciation in a rice ingestion study it was not essential to achieve retention and separation of AsB. The species of concern in this investigation were the toxic inorganic species contained in the rice samples and the methylated arsenic species (MMA and DMA) often found in human urine samples as a result of exposure to arsenic in the diet.

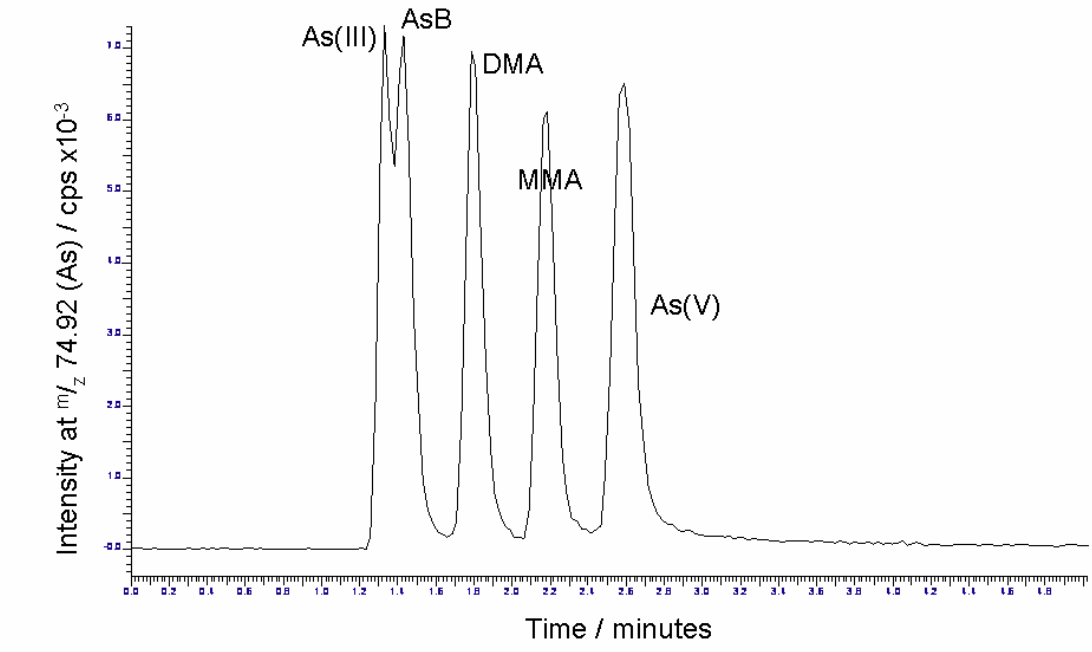

Figure 3.7 Optimised separation of 5 arsenic species. Sample 50 μg As L^{-1} of As(III), AsB, DMA, MMA and As(V). Mobile phase 2.5 mM TBAB, 10.0 mM sodium phosphate buffer, 1.0 % methanol at pH 5.6.

Table 3.4 shows the analytical characteristics of the ion pair LC-ICPMS system. The limit of detection (LOD) was assessed from analysis of a UHQ water blank (n = 10) based upon a signal to noise (S/N) ratio of 3:1 and the limit of quantisation (LOQ) based upon a S/N of at least 10:1 were found for each arsenic species. The precision of the method was calculated from the analysis of a solution containing 15 μg As L^{-1} of each arsenic species. Repeatability was established from RSD of peak area measurements for four replicate measurements performed on the same day. The linearity of the method was assessed by calibration using standard solutions containing 5, 10, 20 and 50 μg As L^{-1} (n = 3). No deviation from linearity was observed with

arsenic concentrations up to 50 μg As L^{-1}. Arsenic recovery from the column was assessed by analysis of a 15 μg As L^{-1} standard for each arsenic species (n = 4). Spike recoveries of individual arsenic species was performed upon a test urine sample with 20 μg L^{-1} As spike. Some example results of the analysis of urine sample with spike additions are shown in Figure 3.8.

The accuracy of the method was evaluated by analysis of freeze-dried human urine certified reference material (CRM) from the National Institute of Environmental Studies (NIES), Japan.[30] The CRM was reconstituted by the addition of 9.57 g of deionised water as recommended (CRM No. 18, NIES, Japan). The results of the CRM analysis were 66.82 ± 1.71 μg As L^{-1} and 44.82 ± 1.53 μg As L^{-1} for AsB and DMA. The certified values are 69 ± 12 μg As L^{-1} for AsB and 36 ± 9 μg As L^{-1} for DMA. The longevity of the column is demonstrated from 342 sample injections being made without any reduction in column efficiency. The column can be regenerated by flushing (and back-flushing) with 100 % acetonitrile, followed by 100 % UHQ water, while disconnected from ICPMS sample introduction.

Table 3.4 Analytical characteristics of ion-pair LC-ICPMS system for arsenic speciation.

	As(III)	**AsB**	**DMA**	**MMA**	**As(V)**
LOD / μg As L^{-1} (n = 10)	0.107	0.084	0.120	0.121	0.101
LOQ / μg As L^{-1} (n = 10)	0.356	0.279	0.399	0.402	0.335
% RSD (n = 4)	5.9	3.9	2.7	5.2	5.4
R^2 (n = 3)	0.9998	0.9999	0.9999	1.0000	0.9993
Recovery / μg As L^{-1} (n = 4)	14.26	14.81	14.36	14.07	13.36
Spike recovery / μg As L^{-1} (n = 3)	15.68	19.51	16.75	18.56	16.24

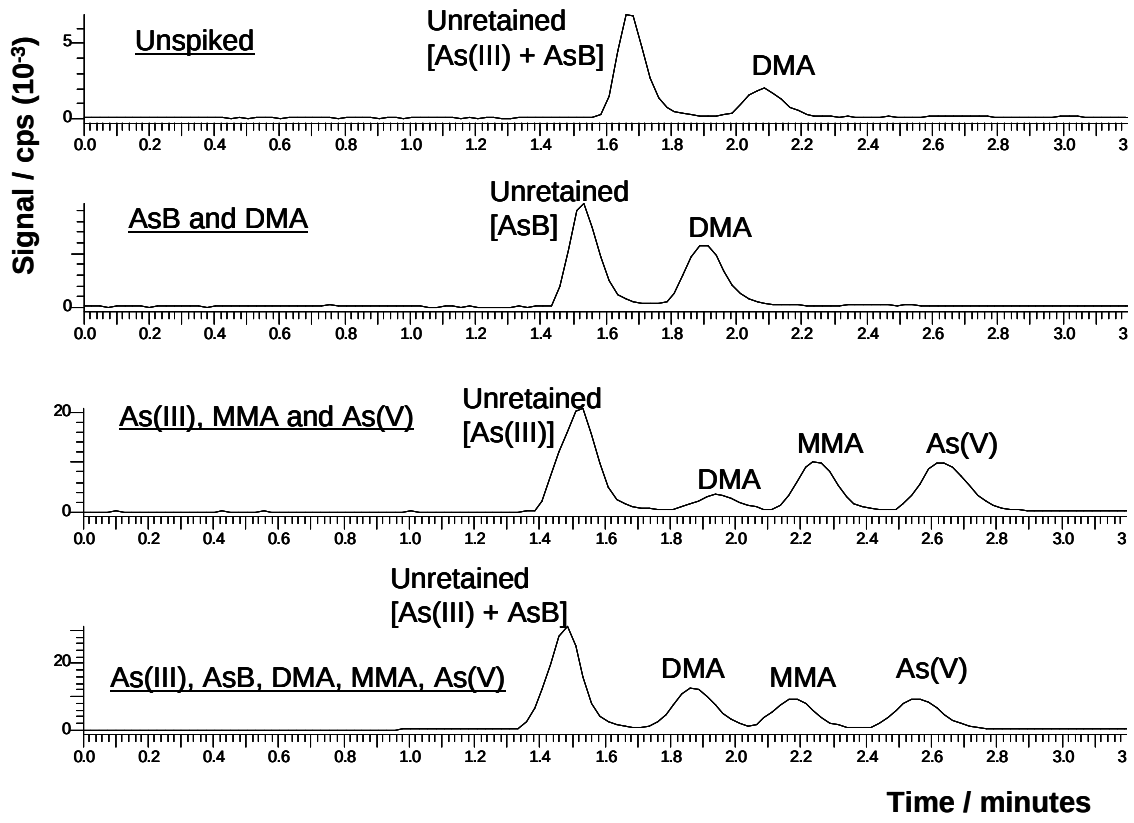

Figure 3.8 Chromatograms produced from the analysis of 5 times diluted urine sample. Underlined are the constituents added as a 20 μg As L^{-1} standard spike.

3.3.2 Application of rapid speciation method to arsenic speciation for human urine samples from an ingestion study

The objective of this study was to demonstrate the applicability of the newly developed rapid arsenic speciation method. A study was carried out in collaboration with Dr. P.I. Haris and E.I. Brima (De Montfort University, Leicester) who designed the investigation to investigate the effect consumption of American long grain rice has on urinary arsenic excretion in a human volunteer. As outlined in the introduction to this

chapter; high levels of arsenic have been reported recently in long grain rice originating from the USA. Arsenic concentrations in American long grain rice have been found to exceed those found in rice from Bangladesh and India, known to suffer from arsenic contamination particularly *via* groundwater.[6] This can present health risks owing to the high amount of rice consumed in the human diet throughout the world.

Selection of the rice sample to be used in the study was based upon the results of a rice survey. Rice was chosen to reflect a wide range of commercially available American rice types, by obtaining examples from different suppliers available from large supermarkets in the city of Leicester, UK.

All procedures followed in the study of rice consumption were in accordance with the ethical guidelines of the Research Ethics Committee, Faculty of Health and Life Sciences, De Montfort University. A volunteer was subjected to a strictly controlled diet for a period of 8 days. During this time the same food was consumed each day with the exception of one meal in the middle of the 8 day period. At this time the rice sample, purchased from a local supermarket, under investigation was ingested. The two diets are presented in Table 3.5 and 3.6. The volunteer refrained from eating fish and seafood for more than one week prior to commencing the diet. The strictly controlled diet was followed for three days in order to build up a background level of urinary arsenic from the same daily food ingestion. On the fourth day the rice sample was consumed, in place of the white bread at dinner. Then the same diet as before was followed for a further four days as samples were taken to investigate the effect of the rice consumption.

Table 3.5 Diet followed by volunteer on each day of the experiment (except for day of rice consumption)

Breakfast	**Lunch**	**Dinner**
Black Tea 3 croissants	White Tea	Meat Okra White Bread 1 Banana Orange juice (1 Litre)

Table 3.6 Diet followed by volunteer on day of rice consumption

Breakfast	**Lunch**	**Dinner**
Black Tea 3 croissants	White Tea	Meat Okra **252g Rice** 1 Banana Orange juice (1 Litre)

Urine samples were collected daily, in the morning, beginning four days prior to the rice ingestion. From the time of ingestion a sample was collected immediately prior to consumption (time 0 hours), 4 hours afterwards, 8 hours afterwards, and then every 8 hours up to 80 hours after ingestion of the rice sample. This resulted in a set of 16 urine samples.

A calibration was performed using the five arsenic species standard reference materials over the range 5.0 to 50.0 μg L^{-1}. Good linearity across this concentration range was achieved, as shown in Figure 3.9.

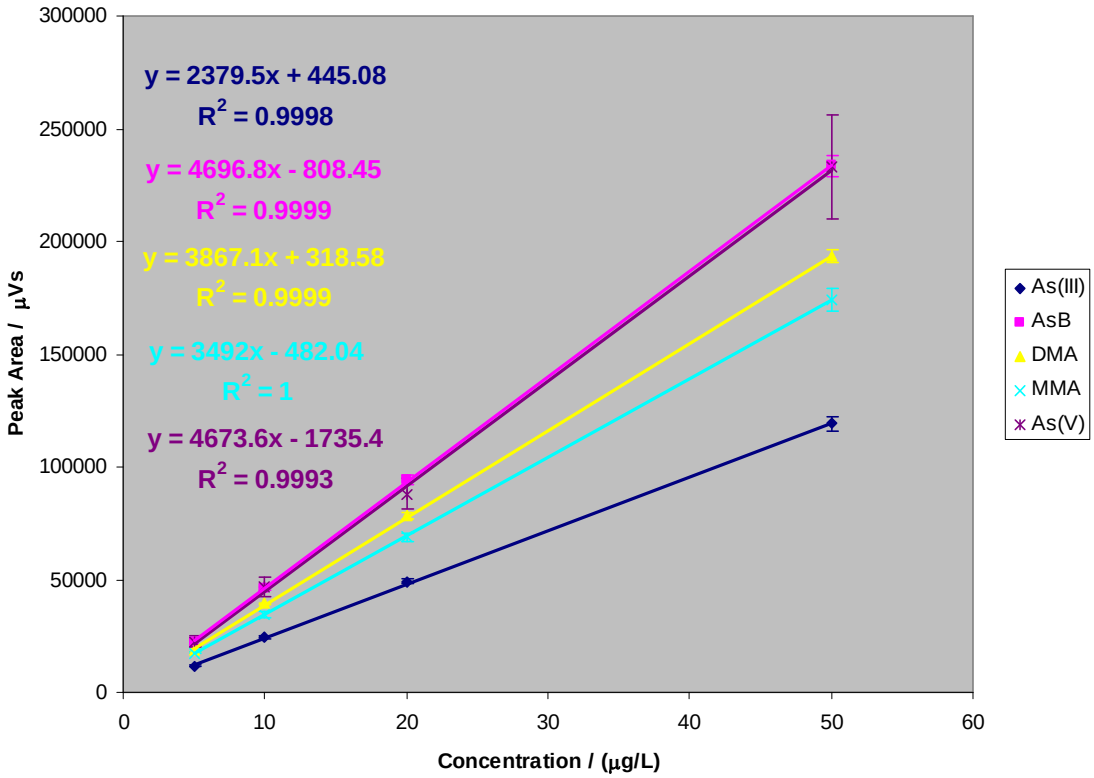

Figure 3.9 Calibration of arsenic certified standards over the range 5.0 to 50.0 µg As L^{-1} for the ingestion study.

The results of the speciation analysis on this set of urine samples are presented in Figure 3.10. These results show that although the volunteer adhered to a very strict diet, there was still a significant background arsenic concentration excreted via urine. This is most significant for DMA, which has higher levels throughout the study in comparison to all other species. Unretained compounds including AsB and As(III) have very low concentrations throughout the study and are unaffected by the ingestion of rice. However consumption of the rice did result in a clear increase in arsenic concentration in the urine. The most dramatic effect was observed for DMA concentration. It has been previously reported by Williams *et al.* that USA long grain rice contains DMA, as well as As(V) and As(III) and that the DMA level of American long grain rice was

particularly high.[6] A further finding of this work was that as well as the increase in DMA, a lower level of As(V) was also detected in the urine after rice ingestion. It is possible that the higher level of DMA detected compared to As(V) could be due to methylation of inorganic arsenic in the human body *via* consecutive reduction and oxidative methylation steps to produce either MMA or DMA species. DMA is the most common species for indicating arsenic exposure, since it generally comprises 60 – 80 % of all arsenic excreted in human urine. MMA and AsB concentration was not effected by ingestion of rice and remained at a low background level throughout the study. DMA was found to be rapidly excreted from the human body, with its concentration rapidly returning to background levels within 16 hours.

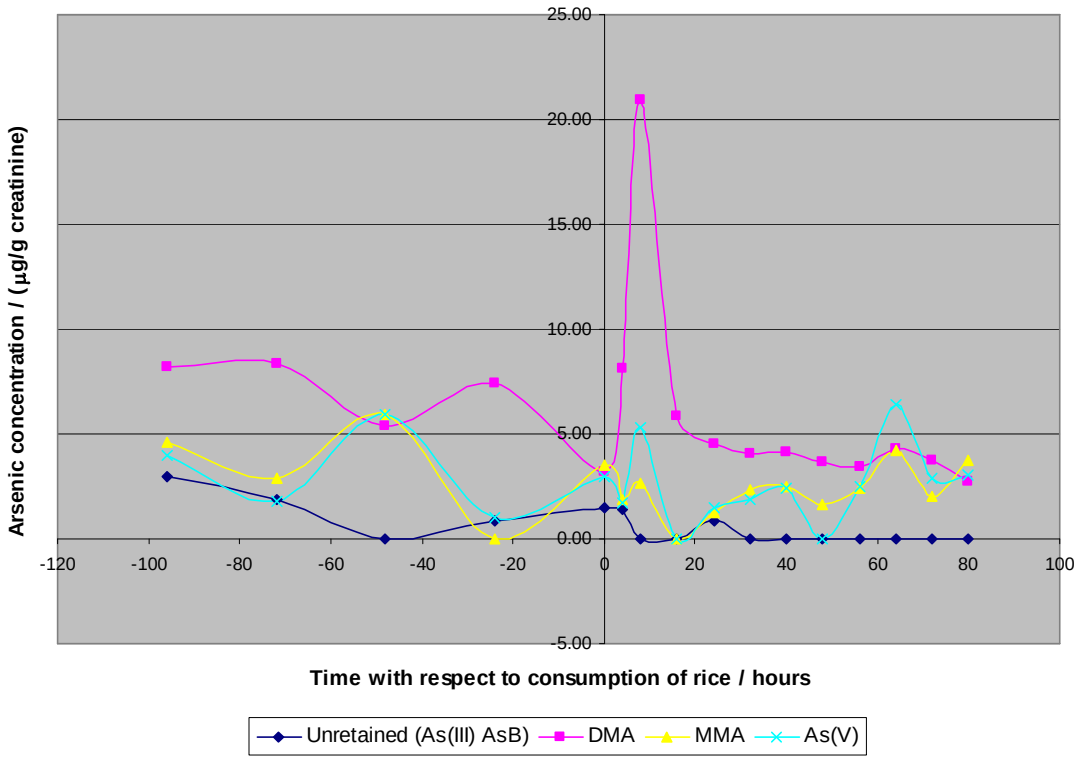

Figure 3.10 Arsenic concentration in urine samples from ingestion study on the consumption of American long grain rice.

A sample of each food contained within the controlled diet was digested and analysed for total arsenic concentration. A second sample of all foods was taken for arsenic speciation analysis and total arsenic determination following extraction. Very low arsenic levels were found in the rest of the food samples with only two species found; being DMA most commonly and As(V) rarely. The arsenic concentrations were approaching the LOD and significantly below the LOQ. However the presence of arsenic is likely to be partially responsible, along with environmental exposure, for the background arsenic concentration found in the urine samples throughout the study. The results of this analysis showed that as expected rice provides the greatest source of arsenic out of all the foods included in the study. Arsenic is present as As(V) and DMA in the uncooked long-grain rice studied at 0.63 and 0.19 μg As g^{-1} respectively. 0.40 μg As g^{-1} was recovered in the column void volume and the contribution corresponding to As(III) would need to be confirmed. This remains unaffected by the cooking process as shown by the recovery of 0.62 μg As g^{-1} As(V), 0.47 μg As g^{-1} DMA and 0.36 μg As g^{-1} in the void volume.

3.4 Conclusions

A rapid speciation method has been described which involved a new application of a Chromolith™ HPLC column for ion-pair chromatography with ICPMS detection. Separation time for arsenic speciation has been reduced to below 3 minutes. Superior LOD *cf.* rapid RP-IPC-ICPMS arsenic speciation methods were obtained.[9] Good precision and accuracy have been achieved and the feasibility of the method has been demonstrated by the analysis of urine and extracted food samples in an ingestion study. We have shown for the first time that consumption of American long-grain rice results

in significant increase in urinary DMA excretion, which supports previous findings that rice contains a high level of arsenic.[7] This method presents the ability to conduct rapid arsenic speciation in clinical and environmental studies. The reduction in separation time affords an increase in sample throughput, reduction in detector idle time and therefore reduction in cost of analysis.

3.5 References

1 B. Welz, *Spectrochim. Acta, Part B*, 1998, **53**, 169.

2 B. Paull and P.N. Nesterenko, *Trends Anal. Chem.*, 2005, **24**, 295.

3 A.H. Smith, C. Hopenhayn-Rich, M.N. Bates, H.M. Goeden, I. Hertz-Picciotto, H.M. Duggan, R. Wood, M.J. Kosnett and M.T. Smith, *Environ. Health Perspect.*, 1992, **97**, 259.

4 A.-L. Lindberg, W. Goessler, E. Gurzau, K. Koppova, P. Rudnai, R. Kumar, T. Fletcher, G. Leonardi, K. Slotova, E. Gheorghiu and M. Vahter, *J. Environ. Monit.*, 2006, **8**, 203.

5 R.A. Schoof, L.J. Yost, J. Eickhoff, E.A. Crecelius, D.W. Cragin, D.M. Meacher and D.B. Menzel, *Food Chem. Toxicol.*, 1999, **37**, 839.

6 P.N. Williams, A.H. Price, A. Raab, S.A. Hossain, J. Feldmann and A.A. Meharg, *Environ. Sci. Technol.*, 2005, **39**, 5531.

7 P.N. Williams, A. Raab, J. Feldmann and A.A. Meharg, *Environ. Sci. Technol.*, 2007, **41**, 2178.

8 Z. Gong, X. Lu, M. Ma, C. Watt and X.C. Le, *Talanta*, 2002, **58**, 77.

9 S. Wangkarn and S.A. Pergantis, *J. Anal. At. Spectrom.*, 2000, **15**, 627.

10 P.A. Gallagher, C.A. Schwegel, X. Wei and J.T. Creed, *J. Environ. Monit.*, 2001, **3**, 371.

11 S. Rattanachongkiat, G.E. Millward and M.E. Foulkes, *J. Environ. Monit.*, 2004, **6**, 254.

12 E. Schmeisser, W. Goessler, N. Kienzl and K.A. Francesconi, *Analyst*, 2005, **130**, 948.

13 M. Chausseau, C. Roussel, N. Gilon and J.-M. Mermet, *Fresenius J. Anal. Chem.*, 2000, **366**, 476.

14 J.A. Brisbin, C. B'Hymer and J.A. Caruso, *Talanta*, 2002, **58**, 133.

15 S. Garcia-Manyes, G. Jimenez, A. Padro, R. Rubio and G. Rauret, *Talanta*, 2002, **58**, 97.

16 A. Raab, H.R. Hansen, L. Zhuang and J. Feldmann, *Talanta*, 2002, **58**, 67.

17 G.F. Pearson, G.M. Greenway, E.I. Brima and P.I. Haris, *J. Anal. At. Spectrom.*, 2007, **22**, 361.

18 L.R. Snyder, J.J. Kirkland and J.L. Glajch, *Practical HPLC Method Development*, Wiley-Interscience, New York, 1997.

19 C. Hopenhayn-Rich, M.L. Biggs, A.H. Smith, D.A. Kalman and L.E. Moore, *Environ. Health Perspect.*, 1996, **104**, 620.

20 M. Vahter, G. Concha, B. Nermell, R. Nilson, F. Dulout and A.T. Natarajan, *Toxicol. Pharm.*, 1995, **293**, 455.

21 A.L. Hinwood, M.R. Sim, N. de Klerk, O. Drummer, J. Gerostamoulos and E.B. Bastone, *Environ. Res.*, 2002, **88**, 219.

22 S.W.A. Rmalli, *Arsenic speciation in foodstuffs from Bangladesh and a method for arsenic removal from water* (M.Phil. Thesis), De Montfort University, Leicester, 2004.

23 E.I. Brima, P.I. Haris, R.O. Jenkins, D.A. Polya, A.G. Gault and C.F. Harrington, *Toxicol. Appl. Pharmacol.*, 2006, **216**, 122.

24 J. Wang, E. Harald Hansen and B. Gammelgaard, *Talanta*, 2001, **55**, 117.

25 X.C. Le and M. Ma, *J. Chromatogr. A*, 1997, **764**, 55.

26 K. Sathrugnan and S. Hirata, *Talanta*, 2004, **64**, 237.

27 A. Huerga, I. Lavilla and C. Bendicho, *Anal. Chim. Acta*, 2005, **534**, 121.

28 E.H. Larsen and S. Sturup, *J. Anal. At. Spectrom.*, 1994, **9**, 1099.

29 P. Thomas and K. Sniatecki, *J. Anal. At. Spectrom.*, 1995, **10**, 615.

30 J. Yoshinaga, A. Chatterjee, Y. Shibata, M. Morita and J.S. Edmonds, *Clin. Chem.*, 2000, **46**, 1781.

4 Development of sample introduction for interfacing microfluidic chips with ICPMS. Part I Evaporation chamber

4.1 Introduction

Spray chambers have a number of functions; the most important of which is to act as a low-pass droplet-size filter. Distribution in droplet size of nebulised sample reduces the analytical precision. Only the smallest droplets are allowed to proceed to the plasma, while any droplets in excess of 10 μm are removed to waste. The spray chamber also helps to dampen noise originating from the peristaltic pump, used to introduce the sample solution. This is achieved by the interaction of several processes; including recombination, inertial impaction, evaporation, charging / discharging and the decay of turbulence.[1] Spray chambers are discussed in Section 1.1.2.2.

The main disadvantage associated with spray chambers is poor transport efficiency, since a large proportion of the sample is removed to waste. This reduces the sensitivity of the analysis typically resulting in less than 5 % of the sample finally reaching the plasma.[2] Further disadvantages are flicker / noise pulses, matrix effects (owing to aerosol transport and filtering), memory effects and long equilibrium times (in the order of 1 – 2 minutes).

Traditional designs include the double pass (a.k.a. Scott) and cyclonic chambers (shown in Figure 1.6). Scott double pass chambers have an internal volume in the region of 100 cm^3 and force the aerosol to follow a complicated path, which very effectively removes larger droplets in excess of 15 – 20 μm. However, they consequently suffer from low analyte transport efficiency and long wash out times. Cyclonic spray chambers have been found to offer an improvement in analytical figures of merit.[3, 4] This improvement stems from increased transport efficiency to the plasma, less severe matrix effects (for inorganic species) and shorter wash out times. These advantages are a result of a simpler aerosol trajectory and the lower internal volume (30 – 40 cm^3) *cf.* the double pass chambers (~ 100 cm^3). Nevertheless, cyclonic chambers do generally produce a coarser tertiary aerosol than the double pass design.[2]

4.1.1 Low flow liquid sample introduction

Extensive reviews considering the elemental analysis of liquid micro-samples have been presented by Todolí and Mermet.[5, 6] The introduction of low liquid sample flow rates using conventional sample introduction for ICPMS results in a sharp decrease in sensitivity. This can be explained by the dramatically reduced amount of analyte present and poorer transport efficiency since conventional nebulisers produce course aerosols when operated a flow rates in the order of tens of microlitres.[6] Low sample consumption systems use components with reduced critical dimensions. Nebulisers have a reduced cross sectional area at the liquid exit, a thinner central capillary and occasionally a smaller gas annulus area. Usually the sample delivery rate is adjusted in order to obtain a signal plateau but a concentric nebuliser is still effective at low flow rates. A range of micro-nebulisers have been developed for the analysis of micro sample volumes, including micro concentric nebulisers (MCN) and the microflow

ultrasonic nebuliser.[7] Some commercial examples include the MicroMist,[8] MiraMist[9] and PFA micronebuliser.[10] A MCN has a reduced inner volume, which in turn reduces washout times. The efficiency of a MCN is high at low flow rates since they have a smaller diameter hence requiring a smaller sample volume, but making them more prone to blockages at their tip. Spray chambers have simply been reduced in volume while maintaining the same design of operation. Mini cyclonic spray chambers (e.g. Cinnabar, Glass Expansion, Australia) have a reduced inner volume of 20 cm^3 *cf.* typical cyclonic chambers 30 – 40 cm^3. The Cinnabar has a marginal increase in signal in comparison to a double pass spray chamber with significantly reduced wash out times (70 seconds, *cf.* 120 seconds) and matrix effects.[5] The wash in / out times are critical for preserving resolution of separations in speciation analysis.[11] A MCN and miniaturised cyclonic spray chamber has proven a suitable method of sample introduction for hyphenated techniques, such as capillary electrophoresis (CE) – ICPMS.[12] This chamber was designed specifically for interfacing CE with ICPMS with low internal volume of 21.0 ml and flow spoiler (to disrupt re-circulatory flow) in order to minimise band broadening.

4.1.2 Total liquid sample introduction

Total consumption of liquid samples would give the advantage of reducing sample consumption, volume of waste produced (particularly significant for toxic and radioactive wastes) and memory effects.[6] These advantages are extremely beneficial in cases in which the amount of sample is limited: semiconductors, clinical, geological and on-chip technology.[2] Total sample consumption also facilitates the coupling of low flow rate separations (e.g. μHPLC, CE) with ICPMS.

Direct injection nebulisers, including the DIN and DIHEN (described in Section 1.1.2.3) provide a method for achieving total liquid sample introduction. Consequently sensitivity and LOD can be significantly improved by a factor of 10 compared with a MCN with cyclone spray chamber.[13] However comparison of MCN with DIHEN has proved that the MCN coupled to either a Scott double pass or cyclonic spray chamber offers improved reproducibility and precision.[14] This has also been investigated in μLC-ICP-MS[15] and CE-ICP-MS systems,[8] and again MCN have proved superior to direct injection nebulisation.

Very low liquid sample flow rates allow simplification of the traditional spray design without the need for an impact bead, drain or complex aerosol trajectory. The internal volume can also be reduced resulting in shorter rinse times and less memory effects. Therefore the conventional chamber can be removed allowing the entire sample to enter the plasma. For these reasons single pass spray chambers have been investigated in the analysis of micro samples. They benefit from a low inner volume and the advantage of providing a simple aerosol trajectory towards the plasma. They can offer an improvement to cyclonic chambers when operated with low liquid flow rates. Matrix effects for organic and inorganic (nitric acid) matrices can be reduced. This is based upon the promotion of solvent evaporation when the gas is not saturated with solvent vapour, i.e. in cases of low liquid to gas ratio (5 – 70 μl min^{-1} liquid; 0.7 L min^{-1} Ar nebuliser gas). Saturation of 0.7 L min^{-1} Argon nebuliser gas at 40 ^{o}C requires 36 μl min^{-1} of water.[4] Upon reaching saturation evaporation is not efficient; therefore at 20 – 200 μl min^{-1} sample flow rate evaporation and filtration occurs in the spray chamber. For flow rates below 20 μl min^{-1} it should therefore be possible to achieve complete evaporation and 100 % transport efficiency into the plasma. Several factors

influence solvent evaporation including the volatility of the solvent, droplet diameter (higher rate for smaller droplets), droplet composition (higher salt concentrations reduce rate), the temperature difference between droplet surface and surrounding gas and the velocity at which the droplet environment is renewed.[2] A CE-ICPMS interface using a single pass spray chamber design has been developed by Prange and Schaumlöffel.[16] this interface has now been commercialised (CEI-100, CETAC Technologies, Omaha, Nebraska, USA).

4.1.3 Torch integrated sample introduction system

Todolí and Mermet have performed a simplification of sample introduction by studying single pass spray chambers operated with low liquid flow rates.[4, 17, 18] A design based upon incorporating a spray chamber into the cavity within the torch has been suggested, termed the torch integrated sample introduction system (TISIS). Modification of the commercial ICPAES torch design allows it to be directly interfaced to the MCN. This chamber has been found to improve sensitivity and reduce sample washout times (i.e. increase sample throughput) for the analysis of very low flow (below 20 μl min^{-1}) liquid samples by ICPAES. Matrix effects from sodium, water or HNO_3 were reduced and shorter equilibrium times achieved.

TISIS has been considered to be an intermediate between direct injection nebulisers (e.g. DIN, DIHEN) and conventional sample introduction with a spray chamber.[17] Two important characteristics of the primary aerosol must be achieved in order to obtain good results with the TISIS. Firstly the nebuliser must provide an aerosol which is as fine as possible to promote efficient solvent evaporation and minimise inertial losses. Secondly the aerosol path towards the plasma must be as

simple as possible. The total aerosol liquid volume is another important factor which governs the transport processes occurring in the TISIS chamber.[18] According to thermodynamic calculations at a given gas flow rate there is a corresponding liquid flow rate at which total solvent evaporation is achieved.[19] Solvent evaporation is promoted at the high gas to liquid ratio provided from introducing very low liquid flow rates. There will therefore be an optimal time period that the primary aerosol resides in the chamber before entering the plasma. Experimentally this will depend on the size (internal volume) of the chamber. The evolution of droplet diameter with time as the solvent evaporates from its surface can be described according to Equation 4.1.[18]

$$d^3 = d_0^3 - Et \qquad \textbf{Equation 4.1}$$

Where d is the droplet diameter at time t, d_0 is the initial droplet diameter and E is the evaporation factor given by Equation 4.2.[18]

$$E = \frac{48 D_v \sigma p_s M^2}{(\rho R T)^2} \qquad \textbf{Equation 4.2}$$

Where D_v is the diffusion coefficient for solvent vapour, σ the solvent surface tension, p_s the saturated vapour pressure, M the molecular mass of the solvent, ρ the solvent density, R the gas constant and T the absolute temperature. Equations 4.1 and 4.2 rely on simplifying assumptions, the most important of which are that the aerosol inside the cavity is under isothermal conditions and its flow regime is laminar. Additionally droplet coalescence is not considered since the liquid flow rate is very low. It has been calculated from Equations 4.1 and 4.2; at the residence time (t = 1.7) and operating temperature of *ca.* 40 °C, droplets below 8.2 μm reach diameters of less than 8.0 μm and are hence ideal for introduction into the plasma.[18] It is therefore obvious that the

flow within the chamber is more complex, and the aerosol has a significantly longer residence time within the chamber allowing evaporation of the larger droplets.

4.1.4 Aim

The aim of this work is to develop an evaporation chamber to facilitate the introduction of very low liquid flow rates into ICPMS. The reasoning behind this is to avoid the sample losses associated with traditional spray chambers and achieve as high as possible transport efficiency of sample to plasma. This design can then be applied to a low flow sample introduction system designed specifically for interfacing microfluidic chips. The evaporation chamber will be based upon work presented by Todolí and Mermet on a TISIS for ICPAES. Modification of the chamber which has been integrated into the vertically aligned ICPAES torch will be undertaken in order to make the design suitable for coupling with the horizontally aligned ICPMS torch. The chamber will then be optimised in order to achieve the best analytical figures of merit.

4.2 Experimental

4.2.1 Instrumentation

The PlasmaQuad II+ (VG Elemental) ICPMS was used for development and optimisation of the evaporation chamber. The final evaluation of the optimised chamber was conducted on the Elan DRC II ICPMS. The ICPMS instruments were optimised and monitored in terms of performance daily (Section 2.1.1) and standard operating conditions for the instruments were used (Table 2.1 and 2.2). The nebuliser gas was optimised based upon maximum signal intensity.

A MicroMist MCN (Glass Expansion, Australia) was used throughout and a miniaturised jacketed cyclonic spray chamber (Cinnabar, Glass Expansion, Australia) was used for reference purposes to evaluate evaporation chamber performance. The Cinnabar was cooled to 4 ^{o}C using a Neslab mini-chiller (Life Sciences International Ltd., Basingstoke, UK) for PlasmaQuad II+ or refrigerating circulating bath (Model 9106, PolyScience, Illinois, USA) with Elan DRC II; as described in Section 2.1.1.3.

Liquid flow for optimisation of the chamber was delivered by the peristaltic pump dedicated to the PlasmaQuad II+ (MiniPuls3, Gilson Inc., Middleton, USA). The flow rate (μl min^{-1}) was calibrated for Orange / Red pump tubing (0.19 mm i.d.) from the pump speed (rev min^{-1}) this resulted in 4.0 μl rev^{-1} (n = 11); see Table 4.1. This was used to convert the desired liquid flow rates into pump speeds for optimisation and operation of the evaporation chamber.

Table 4.1 Liquid flow rates provided by MiniPuls3 peristaltic pump (Gilson Inc., Middleton, USA) with Orange / Red pump tubing (0.19 mm i.d., PVC, Cetac Technologies, Omaha, USA).

Pump speed / rev min^{-1}	Volume / μl	time / s	time / min	flow rate / μl min^{-1}	Pump rate / μl rev^{-1}
4.00	100	372	6.21	16.1	4.0
4.00	100	380	6.34	15.8	4.0
4.00	100	387	6.45	15.5	3.9
5.00	100	319	5.32	18.8	3.8
5.00	100	303	5.05	19.8	4.0
10.00	100	156	2.60	38.4	3.8
10.00	100	148	2.47	40.5	4.0
10.00	100	156	2.59	38.6	3.9
10.00	100	137	2.28	43.8	4.4
10.00	100	140	2.33	42.9	4.3
10.00	250	350	5.83	42.9	4.3
				Average	**4.0**
				Std Dev	0.2
				% RSD	**5.2**

A syringe pump (Bioanalytical Systems Ltd., Kenilworth, UK) was used with the Elan DRC II for the purpose of evaluation of the optimised evaporation chamber. This allowed more acurate control of the liquid flow rate and eliminated the potential for pulsation from using the instrumental peristalic pump at very low flow rates. Clean single use 1 ml disposable syringes were used with this pump. The instruments integrated peristaltic pump was used for investigation of the chamber's rise / wash out times to facilitate the switching between the standard and rinse solutions. The pump was calibrated with small i.d. (orange / red) pump tubing as shown in Figure 4.1.

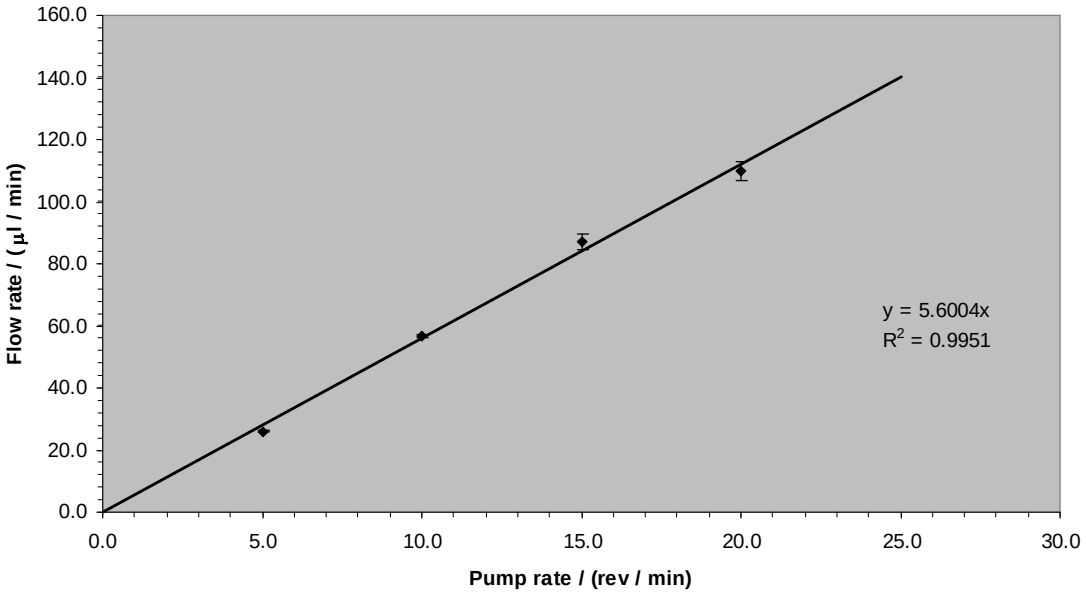

Figure 4.1 Calibration of Elan DRC II integrated peristaltic pump with orange / red pump tubing (Elkay Laboratory Products Ltd., Basingstoke, UK). Time taken (seconds) to deliver 100, 250 and 500 µl solution measured.

4.2.2 Reagents

Optimisation of the evaporation chamber dimensions was conducted using the PlasmaQuad II+ tune solution consisting of 10 μg L^{-1} Be, Co, In, Ce and U in 2 % HNO_3. Evaluation of the optimised chamber was conducted using the Elan DRC II tune solution (comprising of 1 μg L^{-1} Mg, Ce, In, U and 10 μg L^{-1} Ba in 2 % nitric acid) and a multielement standard solution (containing 10 μg L^{-1} Mg, Ce, In, U, As, Se, Mn, Pb, Ni, Mo, Cu, Zn, Co, Cr and 100 μg L^{-1} Ba in 2 % nitric acid). 0.1 % Triton X-100 (Super Purity Solvent™, Romil Ltd., Cambridge, UK) in UHQ water was used in order to clean and condition the chamber, typically aspirated during instrument warm up if the chamber had not been used for some time.

4.2.3 Procedures

4.2.3.1 Fabrication of evaporation chamber

The evaporation chambers were fabricated in house by the chemistry department's glass blowing workshop. Silica tubing with 22 mm i.d. was used for the main body of the chamber. This was narrowed to 14 mm i.d. silica tubing over 10 mm which was fitted with a ground glass cup joint, to fit with the commercial ground glass ball joint on the ICPMS torch. A schematic of the evaporation chamber is shown in Figure 4.2.

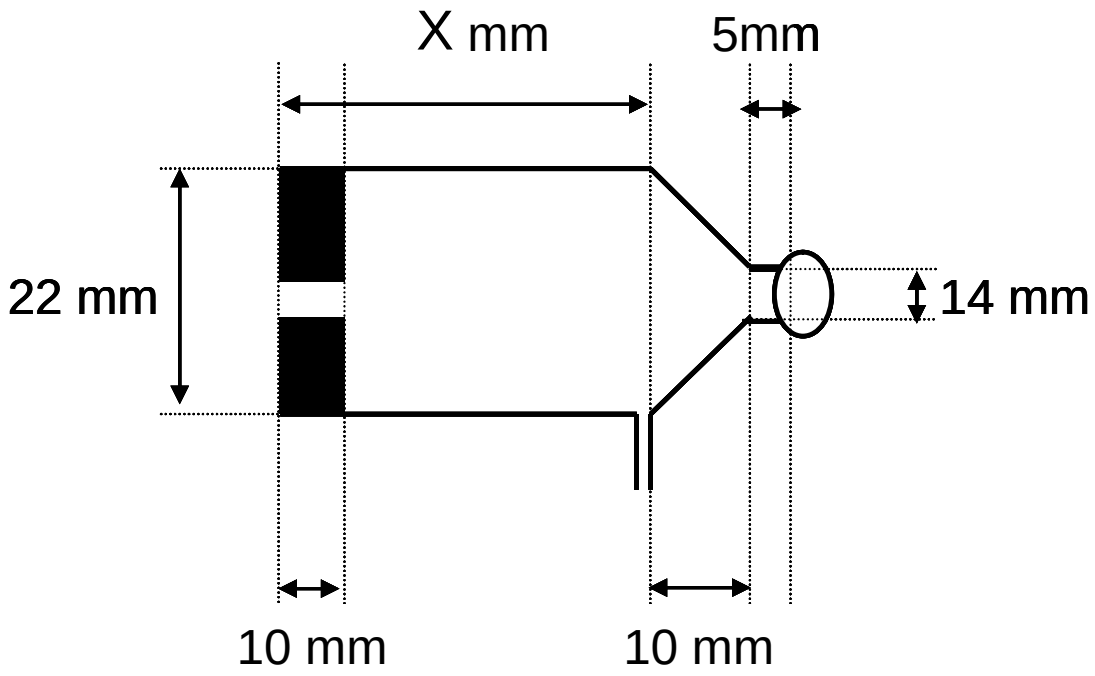

Figure 4.2 Schematic of evaporation chamber with all constant dimensions annotated. Length of main body (X) was varied in order to optimise chamber.

It was decided immediately to use a separate chamber, rather than modifying the existing torch, for ease of changing the sample introduction system. This is the reason for using a ground glass ball and cup joint as used in commercial spray chambers. A similar design was adopted by Mermet *et al.* concurrent to this work.[20] The narrow portion of the chamber (14 mm i.d.) was kept as short as possible to avoid increasing the distance the aerosol has to travel prior to entering the torch injector and therefore plasma. Initially the design included a drain which was fitted at the end of the main body so any liquid recondensation occurring within the chamber could be removed to waste. The drain consisted of a short narrow piece of silica tubing with suitable outer diameter to fit with drain pump tubing, see schematic (Figure 4.2). In the final design this drain was not included. A gas tight seal to hold the MCN in place at the entrance of the chamber was constructed from PTFE by the engineering workshop within the

chemistry department. This fitted tightly into the end of the silica chamber with a rubber 'O' ring ensuring a gas tight seal. A further two 'O' rings were used within a central hole through the PTFE into which the MCN could be inserted and held securely.

4.3 Results and discussion

4.3.1 Modification of TISIS for ICPMS

Todolí and Mermet's original TISIS design utilised a cavity which was an integral part of the silica torch. However the final chamber was made from polyethylene and added to the base of the torch. The reasons for this are that the torch cavity had a limited diameter of 14 mm and a square end at which a PTFE seal was used to hold the injector in place. This increased the turbulence at the exit of the chamber, as demonstrated by the arrows in Figure 4.3.

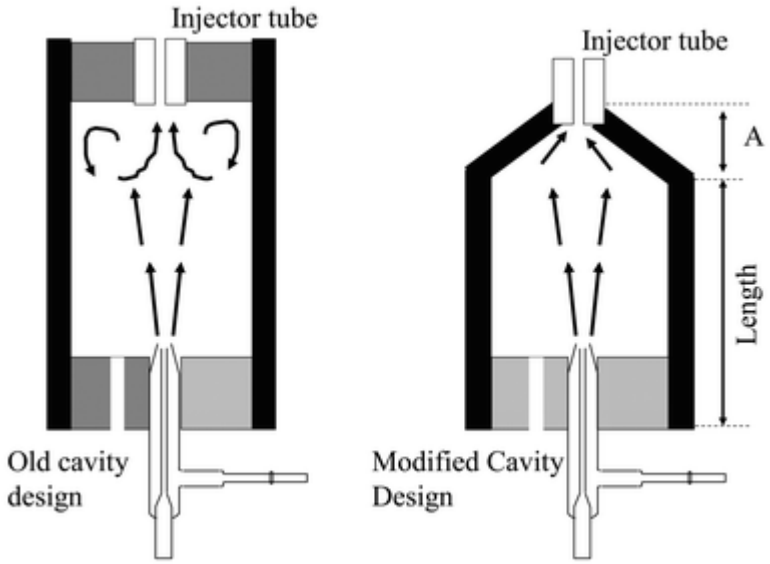

Figure 4.3 Comparison between the old and new TISIS evaporation chambers.[18]

A higher inner diameter of the chamber facilitates the expansion of the primary sample cone and reduces impact losses.[17] Using a conical end to the chamber and a larger internal diameter resulted in greater sensitivity and easier rinsing of the chamber, decreasing the wash out times (20 – 30 seconds, *cf.* 80 – 90 for Cinnabar)[18]. The final TISIS design utilised by Mermet *et al.* for ICPAES is shown schematically in Figure 4.4.

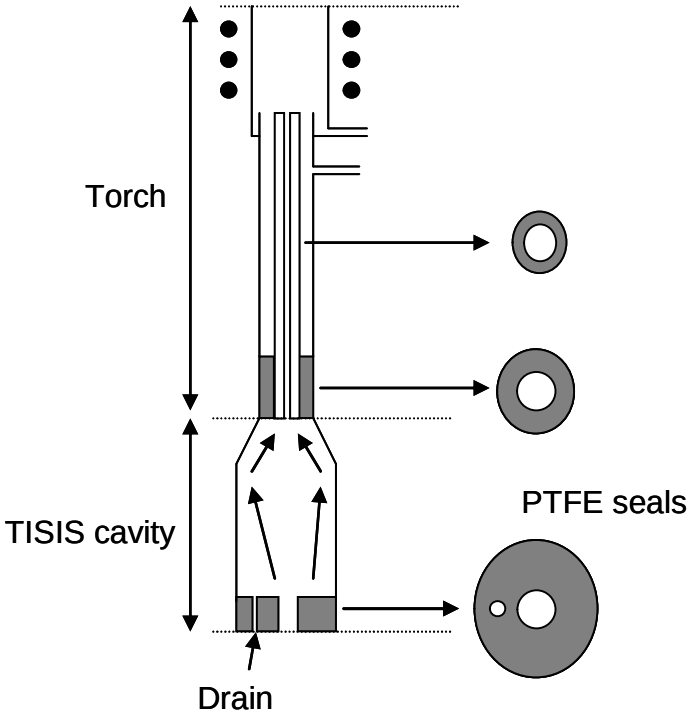

Figure 4.4 Todolí and Mermet TISIS design for ICPAES.[4, 17, 18]

For this work the TISIS design and dimensions were adopted and re-orientated into the horizontal position. The drain was relocated to a side wall for removal of any liquid build up to waste. This resulted in the design shown in Figure 4.5. The fabrication of the evaporation chamber is described in the procedures (Section 4.2.3.1).

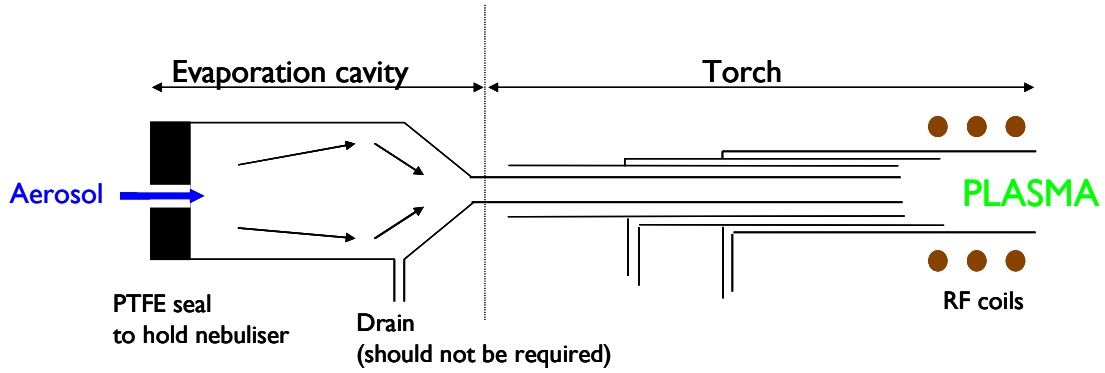

Figure 4.5 Schematic of evaporation chamber designed for use with an existing commercial horizontally aligned ICPMS torch.

4.3.2 Initial test of evaporation chamber with MicroMist nebuliser

As an initial test of the evaporation chamber the instrument was operated with typical conditions likely to be used in final application. The liquid flow was 20 µl min^{-1} of 10 µg L^{-1} tune solution with an optimal nebuliser gas flow rate of 0.98 L min^{-1}. The set up within the ICPMS instrument torch box can be seen in Figure 4.6. The test yielded approximately 50 000 cps for indium ($^{m}/_{z}$ 114.9), which was reasonably stable over a 30 minute period (< 5 % RSD). Primary observations of the chamber during operation showed that droplets were formed in the chamber initially when the instrument was first switched on. This is thought to be due to the chamber dimensions not being optimised, therefore impaction occurs against the chamber walls (particularly the front of the chamber). The recondensation was more prevalent initially since the chamber had not warmed up to normal operating temperature (30 – 35 °C within the torch box).

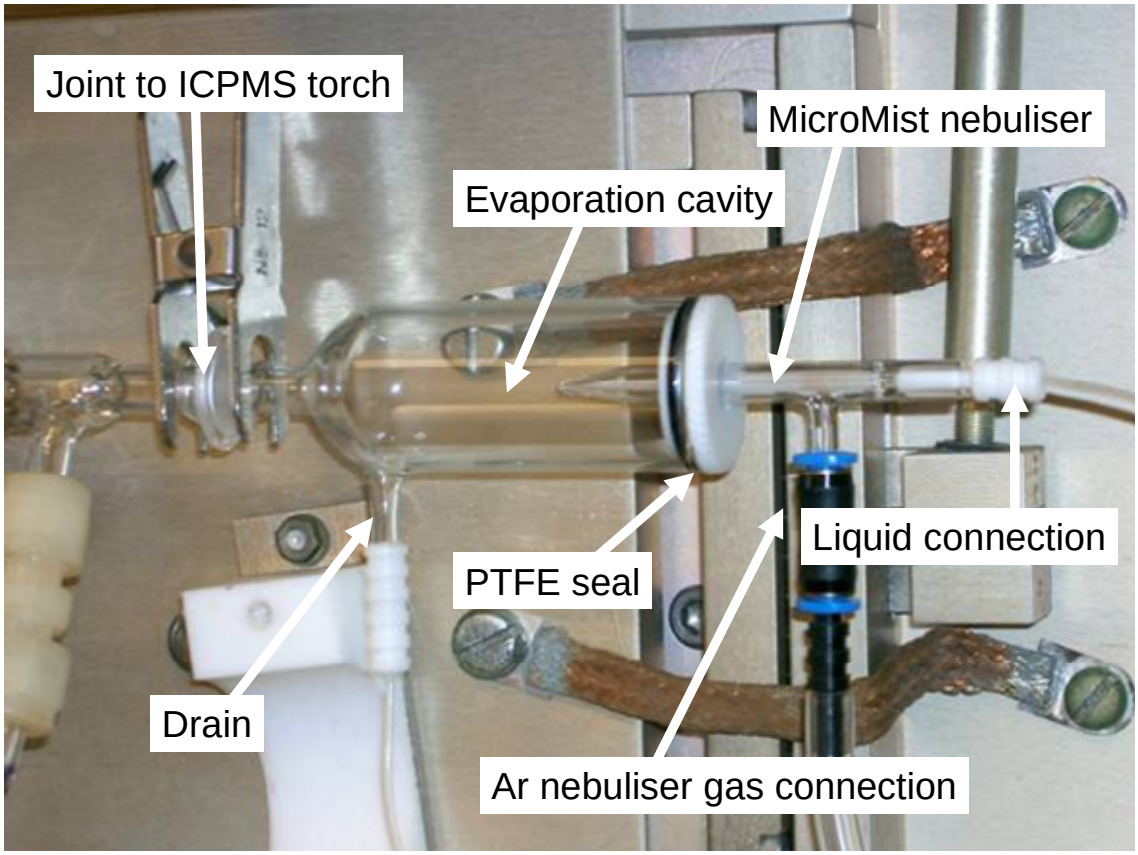

Figure 4.6 MicroMist MCN with evaporation chamber installed within PlasmaQuad II+ ICPMS torch box.

The addition of 0.1 % Triton X-100 to the tune solution was found to help reduce liquid recondensation and droplet formation by reducing the surface tension of the liquid. However initial condensation cleared unaided once the chamber had been allowed to warm during operation. The chamber then remained dry during operation for long periods (in excess of 4 hours). Todolí and Mermet describe the operation of the chamber as achieving efficient evaporation of the primary aerosol so that 57 % of the droplets are below 8 μm and hence contribute efficiently to the signal production.[18] This is true for a MicroMist MCN with 20 μl min^{-1} liquid flow rate and 0.7 L min^{-1} gas flow rate. However the remaining 43 % of the sample aerosol have droplets that are over 8 μm and consequently are lost by impaction against the chamber walls. The fact

that the chamber remains dry during operation suggests that this sample volume is evaporated from the chamber walls and introduced into the plasma.

It was anticipated that the use of a peristaltic pump could introduce pulsation into the analyte signal, especially since it was being operated at low liquid flow rates (in the order of 5.00 rev min^{-1}). However there was little pulsation found in the signal, therefore peristaltic pumping was suitable for sample introduction, at least for the optimisation of the evaporation chamber.

4.3.3 Multivariate optimisation of the evaporation chamber dimensions with PlasmaQuad II+

One of the main problems with previous designs of microchip sample introduction systems for plasma spectrometry has been the low transport efficiency of the sample into the plasma.[21] A key aspect to overcome this was to optimise the evaporation chamber. Since the liquid flow rate in the chip is very low (typically 5 μl min^{-1}) it is highly desirable to attain 100 % transport of the sample out of the end of the chip to the plasma. In order to achieve this it was vital to optimise the evaporation chamber to ensure that all the droplets from the nebuliser are evaporated to form small droplets (< 8 μm) before entering the plasma.

Experimental design was used to optimise the evaporation chamber. Three factors were identified in order to obtain the highest possible transport efficiency of sample into the plasma; namely chamber length, liquid flow rate and gas flow rate. Experiments were designed with two variables; chamber length and liquid flow rate. The nebuliser gas flow rate was adjusted to give maximum intensity at each chamber length / liquid flow rate configuration. Firstly the upper and lower limits of the two

variables were defined and then experiments were designed to cover the area in between these limits. This resulted in a 2-level: 2-factorial experimental design with 13 experiments to sufficiently cover the range, as illustrated in Figure 4.7.

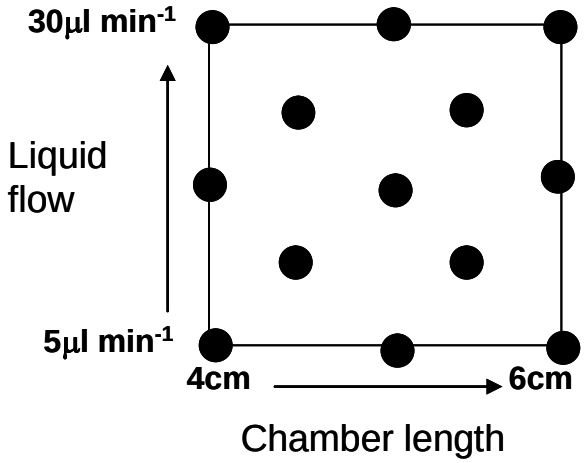

Figure 4.7 2 level: 2 factor experimental design for multivariate optimisation of evaporation chamber. ● indicates one experiment.

The chamber path length was varied between 4.0 to 6.0 cm in order to give a similar chamber volume to that in the work published by Mermet *et al.* for TISIS.[4, 17, 18] This was achieved by fabrication of three chambers with varying main body lengths, as shown with dimensions in Figure 4.8. The path lengths were measured from the tip of the MCN to the exit of the chamber. The chamber diameter was not varied since any increase above 22 mm was not found to significantly affect the signal intensity when a MicroMist MCN was used.[18] This is due to the narrow primary aerosol generated by the MicroMist. The liquid flow rate was optimised between 5.0 and 30.0 μl min^{-1}; selected to give a measurable signal while avoiding excessive dilution of the sample.

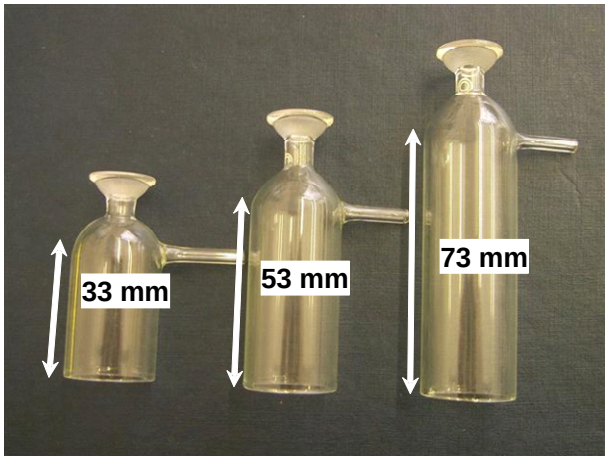

Figure 4.8 Evaporation chambers used in multivariate optimisation on PlasmaQuad II+ ICPMS with MicroMist nebuliser.

A tune solution containing 10 µl L^{-1} indium was delivered to the MCN and the signal at $^{m}/_{z}$ 114.9 monitored. The sensitivity of the system was evaluated in terms of sensitivity (cps) and stability (RSD of 5 replicate measurements). The results are presented in Table 4.2.

Table 4.2 Results from optimisation of evaporation chamber.

Chamber path length / cm	Pump rate / rev min^{-1}	Liquid flow / µl min^{-1}	Gas flow / L min^{-1}	Sensitivity / x10^3 cps	Stability / % RSD
4.0	1.25	5.0	1.21	1.0	50.0
4.0	4.38	17.6	1.00	22.0	5.0
4.0	7.50	30.2	0.95	35.0	5.0
4.5	2.81	11.3	1.11	12.5	7.0
4.5	5.94	23.9	1.02	26.0	4.5
5.0	1.25	5.0	N/A	<1.0	N/A
5.0	4.38	17.6	1.00	36.0	5.0
5.0	7.50	30.2	0.98	43.0	3.0
5.5	2.81	11.3	1.09	24.5	5.0
5.5	5.94	23.9	1.00	42.0	3.0
6.0	1.25	5.0	1.16	10.0	18.0
6.0	4.38	17.6	1.00	42.0	3.5
6.0	7.50	30.2	1.00	52.0	3.0

The sensitivity for 5.0 cm path length with 5.0 μl min^{-1} liquid flow was in the order of a few hundred cps. It was not possible to obtain a stable signal or optimise the gas flow so this result was not included in the data.

Figure 4.9 shows a linear relationship between liquid and gas flow. As the liquid flow is increased the optimal gas flow decreases. This can be explained, as a lower gas flow increases the residence time of the aerosol in the chamber, allowing more complete evaporation to be achieved. Therefore resulting in a higher proportion of droplets being low enough to be introduced into the plasma and significantly contribute to the analyte signal.

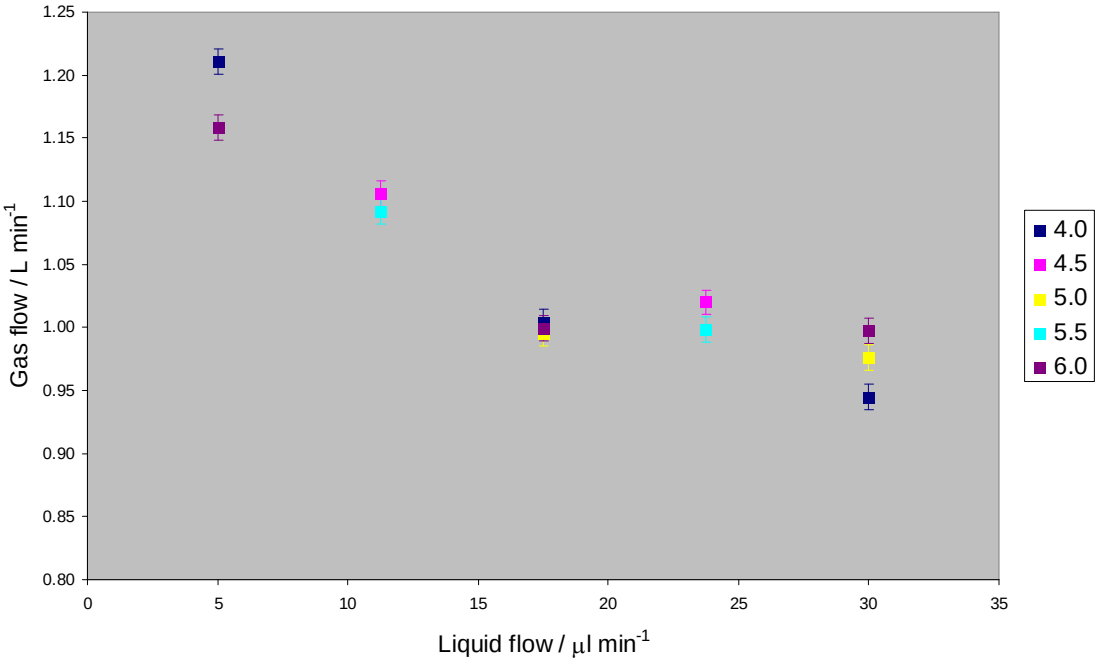

Figure 4.9 Relationship between liquid flow and optimal nebuliser gas flow as demonstrated for various chamber lengths (detailed in the legend: aerosol path length / cm) used in the optimisation of the chamber dimensions. Nebuliser gas optimised on the PlasmaQuad II+ ICPMS based upon the maximum intensity for 10 μg In L^{-1} contained within tune solution (Section 4.2.2).

The use of experimental design to plan experiments enables the detector response (cps) to be plotted with respect to both chamber length and liquid flow rate. This illustrates any interaction between the two variables and enables a visual picture to be created to assist in the interpretation of the results. The results were processed using MATLAB® (MathWorks Ltd., Cambridge, UK) with assistance from Dr. G. R. Flåten.

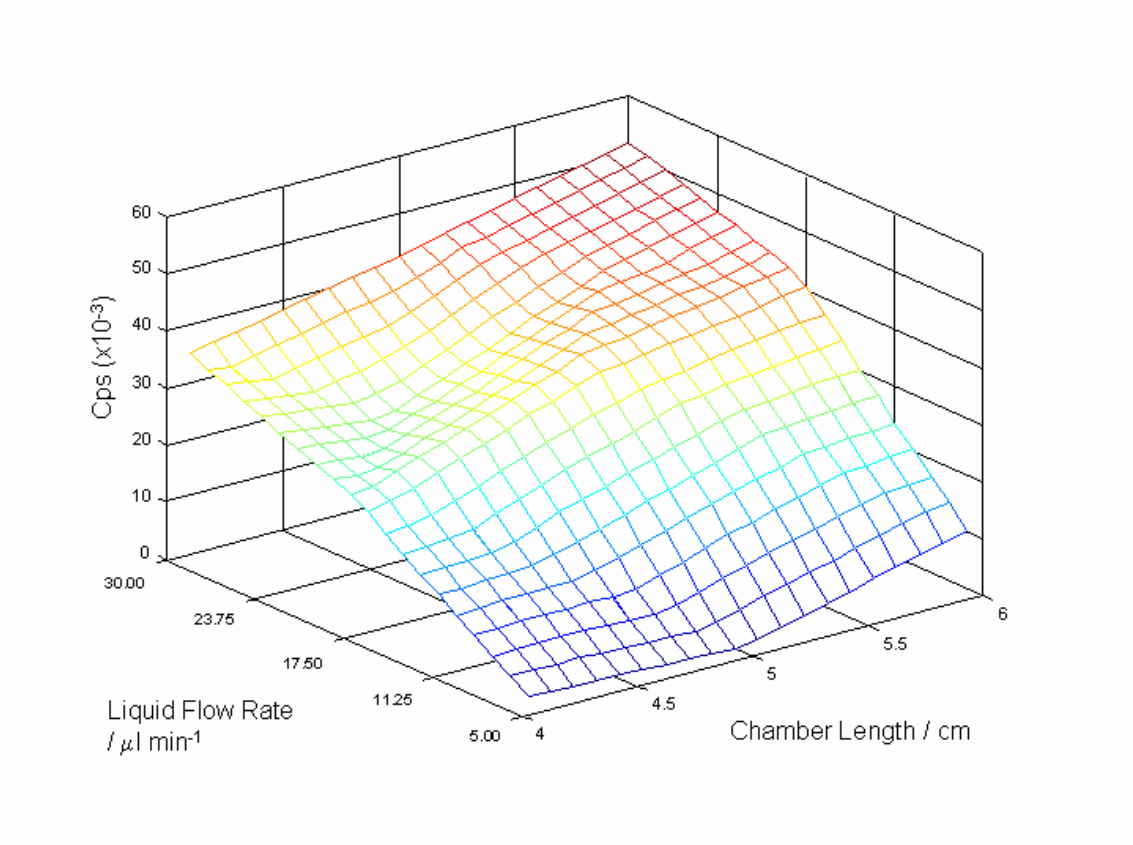

Figure 4.10 Response curve based upon the intensity for 10 µg In L^{-1} contained within tune solution (Section 4.2.2) for the optimisation of evaporation chamber. Effect of chamber length (i.e. internal volume) and liquid flow rate as a function of detector response (cps).

Figure 4.10 shows the response curve for chamber length (cm), flow rate (µl min^{-1}) and the signal response (cps). It was found that the higher the liquid flow rate and the longer the chamber length the greater the cps (i.e. greater sensitivity of analysis). As expected as the liquid flow increases, more counts are generated since there is a

higher concentration of sample introduced into the plasma. Longer chamber lengths result in increased detector response since the inertial impact losses against the front cavity wall are reduced. Additionally at low liquid flow rates droplet coalescence and gravitational losses are reduced. As stated in Section 4.1.3; the chamber provides a simple aerosol trajectory, rather than having a complex path to act as a droplet size filter in order to remove the coarsest droplets, and solvent evaporation is promoted at the high gas to liquid ratio. For the optimal 6.0 cm chamber path length, with an internal diameter of 2.2 cm the internal volume is approximately 23 cm^3. By dividing the internal volume by the nebuliser gas flow rate the aerosol residence time inside the cavity can be approximated. At the optimal gas flow rate of 1.00 L min^{-1} this gives a residence time of approximately 1.4 seconds. Theoretical calculations using Equations 4.1 and 4.2 (Section 4.1.3) support the theory that additional evaporation occurs from the chamber wall, since the larger droplets produced in the primary aerosol would not have sufficient residence time to be reduced in size to below 8.0 μm and introduced into the plasma.

It is accepted that a proportion of droplets in excess of 8.0 μm will be introduced into the plasma. This will have the potential for deteriorating the plasma conditions and will have a negative effect on the stability of the analytical signal. For this reason whilst carrying out these optimisation experiments the stability of the signal was also monitored in terms of the % RSD (n = 5). The most stable results were obtained at the area of maximum sensitivity, shown in Figure 4.11. This is an encouraging result, demonstrating that the method should prove to be sensitive and reproducible for the optimised evaporation chamber.

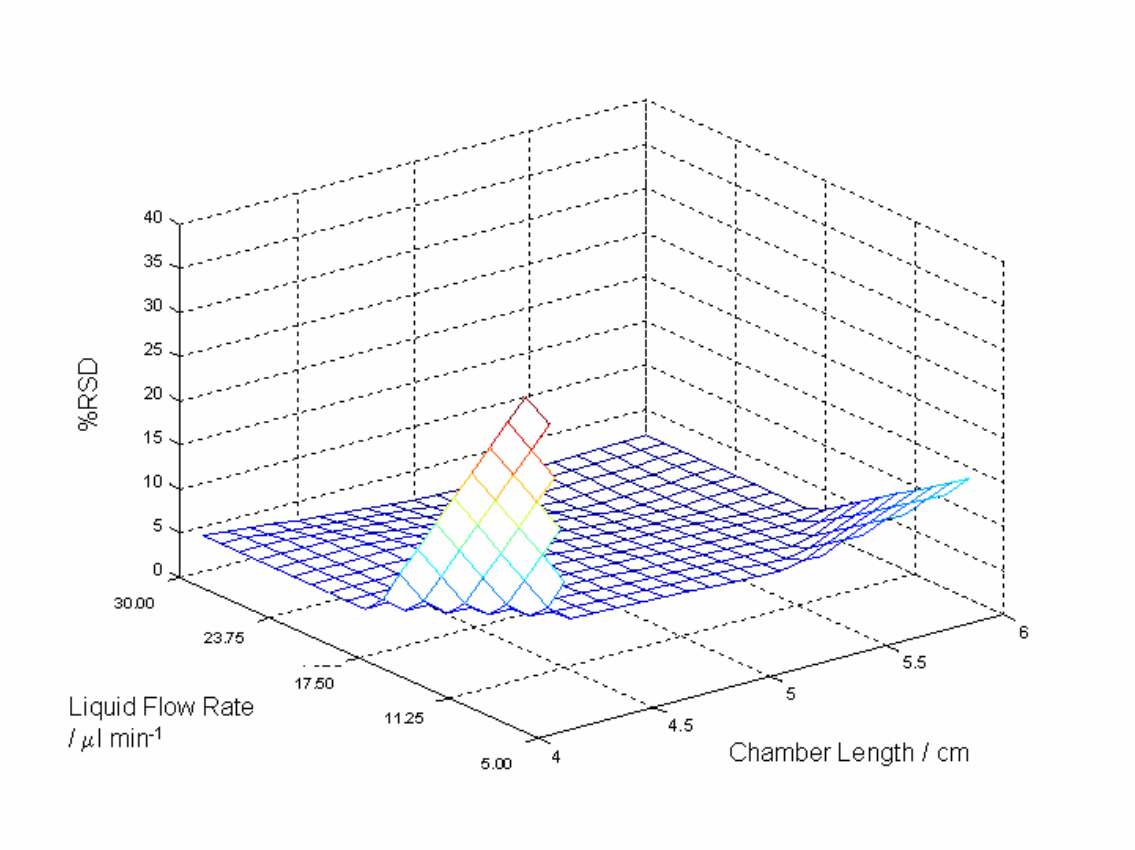

Figure 4.11 Stability of PlasmaQuad II+ ICPMS detector response for based upon the maximum intensity for 10 µg In L^{-1} (% RSD; n = 5) throughout optimisation of evaporation chamber. Most stable signal produced at maximum chamber length and liquid flow rate, coinciding with greatest sensitivity.

It can be seen in Figure 4.10 that the optimum value was obtained at the upper limits set for the experiment. Sample recondensation was observed within the chamber at flow rates in excess of 20 µl min^{-1} (i.e. for both 24 and 30 µl min^{-1}). It was therefore decided that further increasing the liquid flow rate was not beneficial. Additionally the aim of this sample introduction system was to improve the efficiency for introducing very low sample flow rates / volumes *via* a microfluidic chip. Hence increasing the liquid flow rate would increase the sample dilution, negating any improvements in sensitivity. Further optimisation of the chamber was not conducted on the PlasmaQuad

II+ instrument due to its replacement with a Elan DRC II. Optimisation of the chamber length was conducted using the new ICPMS as described later in Section 4.3.5.

4.3.4 Comparison with commercial low flow sample introduction

In order to evaluate the results gained from the use of the evaporation chamber a comparison using a MicroMist and Cinnabar (Glass Expansion, Australia) was conducted. This is the sample introduction system previously used in conjunction with a microfluidic chip in order to obtain high sample introduction efficiency at low flow rates.[22] The standard operating conditions for this sample introduction system uses 0.96 L Ar min^{-1} nebuliser gas flow at 2.3 Bar and approximately 350 μl min^{-1} liquid flow. These conditions typically yield 155 000 cps for 10 μg L^{-1} indium with a stability of 1.5 % RSD. A 10 μg L^{-1} tune solution was introduced and the detector response (cps) for indium was measured ($^{m}/_{z}$ 115.1) with the associated stability (% RSD; n = 5). The liquid flow rate was varied between 5 and 30 μl min^{-1} as for the multivariate optimisation of the evaporation chamber. The nebuliser gas flow was optimised for each liquid flow rate but was not found to alter from 0.89 L Ar min^{-1}. The results presented in Figure 4.12 show that 10 μg L^{-1} indium at a flow rate of 20 μl min^{-1} yields 12 000 cps. This is relatively low, which would result in high detection limits and limited application to the quantitative analysis of real samples. The results from the optimised evaporation chamber were compared to those from the previously used Cinnabar cyclonic spray chamber.[22, 23] Figure 4.13 shows the signal increased for the evaporation chamber over all flow rates investigated, resulting in a 400 % increase in signal intensity.

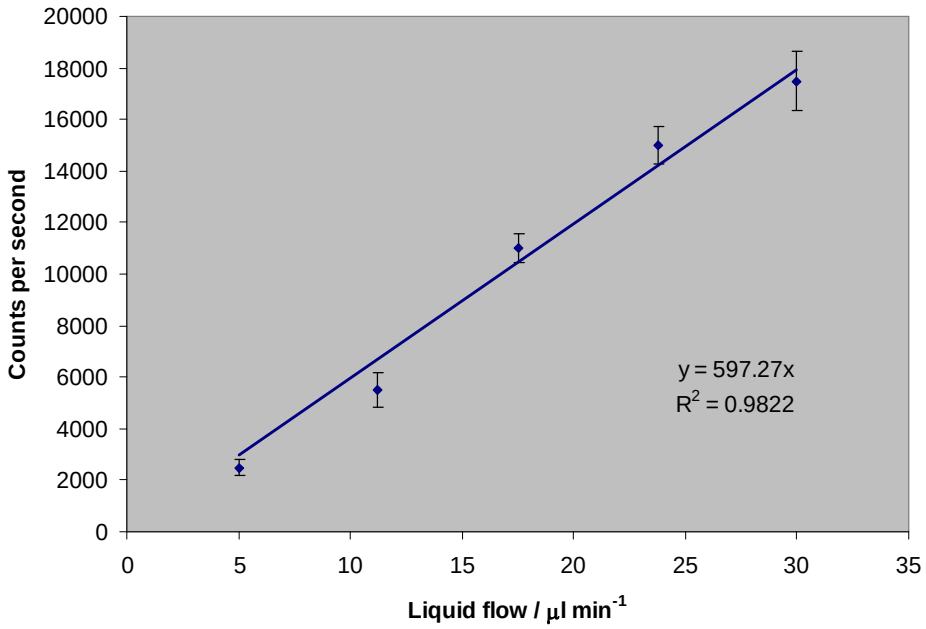

Figure 4.12 Detector response for 10 µg L^{-1} indium ($^{m}/_{z}$ 115.1) at low flow rate with MicroMist MCN and Cinnabar cyclonic spray chamber (4 °C).

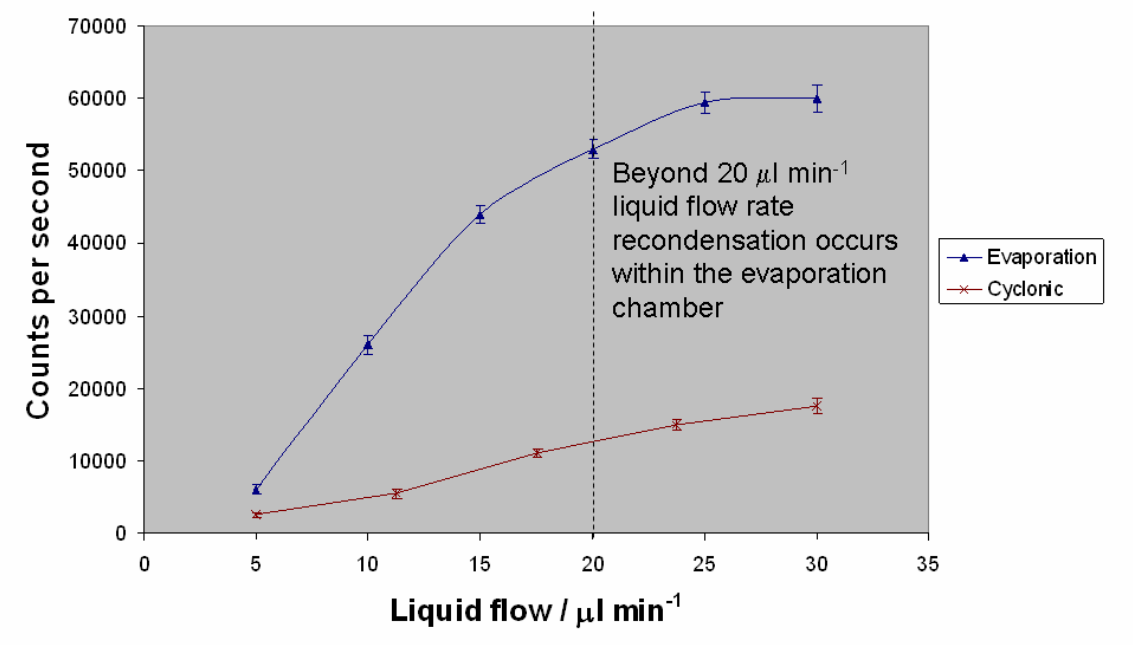

Figure 4.13 Comparison of Cinnabar cyclonic spray chamber (Glass Expansion, Australia) and optimised evaporation chamber. Detector response (cps) for 10 µg L^{-1} indium ($^{m}/_{z}$ 115.1) delivered by peristaltic pump. MicroMist nebuliser (Glass Expansion, Australia) used with both chambers.

This demonstrates the effectiveness of the evaporation chamber for the introduction of low liquid flow rates (< 20 μl min^{-1}). Significant improvements in sensitivity have been achieved in comparison to the commercial low flow sample introduction with a MCN with reduced volume cyclonic spray chamber.

4.3.5 Optimisation of evaporation chamber length with Elan DRC II

Extension of the chamber length optimisation performed in Section 4.3.3 was performed at the optimal liquid flow rate of 20 μl min^{-1} and nebuliser gas flow rate of 0.95 L min^{-1}. A multielement standard solution was used containing a suite of elements across the mass range (10 μg L^{-1} Mg, Cr, Mn, Co, Ni, Cu, Zn, As, Se, Mo, In, Pb, U), 10 μg L^{-1} Ce to permit evaluation of the oxide production (CeO / Ce ratio) and 100 μg L^{-1} Ba for doubly charged species production (Ba^{2+} / Ba^{+} ratio) in 2 % HNO_3. The chamber length was increased by increasing the distance X in Figure 4.2. The chambers were fabricated without a drain as shown in Figure 4.14. The optimal aerosol path length was found to be 10.0 cm, shown by the results presented in Figure 4.15, using a chamber with dimensions as shown in Figure 4.2, where X is 10.5 cm. This gives an internal volume of approximately 35 cm^3, resulting in an aerosol residence time of ~ 2.2 seconds. This is longer than the optimal of 1.7 seconds quoted by Mermet *et al.*[18] and greater than suggested by the optimisation performed with the PlasmaQuad II+. This stems from the positioning of the evaporation chamber on the Elan DRC II in comparison with the PlasmaQuad II+ and ICPAES. The entire sample introduction system is outside the torch box and open to the general laboratory environment. Therefore the operating temperature of the chamber is below that experienced with the previous ICPMS (30 – 35 °C) and that of the ICPAES (*ca.* 40 °C)[18]. In this situation the chamber remained at

room temperature of 27 °C.

Table 4.3 summarises the detector response for the daily performance criteria performed on the Elan DRC II. The optimal aerosol path length of 10.0 cm provides low oxide and doubly charged species production with low background. Table 4.4 demonstrates the detector response for all other elements contained within the multielement standard. The highest sensitivity was achieved consistently for all elements, across the entire mass range.

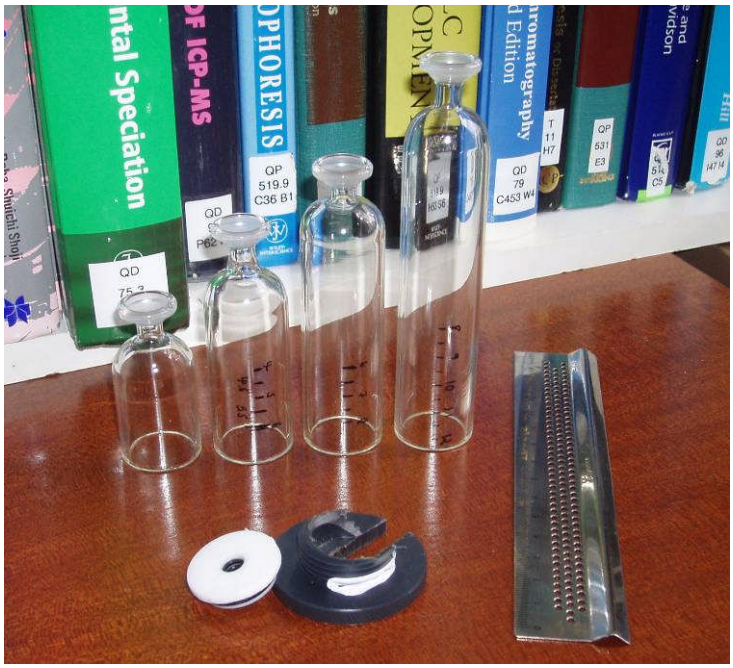

Figure 4.14 Image of 4 chambers used in evaporation chamber length optimisation. No drain provided in chamber. Also showing PTFE adapter to hold MicroMist nebuliser (white) and adapter to secure chamber to Elan DRC II torch (grey), both fabricated by departmental workshop.

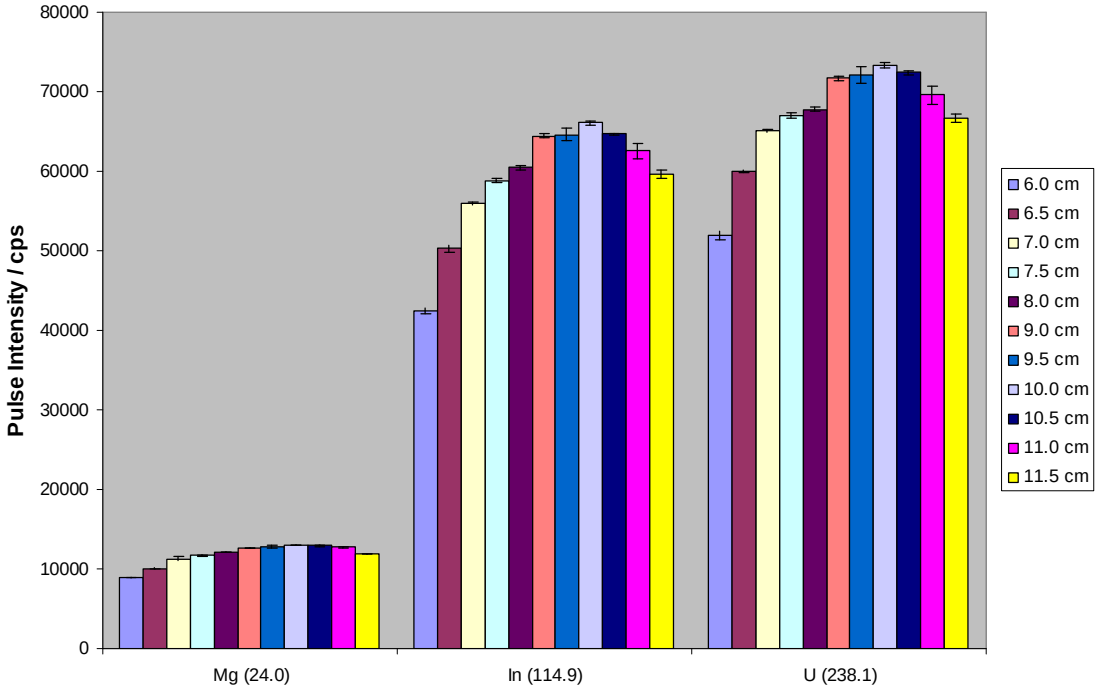

Figure 4.15 Effect of increasing chamber length on the detector response for low to high mass elements. Legend states distance from tip of MicroMist nebuliser to chamber outlet. Error in pulse intensity based upon % RSD of 5 replicate readings.

Table 4.3 Results of daily performance criteria (as described in Section 2.1.1.2) for increasing chamber lengths. Multielement standard (2 % HNO_3) supplied at 20 µl min^{-1} by syringe pump.

Aerosol path length / cm	Pulse intensity / cps ppb^{-1} Mg 24.0	In 114.9	U 238.1	Oxides CeO / Ce %	Doubly charged Ba++/Ba+ %	Background intensity / cps 8.5 amu	220 amu
6.0	899.6	4239.4	5197.7	2.1	2.0	0.6	0.3
6.5	1006.8	5028.4	6000.9	1.4	1.9	0.4	0.6
7.0	1126.8	5591.3	6505.2	1.0	1.8	0.6	0.6
7.5	1166.9	5882.5	6694.7	0.9	1.8	0.6	0.3
8.0	1207.4	6048.6	6777.2	0.8	1.7	0.7	0.6
9.0	1265.5	6445.4	7172.4	0.8	1.6	0.4	0.4
9.5	1275.9	6463.9	7211.4	0.8	1.6	0.6	0.6
10.0	1296.4	6613.2	7334.3	0.8	1.6	0.4	0.5
10.5	1290.5	6466.5	7238.9	0.8	1.6	0.5	0.4
11.0	1272.3	6255.6	6958.7	0.8	1.7	0.5	0.6

Table 4.4 Detector response for a 10 μg L^{-1} multielement standard in 2 % HNO_3 at 20 μl min^{-1}.

Aerosol path length / cm	Pulse intensity / cps ppb^{-1}														
	Cr 51.9	Mn 54.9	Co 58.9	Ni 57.9	Ni 59.9	Cu 62.9	Cu 64.9	Zn 65.9	Zn 67.9	As 74.9	Se 76.9	Se 81.9	Mo 94.9	Mo 97.9	Pb 208.0
6.0	1640.4	2092.0	1600.4	899.1	398.0	1187.8	590.3	456.5	396.4	266.9	33.1	35.9	453.9	720.6	2119.4
6.5	1870.3	2404.0	1870.5	1036.9	458.8	1376.5	680.1	517.3	455.3	317.4	36.0	39.4	530.4	845.1	2428.1
7.0	2037.8	2623.5	2040.4	1134.2	499.5	1499.3	741.6	556.6	483.1	350.4	38.0	42.4	582.6	937.6	2612.8
7.5	2103.4	2727.8	2101.5	1176.7	520.0	1557.3	769.5	570.0	494.0	365.9	38.9	43.4	606.7	982.4	2655.4
8.0	2167.9	2811.3	2177.6	1218.6	535.5	1603.3	791.0	575.8	500.9	376.7	39.3	44.5	626.0	1013.3	2689.5
9.0	2285.8	2945.1	2301.0	1283.6	565.8	1694.9	835.0	638.8	549.0	409.4	44.5	51.4	663.5	1071.6	2843.7
9.5	2276.3	2947.2	2300.1	1286.6	566.7	1699.8	839.0	638.3	545.5	407.8	43.3	49.7	667.1	1078.6	2849.7
10.0	2323.1	3028.2	2345.3	1313.3	575.8	1725.0	854.6	650.5	552.6	417.8	43.9	51.5	673.8	1098.4	2888.8
10.5	2282.1	2981.2	2298.3	1283.2	565.3	1699.8	836.6	637.9	541.5	412.6	43.4	49.7	662.7	1069.9	2837.4
11.0	2249.2	2911.8	2248.0	1263.6	550.9	1656.4	816.1	625.5	535.5	403.1	42.7	48.5	649.8	1043.1	2726.8

The instrumental detection limits (DL) were calculated for Mg, In and U (across the mass range) based upon Equation 4.3.

$$DL = \frac{3SD_{Blank} \times Conc._{Std}}{I_{Std} - I_{Blank}} \qquad \textbf{Equation 4.3}$$

Where; SD_{Blank} is the standard deviation of 10 replicate readings of the blank, $Conc._{Std}$ is the concentration of the element in the multielement standard solution (10 μg L^{-1}), I_{Std} and I_{Blank} are the mean intensities (cps) of 10 replicate readings. This was conducted for both the Cinnabar chamber (at 4 °C) and the evaporation chamber (10 cm). The results, presented in Table 4.5, show that the evaporation chamber consistently yields lower detection limits, generally being 25 to 45 % lower. This is crucial for application to a system for conducting speciation analysis with extremely low analyte concentrations.

Table 4.5 Determination of the instrumental detection limits (DL) for elements across the mass range contained within a 10 μg L^{-1} multielement standard (n = 10). Comparison of the performance for the optimised evaporation chamber with the Cinnabar low volume cyclonic spray chamber.

Element	Mean SD_{Blank} / cps	Mean I_{blank} / cps	Mean I_{Std} / cps	$Conc._{Std}$ / μg L^{-1}	DL / ng L^{-1}
Evaporation chamber (10 cm)					
Mg	16.2	1510.9	11209.1	10	50.1
In	8.7	82.2	54743.3	10	4.8
U	11.6	102.8	66489.8	10	5.2
Cinnabar (4 °C)					
Mg	14.6	806.8	5710.2	10	89.3
In	5.85	68.4	28190.2	10	6.2
U	8.05	72.65	29939.45	10	8.1

4.3.6 Rinse times of chamber

Experiments were conducted to determine the wash out times for both the Cinnabar cyclonic chamber and optimised evaporation cavity. These were based upon the time taken for the signal to decay to 1 % of its steady state value when rinsing the system with UHQ water following a 10 μg L^{-1} multielement standard. All solutions were pumped at 20 μl min^{-1} by peristaltic pump to facilitate easier switching between solutions in comparison with a syringe pump. Figure 4.16 shows a comparison between the two chambers, operated under the same conditions. The nebuliser gas flow was optimised, based upon the maximum intensity for indium, for each chamber independently. No significant differences in the wash out time were found between the two chambers, both resulting in approximately 80 seconds. Although the evaporation chamber provides a simpler aerosol trajectory the optimal internal volume is larger than that of the Cinnabar (approximately 35 cm^3 for the evaporation chamber *cf.* 20 cm^3 for Cinnabar); therefore improvements are not found in the wash out time.

4.4 Conclusions

The aim of this work was to develop an evaporation chamber to facilitate the introduction of very low liquid flow rates into ICPMS. The evaporation chamber is based upon work presented by Todolí and Mermet on a TISIS for ICPAES. The design has been successfully modified to make it suitable for coupling with the commercial horizontally aligned ICPMS torch. The chamber has been optimised in order to achieve the best analytical figures of merit. Combination of the reduced internal volume, low

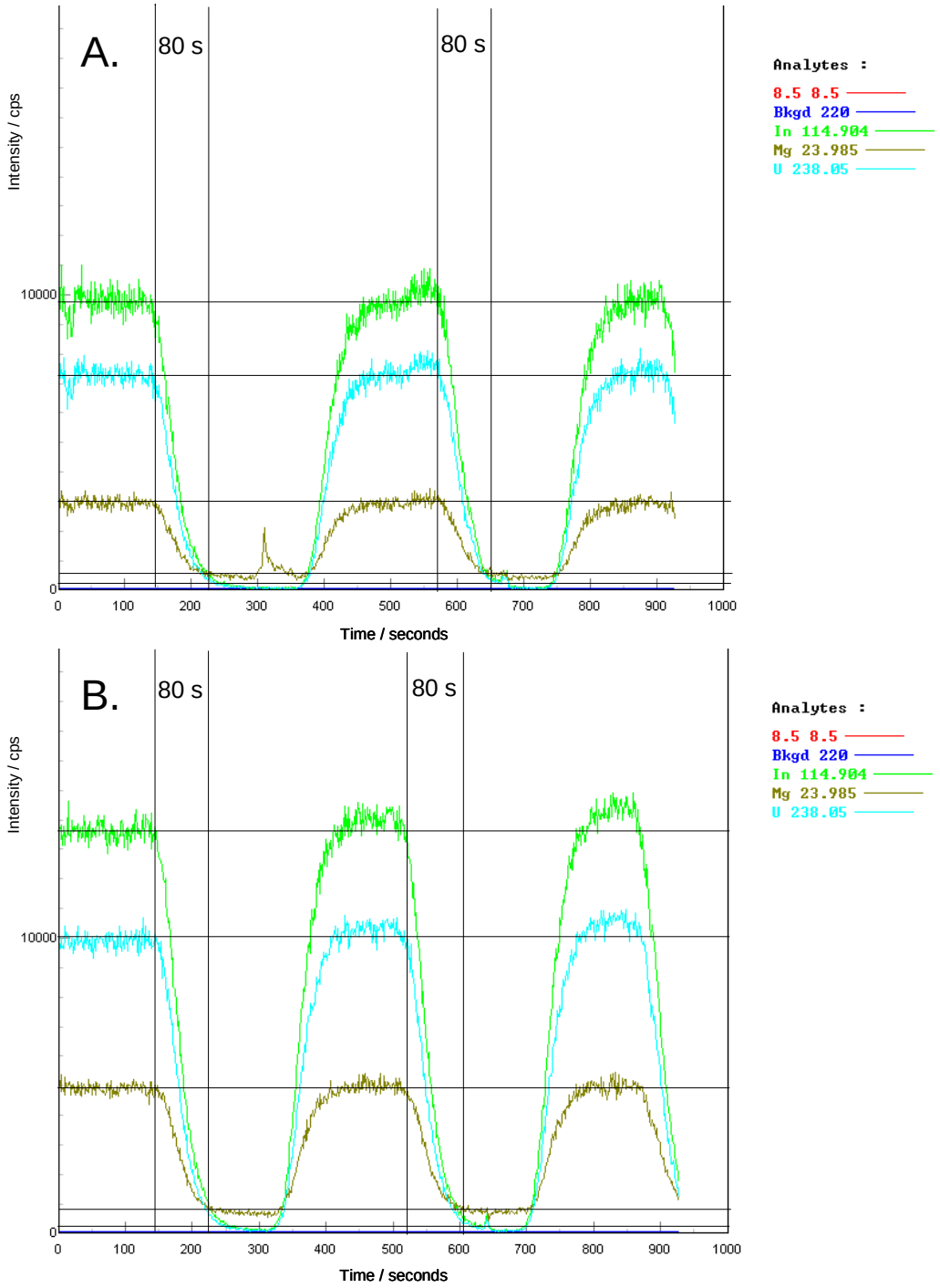

Figure 4.16 Wash out time for: A. Cinnabar spray chamber (4 °C), 0.96 L Ar min^{-1} optimised nebuliser gas flow, B. Optimised 10 cm Evaporation chamber, 0.95 L Ar min^{-1} optimised nebuliser gas flow. 20 µl min^{-1} flow of 10 µg L^{-1} multielement standard solution (Section 4.2.2). Time taken for signal to decrease to 1 % of steady state upon switching to blank solution (2 % HNO_3).

liquid flow rates, promotion of solvent evaporation and the simple aerosol trajectory leads to the increases achieved in sensitivity and instrumental detection limits. The sample losses associated with traditional spray chambers have been minimised and a high transport efficiency of sample to plasma has been achieved. This evaporation chamber is suitable for use with a low flow nebuliser. Inclusion of this chamber into a high efficiency sample introduction system designed specifically for interfacing microfluidic chips with ICPMS is described in Chapter 5. An important factor in the success of this evaporation chamber is the efficiency of the nebuliser. The primary aerosol should have a range of droplet diameters which are as small as possible.

4.5 References

1 B.L. Sharp, *J. Anal. At. Spectrom.*, 1988, **3**, 939.

2 J. Mora, S. Maestre, V. Hernandis and J.L. Todoli, *Trends Anal. Chem.*, 2003, **22**, 123.

3 A. Montaser, *Inductively Coupled Plasma Mass Spectrometry*, Wiley-VCH, 1998.

4 J.L. Todoli and J.-M. Mermet, *J. Anal. At. Spectrom.*, 2002, **17**, 345.

5 J.L. Todoli and J.-M. Mermet, *Trends Anal. Chem.*, 2005, **24**, 107.

6 J.L. Todoli and J.-M. Mermet, *Spectrochim. Acta, Part B*, 2006, **61**, 239.

7 M.A. Tarr, G. Zhu and R.F. Browner, *Anal. Chem.*, 1993, **65**, 1689.

8 E.G. Yanes and N.J. Miller-Ihli, *Spectrochim. Acta, Part B*, 2003, **58**, 949.

9 E.G. Yanes and N.J. Miller-Ihli, *Spectrochim. Acta, Part B*, 2004, **59**, 883.

10 S. Maestre, J.L. Todoli and J.-M. Mermet, *Anal. Bioanal. Chem.*, 2004, **379**, 888.

11 G. Schaldach, H. Berndt and B.L. Sharp, *J. Anal. At. Spectrom.*, 2003, **18**, 742.

12 K.A. Taylor, B.L. Sharp, D.J. Lewis and H.M. Crews, *J. Anal. At. Spectrom.*, 1998, **13**, 1095.

13 J.L. Todoli and J.-M. Mermet, *J. Anal. At. Spectrom.*, 2001, **16**, 514.

14 E. Bjorn, T. Jonsson and D. Goitom, *J. Anal. At. Spectrom.*, 2002, **17**, 1257.

15 Y.C. Sun, Y.S. Lee, T.L. Shiah, P.L. Lee, W.C. Tseng and M.H. Yang, *J. Chromatogr. A*, 2003, **1005**, 207.

16 D. Schaumloffel and A. Prange, *Fresenius J. Anal. Chem.*, 1999, **364**, 452.

17 J.L. Todoli and J.-M. Mermet, *J. Anal. At. Spectrom.*, 2002, **17**, 913.

18 J.L. Todoli and J.M. Mermet, *J. Anal. At. Spectrom.*, 2003, **18**, 1185

19 J.W. Olesik, J.A. Kinzer and B. Harkleroad, *Anal. Chem.*, 1994, **66**, 2022

20 C. Lagomarsino, M. Grotti, J.L. Todoli and J.-M. Mermet, *J. Anal. At. Spectrom.*, 2007, **22**, 523.

21 A.Y.N. Hui, G. Wang, B. Lin and W.-T. Chan, *J. Anal. At. Spectrom.*, 2006, **21**, 134.

22 Q.J. Song, G.M. Greenway and T. McCreedy, *J. Anal. At. Spectrom.*, 2004, **19**, 883.

23 Q.J. Song, G.M. Greenway and T. McCreedy, *J. Anal. At. Spectrom.*, 2003, **18**, 1.

5 Development of sample introduction for interfacing microfluidic chips with ICPMS. Part II Nebuliser

5.1 Introduction

Laboratory on a chip devices provide an excellent opportunity for rapid on chip pre-treatment of samples,[1] conducting separations[2-10] and the full characterisation of a wide range of chemical processes.[11] There have been few attempts to combine the advantages of chip technology with the sensitivity of ICPMS.[12-14] Elemental speciation using microchip electrophoresis successfully interfaced with ICPMS *via* commercial low flow MCN and miniaturised spray chamber has previously been reported within the Department.[13, 14] Problems however remained due to the use of commercial sample introduction with significantly higher liquid flow rate requirements to that generated by the microfluidic device. These included the need for a make up flow to satisfy nebuliser requirements, the inclusion of a relatively large transfer capillary between the chip and the nebuliser and the low transport efficiency of the spray chamber. This resulted in detection limits being increased and broadening of the species separation achieved during electrophoresis.

A discussion of sample introduction for ICPMS has been presented in Section 1.1.2. In order to develop a nebuliser suitable for interfacing a microfluidic chip with ICPMS it is essential to first consider established designs. Efficient aerosol generation requires the nebuliser to supply energy to a liquid bulk. The characteristics of the aerosol produced are highly dependant upon the amount of energy supplied and the

efficiency of the energy transfer. Pneumatic nebulisers (PN) rely on the kinetic energy of a high velocity gas stream. Pneumatic nebulisation is the most common method of aerosol production for liquid sample introduction. PN are popular owing to their simplicity, ease of use and low cost. Numerous different designs have been presented and adapted to specific applications. Some of the most common schemes are presented in Figure 1.6. The concentric design has found the widest application of these schemes.

Commercial PN suffer from the following problems when applied to interfacing with low liquid flow rates supplied from a microfluidic chip. Firstly they have poor analyte transport efficiency (typically 2 % in ICPAES),[15] which significantly impairs the limits of detection. Secondly the method of aerosol production creates suction which induces non-controlled laminar flow within the chip. This therefore dictates a required sample uptake rate (typically 0.5 – 2.0 ml min^{-1}), which is significantly higher than the flow rate in the chip (typically nl up to μl min^{-1}). These problems have been overcome in the past by the introduction of a makeup flow. However this leads to a dilution of the sample and additional reduction in analyte transport efficiency to the plasma, degrading the LOD further. Furthermore if this make up flow rate is pumped pulsation can be introduced, especially with peristaltic pumps operated at low flow rates, adversely affecting the stability (increasing RSD).

In the analysis of small sample volumes with low liquid flow rates (μl min^{-1}) the uptake rate of the nebuliser must be reduced to achieve high transport efficiency and avoid excessive sample dilution. Although conventional nebulisers can be operated at flow rates below 1 ml min^{-1} their design is not optimised for such low flow. The concentric nebuliser has been adapted for low flow rates and several designs have been presented including: the high-efficiency nebuliser (HEN), microconcentric nebuliser

(MCN), the direct injection nebuliser (DIN) and direct injection high-efficiency nebuliser (DIHEN),[15] discussed in Sections 4.1.2 and 1.1.2.3. Generally the liquid and gas cross-sectional areas have been reduced as well as the liquid capillary wall thickness. As a consequence the primary aerosol produced is finer and the natural liquid uptake rate of the nebuliser is reduced. However there are disadvantages associated with these reductions in dimensions. The most prolific of these being the increase risk of blockage at the nebuliser tip, particularly in the analysis of salt containing solutions. The nebuliser becomes more expensive to fabricate and the tip can be easily damaged.

Umemura *et al.* developed a high efficiency cross-flow micronebuliser (HECFMN) for the purpose of interfacing capillary electrophoresis (CE) with ICPMS.[16] Their design aimed to eliminate the problems with band broadening and poor sensitivity seen with the pneumatic micronebuliser, however there remained some issues with stability and run times were of the order of 30 min. In 2006 Hui *et al.* were the first to report a chip based nebuliser however this did not provide the sensitivity that would be required for most applications. A microchip electrophoresis system was interfaced to ICPAES by means of a cross-flow nebuliser.[12] Their system was based upon a polydimethylsiloxane (PDMS) chip but a transport efficiency of only 10 % was achieved, which is not sufficient when introducing very small sample volumes.

5.1.1 Aim

In the present study a new chip based micro cross-flow nebuliser (MCFN) has been developed. This has been specifically been designed for interfacing a microfluidic chip with ICPMS and aims to overcome the problems previously experienced with

commercial sample introduction systems. The MCFN is incorporated in a microchip assembly to provide a rapid and highly efficient sample introduction system into the plasma. The system incorporated an evaporation chamber (described in Chapter 4) in order to achieve high analyte transport efficiency. It is important that the design of the microfluidic sample introduction system is applicable to a wide range of chip designs making it suitable for numerous applications. The application of this sample introduction system to the flow injection analysis of small sample volumes (in the order of nanolitres) and as a potential interface for microchip electrophoresis with ICPMS is investigated.

5.2 Experimental

5.2.1 Instrumentation

Initial investigation into the nebuliser design was conducted on the PlasmaQuad II+ ICPMS. The instrument argon nebuliser gas supply was used in conjunction with the MiniPuls peristaltic pump to assess the aerosol produced by the nebuliser.

The Elan DRC II ICPMS was used for optimisation and evaluation of the sample introduction system. The dynamic reaction cell was used as required to reduce the background signal and eliminate any interfering species present (as described in Section 2.1.1.2). Ammonia was used as the reaction gas (at 0.5 ml min^{-1}) for reducing argon and chloride interferences on the chromium signal (^{52}Cr; $^{40}Ar^{12}C$ and ^{53}Cr; $^{40}Ar^{13}C$, $^{37}Cl^{16}O$). The instrument was optimised (nebuliser gas, Autolens, X-Y position) and its performance was monitored daily as described in Section 2.1.1.2 using standard sample introduction, i.e. glass concentric nebuliser with cyclonic spray chamber (PerkinElmer

SCIEX, Ontario, Canada). The operating conditions for ICPMS when used with MCFN and evaporation chamber are shown in Table 5.1. The X-Y position of the torch was adjusted on changing the selected sample introduction systems in order to give the greatest sensitivity.

Table 5.1 Elan DRC II operating conditions with MCFN and evaporation chamber sample introduction

RF Forward power / W	925
Auxiliary gas flow rate / L min^{-1}	1.2
Plasma gas flow rate / L min^{-1}	15
Nebuliser gas flow rate / L min^{-1}	0.91
DRC nebuliser gas flow rate / L min^{-1}	0.96
NH_3 cell gas flow rate / ml min^{-1}	0.5
RPa	0.0
RPq	0.6
Dwell time per amu / ms	50
Data acquisition mode	Peak hopping
Autolens	On
Detector mode	Dual

Solutions were delivered to the microchip using syringe pumps (Bioanalytical Systems Inc., West Lafayette, USA) capable of providing 0.1 – 100 μl min^{-1}.

The evaporation chamber is described in detail in Chapter 4. The chamber was manufactured in house from quartz tubing. The tube had a 2.2 cm i.d. and the final design was 8.0 cm long with a tapered end and a glass ball joint to fit directly with the

commercial ICPMS torch (PerkinElmer SCIEX, Ontario, Canada) fitted to the Elan DRC II. The wide end of the chamber was sealed into 'O' ring in the nebuliser compartment of the MCFN assembly, described in the procedures.

5.2.2 Reagents

The chromium standards; Cr(VI) (1000 ± 3 μg ml^{-1} in H_2O) and Cr(III) (1000 ± 3 μg ml^{-1} in 2 % HCl), were purchased from Qm_x Laboratory Limited (Thaxted, Sussex, UK). The carrier used throughout was a solution containing 15 mM HNO_3. Yttrium and indium were used as internal standards within the carrier and make up reservoirs respectively; made up from their 1000 μg ml^{-1} standards (Yttrium; PlasmaCAL, Qm_x Laboratory Limited, Thaxted, UK. Indium; BDH Laboratory Supplies, Poole, UK). All solutions were prepared fresh daily using UHQ water.

5.2.3 Procedures

5.2.3.1 Fabrication of PDMS microfluidic chips

A polydimethylsiloxane (PDMS) kit (Sylgard 184, Dow Corning, Germany) was used to rapidly fabricate microfluidic chips. The PDMS was prepared using a 10 : 1 ($^{w}/_{w}$) mixture of silicone elastomer to curing agent by weight. The mixture was combined in a single use sample vial and thoroughly stirred together, with care to avoid forming too many bubbles. The sample vial was then placed in a desiccator under vacuum in order to degas the PDMS mixture. This mixture was then transferred into the chip mould, degassed again as required, and cured at 60 ^{o}C for approximately 2 hours. Once cured the PDMS chip was allowed to cool within the mould before being removed.

Moulds were designed and fabricated in house to form the microfluidic chips. They were constructed from Perspex in order to hold capillaries or formers (in order to produce microfluidic channels directly in the PDMS) in desired positions. The chips were made in two parts for ease of construction. Care was taken in the design of the moulds to ensure that the two surfaces at which the separate chips are compressed together are completely flat to prevent any distortion. The mould was constructed and capillaries or formers inserted to produce the microfluidic channels. This was then sealed with adhesive tape, wax or epoxy resin to prevent any leakage of the uncured PDMS.

Clamps were also manufactured by the departmental engineering workshop in order to compress the PDMS chips and form a liquid / gas tight seal. These consisted of two Perspex plates (50 mm [width] x 50 mm [depth] x 10 mm [thickness]) to cover the top and bottom of the chip. Holes were drilled in the top plate in order to allow access to the chip reservoirs. A hole (5 mm diameter) was drilled in the four corners of both plates, then bolts inserted through in order to form the clamping mechanism. The chip was aligned and compressed in the clamp by tightening the four bolts. Care was taken to tighten the clamp evenly so the chip was compressed evenly. Any distortion of the chip was avoided as this could cause liquid leaks. The arrangement with a clamped PDMS chip can be seen in the example in Figure 5.1.

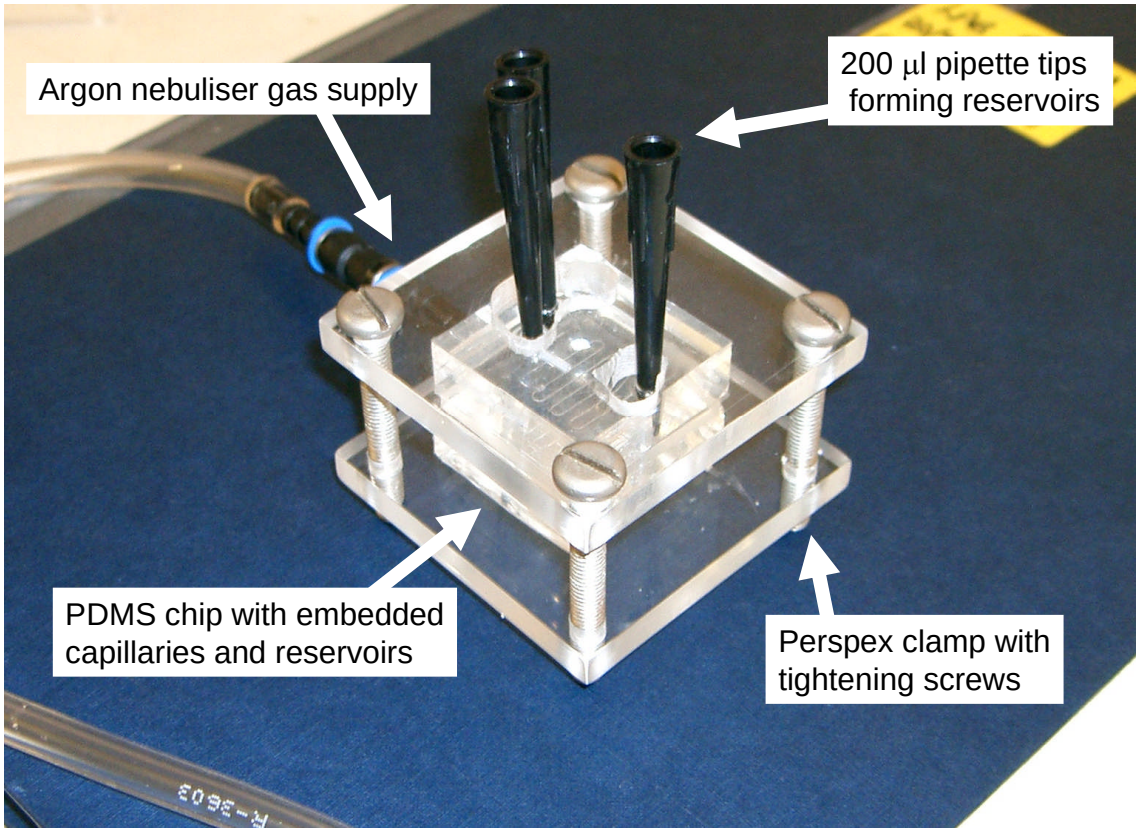

Figure 5.1 Clamped PDMS chip as used in development of chip based nebuliser. Detail of argon nebuliser gas connection, liquid reservoirs and clamp is shown.

5.2.3.2 Fabrication of glass microfluidic chips

The microfluidic chips consisted of two borosilicate glass plates; a bottom (or base) plate into which the channel network is constructed and a top (or cover) plate. The typical dimensions of the chips were 2.5 cm (L) × 2.5 cm (W) ×1.7 cm (H). The device was fabricated by the Microfabrication facility at the University of Hull using a previously reported method.[17] The desired channel network was produced in the base plate by photolithography and wet chemical etching (1 % HF / NH_4F), to produce channels of 100 μm width and 20 μm depth. Wet chemical etching allows freedom in

the channel design and complex patterns can be realised without the need for connectors and the introduction of dead volumes. The same channel network was used throughout the work, which will be discussed later and is shown in Figure 5.2. Briefly the length of the main channel was 10 cm with 8 cm after a sample injection channel in a serpentine pattern. This design allows a longer channel length in a small area, which is useful in conducting separations on such a microchip. A 360 μm i.d. hole was drilled into the base plate at the end of the liquid channel. Holes were drilled into the top plate (typically 2 mm in diameter) in designated positions to form reservoirs and allow connection to liquid handling / pump systems. The two plates were then thermally bonded in a furnace at 570 ˚C for 3 hours. In order to increase the capacity of the reservoirs, 200 μl pipette tips (with ends cut to fit tightly into the drilled holes) were inserted into the top plate and sealed into position with high pressure epoxy resin (Torr Seal®, Varian, Oxford, UK).

5.2.3.3 Fabrication of the micro cross-flow nebuliser assembly

The chip and MCFN assembly consisted of a PTFE block (5.3 x 5.0 x 4.5 cm) into which had been cut, on the top side, a wide channel of 2.5 cm to hold the microchip, as shown in Figure 5.3. A channel for the nebuliser gas was drilled through the back of the PTFE block, with the outside edge being widened and designed to hold screw in HPLC finger tight fitting (Omnifit, Cambridge, UK). The channel met up with a wider cone shaped opening to allow for expansion of the sample aerosol. This opening had a groove with an ‘O’ ring of 2.2 cm i.d. on the front side of the PTFE block in order to provide a gas tight fitting with the evaporation chamber (described in Chapter 4).

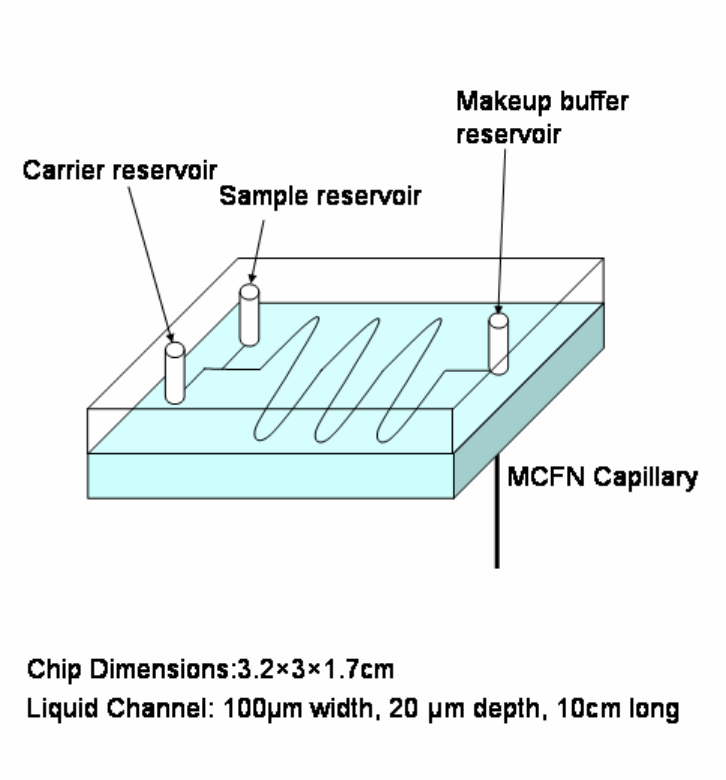

Figure 5.2 Schematic of microchip designed with chip based nebuliser. Top plate contains 3 holes with 2 mm diameter reservoirs which facilitates connection to the pumping system. Bottom plate is etched with liquid channel and has a 360 μm through hole at the end of this channel into which a microcross-flow nebuliser (MCFN) capillary is inserted to transport the liquid to the gas flow for nebulisation.

A 2.0 cm length of 50 μm i.d PEEK capillary (Upchurch Scientific, Oak Harbour, USA) was sealed into the 360 μm i.d. hole in the chip base plate, which was directly under the reservoir at the end of the liquid channel. This capillary (which had a volume of 38 nl) then fitted into a hole (360 μm i.d.) drilled through from the wide channel on the top PTFE block into the opening of the gas channel through the centre of the block. The capillary was aligned perpendicular to the gas flow channel and thus formed the MCFN. The vertical position of the tip of this capillary could be altered by introducing spacers

under the microchip in order to optimise the nebulisation. The gas flow to the nebuliser was delivered by a 250 μm i.d. PEEK capillary (Upchurch Scientific, Oak Harbour, USA), selected to give sufficient gas flow pressure (3 – 5 bar) at suitable flow rate for ICPMS (0.8 – 1.0 L min^{-1}). The horizontal position of the gas capillary could be altered by adjusting the HPLC screw tight fitting; this had a locking nut that could be set once the system was optimised.

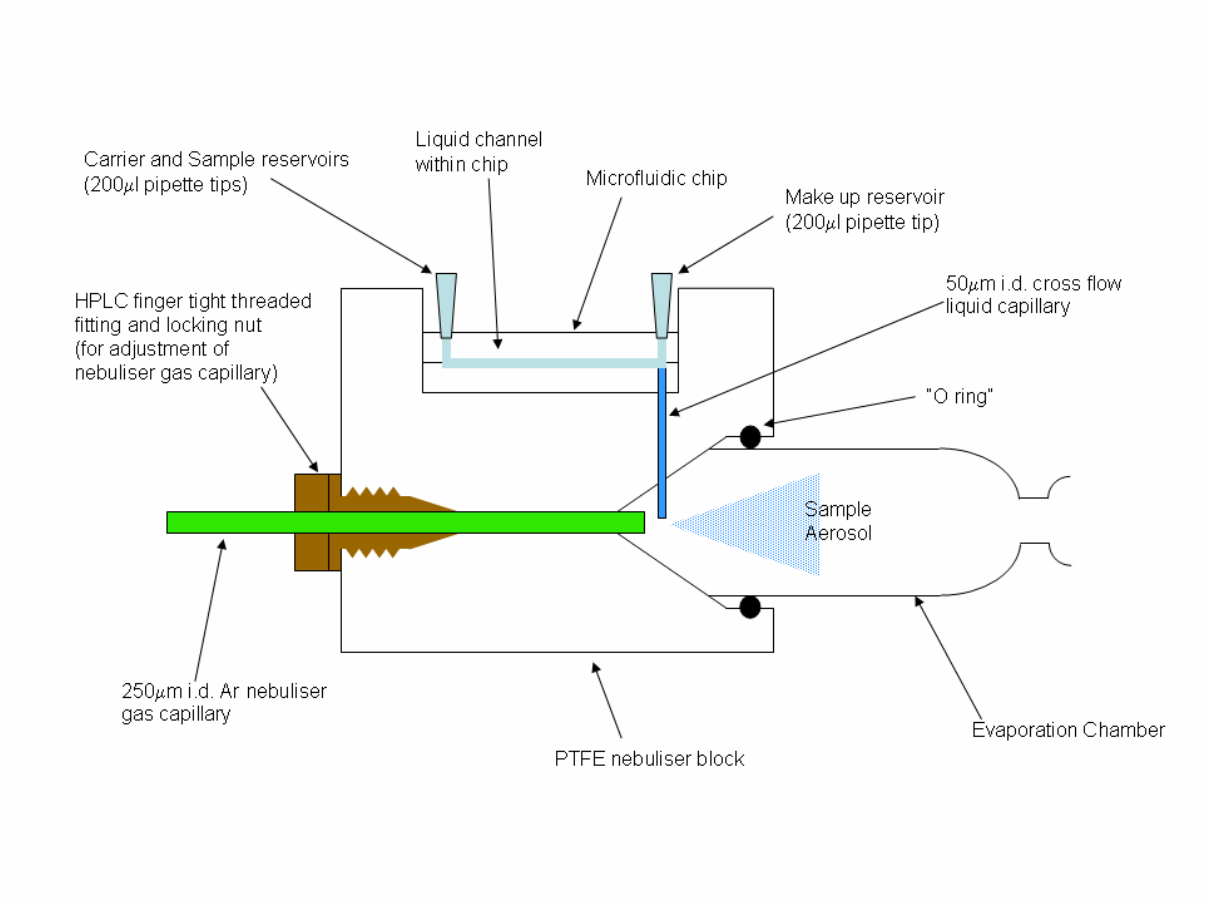

Figure 5.3 Schematic of microchip/nebuliser assembly showing location of microchip in PTFE block, orientation of gas and liquid flows for nebuliser and evaporation chamber which is connected directly to existing ICPMS instrument torch

5.2.3.4 Sample injection

Hydrodynamic sample injection was performed since electrokinetic methods could introduce severe sample bias for the analysis of small ionic molecules.[18] The development of the sample injection procedure is discussed further in Chapter 6. Liquid flow was delivered to the sample and carrier reservoirs by one syringe pump. A 3-way 'Y' manual switching valve (Omnifit, Cambridge, UK) was used to direct the flow to the sample and carrier reservoirs allowing independent control of both. A second syringe pump was used to deliver the make up flow. Tygon peristaltic pump tubing (Elkay Laboratory Products Ltd., Basingstoke, UK) was used to transfer the liquid from syringe pump to the chip reservoirs. The reservoirs were filled with the appropriate solution and then the pump tubing pushed tightly into the reservoir to form a seal. The syringes contained only the carrier solution (15 mM HNO_3). Liquid was pumped to all reservoirs at 10 μl min^{-1} in order to purge the chip for approximately 10 minutes before checking the flow from each reservoir by monitoring the appropriate signal (e.g. Cr: sample, Y: carrier, In: make up). The make up flow and carrier flow was on throughout the sample injection. The sample flow was switched on *via* the 3-way switching valve for a fixed time period to give a known sample volume.

5.3 Results and discussion

5.3.1 PDMS development

The method for making microfluidic chips for the development of a chip-based nebuliser had to be inexpensive, quick and simple as many chips were produced and several of them discarded during investigation into a suitable design. Initial development of a chip-based micro-nebuliser was conducted by fabricating microfluidic chips from polydimethylsiloxane (PDMS). PDMS is a polymeric material well suited to micro fabrication techniques for producing microchips for use in a variety of lab on a chip and micro-total analytical system (μTAS) applications.[17] For these reasons PDMS was a useful starting material for the fabrication of chips in this work.

The fabrication of these chips from PDMS is described in the procedures section. Channels were made either directly within these chips (using formers with appropriate dimensions) or by embedding capillaries to give the desired orientation of gas and liquid flow in order to produce a fine sample aerosol. It was quickly realised that the embedding of a capillary to supply the nebuliser gas was essential within a PDMS chip; since the material deformed at the required flow rate and pressure creating leakage or a change in direction of the gas flow. A short length (30 – 40 mm) of PEEK (250 μm i.d.) capillary (Upchurch Scientific, Oak Harbour, USA) was selected to give sufficient gas flow pressure (3 – 5 bar) at suitable flow rate for ICPMS (0.8 – 1.0 L min^{-1}). This was sealed into an EzyLok connector (Glass Expansion, Austrailia) using epoxy resin (Bondmaster®, Eastleigh, UK); allowing simple connection to Tygon tubing ($^1/_4$" diameter) used for connection of the gas flow to both ICPMS instruments.

Firstly the orientation of gas and liquid flow for efficient nebulisation was investigated. A key factor in the final design is the ease of fabrication for the final chip. Ideally all channels, carrying both gas and liquid, would be in one plane on the surface of the chip, and hence etched in one step. For this reason the initial designs were based upon the gas and liquid flow meeting at varying angles on a planar surface. Nebulisation was achieved, with varying degrees of success, but the aerosols produced were highly pulsed. This was due to the formation of droplets at the end of the liquid capillary, before being nebulised by the gas flow.

Included in this investigation was a design based upon the parallel path design reported by Burgener (Burgener Research Inc., Ontario, Canada).[19, 20] A high gas flow, under high pressure, flowing in very close proximity and parallel to a liquid flow will shatter the liquid into a fine mist of droplets. This design is advantageous for a chip based nebuliser since as all channels would be at the surface of the chip. However efficient nebulisation was not achievable due to the use of capillaries. The spacing dictated by the two neighbouring capillary walls separate the gas and liquid flow sufficiently to hamper the liquid being drawn into the gas flow by the pressure difference created by the gas flow exiting the capillary. Therefore this design may be effective on an accurately engineered chip design, ideally encompassing the more efficient enhanced parallel path design. This involves the inclusion of a small lip to guide the liquid flow into the centre of the gas flow. An illustration of such a microfluidic device is shown in Figure 5.5. This was not investigated further in this study owing to the required chip engineering imposing limitations on the applicability to a wide range of microfluidic designs.

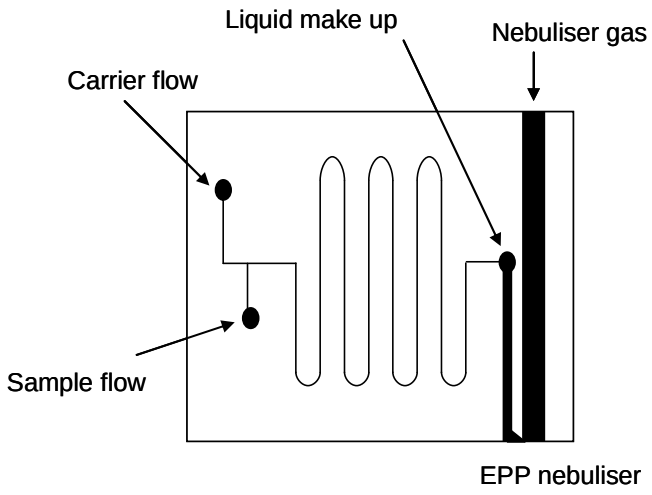

Figure 5.4 Design for microfluidic chip with integrated enhanced parallel path (EPP) nebuliser.

A design based upon the concentric nebulisers, while providing efficient nebulisation, was not investigated in the chip based nebuliser design. Integrating such a design would require a high degree of engineering making the microfluidic chips expensive. Additionally one of the disadvantages associated with microfluidic chips is the potential for blockages. A concentric nebuliser design would exacerbate this problem.

5.3.2 Cross-flow design

A proven nebuliser design with the liquid and gas flows meeting perpendicular to each other produced the best results based upon visual inspection of the aerosol. A cross-flow or V-groove design could be integrated readily into a chip based design due to the ease of engineering. It would conceivably be possible to alter an existing microchip to encompass such a design. The cross-flow orientation is more desirable than a V-groove design as it can be more easily incorporated into an enclosed system, suitable for use with an ICP source. The V-groove design (Figure 1.6 d) involves liquid flow through an external v-shaped groove. With this system it would be harder to achieve a gas

tight seal when incorporated into the front face of the chip within an evaporation chamber.

A cross-flow PDMS chip was constructed following the same preparation procedure as before. The chip was in two pieces, using the same orientation for the gas flow within a centrally embedded capillary, with the liquid capillary being aligned perpendicular to the gas flow outlet to form an arrangement as shown in Figure 1.6 b. This proved effective for the nebulisation of water, and no problems with droplet formation at the nebuliser tip were observed. The aerosol was visualised by spraying onto absorbent blue paper illuminated from behind. Inspection demonstrated that the aerosol consisted of finer droplets, *cf.* previous designs, and no obvious pulsation was observed.

5.3.3 Aerosol droplet size measurements

In the development of a new nebuliser it is desirable to measure the mean size distribution of the droplets produced, in order to ascertain the efficiency of the nebulisation and suitability for sample introduction into the plasma.[21] In order to gain an understanding of how aerosol properties affect ICP detection quantitative tertiary aerosol drop size distributions are required. An aerosol is a mixture of gases, particles and solvent vapour. The particles are either solid or liquid droplets with diameters ranging from > 0 to 200 μm. Droplets are assumed to be spherical, i.e. the effect of particle shape is neglected. Numerous studies on droplet sizing have been conducted and the effects on ICPMS evaluated.[22-24]

The facility to measure aerosol droplet size distributions was not available during this work; therefore the performance of the nebuliser was assessed directly by

operation with the ICPMS instrument, by observing the sensitivity and stability of the detector response. Precise measurement of the aerosol characteristics and analyte mass transport efficiency for very low liquid flow rates (μl min^{-1}) has been reported to be difficult.[25] This is due to the limited aerosol – liquid volume at liquid flow rates below 100 μl min^{-1}.[26] Therefore there is a lack of fundamental studies concerning the processes occurring at low liquid flow rates.

5.3.4 Micro cross-flow nebuliser for use with glass microfluidic chip

Several designs were initially investigated for the chip based cross-flow nebuliser. It was soon found that several factors had to be considered that limited the options. These included the need to have access to the top of the chip for sample injection (i.e. chip to be horizontally aligned) and the horizontal alignment of the ICPMS torch and evaporation chamber. Since the nebuliser gas flow dictates the direction of the aerosol produced this must be on the same plane as the evaporation chamber and torch. Therefore the liquid flow must flow vertically up or down. This presents problems for the incorporation into a microfluidic chip since small vertical channels are not easily fabricated through the device. Only holes greater than 360 μm can be drilled, which is too large. Smaller channels can be laser ablated, but this would not produce a smooth circular channel surface. It was also essential to have a gas tight system from the liquid entering the chip to reaching the plasma to prevent air extinguishing the plasma. These factors eliminated incorporation of the cross-flow nebuliser into the microfluidic chip due to engineering problems of the chip and creating an interface to achieve a reliable gas tight seal.

A design based upon transferring the liquid from the microfluidic chip to a cross-flow nebuliser arrangement sited directly above the liquid exit of the chip was developed. This was constructed from a glass bottom plate, with etched channel, and PDMS top plate. The nebuliser gas capillary and reservoirs (200 μl pipette tips) for carrier and sample were embedded within the PDMS during fabrication. This is shown schematically in Figure 5.5.

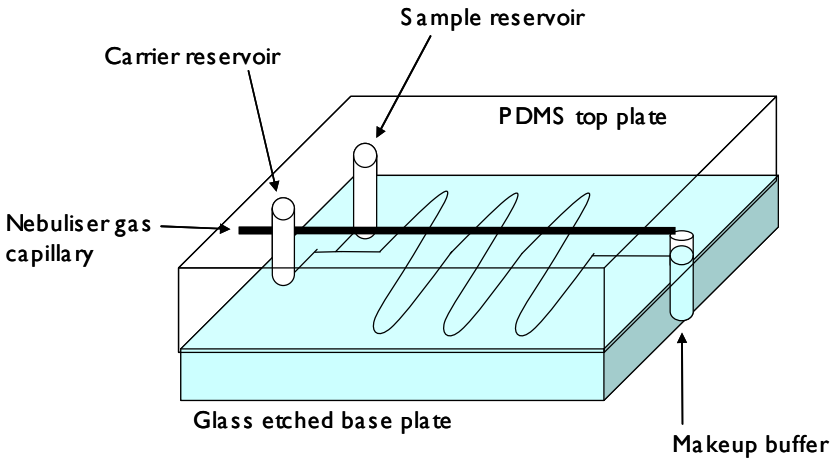

Figure 5.5 Schematic of chip based cross-flow nebuliser design with nebuliser sited directly above liquid exit of chip.

The make up buffer was supplied by a 500 μm i.d. capillary sealed into the hole through the glass base plate using PDMS. A second capillary, termed the cross-flow capillary, was embedded within the PDMS top plate above the liquid exit to facilitate the transfer of the make up and chip flow vertically up to meet the nebuliser gas stream. The cross-flow capillary was a very short length (approx. 4 mm) of 150 mm i.d. PEEK (Upchurch Scientific, Oak Harbour, USA). This could be adjusted vertically, using tweezers, within the PDMS to meet with the gas flow capillary. This composite PDMS / glass chip was clamped together as described in procedures (Section 5.2.3.1) and is shown in Figure 5.6. The evaporation chamber was sealed into this assembly using a

PTFE adapter. This was screwed into the face of the clamp and a gas tight seal to the chip / clamp was formed by PDMS. The adapter had a 26 mm diameter central hole to hold the evaporation chamber. This contained a rubber 'O' ring to form a seal around the outside of the chamber.

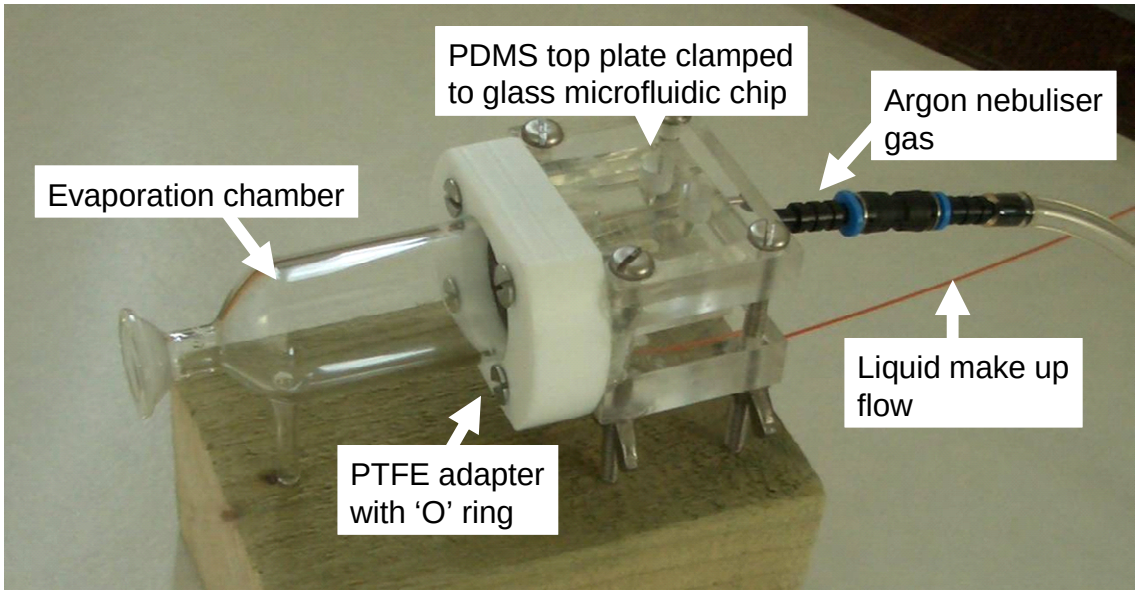

Figure 5.6 Composite PDMS / glass chip with micro cross flow nebuliser and evaporation chamber.

Careful alignment of the gas and liquid capillaries resulted in production of a fine sample aerosol, generating 30 000 cps with < 5 % RSD over 30 minutes (liquid 20 µl min^{-1}; gas 0.88 L Ar min^{-1}). However no adjustment of the gas or liquid capillaries could be made once the evaporation chamber was connected. It became obvious that any gas or liquid tubes must be held rigidly, but at same time be adjustable if reproducible results were to be obtained. Additionally the use of a PDMS top plate made sealing the chip difficult and frequent leaks were experienced. For this reason it is desirable to use a thermally bonded glass microfluidic chip. With the current design changing the chip or any of the capillaries would be complex and require the entire assembly to be dismantled and resealed (requiring curing of PDMS). While it is

conventional to have the liquid flowing up to meet the gas flow; upward flow of liquid created excessive back pressure within the channels of the chip and affected the liquid flow. In this cross-flow design it was found to be better to have the liquid flowing down in the opposite geometry.

These factors led to the final design of a micro cross-flow nebuliser (Figure 5.3) with a glass microfluidic chip (Figure 5.4). Figure 5.7 shows the resulting sample introduction system with the Elan DRC II ICPMS.

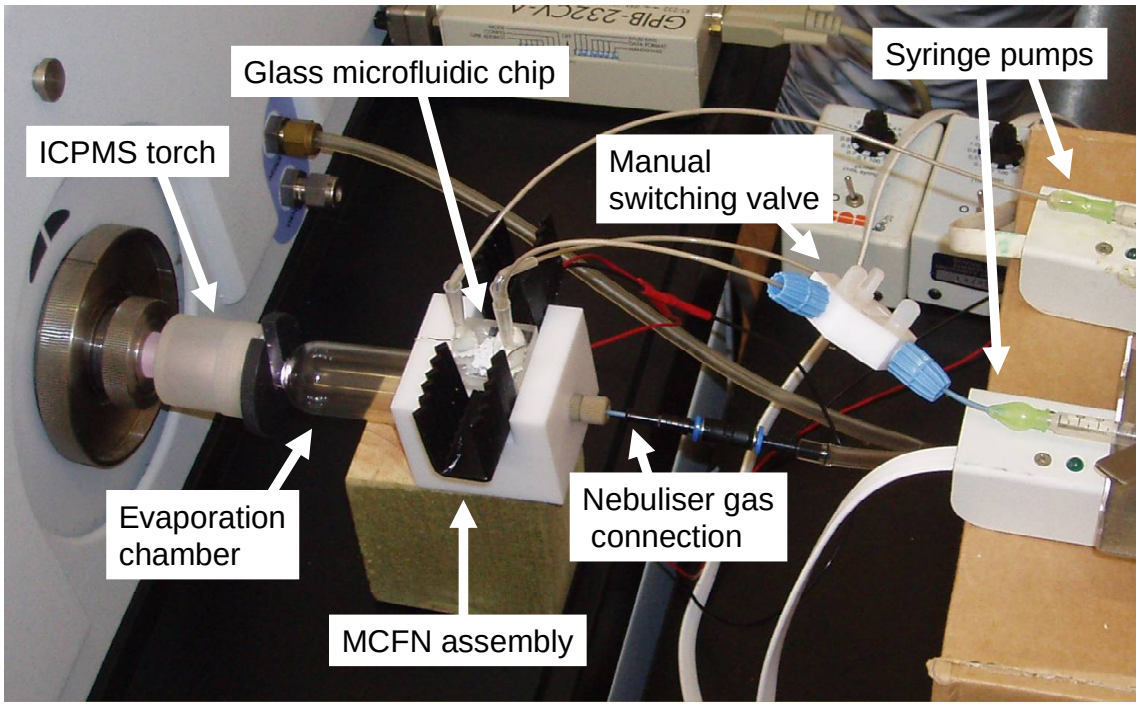

Figure 5.7 Microfluidic chip sample introduction system for ICPMS. Comprising of micro cross flow nebuliser (MCFN) and integrated evaporation chamber. Liquid supplied to microchip reservoirs by two independent syringe pumps. Sample injection performed by means of a manual switching valve to direct flow between sample and carrier reservoirs.

A very short 2.0 cm length of PEEK tubing (50 μm i.d.) was used both as an interface and as the sample delivery tube for the nebuliser, introducing a dead volume of just 38 nl (*cf.* 995 nl, with previous design to utilise commercial sample introduction)[14]. The

capillary was held rigidly in place within the PTFE block and also had the advantage of being easily replaced if it became blocked or damaged. The nebuliser gas tube was held at right angles to the sample tube by the PTFE block and its position could be adjusted by a locking screw as described in the procedures (Section 5.2.3.3). Both the gas and liquid capillaries could be aligned and adjusted with the evaporation chamber in place while connected to the ICPMS with the plasma on. This allowed accurate optimisation of the nebuliser using the signal generated (cps). This arrangement also permits the microfluidic chip to be easily replaced and any chip design to be used (as long as the external dimensions of the chip fit within the PTFE block, or the cavity in the block is modified as required).

5.3.4.1 Optimisation of ICPMS sample introduction

The Elan ICPMS was optimised with standard sample introduction and the performance checked as recommended by the instrument manufacturer. Upon switching to the MCFN and evaporation chamber the positioning of the sample delivery and nebuliser gas capillaries were adjusted followed by the X-Y position of the torch to obtain the maximum signal (based upon Mg, In, and U using 1 μg L^{-1} tune solution).

The nebuliser gas flow rate and RF power were optimised for the chip-based MCFN with the optimised evaporation chamber sample introduction system. A solution containing 10 μl L^{-1} indium was delivered at 5.0 μl min^{-1} to the make up reservoir by the syringe pump, with the sample and carrier reservoirs being filled with 15 mM nitric acid. The effects were monitored by measuring the signal for indium at $^{m}/_{z}$ 114.9. For the gas flow study, the flow rate was varied between 0.6 – 1.2 L min^{-1} argon in steps of 0.01 L min^{-1}. The optimum was selected based upon maximum intensity for indium

rather than the oxide ratio (CeO / Ce) to provide below 3 % oxide formation. This was because oxide interferences were found to be significantly lower than 3 % at all gas flows investigated and for the introduction of such a low sample flow rate the most important factor is to achieve the greatest analyte signal as possible. For the RF power study the power was varied from 900 to 1400 W in steps of 25 W and optimised on maximum sensitivity for indium. Example results of this optimisation are shown in Figures 5.8 and 5.9.

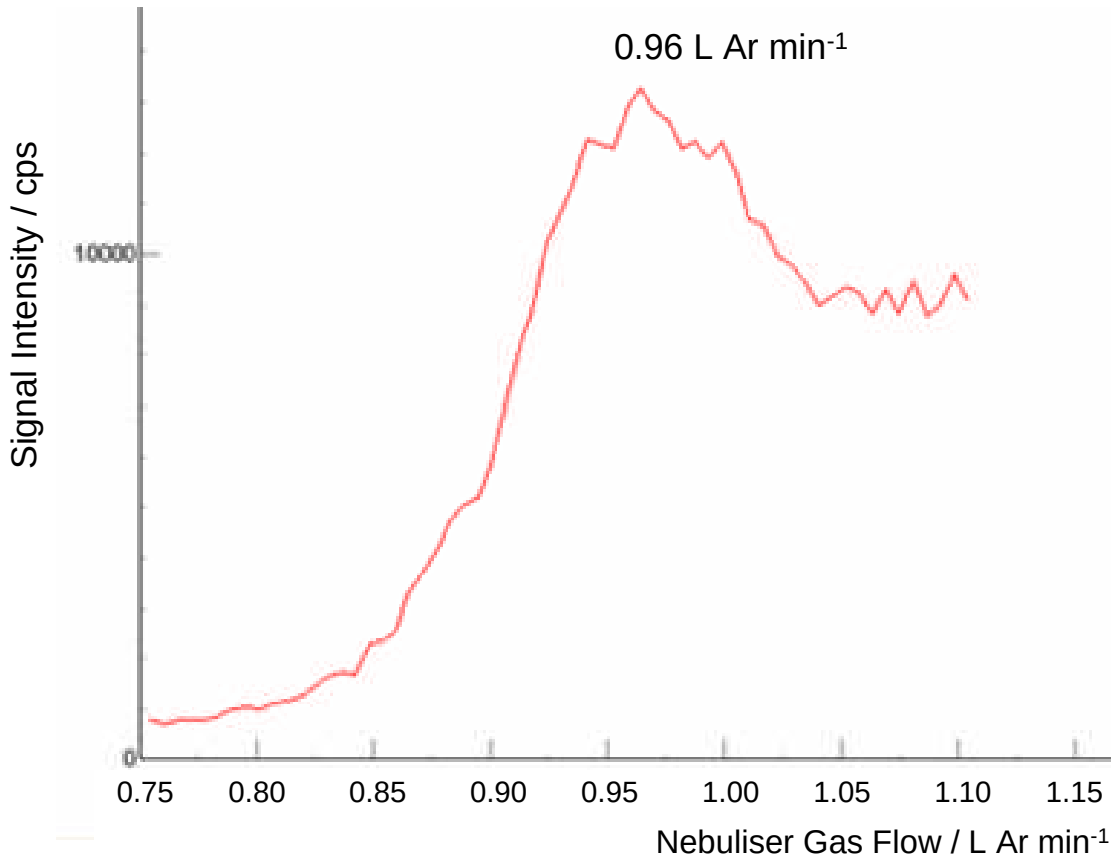

Figure 5.8 Ar nebuliser gas optimisation with DRC (0.5ml min^{-1} NH_3) based upon maximum intensity at $^{m}/_{z}$ 114.904 for 10 µg L^{-1} indium at 5.0 µl min^{-1}. MCFN with optimised evaporation chamber.

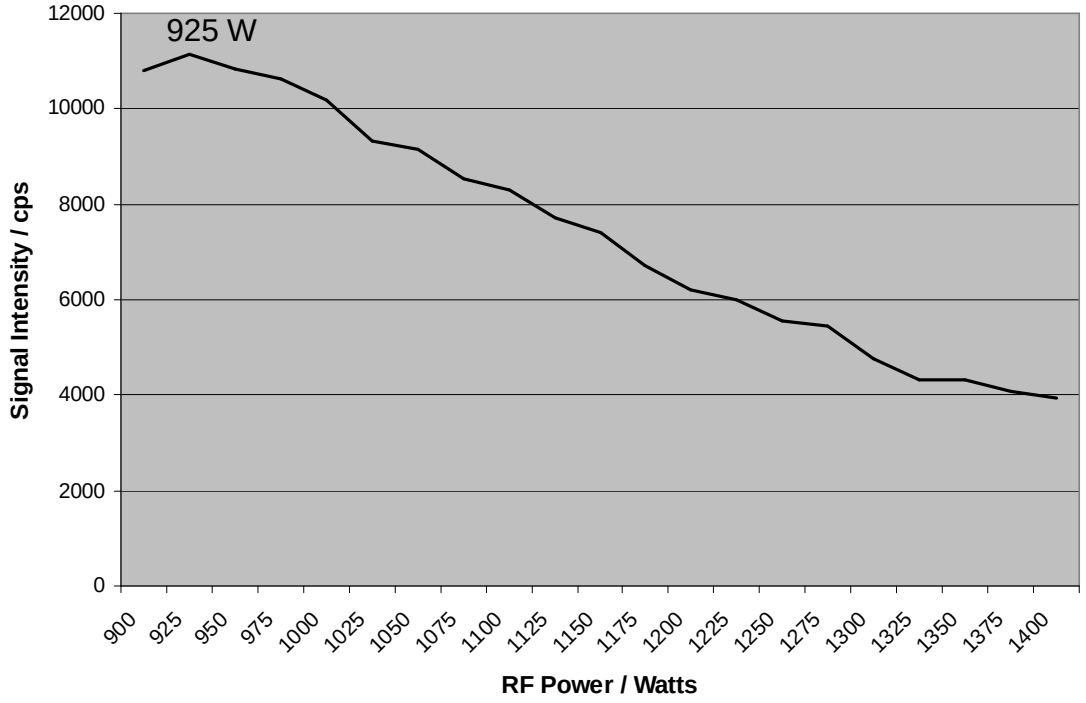

Figure 5.9 Optimisation of RF power for MCFN with optimised evaporation chamber. Based upon the sensitivity for indium (5.0 μl min^{-1}) at $^{m}/_{z}$ 114.9 contained within make up reservoir.

The optimal RF power was 925 W and nebuliser gas flow was 0.91 L Ar min^{-1} in standard mode (without use of DRC) and 0.96 L Ar min^{-1} in DRC mode. The RF power is slightly lower than usual due to the lower flow rate of the sample, hence drier plasma conditions. The optimisation resulted in 13 500 cps for 10 μg L^{-1} indium at 5 μl min^{-1}. This demonstrates the ability to achieve good sensitivity for trace element detection operated at very low flow rates (μl min^{-1} *cf.* ml min^{-1} usually required). The stability of the chip sample introduction was evaluated by measuring the signal for 10 μg L^{-1} indium at 5 μl min^{-1} for 10 minutes (n = 453), which resulted in 2.6 % RSD. No sample recondensation was ever observed within the optimised evaporation chamber provided that the liquid flow rate was below 20 μl min^{-1}. Hence the chip MCFN sample introduction interface is both stable to achieve reproducible results and sensitive,

achieving high transport efficiency.

5.3.4.2 Flow injection analysis of small sample volumes

The optimised sample introduction system was evaluated for the analysis of extremely small sample volumes, in the order of nanolitres. These experiments were carried out using continuous liquid flow providing constant plasma conditions. Hydrodynamic sample injection was performed as described in the procedures. The sample contained 150 μg Cr L^{-1} in 15 mM HNO_3. The sample volume was easily calculated from the flow rate and injection time.

Firstly the control and stability of the liquid pump and injection system was investigated. The signal for yttrium contained within the carrier reservoir was monitored throughout switching of the sample flow and remained stable throughout. A chromium standard was monitored as the sample and the flow applied at 0.25 μl min^{-1}. Figure 5.10 shows the chromium signal rose up to a stable level until it was switched off again, at which point it dropped off sharply to the baseline. The rise time for the sample can be estimated at 50 seconds, while the signal falls to 1 % of the background within 30 seconds. This demonstrates the flow can effectively be controlled by the external syringe pumps and switching valve.

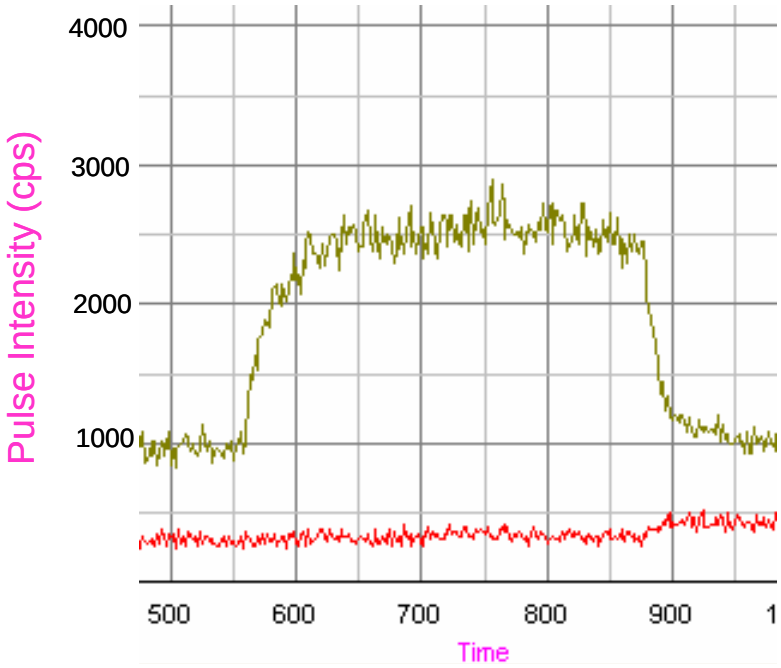

Figure 5.10 Control of hydrodynamic carrier and sample flow. Sample reservoir containing 100 μg L^{-1} Cr(III) / 50 μg L^{-1} Cr(VI) mixed standard in 15 mM HNO_3. Make up and carrier reservoirs containing 15 mM HNO_3 spiked with 10 μg L^{-1} indium and 100 μg L^{-1} yttrium respectively. Flow rate 0.5 μl min^{-1} to both sample and carrier reservoirs and 5.0 μl min^{-1} to make up. Signal monitored for Cr ($^{m}/_{z}$ 51.9) [green] and Y ($^{m}/_{z}$ 88.9) [red].

The reproducibility of the sample injection procedure was evaluated by comparison of six 20 second consecutive injections at 0.4 μl min^{-1} corresponding to a 130 nl sample volume. Figure 5.11 shows the peaks obtained. Table 5.2 shows the results for the reproducibility for the injection procedure assessed by peak height and integration of the peak area. The data was processed using Turbochrom Workstation and Chromlink™ for the Elan ICPMS (PerkinElmer LAS Ltd., Beaconsfield, UK). The best results were obtained from the peak area, resulting in 5.1 % RSD.

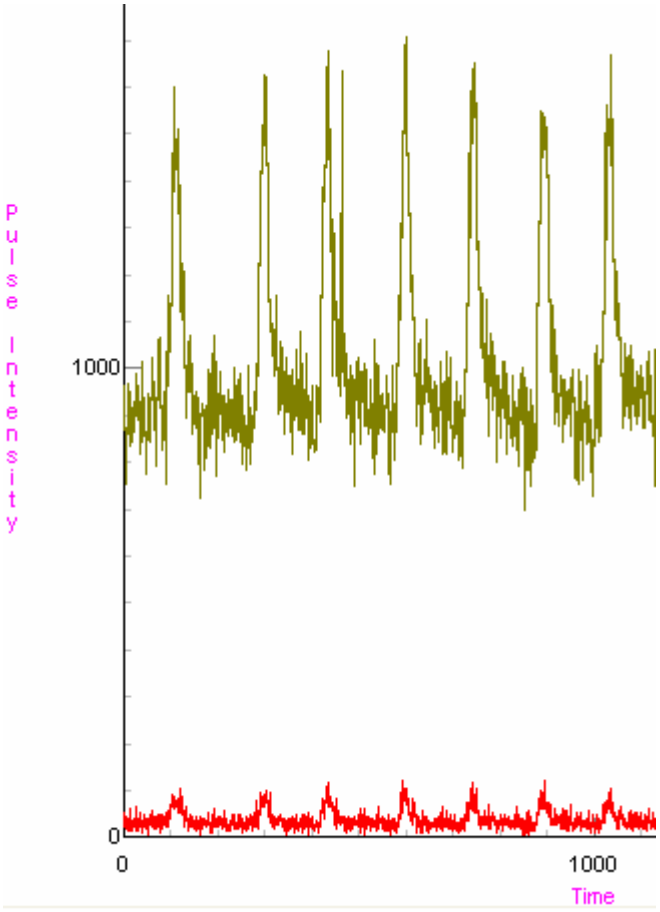

Peak	Area	Height
1	14581	710.67
2	15646	768.9
3	16743	881.9
4	16441	836.7
5	15929	719.8
6	15159	857.5
Mean	15750	795.9
SD	803	73.0
RSD / %	**5.1**	**9.2**

Table 5.2 and Figure 5.11 Injection reproducibility of consecutive 20 second (130 nl) sample injections. Sample reservoir containing 100 μg L^{-1} Cr(III) / 50 μg L^{-1} Cr(VI) mixed standard in 15 mM HNO_3. Make up and carrier reservoirs containing 15mM HNO_3 spiked with 10 μg L^{-1} indium and 100 μg L^{-1} yttrium respectively. Flow rate 0.8 μl min^{-1} to both sample and carrier reservoirs and 5.0 μl min^{-1} to make up. Signal monitored for Cr ($^{m}/_{z}$ 51.9) [green] and Y ($^{m}/_{z}$ 88.9) [red].

The reproducibility, while not ideal is reasonable considering the extremely low sample volumes and manual injection procedure. Further discussion and suggestions for improving injection are presented in Chapter 6.

The response of increasing sample volume was then investigated by means of increasing the injection time from 5 seconds up to 30 seconds. This corresponds to sample volumes from 40 nl up to 250 nl. Figure 5.12 shows the results of six consecutive injections with increasing volume of a chromium standard.

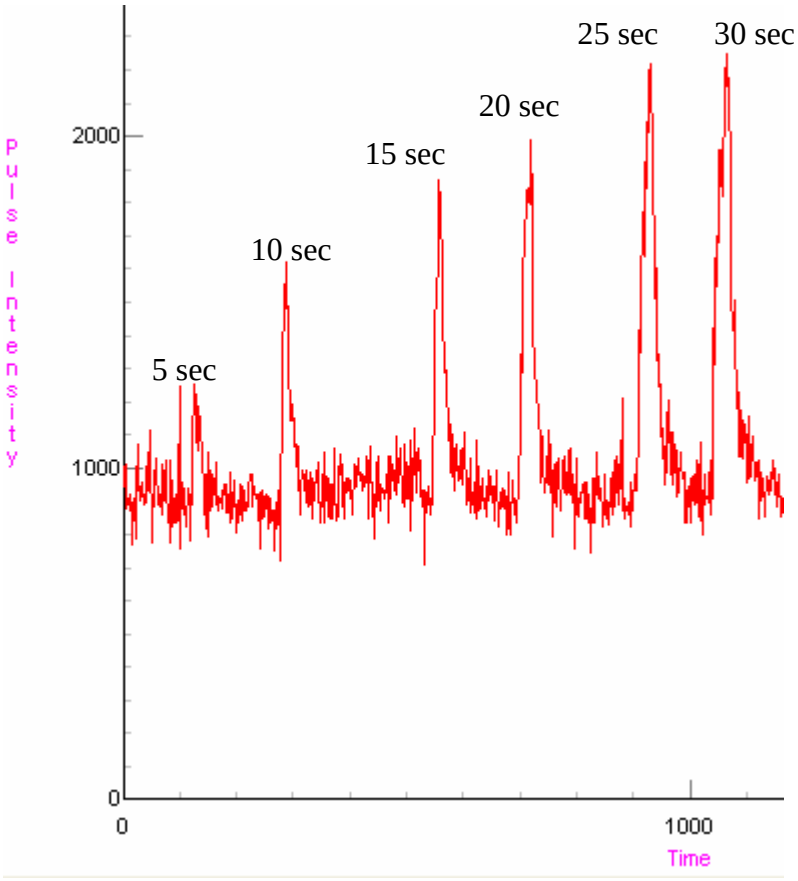

Figure 5.12 Increasing injection time for 6 consecutive injections. Flow rate 0.5 µl min^{-1} to sample reservoir containing 100 µg L^{-1} Cr(III) / 50 µg L^{-1} Cr(VI) mixed standard in 15 mM HNO_3. Make up and carrier reservoirs containing 15mM HNO_3 pumped at 1.0 and 5.0 µl min^{-1} respectively.

Figure 5.13 shows the relationship between peak area produced by sample injection and the sample volume. A linear increase in the intensity is found as the sample volume increases. This demonstrated that the sample injection technique effectively controls the injected sample volume. Therefore this sample introduction system encompassing a microfluidic chip provides an effective method to introduce nanolitre sample volumes for ICPMS.

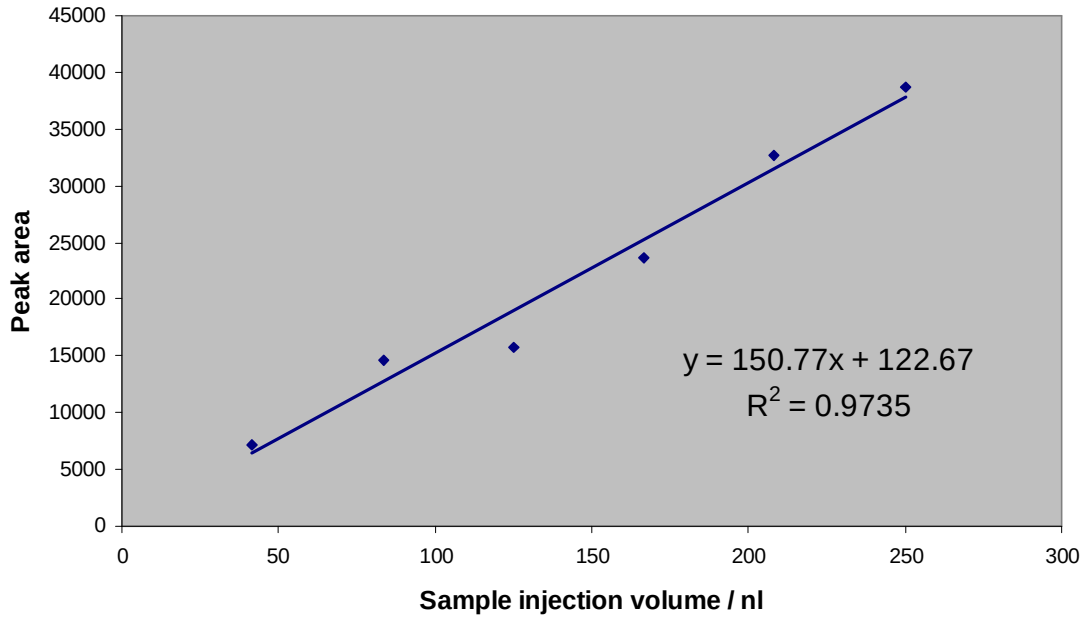

Figure 5.13 Sample injection volume against the area of peak produced. Sample consists of 100 μg L^{-1} Cr(III) / 50 μg L^{-1} Cr(VI) mixed standard in 15 mM HNO_3. Flow rate 0.5 μl min^{-1} to sample reservoir. Make up and carrier reservoirs containing 15mM HNO_3 pumped at 1.0 and 5.0 μl min^{-1} respectively.

It is possible to estimate the lowest sample injection volume that can reproducibly give a practical signal. 40 nl sample volume of 150 μg Cr L^{-1}, resulted in 1250 cps. However; it was noted throughout these experiments that the background signal for chromium was relatively high (*ca.* 1000 cps). When using a chromium

sample the signal corresponding to ^{52}Cr is interfered (e.g. $^{40}Ar^{12}C$). This interference can be reduced by using the DRC with 0.5 ml min^{-1} NH_3 to yield greatly improved signal to noise ratios. Figure 5.14 shows the background signal was subsequently reduced from almost 1000 cps to below 300 cps. Therefore 1000 cps for 30 nl sample volume gives a signal to noise (S/N) ratio of 3.3, which is above the criteria for limit of detection.

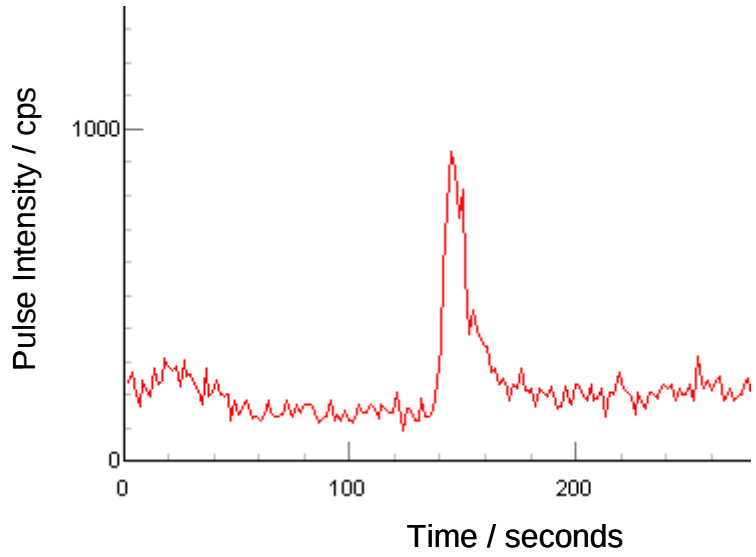

Figure 5.14 Reduction of Cr ($^{m}/_{z}$ 51.9) background using DRC (0.5 ml min^{-1} NH_3, RPq 0.6). Sample injection of 30 nl (0.4 µl min^{-1} flow rate, 5 second injection) 100 µg L^{-1} Cr(III) / 50 µg L^{-1} Cr(VI) mixed standard in 15 mM HNO_3.

5.3.4.3 Application to microchip electrophoresis

The sample introduction system was then investigated as an interface for microchip electrophoresis with ICPMS detection. Speciation of chromium (Cr^{VI} / Cr^{III}), arsenic (As^{III} / As^{V}), and copper (Cu-$EDTA^{2-}$ / Cu^{2+}) has previously been achieved with such a system interfaced to ICPMS *via* commercial sample introduction.[14]

5.3.4.3.1 Benefits of microchip electrophoresis

The benefits of electrophoresis within a microfluidic chip, compared with capillary electrophoresis, include reduced dimensions (channel diameter, length), minimisation of dead volumes from the use of etched channel networks and more efficient heat dispersion. These advantages can afford a significant reduction in separation time, from several minutes to 30 – 60 seconds. This is highly desirable when using highly sensitive detection provided by ICPMS, since the detector idle time is reduced as is the cost of analysis and the sample throughput can be greatly increased.

These advantages result from Ohm's law, which states the electric field (E) in V cm^{-1} is equal to:

$$E = IR \qquad \textbf{Equation 5.1}$$

Where; I is the current and R is the resistance to the current flow.[27] Since in the microfluidic device the channel length is constant the applied voltage (V) is equal to the electric field. An Ohm's law plot of Equation 5.2 defines the maximum voltage that can be applied by the upper limit of linearity.

$$I = \left(\frac{1}{R}\right)V \qquad \textbf{Equation 5.2}$$

This maximum voltage is dependent upon the buffer composition, pH and concentration as well as the capillary dimensions. A shorter separation channel increases E (V cm^{-1}) and hence reduces the maximum voltage. A smaller diameter channel decreases E (V cm^{-1}) and hence increases the maximum voltage.

5.3.4.3.2 Chip arrangement and conditions

Figure 5.15 shows the microfluidic chip channel design adapted from previous electrophoretic work. Sample injection was performed as described in procedures and evaluation for flow injection analysis. The separation channel followed a serpentine pattern in order to provide a longer channel length in a small area. This is a compromise however since a straight channel would minimise band-broadening contributions from electric field and geometric effects.[18]

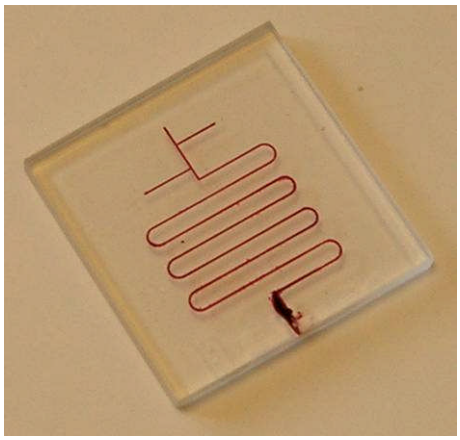

Figure 5.15 Microchip channel layout used in electrophoresis experiments. Channel has been filled with water soluble dye for visualisation (Rose Bengal, Sigma-Aldrich Ltd., Gillingham, UK). Chip dimensions: 2.5 cm (L) × 2.5 cm (W) ×1.7 cm (H). Channel length 10 cm with 8 cm serpentine separation channel following sample injection. Channels 100 μm wide and 20 μm deep formed *via* wet chemical etching of borosilicate glass.

By bending the separation column through 180° turns the difference in the length (d*l*) of the column between the inside and the outside is given in Equation 5.3.[18]

$$dl = \vartheta dr \qquad \textbf{Equation 5.3}$$

Where θ is the angle of the turn (π) and d*r* is the difference in the radius of the turn, i.e. the channel width (100 μm). The difference in channel length is therefore 314 μm

per turn. The effect on the plate height (H) due to this geometric dispersion can be estimated using the relationship in Equation 5.4.[18]

$$H = \frac{n(w\theta)^2}{12L} \qquad \textbf{Equation 5.4}$$

Where L is the length of the channel (80 mm). For simple geometrical broadening it is assumed that the sample is travelling at the same velocity on both the inside and outside of the channel throughout the turn. Therefore with the dimensions in the device above (w = 100 mm; $\theta = \pi$; n = 8 [7 x 180° turns and 2 x 90° turns]) the distortion in the band profile is equivalent to 0.82 μm. It is important to note that the contribution to the plate height by geometric dispersion decreases as the square of the channel width. Therefore reducing the channel dimensions effectively reduces dispersion due to compact serpentine designs. The geometry of the turns could also produce an additional distortion due to spatially varying electric field strengths within the turn. An ion on the inside of the turn would experience a higher electric field than an ion on the outside, resulting in a greater linear velocity.

Platinum wire electrodes were inserted through the side of the carrier and sample reservoirs into the base of the separation channel. The holes were sealed with a high pressure sealant (Torr Seal®, Varian, Oxford, UK). A high voltage power supply (Wallis Hivolt, Advance Hivolt, West Sussex, UK) capable of supplying 30 kV at 2.0 mA was used to supply the high voltage for the separation. Platinum wires were inserted into the carrier and makeup reservoirs to form electrodes and voltages up to 10 kV were applied *via* these across the separation channel.

Speciation of chromium was attempted using the same conditions as in previous works.[13] The carrier electrolyte was 15 mM HNO_3 at pH 2.0, chosen in order to minimise any EOF of the bulk solution to allow hydrodynamic control *via* the syringe pumps. This was spiked with 100 μg L^{-1} yttrium standard in order to monitor flow and injection procedure. The sample solution consisted of 100 μg L^{-1} Cr(III) / 50 μg L^{-1} Cr(VI) mixed standard in UHQ water. The make up solution was 15 mM HNO_3 spiked with 10 μg L^{-1} indium standard in order to monitor flow and optimise the sample introduction system. The make up flow was 5 μl min^{-1} throughout as this was the optimum found in order to achieve the greatest transport efficiency using the MCFN and evaporation chamber. The sample flow rate was varied between 0.25 and 1.00 μl min^{-1}, resulting in residence times for the sample plug within the separation chamber between approximately 15 and 60 seconds (*cf.* 30 seconds previously required to achieve baseline separation).

The microfluidic separation channel was conditioned prior to electrophoresis using a previously reported method.[2] 1.0 mol L^{-1} NaOH was pumped at 10 μl min^{-1} for 10 minutes in order to regenerate the silanol groups on the surface of the glass. The chip was thoroughly rinsed with UHQ water for 10 minutes and finally the run buffer was pumped for a further 10 minutes. This was performed prior to connection to the ICPMS.

5.3.4.3.3 Conductivity

Conductivity is defined as the ability of a substance to conduct electrical current and is effectively the reciprocal of resistivity. Conductivity is measured in terms of Siemens (S) as the conductance between opposite faces of 1 cm^3 of material, therefore has units

of S cm^{-1} (commonly μS cm^{-1} up to mS cm^{-1}). Pure water has a conductivity of 0.055 μS cm^{-1} and resistivity of 18.3 MΩ cm.[27]

The conductivity of nitric acid (69 %, Super Purity Acid, Romil Ltd., Cambridge, UK) is 6380 μS cm^{-1} at 25 °C for 1000 mg L^{-1}. The conductivity of the 15 mM HNO_3 (945.15 mg L^{-1}) used as carrier electrolyte can therefore be calculated as 6030 μS cm^{-1}. Solid chromium has a conductivity of 77.519 mS cm^{-1}. The conductivity of the sample must be lower than that of the carrier otherwise the applied voltage will be consumed by the carrier.

The conductance (μS) of the sample, make up and carrier solutions were determined by application of HV in a bridge cell. This cell was fabricated using two 50 cm^3 sample tubes with a borosilicate capillary (1.5 mm i.d. x 40 mm length) connecting them. Voltage was applied *via* platinum electrodes placed in each sample vial and the current through the solution measured. Resistance (MΩ) was calculated using Equation 5.5 and the reciprocal used to evaluate conductance (μS).

$$R = \frac{V}{I} \qquad \textbf{Equation 5.5}$$

Conductance was measured for a sample solution containing 200 μg L^{-1} Cr(III) / 100 μg L^{-1} Cr(VI) in UHQ water. Application of 450 V gave 1.0 mA, resulting in a conductance of 2.2 μS. A solution of 15 mM HNO_3 spiked with 200 μg Y L^{-1} and 10 μg In L^{-1} resulted in 11.2 μS, while 15 mM HNO_3 without such additions gave 11.8 μS. This effectively proves that the conductivity of the sample solution is significantly lower than that of the carrier providing it is made up in UHQ water.

5.3.4.3.4 Operation of electrophoretic chip

Problems were encountered during the application of the high voltage (HV) required for performing electrophoretic separation. On applying (and disconnecting) the HV a large drop in signal intensity for all analytes (In, Y and Cr) was observed. This was seen even for low applied voltages (100 – 200 V). The signal recovered slowly, on occasion increased to a higher intensity than prior to the application of HV, before returning to normal. Figure 5.16 shows an example of the signal loss and recovery.

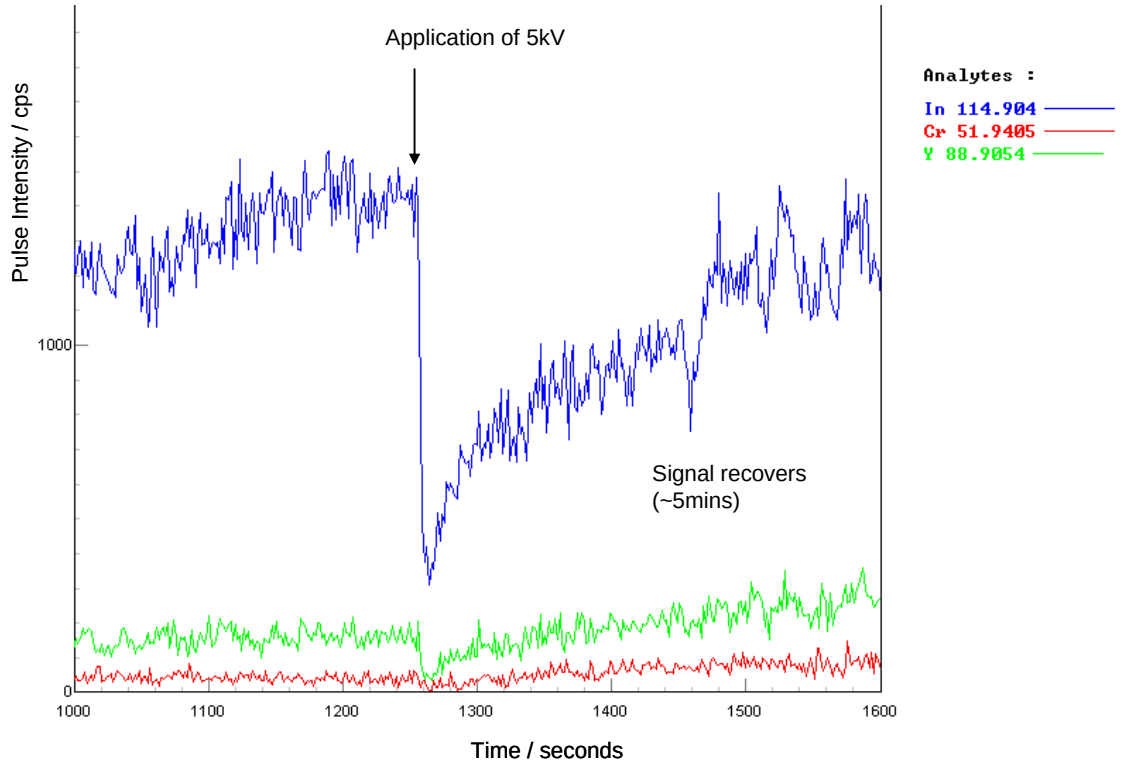

Figure 5.16 Loss of signal intensity of application of HV (5 kV). Signal recovery and stabilisation takes in excess of 5 minutes. 10 μg L^{-1} indium in make up, 150 μg L^{-1} chromium in sample and 100 μg L^{-1} yttrium in carrier reservoirs respectively.

Several checks of the system were conducted in order to ascertain the cause of this signal loss. The d.c. voltage was checked across the electrodes and the liquid within the carrier and make up reservoirs. The result showed that the voltage was

supplied by the power supply, applied across the electrodes and flows through 15 mM HNO_3 between carrier and make up reservoirs. There was no discharge found to the sample reservoir or the syringe pumps. A different power supply (2 kV) was tested, to see if the problem related to the Wallis Hivolt supply, however no improvement was seen. The same effect was seen upon reversing the polarity of the applied HV and increasing the make up flow from 5 up to 20 μl min^{-1} (the limit for operation of the evaporation chamber).

On application of 4.0 kV the current generated is typically 0.1 mA and the chip remains cool. However on removal from the MCFN assembly application of 4.0 kV; 0.5 mA current was generated and the chip heated up significantly over 2 minutes. It is suggested that the liquid flow is disrupted by bubbles produced at the electrode surface, causing a loss of signal and a break in the electrical circuit. A diagnostic test using two platinum wire electrodes placed in a flow cell, consisting of two chambers (10 ml) joined by a glass tube, was performed. The system was filled with 15 mM HNO_3 and 4.0 kV applied. Instantly bubbles were produced at the electrode surfaces. This confirms the hypothesis that bubbles are introduced into the microfluidic channel. As a result further investigation into other electrolytes was performed. Some carrier electrolytes recently applied to chromium speciation by capillary electrophoresis are shown in Table 5.3.

Table 5.3 Buffer systems recently applied to electrophoretic separation of chromium species

Buffer	pH	Reference
15 mM HNO_3	2	[13]
20 mM Sodium acetate	7.2	[16]
13 mM CaCl2	6	[28]
10 mM Ammonium citrate	7.7	[29]

20 mM sodium acetate was placed into flow cell and 500 V was applied, which was current limited at 2.0 mA, and bubbles were once again generated at the electrode surface. This is likely to be a problem in any aqueous buffer because of the high electric field required for separation is above the limit for hydrolysing water. Generally aqueous solutions are hydrolysed at electric fields above 700 V cm^{-1}.

As a result of this investigation the movement of the electrodes was investigated in order to prevent the bubbles generated at the electrode surface entering the channels on the chip. Platinum wire electrodes were sealed into glass flow cells placed within the pump tubing, as shown in Figure 5.17. This arrangement was tested by connecting a glass capillary tube (1.5 mm (D) x 100 mm (L) borosilicate) to the two electrodes contained within the flow cells with peristaltic pump tubing. A syringe pump was used to supply 15 mM HNO_3 and HV was applied across the electrodes. Only 500 V could be applied before 2.0 mA limit was reached. Bubbles evolved around the electrodes were effectively contained within the flow cells and no disturbance to flow was observed.

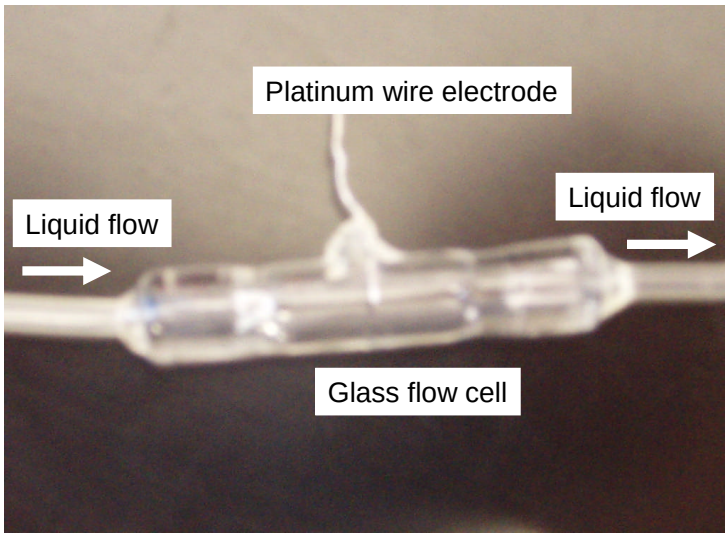

Figure 5.17 Image of glass flow cell (fabricated by departmental glass blowing workshop), with electrode and peristaltic pump tubing sealed into the chamber. Flow cell placed in between syringe pump and microchip reservoir.

The electrode system was then tested on the microfluidic chip and it was possible to apply up to 10.0 kV (generating 0.5 mA). Higher voltages will be required to produce the same electric field since the distance over which the voltage is applied has been increased by moving the electrodes to the pump tubing. However upon monitoring the signal on the ICPMS the same decrease in signal was observed on application of HV *via* the electrodes sited in the flow cells.

On further investigation it was suggested that the problem could be due to electrical interference. Therefore shorter shielded wires were used for the connection of the HV supply to the platinum electrodes. Additionally the HV was applied and sample injection performed once the signal had recovered from the initial drop. This approach had a limited success. It was possible to successfully inject a sample plug, however no separation was achieved. Application of the HV for a sustained period induced excessive heat build up in the microfluidic chip. This was observed as a steady loss of signal, illustrated by Figure 5.18, and increase in current flow. Despite the dispersion of

heat from the separation channel being more efficient than from within a capillary, once the main body of the chip had heated the chip could not cool rapidly enough in the general laboratory atmosphere.

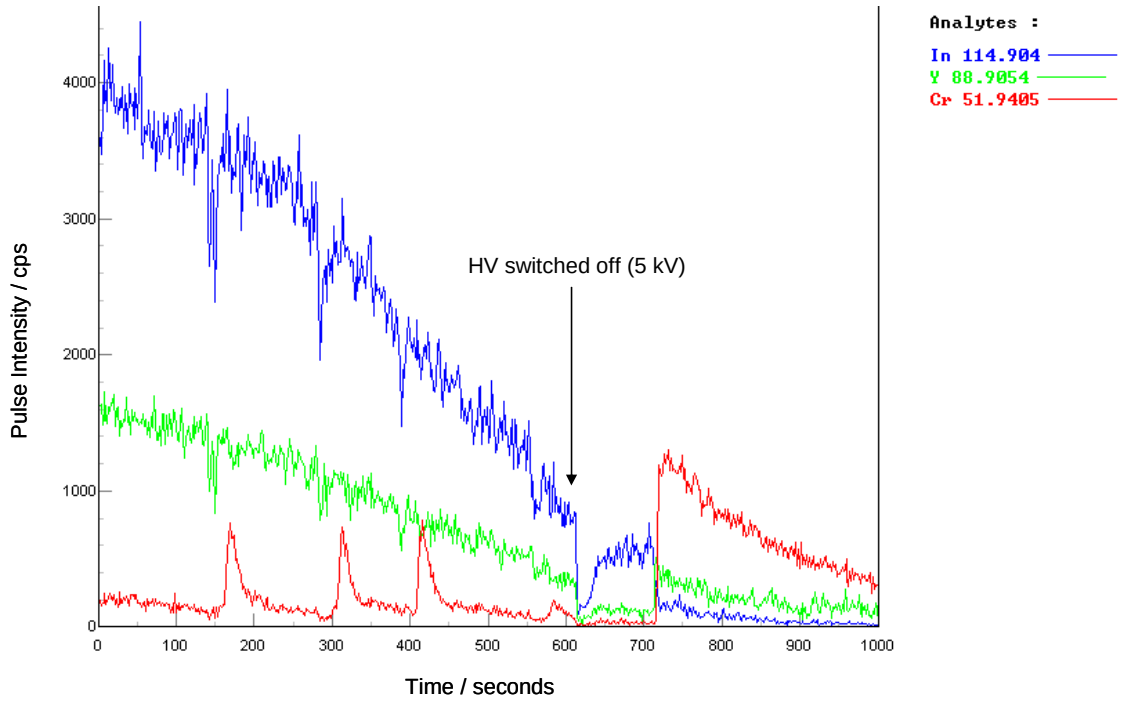

Figure 5.18 Signal decrease caused by overheating of electrophoresis microchip. Application of 5.0 kV for 45 minutes prior to signal decrease observed.

5.3.4.3.5 Temperature control of chip

Raising the applied HV has the benefits of decreasing migration times and achieving higher efficiencies. However Joule heating and hence the current flow are increased.[27] In this system the HV required to achieve separation causes excessive joule heating. Joule heating is refers to the increase in temperature of a conductor as a result of resistance to an electrical current flowing through it. It is a particular problem in microfluidic devices since it alters the liquid flow. Joule heating is proportional to power (P), which is related to the applied voltage as in Equation 5.6.

$$P = VI \qquad \textbf{Equation 5.6}$$

Where V is the applied voltage and I is the current generated. The production of excess heat causes the viscosity of the buffer to be decreased causing increased current flow. In electrophoresis broader peaks are generated with non-reproducible migration times and sample decomposition / denaturing or boiling of the buffer leading to electrical discontinuity can result.

In order to overcome the build up of heat in the microfluidic device a thermoelectric cooling device was employed. The solid state heat pump operates *via* heat absorption by electrons as they pass from a low energy level in the p-type semiconductor element (electron deficient), to a higher energy level in the n-type semiconductor element (excess of electrons). A power supply is required to provide the energy to move the electrons through the system. At the hot junction energy is expelled to a heat sink as electrons move from their high energy level element (n-type) to a lower energy level element (p-type). A thermoelectric cooling couple consists of n- and p-type semiconductor material, primary heavily doped bismuth telluride, as illustrated in Figure 5.19. A device comprises of these couples connected electrically in series and thermally in parallel. The heat absorbed at the cold junction and pumped to the hot junction is proportional to the number of couples and the current passing through the circuit.[30]

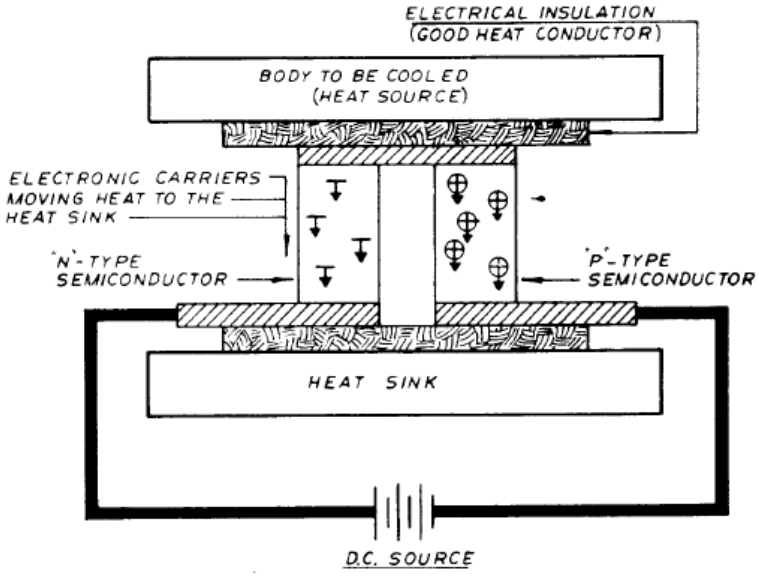

Figure 5.19 Cross section of a typical thermoelectric cooler (Melcor, Trenton, USA).[30]

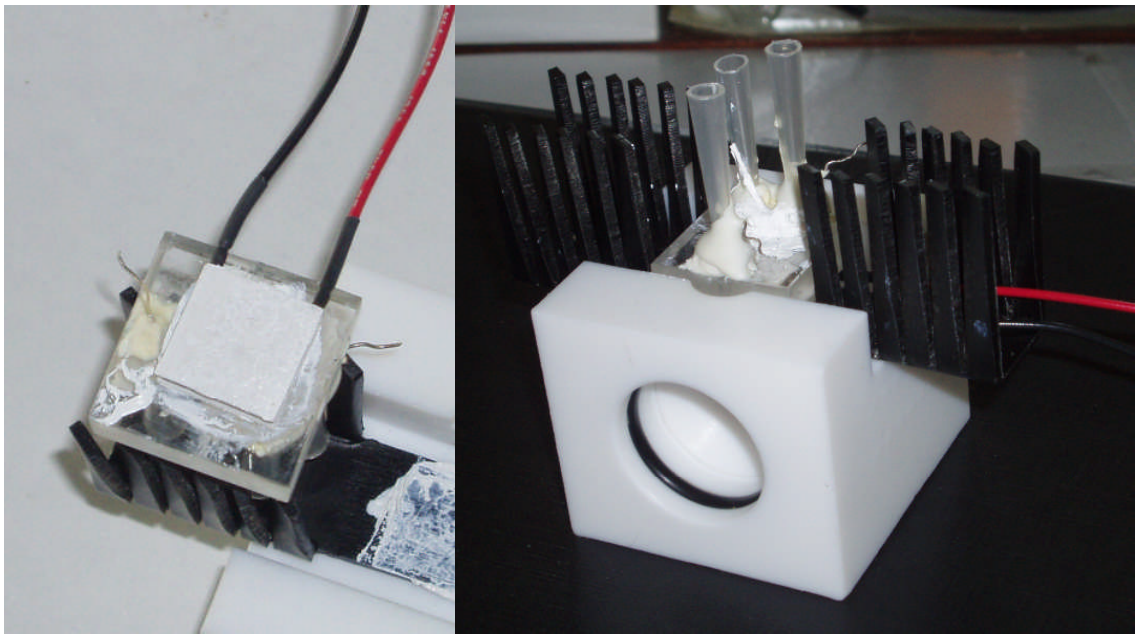

Figure 5.20 Microchip electrophoresis system with thermoelectric cooling and MCFN.

The principal advantage of this type of device for cooling a microfluidic chip is the available dimensions. A thermoelectric cooler (15 mm [L] x 15 mm [W] x 4 mm [D]) was sited directly underneath the separation serpentine on the electrophoresis microchip (RS Components Ltd., Corby, UK). This was used in conjunction with a heat sink under the hot junction to dissipate the heat produced. Figure 5.20 shows the set up with the electrophoretic microchip and MCFN assembly. The cooling device effectively cooled the chip maintaining the temperature below 15 °C at applied HV of 8 – 10 kV.

Unfortunately despite overcoming the problems discussed, including the loss of signal due to the application of HV and the joule heating of the microchip, electrophoretic separation was not achieved within the time constraints of this period of study.

5.4 Conclusions

This study has demonstrated the development of a highly efficient sample introduction system designed specifically for interfacing lab on a chip or microfluidic devices with ICPMS. This was achieved by a micro cross-flow nebuliser (MCFN) providing efficient pneumatic nebulisation of the extremely low liquid flow rate. The liquid flow within the chip was unaffected by nebulisation and there was no requirement for excessive dilution of the sample by a make up flow. An evaporation chamber was used in order to facilitate the transport of the entire primary aerosol into the plasma; hence improving the sensitivity of analysis. The MCFN design allows the microfluidic chip to be replaced simply without altering the sample introduction. Any design of microfluidic channel layout can be used, allowing the devices to be tailored to specific applications. The cost of the microchip is kept low, since there is no additional

engineering of the microchip for use with the interface. Single use disposable chips could even be used with this ICPMS sample introduction system. The application of the sample introduction system to the flow injection analysis of nanolitre sample volumes has been demonstrated. The potential for conducting microchip electrophoresis with ICPMS detection has been shown.

5.5 References

1 J. Lichtenberg, N.F. de Rooij and E. Verpoorte, *Talanta*, 2002, **56**, 233.

2 C.-C. Lin, C.-C. Chen, C.-E. Lin and S.-H. Chen, *J. Chromatogr. A*, 2004, **1051**, 69.

3 Y.-C. Lin, *Sens. Actuators, B*, 2001, **80**, 33.

4 G. Deng and G.E. Collins, *J. Chromatogr. A*, 2003, **989**, 311.

5 K. Tsukagoshi, M. Hashimoto, R. Nakajima and A. Arai, *Anal. Sci.*, 2000, **16**, 1111.

6 G.E. Collins and Q. Lu, *Sens. Actuators, B*, 2001, **76**, 244.

7 R. Wilke and S. Buttgenbach, *Biosens. Bioelectron.*, 2003, **19**, 149.

8 Q. Lu and G.E. Collins, *Analyst*, 2001, **126**, 429.

9 J. Wang, M.P. Chatrathi, B. Tian and R. Polsky, *Anal. Chem.*, 2000, **72**, 2514

10 S.C. Jacobson, R. Hergenroder, L.B. Koutny and J.M. Ramsey, *Anal. Chem.*, 1994, **66**, 1114.

11 P.D.I. Fletcher, S.J. Haswell and V.N. Paunov, *Analyst*, 1999, **124**, 1273.

12 A.Y.N. Hui, G. Wang, B. Lin and W.-T. Chan, *J. Anal. At. Spectrom.*, 2006, **21**, 134.

13 Q.J. Song, G.M. Greenway and T. McCreedy, *J. Anal. At. Spectrom.*, 2003, **18**, 1.

14 Q.J. Song, G.M. Greenway and T. McCreedy, *J. Anal. At. Spectrom.*, 2004, **19**, 883.

15 J. Mora, S. Maestre, V. Hernandis and J.L. Todoli, *Trends Anal. Chem.*, 2003, **22**, 123.

16 J. Li, T. Umemura, T. Odake and K. Tsunoda, *Anal. Chem.*, 2001, **73**, 5992.

17 T. M^{c}Creedy, *Anal. Chim. Acta*, 2001, **427**, 39.

18 S.C. Jacobson, R. Hergenroder, L.B. Koutny, R.J. Warmack and J.M. Ramsey, *Anal. Chem.*, 1994, **66**, 1107.

19 J. Burgener, *http://www.burgenerresearch.com* (accessed 10/12/2003)

20 J. Burgener, *New Developments in Burgener Nebulisers*, New Directions in ICP Mass Spectrometry at University of Sheffield, 05/11/2003

21 B.L. Sharp, *J. Anal. At. Spectrom.*, 1988, **3**, 939.

22 J.W. Olesik and L.C. Bates, *Spectrochim. Acta, Part B*, 1995, **50**, 285.

23 T.E. Corcoran, R. Hitron, W. Humphrey and N. Chigier, *J. Aerosol Sci.*, 2000, **31**, 35.

24 R.D.B. Gatherer, R.M. Sayer and J.P. Reid, *Chem. Phys. Lett.*, 2002, **366**, 34.

25 J.L. Todoli and J.-M. Mermet, *Spectrochim. Acta, Part B*, 2006, **61**, 239.

26 J.L. Todoli and J.-M. Mermet, *Trends Anal. Chem.*, 2005, **24**, 107.

27 D.R. Baker, *Capillary Electrophoresis*, Wiley-Interscience, New York, 1995.

28 B. Michalke and P. Schramel, *Fresenius J. Anal. Chem.*, 1997, **357**, 594.

29 S. Pozdniakova and A. Padarauskas, *Analyst*, 1998, **123**, 1497.

30 *http://www.melcor.com/handbook.html* (accessed 23/03/2007)

6 Microchip Sample Injection

6.1 Introduction

Accurate and precise sample introduction is crucial to obtain good quality data in quantitative analysis. This is particularly true when handling small sample volumes (sub-microlitre). A significant advantage of microfluidic devices is the high degree of control over liquid flow. The functionality of micro-separation systems is limited by fluid control. There have been numerous schemes presented for liquid handling within such devices, tailored to suit specific applications. A comprehensive review has been reported by Bayraktar and Pidugu.[1] Various separation techniques have been incorporated into microfluidic devices with the most common separation mechanisms being isotachophoresis,[2-5] electrophoresis[6] and liquid chromatography.[7] Commercial systems employing microchip electrophoretic separation (2100 Bioanalyzer kit, Agilent Technologies Ltd., Stockport, UK) and μHPLC (1200 Series HPLC-Chip / MS system, Agilent Technologies Ltd., Stockport, UK) are now available. Considerations for any liquid handling scheme that these techniques evoke include the use of high pressure, high applied voltages and the use of a wide range of solvents. As previously discussed work within this group has been focussed upon microchip based electrophoresis; therefore this is the main consideration in the design of the sample injection procedure.

6.1.1 Electrokinetic injection

The majority of sample introduction procedures used in electrophoresis involve electrokinetic injection. This is because the technique has most frequently been applied to the separation of large biomolecules; such as DNA fragments, proteins and peptides. Electrokinetic sample injection within microfluidic devices generally employs electroosmotic flow to perform valveless injections.[8-10] Defined volumes can be introduced using EOF; generally *via* two modes, floating or pinched injection.[11] Experimentally floating is the simpler of the two requiring one pair of electrodes, however pinched injection has been found to result in a more defined sample volume which is less affected by dispersion effects. The amount of sample injected is dependant upon the applied electric field and time period for which it is applied. However, several parameters of the sample solution affect the electrophoretic mobility including; pH, temperature, viscosity, ionic strength and dielectric constant.[12] A significant disadvantage with an electrokinetic injection scheme for the analysis of small ionic molecules is the introduction of severe sample bias / discrimination. Ions with greater mobilities are disproportionally introduced in larger quantities.[13] For molecules with high electrophoretic mobilities a positive injection potential would induce a bias towards anions over neutrals and hamper or even exclude the injection of cations. For this reason in elemental speciation a hydrodynamic injection technique is more appropriate.[14-16]

6.1.2 Hydrodynamic injection

Hydrodynamic sample injection performed with traditional capillary electrophoresis is time consuming and lacks precision.[13] This involves the mechanical exchange of capillary between the sample and buffer reservoirs, which is not possible with a

microfabricated chip device. Within a microchip this can be achieved by use of a simple switching valve, as in previous work,[17] a pressure driven PDMS passive valve,[15] electro-fluidic solenoid valves (e.g. Lee Products Ltd., London, UK), or by use of specially adapted low volume rotary valves (similar to those used in liquid chromatography).[12] Another possible method in microchip based systems is the use of microvalves formed within the channel network of the microchip.

6.1.2.1 Polymer monolith microvalves

The requirements of microvalves for use in a microfluidic separation device include the ability to seal against high pressures required for driving fluid through chromatographic stationary phases and remain unaffected by application of high voltage. They must have negligible leak rates *cf.* flow rates, be resistant to wide range of solvents, mechanically stable and not bind to channel walls so they can be actuated with liquid or gas pressure. Ideally they should be constructed in *situ* with precise control of dimensions, hence preventing any bypassing of liquid flow. Practically they should be inexpensive to fabricate and compatible with the substrate materials.[18] Polymer monoliths are particularly suited to this application since their fabrication is possible within a micro-channel and the chemistry can be designed in order to give desired properties. Once the valves have been formed there is no bypassing, and they have a robust, fixed structure within the channel.

Microvalves formed from polymer monoliths were first presented by Unger *et al.* in Science 2000.[19] This methodology was adopted by Kirby, Hasselbrink and Shepodd in the development of on / off microvalves that could withstand high-pressures for microfluidic control in separation chips.[18, 20, 21] These were produced from highly cross-linked and fluorinated polymers in order to produce rigid valves that resist

deformation and do not adhere to the microchip channel walls. The microvalves were produced accurately in *situ* by photo-polymerisation initiated by UV light from a laser source.

6.1.3 Aim

The aim of this study is to evaluate and improve the manual injection technique used with the microchip ICPMS system (as described in Section 5.2.3.4) to achieve better precision and accuracy. With the objective to look towards automation of the sample introduction of a discrete sample plug. A fixed sample volume is to be injected into a continuous carrier flow in a reproducible manner. Investigation into the use of on / off microvalves formed in *situ* within the microfluidic device is described. This involves the development of Teflon-like, rigid polymer monoliths and an assessment of their incorporation into an electrophoretic microchip to form a discrete sample loop for sample injection.

6.2 Experimental

6.2.1 Instrumentation

A UV lamp source (Spectroline ENF-260 C/F, Spectronics Corporation, New York, USA) or a XeCl laser source (Eximer-500, Lumonics, Ontario, Canada) was used for the photo-polymerisation of the microvalves. The lamp source provided emission in the ultraviolet (UV) region at 365 nm, with the laser source at 308 nm. For the laser source the energy (following a 4 mm x 10 mm mask) was measured using a piezoelectric crystal. 24.4 mV were produced at 13.2 V J^{-1} (± 10 %) resulting in an energy of 1.8 mJ. The fluence is equivalent to the energy per square cm. Therefore in this case the fluence was 4.5 mJ cm^{-2}. The laser was operated at 10 Hz (pulses s^{-1}) with each pulse

lasting approximately 8 ns. The dose can be calculated from the laser fluence (F), unmasked area of capillary (A) and the number of pulses (P) by the relationship shown in Equation 6.1.

$$Dose = \left(\frac{F}{A}\right) \times P \qquad \textbf{Equation 6.1}$$

6.2.2 Reagents

Certified reference standards (1000 μg ml^{-1}) were used in the preparation of all solutions. Chromium, yttrium and indium standards were contained within the sample, carrier and make up reservoirs respectively. Yttrium and chromium standards were purchased from Qm_x Laboratory Limited (Thaxted, UK) and indium from BDH Laboratory Supplies (Poole, UK). All solutions were prepared fresh daily using UHQ water and high purity nitric acid (HNO_3) was used throughout (SuperPurityAcid 69 %, Romil Ltd., Cambridge, UK).

Rose Bengal (Sigma–Aldrich Chemie GmbH, Steinheim, Germany) water soluble dye was used to visualise liquid flow within the microchip. The disodium salt was dissolved in UHQ water to give appropriate colour intensity. The resulting solution was filtered through a 0.45 μm cellulose filter unit (MF-Millipore, Cork, Ireland) prior to use within microfluidic device.

6.2.2.1 Polymer monoliths

A mixture of monomers, solvents and a photo-initiator were used to form polymer monoliths. The monomers used were trifluoroethylacrylate and 1,3- butanediol diacrylate (Sigma–Aldrich Chemie GmbH, Steinheim, Germany). Solvents included methoxyethanol, 1,4- dioxane and 5 mM TRIS buffer (Sigma–Aldrich Chemie GmbH,

Steinheim, Germany). The photo-initiator used was 2,2'- azobisisobutyronitrile (AIBN, Sigma–Aldrich Chemie GmbH, Steinheim, Germany).

6.2.3 Procedures

6.2.3.1 Manual sample injection

Liquid flow was delivered to the sample and carrier reservoirs by one syringe pump. A 3-way 'Y' manual switching valve (Omnifit, Cambridge, UK) was used to direct the flow to the sample and carrier reservoirs allowing independent control of both. A second syringe pump was used to deliver the make up flow. Tygon peristaltic pump tubing (Elkay Laboratory Products Ltd., Basingstoke, UK) was used to transfer the liquid from syringe pump to the chip reservoirs. The reservoirs were filled with the appropriate solution and then pump tubing pushed tightly into the reservoir to form a seal. The syringes contained only the carrier solution, 15 mM HNO_3. Liquid was pumped to all reservoirs at 5 μl min^{-1} in order to purge the chip for approximately 15 minutes before checking the flow from each reservoir by monitoring the appropriate signal (e.g. Cr: sample, Y: carrier, In: make up). The make up flow and carrier flow was on throughout the sample injection. The sample flow was switched on *via* the 3-way switching valve for a fixed time period to give a known sample volume.

6.2.3.2 Formation of in *situ* micro-valves

Microvalves were produced within capillaries / channels using polymer monoliths adapted from a method by Kirby, Shepodd and Hasselbrink Jr.[18, 20] These were formed *via* UV photo-initiated polymerisation. The channel was completely filled with a monomer (60%) / solvent (40%) / initiator mixture (0.5 % $^{w}/_{w}$). The monomers used were trifluoroethylacrylate and 1,3- butanediol diacrylate (1 : 1); solvents

methoxyethanol, 1,4- dioxane and 5 mmol L^{-1} TRIS buffer (1 : 1 : 1); and photo-initiator AIBN. The polymer mixture was sonicated under vacuum for 15 minutes immediately prior to pressure injection into the channel in order to reduce inhibition to polymerisation (for example by dissolved oxygen).[20] This was then sealed to the environment using wax or fast curing epoxy resin, while taking care to allow the channel to be easily opened again following formation of the microvalves. The mixture was allowed to become quiescent then polymerisation was then performed *via* exposure to ultraviolet light. The channel was then flushed with acetonitrile in order to wash away any residual reagents and prevent any further polymerisation.

6.3 Results and discussion

6.3.1 Manual switching valve

The manual sample injection technique described in the procedures was established by visualisation of the liquid flow using water soluble dye (Rose Bengal). If careful systematic connection of the sample reservoirs to the syringe pump tubing was not performed the chip would become flooded with the sample (Cr), carrier (Y) or make up (In) solution. This can cause contamination of the chip reservoirs with other solutions; creating a high background signal and inability to perform sample injection. The make up tubing was therefore connected first and pumped at 10 μl min^{-1}, followed by connection of both the sample and carrier tubing simultaneously. Then the chip was purged at 5 μl min^{-1} for at least 15 minutes (generally conducted during ICPMS instrument warm up).

Results of the manual sample injection technique applied to the microfluidic sample introduction system are presented in Chapter 5 (section 5.3.4.2). The sample

contained 150 μg Cr L^{-1} in 15mM HNO_3. The precision based upon peak area of a sample volume of 133 nanolitres (flow rate 0.4 μl min^{-1}) was 5.1 % RSD (n = 6). The lowest sample injection volume that could reproducibly give a usable signal was 42 nanolitres (corresponding to a 5 second injection at 0.5 μl min^{-1}) resulting in a signal to noise (S/N) ratio of 3.6.

6.3.2 Polymer monoliths as microvalves

The most fundamental fluid control element is an on / off valve. The microvalves were designed to be non-porous, rigid and not adhere to the capillary / channel walls. In order to achieve this monomers were carefully selected to give the desired properties. Choice of monomers affects pore size, surface energy and mechanical strength.[20] A highly fluorinated acrylate, which repels silanol groups on surface of glass capillary, was used to produce a Teflon-like polymer. A cross-linked acrylate was used to provide mechanical strength, low porosity and solvent resistance. Solvents were used as described by Hasselbrink Jr. *et al.*[18] and were chosen to control the phase separation properties of the mixture, hence polymerisation times and pore sizes.[20]

6.3.2.1 Glass capillaries

For development of the fabrication of the monoliths it was planned to use PDMS chips since these could be rapidly fabricated with various channel designs appropriate for the formation of microvalves. Unfortunately the cured PDMS was found to absorb in the UV region, preventing photo-polymerisation of the monoliths. Therefore borosilicate capillaries were used since this is the material used for the fabrication of the glass microfluidic chips. An initial test was conducted using a glass microchip with a single central channel which had a short constriction in the centre. A mask was applied to the chip to leave 1 mm of the channel length exposed to form a piston shaped monolith.

The chip was exposed to UV radiation at 365 nm provided by a bench top lamp source. Photo-polymerisation was achieved; however using this UV source it took in excess of 2 hours. The resulting monolith formed was 3 times the size of the masked off area, as shown in Figure 6.1.

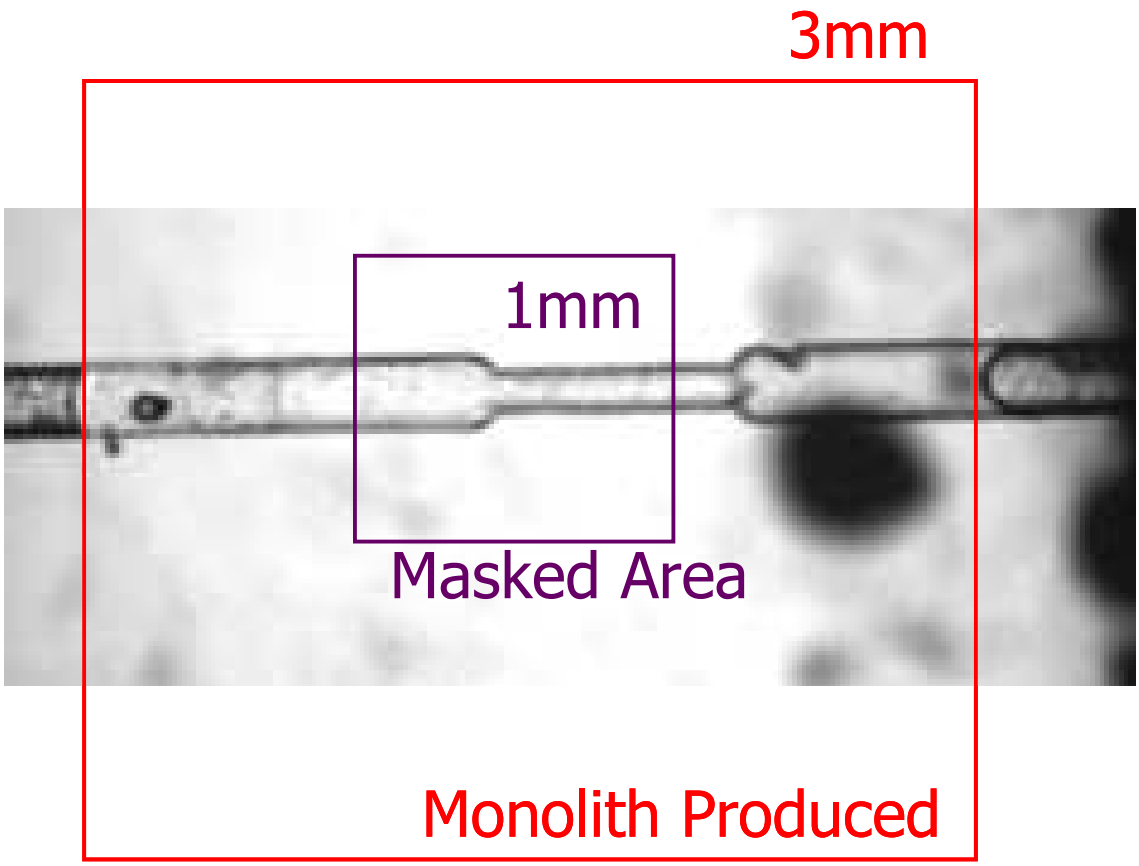

Figure 6.1 Optical microscope image of polymer monolith produced using UV lamp at 365 nm with an exposure time of approximately 2.5 hours.

It was therefore obvious that the use of a low power UV lamp source was not suitable for production of the microvalves. The problems with diffusion and time taken to cure polymer could be overcome using carefully designed optics to focus the light or a UV laser source. Lasers have numerous advantages since they inherently do not suffer from diffusion problems. Therefore simple masks can be used to define the microvalve area with no requirement for more complex optics. This permits the formation of monoliths

with accurate and precise critical dimensions. Additionally they provide high intensity emission and high radical populations, which afford a significant reduction in time for laser to cure polymer (seconds rather than hours). Lasers also exhibit relative insensitivity to inhibitors.

Advice was sought from Dr. Howard Snelling of the physics department at the University of Hull and a XeCl (308 nm) UV laser was made available for the work. The transmission spectrum of borosilicate glass was measured in order to ensure that it does not absorb strongly at 308 nm, shown in Figure 6.2. The actual dose absorbed by the polymer monolith reactants is affected by reflectance losses, lens effects from using a circular capillary, absorption by borosilicate capillary and the cured / uncured polymer material. Figure 6.3 shows the absorption spectrum of a thin layer of the cured polymer monolith formed on the surface of a microscope slide.

A borosilicate capillary with 0.5 mm i.d. (external dia 5 mm) was exposed to 308 nm UV through a 1.0 mm mask (exposed area 5 $x10^{-3}$ cm^2). Figure 6.4 outlines the experiments conducted in order to optimise the photo-polymerisation by increasing the dose from 0.06 up to 0.90 mJ (calculated from relationship in Equation 6.1).

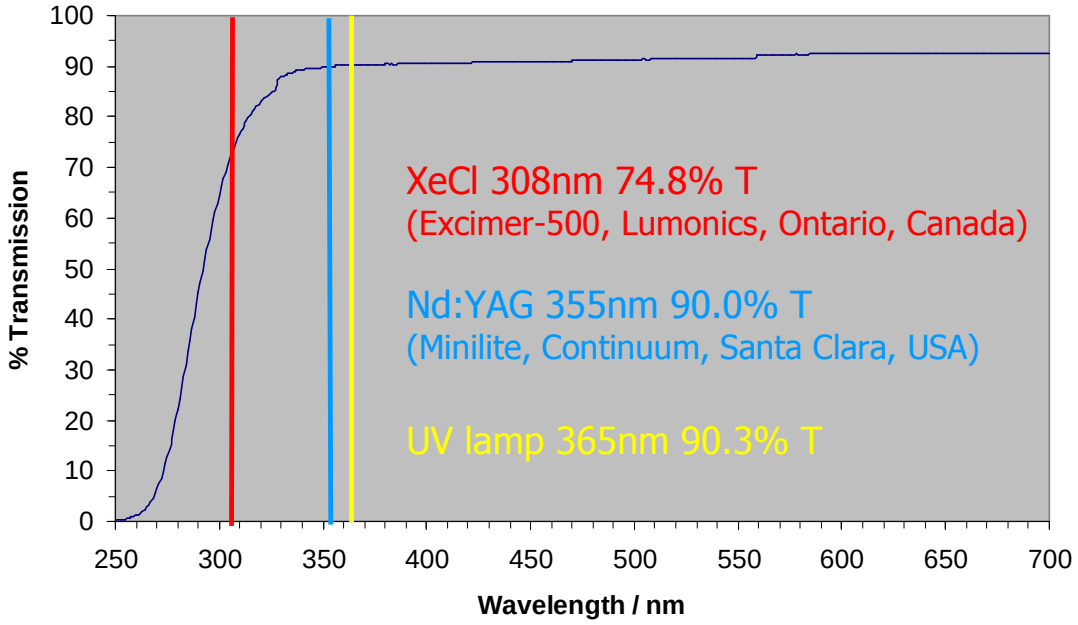

Figure 6.2 Transmission of light in the ultraviolet region through 1.0 mm (0.5 mm i.d. with 1.5 mm o.d.) borosilicate glass capillary. The absorbance for the UV lamp and XeCl laser used in this work is annotated along with the Nd:YAG laser used in previous work by Hasselbrink *et al.*[18]

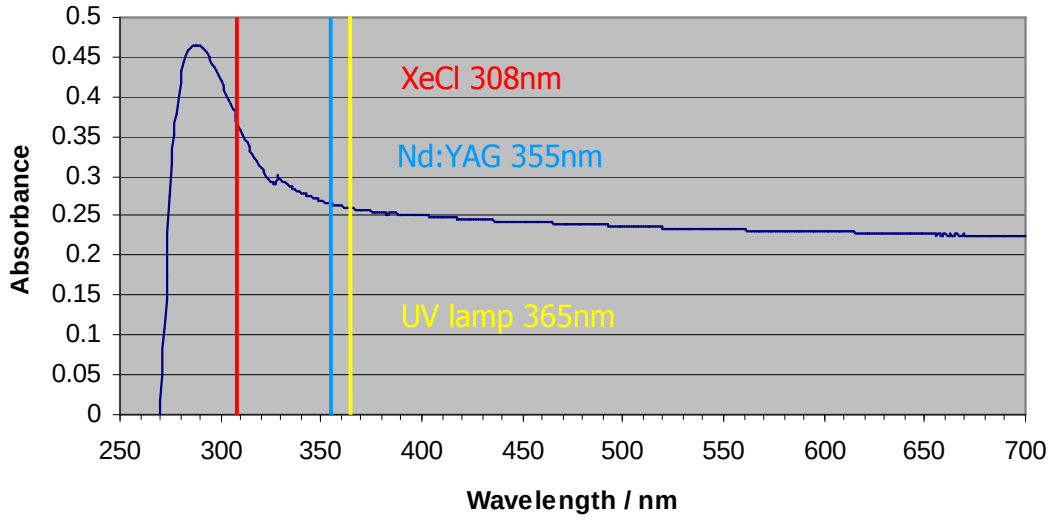

Figure 6.3 Absorption spectrum for cured polymer monolith formed on a microscope slide. Reaction mixture consisting of 60 % monolith and 40 % solvent with excess AIBN.

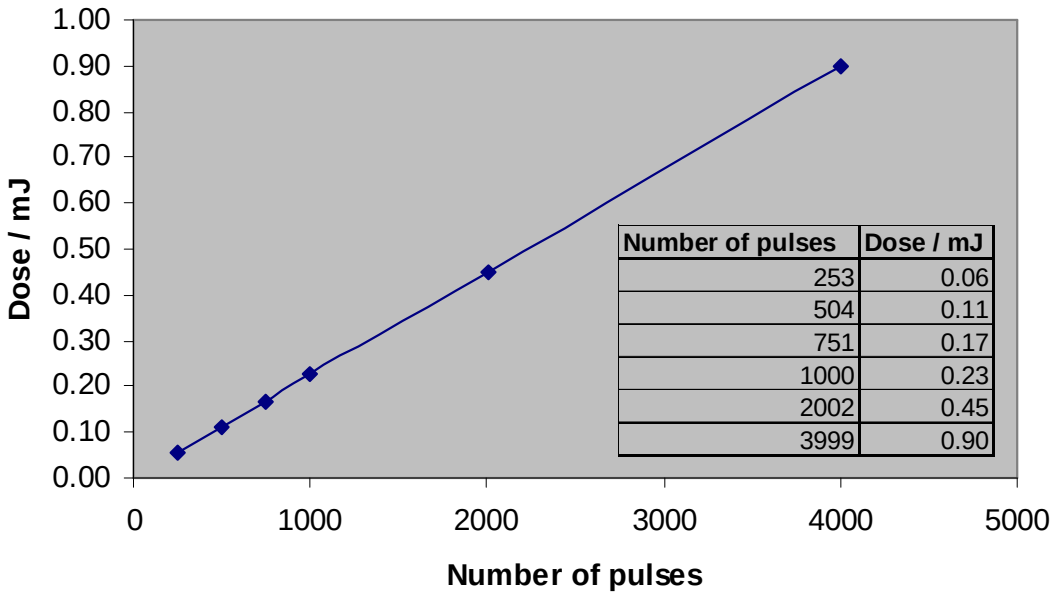

Figure 6.4 Illustration of the experiments conducted in order to achieve the correct dose of UV laser energy (308 nm) to form a microvalve within borosilicate glass capillary (0.5 mm i.d.).

Figure 6.5 shows the results of microvalve formation obtained throughout the laser energy optimisation. The exposed capillary area was designed to produce microvalves with dimensions of 0.5 mm diameter and 0.5 mm in length. Figure 6.5 a. shows a dose of 0.11 mJ is not sufficient to induce polymerisation. Upon increasing the dose to 0.17 mJ polymerisation begun to partially form a microvalve structure. Figure 6.5 (c. and d.) illustrates that using a dose above 0.20 mJ a complete polymer monolith is formed throughout the entire channel cross sectional area. Further increasing the dose above 0.60 mJ resulted in over curing of the polymer monolith, visualised by the evolution of gas bubbles and incomplete structure (Figure 6.5 e.). On removal of the microvalves from the capillary any which had been over cured crumbled.

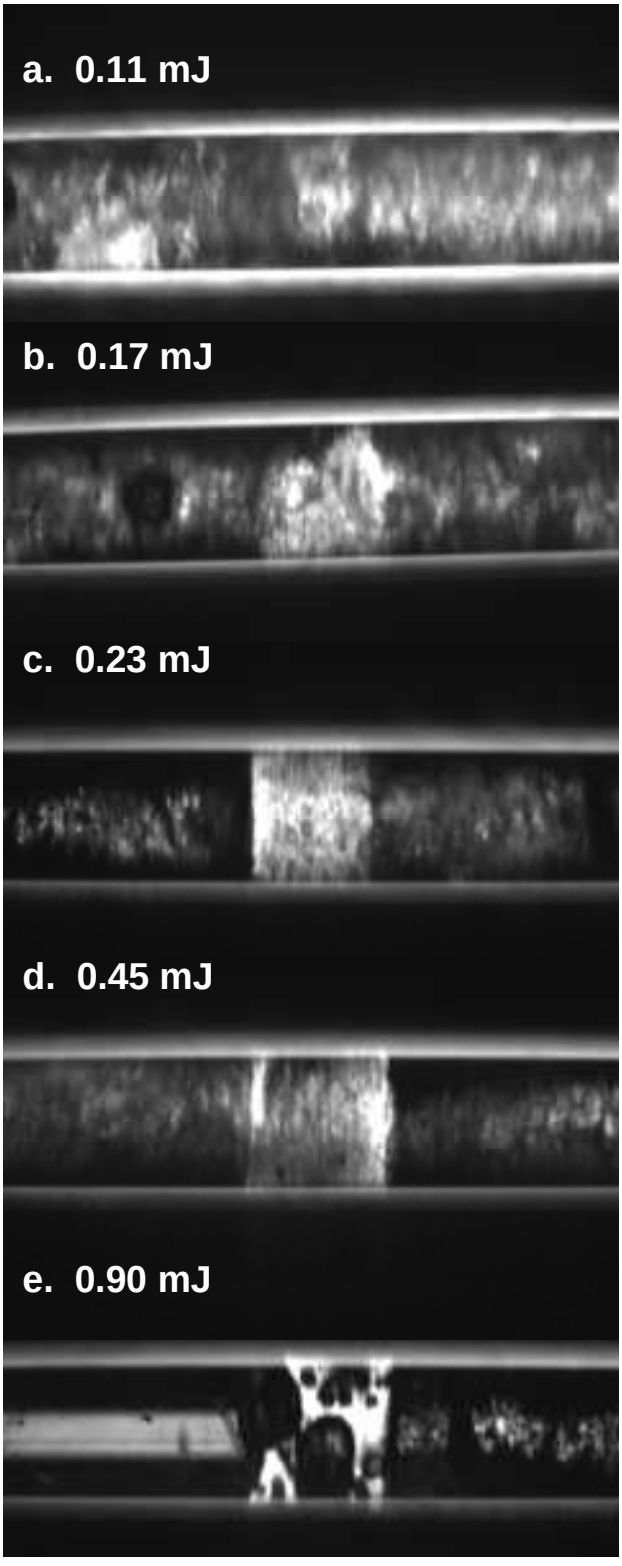

Figure 6.5 Optical microscope images of the microvalves produced as the dose was increased. XeCl laser (308 nm), 0.5 mm i.d. borosilicate capillary.

A UV laser dose of 0.45 mJ (Figure 6.5 d.) was found to be optimal for production of microvalves with these critical dimensions. The resulting polymer monolith completely

sealed the capillary channel and had the same dimensions as the exposed area. Figure 6.6 shows SEM images of the microvalve structure produced by laser photo-polymerisation with 60 % monomer: 40 % solvent mixture. The smooth outer (Teflon-like) surface can be seen which coupled with the repulsive negative charge provided by the highly-fluorinated composition ensured the microvalve did not adhere to the capillary wall. Figure 6.6 b. shows a larger scale image detailing the internal structure and pore size which provides the microvalves with rigidity preventing deformation under pressure and any bypassing or leakage.

It was possible to actuate the microvalves along the length of the channel using either gas or liquid (acetonitrile or UHQ water) pressure supplied by a syringe. No obvious leakage of liquid or gas was observed. Therefore incorporation of the microvalves into an electrophoresis microchip was evaluated. A suitable microfluidic device was designed and submitted for fabrication by the Microfabrication facility at the University of Hull. Figure 6.7 shows a schematic of such an electrophoresis microchip design submitted for fabrication. This design utilises three microvalves, which would all be linked to one pressure driven actuator, in order to create a discrete sample loop. Unfortunately the device was not fabricated in time for the system to be tested during this prescribed period of study.

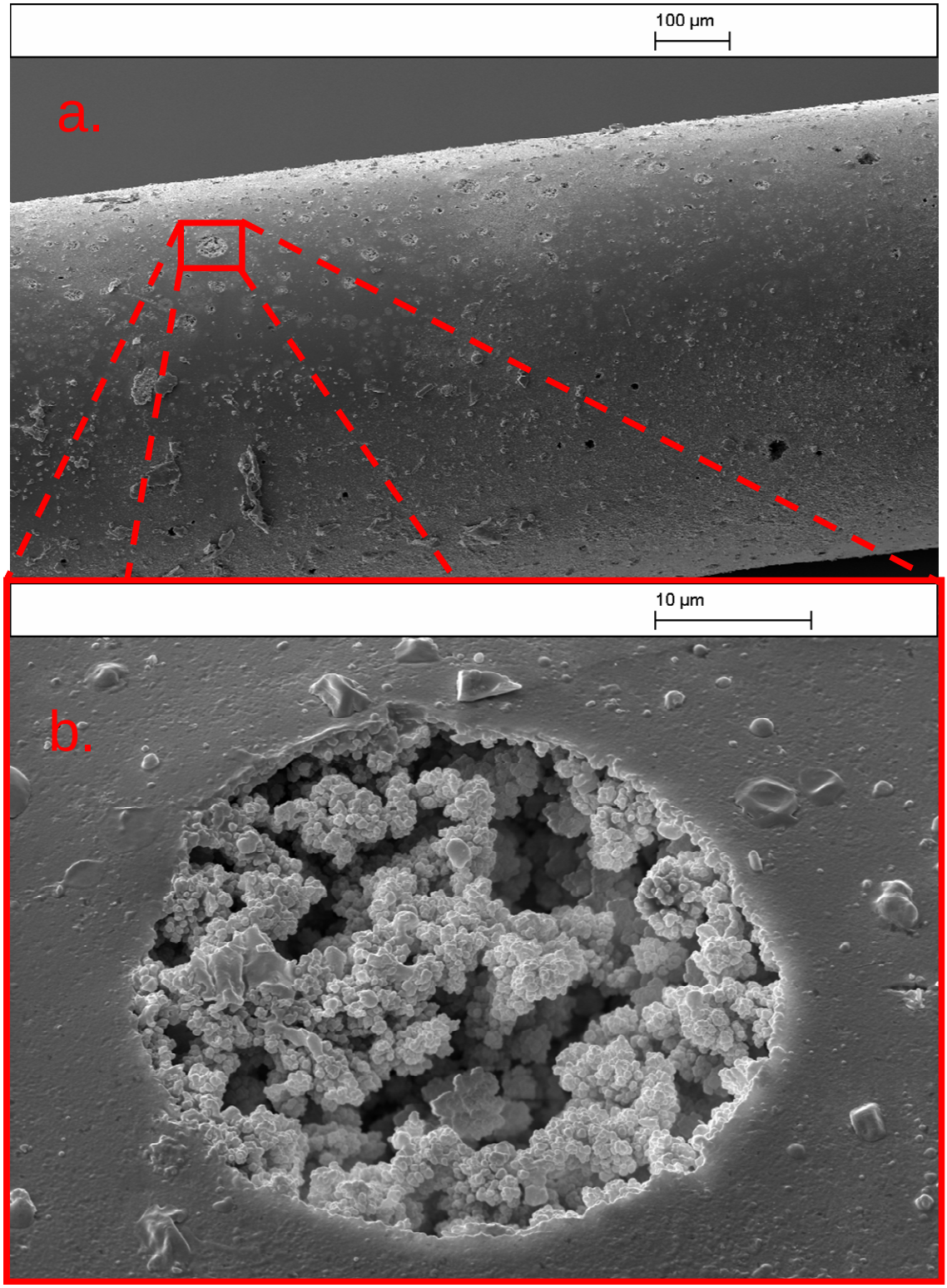

Figure 6.6 SEM images of polymer monolith. a. Teflon-like surface structure ensuring the monolith does not adhere to the channel wall. b. Large scale image showing the inner structure of the monolith.

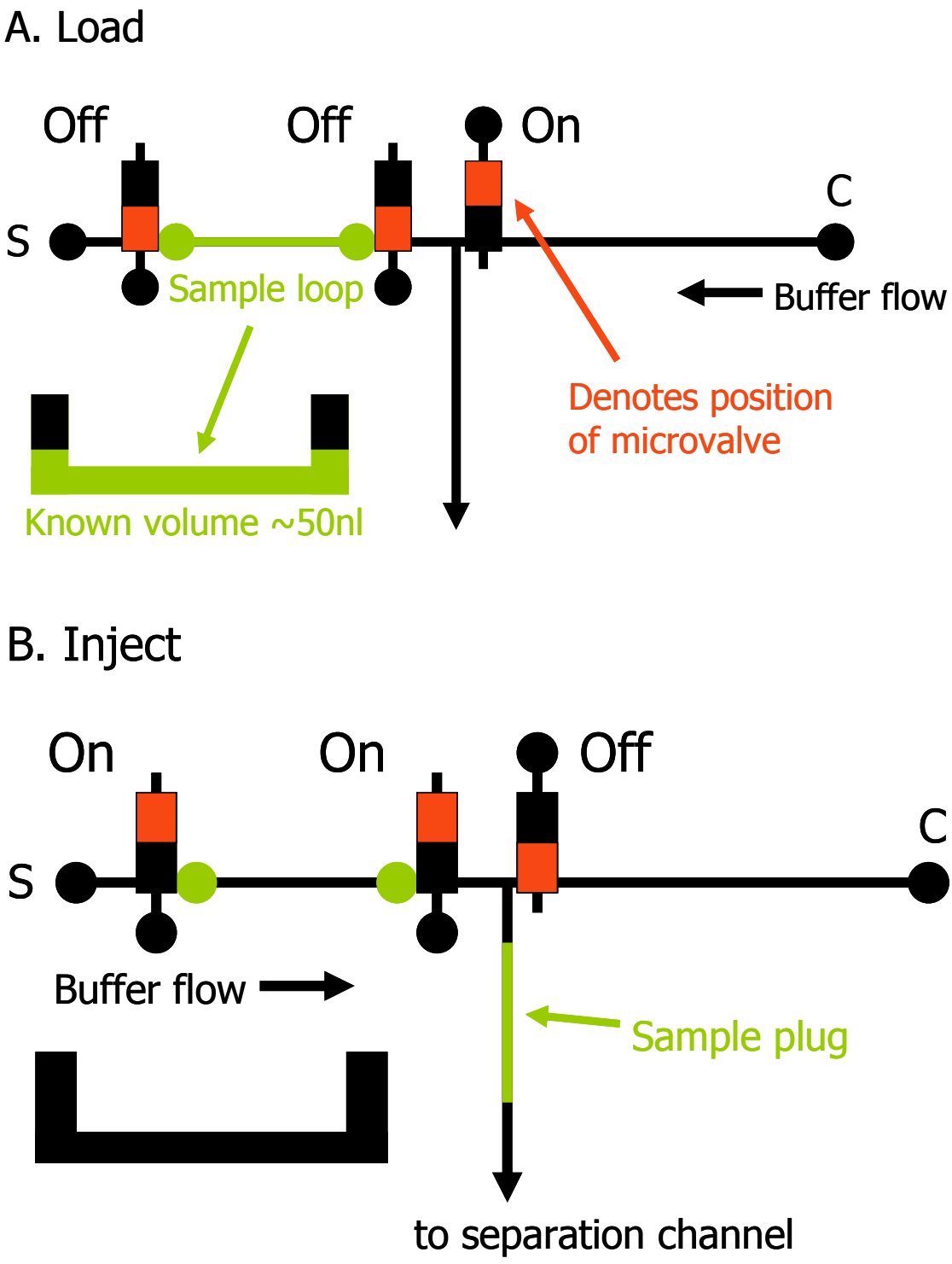

Figure 6.7 Microfabrication chip design for an electrophoresis microchip incorporating channels for in *situ* fabrication of microvalves formed by polymer monoliths. Microvalves actuated by carrier buffer liquid pressure in order to switch flow between the carrier inlet reservoir (C) during sample loading (6.7A) and the sample inlet reservoir (S) during sample injection (6.7B).

6.4 Conclusions

The aim of this work was to evaluate and improve the manual injection technique previously used in order to achieve better precision and accuracy. Investigation into the use of on / off microvalves formed in *situ* within glass capillaries was performed. Teflon-like, rigid polymer monoliths were produced by photo-polymerisation using a UV (XeCl 308 nm) laser source. Successful fabrication of microvalves was achieved which proved effective at sealing and controlling liquid flow within the capillary channel. The valves could be actuated along the channel length using liquid pressure. Microvalves of the type described in this work have the potential for integration into a microfluidic device in order to form a discrete sample loop. This type of microchip could provide an attractive method for automation of the sample introduction procedure in order to inject a discrete sample plug into a continuous carrier flow in a reproducible manner.

6.5 References

1 T. Bayraktar and S.B. Pidugu, *Int. J. Heat Mass Transfer*, 2006, **49**, 815.

2 B. Graβ, G. Weber, A. Neyer, M. Schilling and R. Hergenroder, *Spectrochim. Acta, Part B*, 2002, **57**, 1575.

3 J.E. Prest, S.J. Baldock, P.R. Fielden, N.J. Goddard and B.J. Treves Brown, *J. Chromatogr. A*, 2003, **990**, 325.

4 J.E. Prest, S.J. Baldock, P.R. Fielden and B.J. Treves Brown, *Analyst*, 2001, **126**, 433.

5 J.E. Prest and P.R. Fielden, *Anal. Commun.*, 1999, **36**, 333.

6 G. Alvarez-Llamas, M.R.F. de laCampa and A. Sanz-Medel, *Trends Anal. Chem.*, 2005, **24**, 28.

7 J.P. Kutter, *Trends Anal. Chem.*, 2000, **19**, 352.

8 R. Wilke and S. Buttgenbach, *Biosens. Bioelectron.*, 2003, **19**, 149.

9 J. Wang, M.P. Chatrathi, B. Tian and R. Polsky, *Anal. Chem.*, 2000, **72**, 2514

10 S.-H. Chen, Y.-H. Lin, L.-Y. Wang, C.-C. Lin and G.-B. Lee, *Anal. Chem.*, 2002, **74**, 5146.

11 S.J. Haswell, *Analyst*, 1997, **122**, 1R

12 C. Yao, R. Gao and C. Yan, *J. Sep. Sci.*, 2003, **26**, 37.

13 S.C. Jacobson, R. Hergenroder, L.B. Koutny, R.J. Warmack and J.M. Ramsey, *Anal. Chem.*, 1994, **66**, 1107.

14 C.-C. Lin, C.-C. Chen, C.-E. Lin and S.-H. Chen, *J. Chromatogr. A*, 2004, **1051**, 69.

15 S. Buttgenbach and R. Wilke, *Anal. Bioanal. Chem.*, 2005, **383**, 733.

16 U. Backofen, F.-M. Matysik and C.E. Lunte, *Anal. Chem.*, 2002, **74**, 4054.

17 Q.J. Song, G.M. Greenway and T. McCreedy, *J. Anal. At. Spectrom.*, 2004, **19**, 883.

18 E.F. Hasselbrink Jr., T.J. Shepodd and J.E. Rehm, *Anal. Chem.*, 2002, **74**, 4913.

19 M.A. Unger, H.-P. Chou, T. Thorsen, A. Scherer and S.R. Quake, *Science*, 2000, **288**, 113.

20 B.J. Kirby, T.J. Shepodd and E.F. Hasselbrink Jr., *J. Chromatogr. A*, 2002, **979**, 147.

21 B.J. Kirby, D.S. Reichmuth, R.F. Renzi, T.J. Shepodd and B.J. Wiedenman, *Lab Chip*, 2005, **5**, 184.

7 General Conclusions and Future Work

The superior analytical characteristics of ICPMS, including extremely low detection limits, good precision and simultaneous multielement detection, makes it the single most powerful technique for elemental analysis. The introduction and development of reaction / collision cell technology over the past 20 years has opened up tolerance to a wide range of interfering species / matrices and made available isotopes previously hindered by spectroscopic interferences, particularly from argon species. Sample introduction has always been a hindrance in plasma spectrometry and careful selection and optimisation is essential to achieve good analytical results. Conventional sample introduction systems generally suffer from low transport efficiency and require relatively large volumes of solution. Developments in solid sample introduction, by laser ablation, and the analysis of low flow / microsample volumes, by direct injection or highly efficient sample introduction systems, have opened up new possibilities. While ICPMS can provide isotopic information it can not directly provide speciation information owing to the destructive nature of the technique. However it has become the detector of choice for elemental speciation analysis coupled with a highly efficient separation scheme (GC, LC, CE). The high running cost of ICPMS does not lend itself well to lengthy separations. A reduction in separation time affords an increase in sample throughput, reduction in detector idle time and therefore reduction in cost of analysis.

7.1 Monolithic silica HPLC for rapid arsenic speciation

In this thesis a rapid speciation method has been described by means of a new application for a Chromolith™ HPLC column. Development of an ion-pair liquid chromatographic method for this monolithic silica stationary phase material has been described. The system has been applied to arsenic speciation, owing to the global interest in arsenic contamination / exposure. Optimisation was performed in order to achieve good resolution with a short separation time. The separation of arsenic species has been demonstrated within 3 minutes, providing a significant improvement to sample throughput and hence a reduction in the analysis cost. The separation was achieved by ion-pair liquid chromatography using 2.5 mM tetrabutylammonium bromide (TBAB), 10 mM phosphate buffer (pH 5.6) and 1.0 % ($^{v}/_{v}$) methanol as the mobile phase. Baseline resolution was achieved for 3 of the 5 arsenic species investigated. Inorganic As(III) was unretained and arsenobetaine (AsB) only achieved very slight retention; hence both were eluted in the column void volume. Detection limits of 0.107, 0.084, 0.120, 0.121 and 0.101 μg As L^{-1} for As(III), arsenobetaine (AsB), dimethylarsinate (DMA), monomethylarsonate (MMA) and As(V), respectively were achieved. The precision of the method, based upon analysis of 15 μg L^{-1} As, was better than 5.9 % for all species. The accuracy of the determination within biological samples was confirmed by the analysis of a human urine certified reference material with good agreement found with the certified values. The feasibility of the method has been demonstrated by the analysis of urine and extracted food samples in an ingestion study. It has been shown for the first time that consumption of American long-grain rice results in significant increase in urinary dimethylarsinate (DMA) excretion. This supports previous findings that rice grown in the USA contains a high level of arsenic compared with rice from

other regions (Europe, Bangladesh and India) and other widely consumed food types (bread, milk, pork meat, chicken meat, cabbage and potatoes). The results also confirm that the primary pathway for removal of arsenic in humans is *via* methylation and urinary excretion. Arsenic speciation in urine can be considered as a biomarker for arsenic exposure since arsenic levels in urine have a relatively short half life; and hence represent recent exposure. The results of this ingestion study showed that arsenic concentrations in urine dropped back to their original levels within 16 hours of the rice consumption. This method presents the ability to employ a monolithic silica stationary phase material to conduct rapid arsenic speciation in clinical and environmental studies.

7.2 Highly efficient microchip sample introduction system

The development of a highly efficient sample introduction system designed specifically for interfacing lab on a chip or microfluidic devices with an ICPMS has been described. This is achieved by a micro-cross-flow nebuliser (MCFN) incorporated into the end of the chip, providing nebulisation of the extremely low liquid flow rate without affecting the liquid flow within the chip or requiring excessive dilution of the sample by a make-up flow. An evaporation chamber is used in order to facilitate the introduction of very low liquid flow rates and provide transport of the entire primary aerosol into the plasma. Combination of the reduced internal volume, low liquid flow rates, promotion of solvent evaporation and the simple aerosol trajectory leads to the increases achieved in sensitivity of analysis. A comparison with a commercial low volume cyclonic spray chamber (Cinnabar) was performed. The optimised evaporation chamber resulted in a 400 % increase in signal intensity and instrumental detection limits are improved by an average 34 %. The optimised sample introduction system achieved a sensitivity of 13

500 cps for 10 μg L^{-1} indium at the extremely low liquid flow rate of 5 μl min^{-1}. The stability of the sample introduction over 10 min was 2.6 % RSD (n = 453) and no sample recondensation was ever observed in the evaporation chamber at flow rates up to 20 μl min^{-1}. Hydrodynamic sample injection was performed via a manual switching valve, with a reproducibility of 5.10 % RSD (n = 6). The system facilitates the flow injection analysis of very low sample volumes (> 40 nl). The MCFN design allows the microfluidic chip to be replaced simply without altering the sample introduction. Any design of microfluidic channel layout can be used, allowing the devices to be tailored to a wide range of specific applications. The cost of the microchip is kept low, since there is no additional engineering of the microchip for use with the interface. Single use disposable chips could even be used with this ICPMS sample introduction system.

Improvement of the manual injection technique previously used has been discussed in order to achieve better precision and accuracy. Investigation into the use of on / off microvalves formed in *situ* within glass capillaries was performed. Teflon-like, rigid polymer monoliths were produced by photo-polymerisation using a UV laser source. Successful fabrication of microvalves was achieved which proved effective at sealing and controlling liquid flow within the capillary channel.

7.3 Suggestions for future work

The application of monolithic silica stationary phase material has proved effective at greatly reducing the separation time, while only requiring tailoring of methods originally developed for traditional packed silica columns. It is therefore anticipated that the application of this stationary phase media to the separation of a wide range of other analyte species using methods described in the literature could provide similar

improvements. Owing to the multielement specificity of the ICPMS detection it would be conceivable that a number of elemental species could be separated in a single run. Investigation into the chromatographic separation of several elements under the same conditions could result in significantly more information being obtained without increasing the analysis time. The author is currently developing a method for the simultaneous separation of inorganic arsenic and chromium species in order to investigate leaching from chromated copper arsenate (CCA) treated wood in collaboration with the geography department (University of Hull). Additionally it would be particularly interesting to study the simultaneous speciation of arsenic, selenium and manganese. Dietary ingestion of selenium has been found to assist the excretion of toxic arsenic species, while there is evidence that high levels of manganese and arsenic in combination can increase associated neurotoxic effects. The effects of exposure to chemical mixtures are not widely known. Further research is required on the effect of exposure to combinations of toxic element species in order to assess any contributory effects.

The interfacing of microfluidic chips with ICPMS is desirable to take advantage of the superior multielement limits of detection that ICPMS offers. The development of a dedicated sample introduction system for this purpose is essential to afford the advantages microchips can provide. Lab on a chip devices can be used to perform rapid separation of elemental species by chromatographic or electrophoretic methods; hence reducing time per sample, therefore detector idle time and the cost of analysis. This is particularly of benefit for ICPMS detection owing to the high running costs. Application of the sample introduction system described in this thesis to interface an electrophoretic chip for speciation analysis is ongoing. This system is expected to

afford a significant reduction in separation times and improvements in detection limits and separation efficiency, since the separation will not be degraded by the sample introduction into the ICPMS. Further investigation into the evaporation cavity, regarding the use of a sheath gas to prevent impaction losses and heating of the chamber to promote evaporation further is desirable in order to achieve even greater analyte transport and reduce rinse times. Characterisation of the primary aerosol generated by the micro-cross-flow nebuliser assembly and tertiary aerosol exiting the evaporation chamber would be useful and highlight possibilities for improving the efficiency of the interface. The interface is also being investigated for use with micro-HPLC – ICPMS, in order to improve the sample introduction efficiency.

The sample injection technique is instrumental in obtaining good quality analytical data from microfluidic devices. Accurate and precise sample volumes must be introduced into a separation micro-channel for elemental speciation. Microvalves of the type described in this thesis have the potential for integration into a microfluidic device in order to form a discrete sample loop. This type of microchip could provide an attractive method for automation of the sample introduction procedure in order to inject a discrete sample plug into a continuous carrier flow in a reproducible manner. On incorporation into a microchip the microvalves must be fully characterised, in terms of actuation pressures and leakage rates, and methods for breaking down / removing them from the chip. This could initially βε περφορμεδ ωιτηιν μιχρο−σλιδε χαπιλλαριεσ ωιτη σιμιλαρ διμενσιονσ το μιχ ροχηιπ χηαννελ (50 μm path length; 0.15 mm by 0.6 mm o.d.).

Publications

1. **Recent developments in manganese speciation.**

   G.F. Pearson and G.M. Greenway, *Trends Anal. Chem.*, 2005, **9**, 803.

2. **Rapid arsenic speciation using ion pair LC-ICPMS with a monolithic silica column reveals increased urinary DMA excretion after ingestion of rice.**

   G.F. Pearson, G.M. Greenway, E.I. Brima and P.I. Haris, *J. Anal. At. Spectrom.*, 2007, **22**, 361.

3. **A highly efficient sample introduction system for interfacing microfluidic chips with ICPMS.**

   G.F. Pearson and G.M. Greenway, *J. Anal. At. Spectrom.*, 2007, **22**, 657.

Oral Presentations

1. **Development of on-chip nebulisation for μCE with ICPMS Detection.**

   12th Biennial National Atomic Spectroscopy Symposium, University of Plymouth, July 2004.

2. **Miniaturisation of sample introduction for ICPMS.**

   Departmental research colloquium, University of Hull, June 2006.

3. **New Approaches for Elemental Speciation with ICPMS Detection.**

   13th Biennial National Atomic Spectroscopy Symposium, University of Glasgow, July 2006.

4. **New Approaches for Elemental Speciation with ICPMS Detection.**

   Analytical Research Forum, University of Cork, July 2006.

5. **Novel techniques in Arsenic Speciation.**

   Elan User Group meeting, PerkinElmer LAS, Beaconsfield, November 2006.

Poster Presentations

1. **Development of Microchip Capillary Electrophoresis with ICPMS for Speciation.**

   Analytical Research Forum, University of Plymouth, July 2005.

Collaborative Studies

1. **Interfacing microfluidic chips with microwave induced plasma optical emission spectrometry.**

   Short-term scientific mission for Chemistry in High-Energy Microenvironments.

   COST-STSM-D32-01815

   Prof. Henryk Matusiewicz, Poznan University of Technology, Poznan, Poland.

   5th – 10th February 2006.

2. **Investigation of total arsenic and selenium ratios in human urine, hair and nail samples. Arsenic speciation in human urine and food samples for an ingestion study on American long grain rice.**

   Dr. Parvez I. Haris and Eid I. Brima, De Montfort University, Leicester, UK.

   July 2005 – October 2006.

   E.I. Brima, P.I. Haris, R.O. Jenkins, D.A. Polya, A.G. Gault and C.F. Harrington, *Toxicol. Appl. Pharmacol.*, 2006, **216**, 122.

   E.I. Brima, R.O. Jenkins and P.I. Haris, *Spectroscopy*, 2006, **20**, 125.

Technical Abbreviations and Acronyms

AAS	atomic absorption spectrometry
AC	alternating current
AES	atomic emission spectrometry
AFS	atomic fluorescence spectrometry
AFT	axial field technology
amu	atomic mass unit
AsB	arsenobetaine
BEC	background equivalent correction
CE	capillary electrophoresis
CF	cross-flow
CFN	cross-flow nebuliser
CGE	capillary gel electrophoresis
CITP	capillary isotachophoresis
cps	counts per second
CRM	certified reference material
CZE	capillary zone electrophoresis
DBT	dynamic bandpass tuning
DC	direct current
DF	double focussing
DIHEN	direct injection high efficiency nebuliser
DIN	direct injection nebuliser
DL	(instrument) detection limit
DMA	dimethylarsinic acid
DRC	dynamic reaction cell
EOF	electroosmotic flow
ETV	electrothermal vaporisation
eV	electron volts
FAAS	flame atomic absorption spectrometry
GC	gas chromatography
HECFMN	high efficiency cross-flow micronebuliser
HEN	high efficiency nebuliser
HG	hydride generation
HPLC	high performance liquid chromatography
HR	high resolution
HV	high voltage
ICP	inductively coupled plasma
IE	ionisation energy
IP	ionisation potential
IPC	ion pair chromatography
IPR	ion pair reagent
ITP	isotachophoresis
IUPAC	international union for pure and applied chemistry
LC	liquid chromatography
LOD	limits of detection
LTE	local thermal equilibrium
m/z	mass to charge ratio
MC	multicollector
MCN	microconcentric nebuliser
MEKC	micellar electrokinetic capillary chromatography
MIP	microwave induced plasma
µl	microlitre
MMA	monomethylarsonic acid
MP	mobile phase
MS	mass spectrometry
nl	nanolitre
OES	optical emission spectrometry
PDMS	polydimethylsiloxane
PMT	photomultiplier tube
PN	pneumatic nebuliser
ppb	parts per billion
ppm	parts per million
ppt	parts per trillion
PTFE	polytetrafluoroethylene
Q	quadrupole
q/r	charge to size ratio
RF	radiofrequency
RP	reversed phase
RSD	relative standard deviation
S/N	signal to noise ratio
SD	standard deviation
SEC	size exclusion chromatography
SF	sector field
SP	stationary phase
SPE	solid phase extraction
TDS	total dissolved solids
TISIS	torch integrated sample introduction system
TOF	time of flight
UHQ	ultra high quality
USN	ultrasonic nebuliser
UV	ultraviolet